

Aus dem
Institut für Physiologische Chemie
der Medizinischen Fakultät
der Martin-Luther-Universität Halle-Wittenberg

(Direktor: Prof. Dr. rer. nat. Guido Posern)

**Ubiquitin regulated processes: from single cell nutrient sensing
and signal transduction to organismal development and human
disease**

Habilitationsschrift
zur Erlangung des akademischen Grades
eines habilitierten Doktors
der Medizinischen Wissenschaften (Dr. rer. nat., rer. medic. habil.)
für das Fachgebiet Biochemie

vorgelegt
der Medizinischen Fakultät
der Martin-Luther-Universität Halle-Wittenberg
von: Dr. rer. nat. Thorsten Bernd Pfirrmann
geboren am 08.12.1974 in Heidelberg

Gutachter: Prof. Hoppe
Prof. Grune

Datum der Verteidigung: 22.05. 2018

1 Abstract

All cells share some evolutionary conserved features with each other, e.g. cells are able to sense their environment in order to quickly adapt to changing environmental conditions. Signals like a change in temperature, lack or availability of certain nutrients and pheromones induce a rapid but highly specific change in the transcriptional profile, so that redundant or dispensable genetic programs are switched off, while others are turned on. These regulatory programs, collectively called signal transduction pathways, secure cellular adaptation to environmental changes and thus cellular or organismal survival. Aberrations in nutrient sensing and signaling pathways lead to pathologies and severe diseases, ranging from obesity, diabetes type II, cancer, molecular ageing and many more.

Since the early days of molecular biology and biochemistry, *Saccharomyces cerevisiae* (bakers yeast) is a popular eukaryotic model to study all aspects of cell organization, communication and regulation. During the last three decades, the combination of powerful yeast genetics and genome-wide approaches has led to a more integrated view of metabolic regulation and signal transduction. Often these findings are conserved in higher organisms allowing a more comprehensive understanding of our species. The detailed understanding of such processes is the essence of basic research and the basis for translational research approaches to develop novel diagnosis tools or even therapies.

In this work we first discuss novel insights into the function of the SPS-amino-acid sensing and signaling pathway in yeast. A central component of the pathway is the protease Ssy5 that specifically processes an N-terminal regulatory domain of the transcription factor Stp1. Upon amino acid induced cleavage, Stp1 can enter the nucleus and activate transcription of amino acid permease genes to ensure cellular uptake of extracellular amino acids. My studies show that Ssy5 is directly activated by ubiquitin proteasome mediated polyubiquitination and subsequent degradation of an inhibitory Pro-domain and describe a previously unknown mechanism to activate a latent transcription factor. Second, we discuss the finding of a novel yeast ubiquitin ligase complex, the Gid/CTLH complex that regulates the metabolic switch from gluconeogenesis to glycolysis and plays a central role in glucose sensing and energy homeostasis in the cell. We show, that Gid subunits are evolutionary conserved at the level of the primary structure but also functionally. A protein complex composed of these proteins functions as a ubiquitin ligase complex in yeast and higher vertebrates, where it is called the Gid/CTLH complex. Very surprising novel unpublished results connect the function of the Gid/CTLH complex to the basal body of the primary cilium. The primary cilium is a cell organelle of higher vertebrate cells that functions e.g. as a sensor for extracellular morphogens like sonic hedgehog. It consists of a ciliary axoneme build-up of a nine-duplet microtubular filament ring that arises from the basal body and is surrounded by the ciliary membrane. Our data suggests, that the Gid/CTLH complex functions as a basal body localized nutrient sensor that regulates energy homeostasis by directly influencing mTOR signaling and autophagy.

Pfaffmann, Thorsten. Ubiquitin regulated processes: from single cell nutrient sensing and signal transduction to organismal development and human disease. Halle, Univ., Med. Fak., Habil., 41 Seiten, 2017

2 Table of Contents

1	Abstract	II
2	Table of Contents.....	III
3	List of Abbreviations.....	IV
4	Chapter I – The Ubiquitin Proteasome system in nutrient sensing and signaling	
1		
4.1	Introduction.....	1
4.2	Amino acid sensing and the SPS-sensing system.....	3
4.3	Glucose sensing, catabolite degradation and the Gid/CTLH ubiquitin ligase complex.....	11
5	Chapter II - The vertebrate Gid/CTLH ubiquitin ligase complex in development and disease	17
5.1	Introduction.....	17
5.2	The Gid/CTLH ubiquitin ligase complex is associated with ciliopathies in Humans and <i>Xenopus laevis</i>	20
6	Outlook and future perspectives	27
7	Literature.....	31
8	Published articles relevant for this work*	39
9	Thesises	40
10	Eidesstattliche Erklärung.....	V
11	Curriculum vitae	VI
12	Appendix	IX

Figure 1: The Ubiquitin-Proteasome-System.....	3
Figure 2: Amino acid-induced proteasomal degradation of the Ssy5 Pro-domain correlates with Stp1 processing	6
Figure 3: Synthetic N-degron-regulated Pro-domain degradation results in temperature-controlled Stp1 processing.....	7
Figure 4: Casein kinase I and Grr1 are required for amino acid-induced degradation of the Ssy5 Pro-domain.....	9
Figure 5: Current model of Receptor-Activated proteolysis of Ssy5.....	9
Figure 6: Catabolite degradation of fructose-1,6-bisphosphatase (FBPase).....	12
Figure 7: Comparative representation of orthologous Gid2/Rmd5 proteins.....	13
Figure 8: Gid2/Rmd5 shows E3 activity.....	14
Figure 9: Gid4 expression regulates FBPase degradation.....	16
Figure 10: Spatial analysis of <i>rmnd5</i> (A) and <i>mkln1</i> (B) expression.....	21
Figure 11: <i>rmnd5a</i> loss of function results in morphological changes of the pronephric kidney in <i>Xenopus laevis</i>	22
Figure 12: <i>rmnd5a</i> knock down alters ciliogenesis of multi-ciliated cells of the skin (MCCs) in <i>Xenopus laevis</i>	24
Figure 13: Ciliopathy typical phenotypic features in RMND5a LoF <i>Xenopus laevis</i> and a patient with a partial RMND5a duplication.....	25
Figure 14: RMND5a loss-of-function alters primary cilia dependent sonic hedgehog signaling in NIH3T3 cells.....	25
Figure 15: Co-localization of RMND5a with the basal body of the primary cilia in NIH3T3 cells.....	26
Figure 16: The Gid/ CTLH ubiquitin ligase complex in yeast and homo sapiens. ...	29

3 List of Abbreviations

°C	degree celsius
A	alanine
AMP	adenosine monophosphate
AP	alkaline phosphatase
ATP	adenosine triphosphate
BBS	Bardet Biedel syndrome
Cat-domain	catalytic domain
CFP	cyan fluorescent protein
CHX	cycloheximide
CTLH domain	C-terminal to LisH domain
D	aspartic acid
DHFR	dihydrofolate-reductase
DNA	deoxyribonucleic acid
e.g.	<i>exempli gratia</i>
E1	ubiquitin activating enzyme
E2	ubiquitin conjugating enzyme
E3	ubiquitin ligase
EGFR	epidermal growth factor receptor
ESEM	environmental scanning electron microscope
Fbpase	fructose-1,6-bisphosphatase
FCS	fetal calf serum
GFP	green fluorescent protein
H	histidine
JBS	Joubert syndrome
K	lysine
kDA	kilodalton
LCA	Leber-congenital amaurosis
leu	leucine
LisH domain	Lis homology domain
MCC	multi-ciliated cells
min	minute
MKS	Meckel Gruber syndrome
MM	DuPont Ally®
MO	morpholino
ODC	Oral facial digital syndrome
PEPCK	phosphoenolpyruvat-carboxykinase
PhD	doctor of philosophy
Prof.	professor
R	arginine
RAP	receptor activated proteolysis
RFP	red fluorescent protein
RIP	regulated intra-membrane proteolysis
RNA	ribonucleic acid
RUP	ubiquitin/proteasome-dependent processing
S	serine
SCF complex	Skp1/Cdc53/F-box protein complex
SD-medium	synthetic defined medium
SDS	sodium dodecyl sulfate
SHH	sonic hedgehog
SPS-sensor	Ssy1-Ptr1-Ssy5-sensor
STRD	standard
UBP	ubiquitin-specific-protease
UPS	ubiquitin-Proteasome-System
WB	Western bot
WMISH	whole mount <i>in situ</i> hybridisation
WT	wild type

4 Chapter I – The Ubiquitin Proteasome system in nutrient sensing and signaling

4.1 Introduction

4.1.1 Ubiquitin

The protein ubiquitin was discovered and described more than 40 years ago by Goldknopf and colleagues in a series of publications that led to the description of the small 76 amino acid protein as a posttranslational modifier. At that time, it was first found attached to histone H2B with an isopeptide bond of the ubiquitin C-terminus and an internal lysine residue (K119) within H2B. Today we know, that H2B can be tagged with a single ubiquitin molecule in a process called mono-ubiquitination or mono-ubiquitylation and it was the first of many different posttranslational modifications to come that modify lysine residues within histones to regulate gene expression (Pavri et al., 2006). Today, it turns out that the variety and complexity of the posttranslational modification system with ubiquitin is much more complicated and probably the most versatile and potent posttranslational modifier in existence.

Ubiquitin is a 76 amino acid protein with a molecular mass of 8.5 kDa. It is ubiquitously expressed and highly evolutionary conserved, the human and the *Sacharomyces cerevisiae* protein differs in only three amino acids. In humans there are four known genes that code for ubiquitin, all of them are fusion proteins that need to get processed by specific proteases in order to produce functional single moiety ubiquitin (Wiborg et al., 1985). Interestingly, two fusion proteins are chimeric proteins fused to ribosomal subunits (RPS27A, UBA52), while the UBB and UBC genes code for in tandem fusions of ubiquitin. Its remarkable conservation is thought to be caused by the immense selective pressure on the molecule as a result of its diverse essential biological functions (Pickart and Eddins, 2004). These functions include the targeted degradation of proteins by the 26S proteasome, the unspecific degradation of proteins in the lysosome (vacuole), endocytosis of membrane proteins (e.g. EGFR), intracellular trafficking and regulation of the secretory pathway, transcriptional regulation and many more (reviewed in Figure 1). It is really surprising that a single posttranslational modifying protein is the main regulator of all of these processes and the question remains how the cellular recognition machineries are able to distinguish between these processes. Answers, at least in part, might be found in the primary sequence and the structure of ubiquitin itself but also in the enzymatic machinery that targets substrates

for ubiquitination (also called ubiquitylation). To be able to understand this, one must first look at the biochemical principles behind the ubiquitination process. The ubiquitination machinery requires the sequential and hierarchical reaction of a set of three enzyme classes to catalyze mono-ubiquitination, multi-monoubiquitination or polyubiquitination of a substrate (Sadowski et al., 2012). The ubiquitin-activating-enzyme activates ubiquitin by ATP hydrolysis (E1) which is then transferred to the ubiquitin-conjugating-enzyme (E2) and finally the substrate specific ubiquitin ligase (E3) will transfer ubiquitin onto a lysine residue of the substrate forming a covalent isopeptide bond. In the final step of substrate ubiquitination an activated ubiquitin is covalently attached to either a substrate lysine residue or to one of the seven lysine residues of ubiquitin itself, thus forming polyubiquitin chains with homotypic chains on one particular lysine residue of ubiquitin or mixed polyubiquitin chains generated by polymerization of different ubiquitin lysines. In some rare cases mono-ubiquitination does not require an E3 at all (Woelk et al., 2006).

The catalytic specificity for the substrate and for the kind of ubiquitination is mostly dependent on the ubiquitin-ligase and thus forms the molecular reason for the plethora of different functions regulated by ubiquitination. In a reverse process, so called ubiquitin-specific-proteases (UBPs) can remove polyubiquitin chains from substrate molecules or trim chains. Consequently, these enzymes add an additional layer of control to the system and act as E3 antagonists. Both enzyme classes are the main focus of my scientific career, but only work on ubiquitin ligases will be presented in this review.

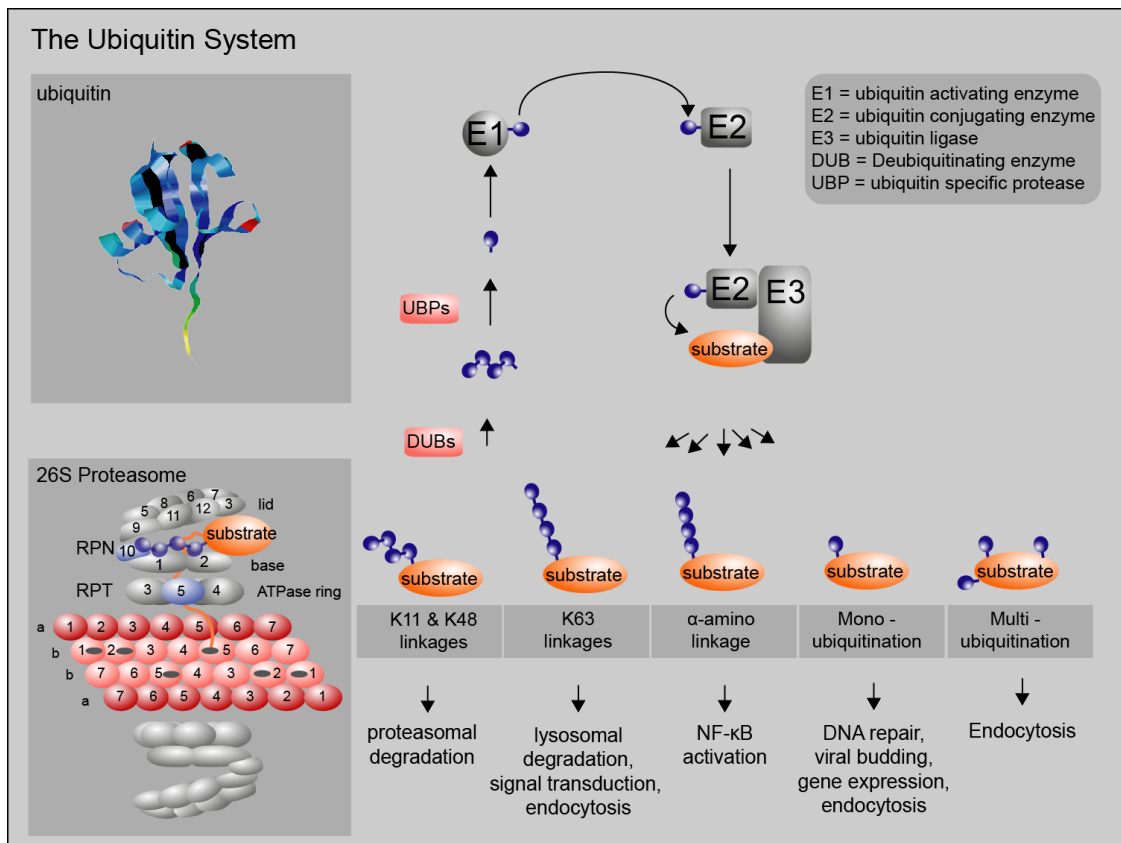


Figure 1: The Ubiquitin-Proteasome-System. The UPS requires the sequential hierarchical reaction of a class of three enzymes to ubiquitinate a substrate protein: The „ubiquitin activating enzyme“ (E1), the „ubiquitin conjugating enzyme“ (E2) and the corresponding substrate specific „ubiquitin ligase“ (E3). E3-antagonists, so called „ubiquitin specific proteases“ do remove ubiquitin moieties from chains or the substrate. Lysine residues (K) within ubiquitin are used to form polyubiquitin chains: K11- and K48-polyubiquitin chains induce 26S proteasome dependent substrate degradation, K63-polyubiquitin chains regulate endocytosis and other processes, while chains via the N-terminus regulate NF κ B signaling. Mono-ubiquitination and multiubiquitination regulate processes like endocytosis and DNA repair. The 26S-proteasome binds K48, K11 polyubiquitinated substrate, unfolds and degrades it in the interior of the barrel shaped 20S proteasome. A schematic view of the 26S proteasome and its subunits is shown (left lower figure) adapted from (Wolf et al., 2004).

4.2 Amino acid sensing and the SPS-sensing system

The Ssy5 signaling endo-protease is the core component of the Ssy1-Ptr3-Ssy5 (SPS) sensor, a yeast plasma membrane localized protein complex that senses extracellular amino acids. This pathway enables yeast cells to take up extracellular amino acids by induction of genes encoding for broad specificity amino acid permeases (Forsberg and Ljungdahl, 2001, Pfirrmann, 2012). In our current model that includes data from three of my first author publications, Stp1 and Stp2 are synthesized as latent precursors excluded from the nucleus due to the presence of negative regulatory domains at their N-terminus (Andréasson and Ljungdahl, 2002). The primary amino acid-induced signal is initiated by the plasma membrane-localized receptor Ssy1 that transmits Ptr3 dependent activation of the Ssy5 signaling-protease. A key event in this pathway is the endoproteolytic Ssy5 dependent proteolytic processing and activation of the homologous transcription factors, Stp1 and Stp2 (Stp1/2), a process we named RAP

(receptor activated proteolysis). Processed Stp1/2 can actively enter the nucleus and initiate the transcription of amino acid permease genes. The gene products will then allow cells to take up amino acids from the medium.

For a long time the function of Ssy5 in the SPS sensing complex remained unclear. However, several recent reports show now that Ssy5 has sequence similarities to chymotrypsin-like proteases (Abdel-Sater et al., 2004, Andréasson et al., 2006, Poulsen et al., 2006). Point mutations of the proposed catalytic triad of Ssy5 (H465, D545 and S540) lead to a complete loss of Stp1 processing (Abdel-Sater et al., 2004, Andréasson et al., 2006) and inactivate the intrinsic autoprocessing activity. Like all chymotrypsin like proteases (clanA) Ssy5 is expressed as an inactive zymogen and undergoes autoproteolytic processing between aminoacid 381 and 382 to generate an N-terminal Pro-domain and a C-terminal catalytic domain (Andréasson et al., 2006, Barrett and Rawlings, 1995, Poulsen et al., 2006). Expression of proteases as inactive zymogens has several functions: The Pro-domain of α -lytic enzyme for example is necessary to overcome an extremely high folding barrier of 30 kcal/mol. The Pro-domain is thus necessary to mediate proper folding of the catalytic domain (Baker et al., 1993, Baker et al., 1992) and the tight fit of the Pro-domain into the catalytic domain of alpha lytic enzyme keeps the enzyme inactive until the Pro-domain is removed (Cunningham and Agard, 2003).

This knowledge set the base for our hypothesis that Ssy5 is activated by a regulated removal of the Ssy5 Pro-domain. Key experiments that support this hypothesis will be presented in the following two chapters and are reviewed in chapter 685 of the 'Handbook of Proteolytic Enzymes' (Pfirrmann, 2012). A concluding model of our findings is presented in Figure 5.

4.2.1 The Prodomain of Ssy5 Protease Controls Receptor-Activated Proteolysis of Transcription Factor Stp1

Proteolytic processing is a mechanism used by eukaryotes to control the activity of latent transcription factors (Brivanlou and Darnell, 2002). For example, regulated intra-membrane proteolysis (RIP) and ubiquitin/proteasome-dependent processing (RUP) are two mechanisms that employ proteolysis-dependent activation of latent membrane-anchored transcription factors (Brown et al., 2000, Hoppe et al., 2001). RIP is catalyzed by membrane bound proteases that cleave inactive precursor molecules to release active transcription factors from their membrane anchor. In the RUP mechanism, a

polyubiquitinated membrane anchored precursor is partially degraded by the 26S Proteasome and active transcription factor is released to target the nucleus. Both RIP and RUP rely on constitutively active proteases that process substrate transcription factors when available to bind the protease. Control of substrate availability is achieved by changing the intracellular compartmentalization of the substrate (RIP) or covalent modification to modify substrate targeting to an enclosed protease compartment (RUP). Consequently, in these pathways the regulation of signal transduction occurs at the level of the substrate availability and not by directly regulating the proteolytic activity of the processing protease. RAP is distinguished from the previously described protease-based signaling mechanisms, RIP and RUP, in that it does not rely on modulating substrate accessibility but instead is based on direct protease regulation.

The mechanism of RAP-dependent activation of Stp1 and Stp2 is not well understood, but several observations point to an important regulatory function of the Ssy5 Pro-domain (Andréasson et al., 2006). First, the Pro-domain appears to be required in the co-translational maturation of the protease. Further, after autoproteolytic processing the Pro- and Cat-domains remain associated forming a catalytically competent but inactive protease that associates with Stp1 *in vivo* and *in vitro*. Accordingly after assembly into a functional protease, the Pro-domain acts as an effective Cat-domain inhibitor that must be removed for protease activation.

The following key experiments will be presented to demonstrate that the Pro-domain of Ssy5 is degraded by the 26S proteasome in a SPS-dependent and -regulated manner and that Pro-domain degradation is sufficient for Ssy5 activation. Figure 2 shows the degradation kinetics of the Pro-domain of Ssy5 (upper panel) as well as Stp1 processing and degradation (lower panel) after addition of leucine (+ leu) to induce the SPS signaling pathway. Samples were taken after cycloheximide (CHX) and leucine (+ leu) addition at the indicated timepoints (min) and subjected to SDS Page and subsequent Western blot analysis. In a control strain (CIM3) and a conditional temperature sensitive mutant of a proteasomal subunit (*cim3-1*) the fate of the Ssy5 Pro-domain (upper panel) and Stp1 processing (lower panel) was followed by detection with an anti-HA antibody (α -HA), α -Pgk1 was used as a loading control. While the Pro-domain is stable without the addition of leucine (no leu) it is degraded within 15 min after leucine addition (+leu) followed by a rapid proteolytic cleavage of Stp1. In contrast, in the proteasomal mutant (*cim3-1*) the Pro-domain remains stable and Stp1 full length as well as active Stp1 can be detected at restrictive temperatures. This

experiment underlines the significance of 26S proteasome activity for Ssy5 activation and strengthens our hypothesis that SPS-dependent Pro-domain degradation is the trigger and main regulator of Stp1 activation.

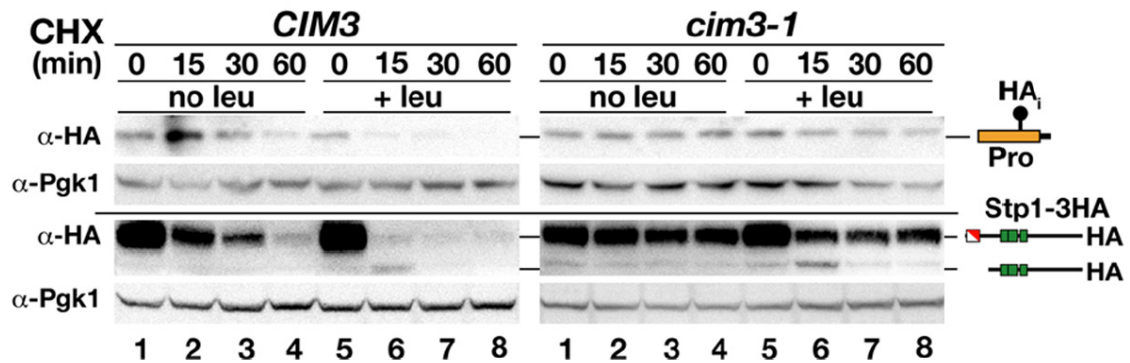


Figure 2: Amino acid-induced proteasomal degradation of the Ssy5 Pro-domain correlates with Stp1 processing. Immunoblot analysis of cell extracts from *CIM3* (CAY220) and the conditional temperature sensitive proteasomal *cim3-1* (CMY763) mutant strains carrying pRS315 (LEU2) and pSH120 (HAi-Ssy5-GST) or pCA047 (Stp1-HA). Cells were pregrown in SD at 25°C, and cultures were split into two equal volumes and incubated at 37°C for 30 min prior to the addition of CHX and leucine as indicated. Samples were taken at the indicated time points after CHX addition. The immunoreactive forms of the Ssy5 Pro-domain and Stp1 are schematically represented at their corresponding positions of migration. Levels of Pgk1 served as an internal control for protein loading (taken from (Pfirrmann et al., 2010)).

In a next important key experiment we designed and employed a synthetic temperature regulated instable Pro-domain, to be able to degrade the Pro-domain SPS-sensor independent by simply changing growth temperature. A tool employed in the experimental setup is based on the temperature-controlled N-degron described by the group of Alex Varshavsky (Dohmen et al., 1994). It functions on the fact that ubiquitin fusion proteins are processed by endogenous ubiquitin-specific-proteases leaving an N-terminal residue that decides over the stability of the following protein. This pathway generally named the N-end rule pathway describes a set of different N-terminal proteins that either stabilize or destabilize a protein. For example an N-terminal arginine (R) renders a protein unstable, while an N-terminal alanine (A) stabilizes proteins. The protein dihydrofolate-reductase (DHFR) is tightly folded and despite N-terminal destabilizing residues cannot be unfolded and degraded by the 26S proteasome at lower growth temperatures (25°C), however at higher growth temperatures (35°C) a fusion protein is turned over by the proteasome. As shown in Figure 3A two different fusion proteins were constructed leaving either a destabilizing arginine (Ssy5-Rds) or a stabilizing alanine (Ssy5-As) at the N-terminus of DHFR protein fused to the Pro-domain of Ssy5. A growth based functional assay, shows that a HA-tagged Ssy5 and Ssy5-Rds can complement a *ssy5*-deletion as seen by growth on YPD + MM at 25°C

and 35°C (Figure 3A). A constitutive active Ssy5 allele is the $\Delta 60$ allele, that allows growth on YPD + MM in a strain additionally deleted in the SPS-sensor Ssy1. This indicates Ssy1 independent activation of the protease. Interestingly, the synthetic Ssy5-Rds construct does not allow growth on YPD + MM at 25°C, but is fully active at 35°C. As seen in Figure 3B Ssy5 activation correlates with the temperature induced degradation of the Pro-domain and Stp1 processing. This indicates that the artificial removal of the Pro-domain is sufficient to fully activate Ssy5 and demonstrates the inhibitory function of the Pro-domain. Further experimental details are given in (Pfirrmann et al., 2010).

Taken together, we do not only demonstrate the biological function of the Pro-domain as a potent Cat-domain inhibitor, but additionally set an example of state-of-the-art synthetic biology that employs biological building blocks to engineer novel synthetic biological tools.

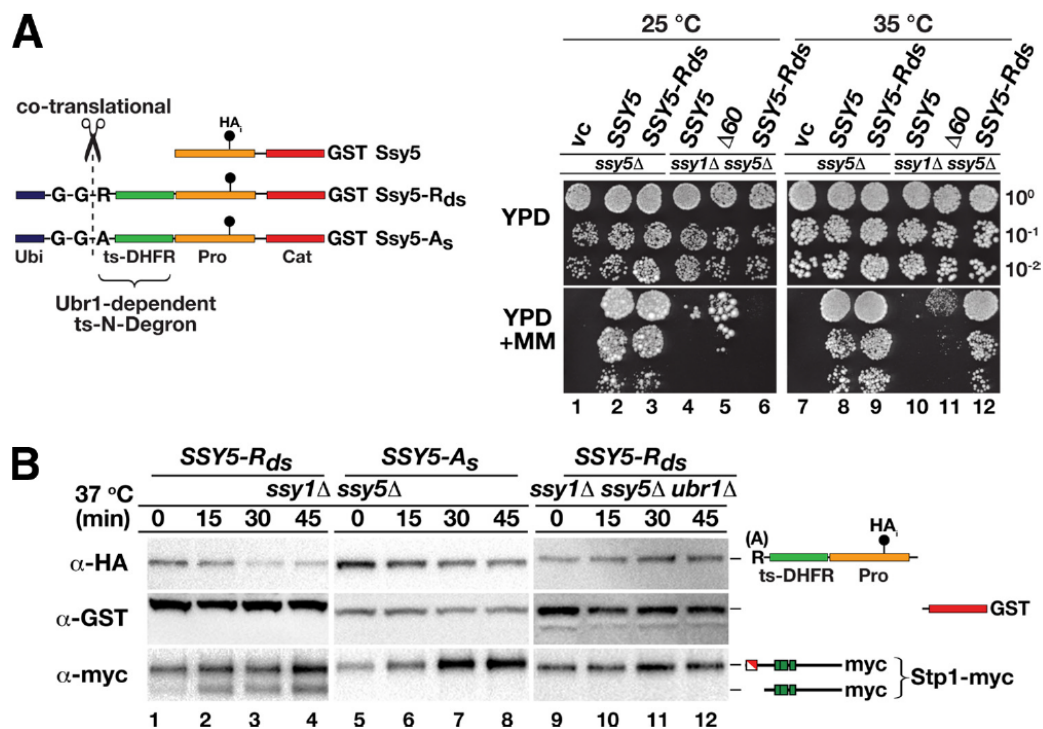


Figure 3: Synthetic N-degron-regulated Pro-domain degradation results in temperature-controlled Stp1 processing. (A) Ssy5 N-degron constructs are schematically represented. The constructs have an N-terminal ubiquitin moiety (Ubi), a destabilizing arginine (R) or a stabilizing alanine (A) residue, and a temperature-sensitive dihydrofolate reductase (ts-DHFR) linker fused at the N-terminus of Ssy5 with an internal Pro-domain HA epitope (HAi) and a C-terminal GST tag. The ubiquitin is cotranslationally cleaved (scissors) following the diglycine (G-G) residues, resulting in proteins with an N-terminal arginine or alanine residue. Arginine, but not alanine, is an N-end rule substrate recognized by Ubr1. Growth of HKY77 (Δ ssy5) and HKY84 (Δ ssy5 Δ ssy1) carrying a vector control (vc), pSH120 (SSY5), pSH106 ($\Delta 60$), or pTP110 (SSY5-Rds) is shown. Cells were pregrown in SD, dilutions were prepared and spotted onto YPD and YPD plus MM, and the plates were incubated at 25 or 35°C for 6 or 3 days, respectively. pSH106 ($\Delta 60$) was used as a positive constitutive control (right panel). (B) Immunoblot analysis of protein extracts from HKY84 (Δ ssy5 Δ ssy1) carrying pCA204 (Stp1-myc) and pTP110 (SSY5-Rds, lanes 1 to 4) or pTP111 (SSY5-As, lanes 5 to 8) and from TPY101 (Δ ssy5 Δ ssy1 Δ ubr1) carrying pCA204 (Stp1-myc) and pTP110 (SSY5-Rds, lanes 9 to 12). Cells were grown in SD at 25°C, cultures were shifted to 37°C at t=0, and extracts were prepared from equivalent numbers of cells harvested at the indicated time point (taken from Pfirrmann et al., 2010).

4.2.2 A phosphodegron controls nutrient-induced proteasomal activation of the signaling protease Ssy5

In a following step we set out to investigate the mechanism behind regulated Pro-domain degradation. Proteasomal degradation of the Ssy5 Pro-domain most likely involves a specific ubiquitin ligase that mediates polyubiquitination of the Pro-domain in response to SPS signaling. A potential candidate was the general Skp1/Cdc53/F-box protein (SCF) complex, an E3 ubiquitin ligase that at the time of the study was already known to be required for Ssy5 activation (Andréasson et al., 2006, Bernard and André, 2001). SCF complexes achieve substrate specificity through association with exchangeable F-box proteins that enable specific binding and subsequent polyubiquitination of target proteins (Jonkers and Rep, 2009). Grr1 is one of the best-characterized F-box proteins in yeast, and Grr1 is known to recognize and bind phosphorylated substrates, so called phosphodegrons. Notably, several proteins have been found to be inducibly phosphorylated by casein kinase I (Yck1, Yck2) leading to their SCF^{Grr1}-dependent proteasomal degradation. Both Yck1/2 and SCF^{Grr1} are required for SPS sensor signaling (Abdel-Sater et al., 2004, Abdel-Sater et al., 2011, Spielwoy et al., 2004). Through extensive reverse genetic approaches, structure function analysis and biochemical binding assays, we were able to characterize an intrinsic phosphodegron within the Pro-domain of Ssy5. This motif strikingly resembles the Yck1/2- and Grr1-dependent degrons required for the degradation of transcriptional regulators in the Snf3/Rgt2 glucose-sensing pathway (Moriya and Johnston, 2004). We show that Yck1/2 phosphorylates several serine residues within this motif in an SPS dependent fashion. According to our data, this modification induces a transformational rearrangement that now is capable of binding the SCF^{Grr1}-complex. In contrast to wild type Ssy5, a constitutive Pro-domain Ssy5 mutant isolated from a semi-directed evolution assay, binds Grr1 directly and thus most probably mimicks a conformation that resembles phosphorylated Pro-domain. This conformational change leads to a sudden polyubiquitination of the Pro-domain, followed by 26S proteasomal degradation and thus activation of the protease. Details of the experimental setups can be found in our publications (Omnus et al., 2011, Pfirrmann et al., 2010) and are reviewed in chapter 685 of 'The Handbook of Proteolytic Enzymes' (Pfirrmann, 2012).

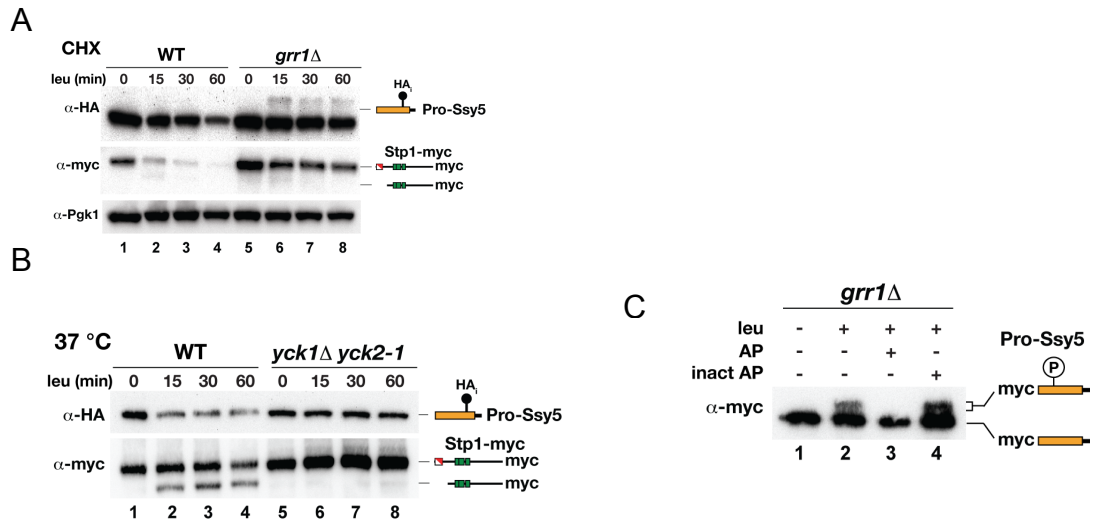


Figure 4: Casein kinase I and Grr1 are required for amino acid-induced degradation of the Ssy5 Pro-domain. (A) Immunoblot analysis of cell extracts from HKY77 (*ssy5Δ YCK1 YCK2*) (WT) and CAY320 (*yck1Δ yck2-1*) carrying pSH120 (HA₃-SSY5-GST) and pCA204 (STP1-MYC). Cells were pregrown in SD medium at room temperature and incubated at 37°C for 30 min, then samples were taken at the indicated time points after leucine addition. (B) Immunoblot analysis of cell extracts from HKY77 (*ssy5Δ*) and CAY276 (*ssy5Δ grr1Δ*) carrying plasmids as in (A); extracts were prepared from cells grown in SD medium after the addition of CHX and leucine at the indicated time points. (C) Immunoblot analysis of immunoprecipitated Pro-domain from extracts from cultures of CAY276 (*ssy5Δ grr1Δ*) carrying pHK048 (MYC-SSY5) and pRS317 induced with leucine as indicated. Immunoprecipitated material was incubated with active (AP) or heat-inactivated (inact AP) alkaline phosphatase as indicated. Immunoreactive forms of phosphorylated and dephosphorylated Ssy5 prodomain and Stp1 are schematically represented at their corresponding positions of migration (taken from Omnus et al., 2011).

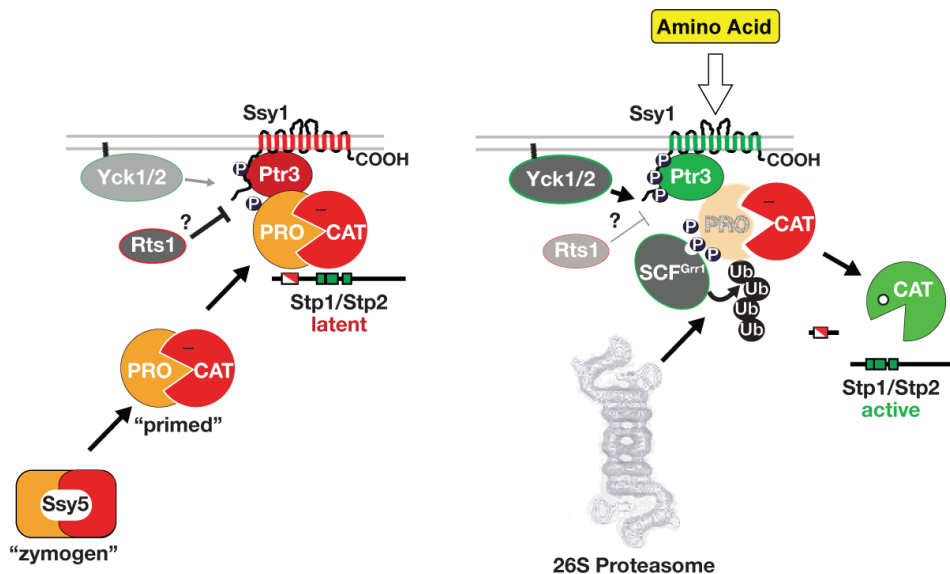


Figure 5: Current model of Receptor-Activated proteolysis of Ssy5. *left: The SPS sensing system in the 'off state'.* The protease Ssy5 is expressed as an inactive zymogen and consists of a Pro-domain (Pro) and a catalytic-domain (Cat). The Pro-domain is essential for the proper folding of the Cat-domain after translation. After folding, active Ssy5 auto-processes itself and the Pro-domain inhibits the Cat-domain by inhibiting the catalytic sites of the protease (primed Ssy5). Primed Ssy5 binds Ptr3 and the two latent transcription factors Stp1/2. *right: The SPS sensing system in the 'on state'.* As soon as amino acids are present and detected by the amino acid sensor Ssy1, Ptr3 and the Pro-domain of Ssy5 are getting phosphorylated by casein-kinase I (Yck1/2). The phosphatase Rts1 acts as an antagonist to Yck1/2. Subsequently, phosphorylated Pro-domain will be polyubiquitinated in a SCF^{Grr1} dependent manner and be degraded by the 26S proteasome. The proteolytic degradation of the Pro-domain is the activating step that induces Stp1/2 proteolytic processing and subsequent accumulation in the nucleus. Active Stp1 activates the transcription of amino acid permease genes, which in turn allows the cells to take up amino acids from the medium.

Our studies on amino-acid signaling in yeast exemplify a novel strategy within a cells repertoire to activate latent transcription factors. Several publications describe a direct involvement of the 26S proteasome in the partial processing of latent transcription factors. A prominent example is the proteolytic activation of the endoplasmic reticulum associated transcription factor Nrf1 (Sha and Goldberg, 2014). This transcription factor regulates the transcription of all 26S proteasomal subunits including p97. While it is not entirely understood how 26S-dependent proteolytic processing can be achieved without degrading the entire transcription factor, the proteolytic processing of Stp1/2 offers a novel alternative strategy. A very recent finding describes a 26S proteasome independent activation of Nrf1 (Vangala et al., 2016). This raises the important question if mechanisms like RAP appear more frequent than we do anticipate right now and if Nrf1 might be processed by a yet unidentified protease.

4.3 Glucose sensing, catabolite degradation and the Gid/CTLH ubiquitin ligase complex

Glucose serves as a high-energy carbon source and its availability is constantly monitored by yeast. Thus glucose sensing- and signaling-systems are extremely advanced and sensitive. Specialized hexose sensors, e.g. Snf3 and Rgt2 react to its presence by affecting metabolism on all layers of control (Celenza et al., 1988, Ozcan et al., 1996), e.g. on transcriptional, posttranscriptional, translational and posttranslational level (Rolland et al., 2002). During glycolysis glucose is metabolized to pyruvate under aerobic conditions or to ethanol under anaerobic conditions in yeast. Gluconeogenesis is the antagonistic reciprocally controlled pathway that is required to synthesize glucose *de novo* from precursor molecules. To prevent a futile cycle of ATP hydrolysis either one or the other is active or inactive (Purwin et al., 1982). Both pathways share a major part of their enzymatic equipment, however some reactions are thermodynamically irreversible and require key enzymes specific for gluconeogenesis, e.g. fructose-1,6-bisphosphatase (FBPase). In *homo sapiens* the expression of FBPase is restricted to the liver, kidneys and the pancreas (Yanez et al., 2005). In yeast FBPase is expressed when cells are grown on a non-fermentable carbon source, e.g. ethanol. In a process called catabolite inactivation the pathway is shut off after glucose supplementation in a series of events. First, the transcription of FBP1 is repressed by Mig1 (Klein et al., 1998, Rolland et al., 2002) and second FBPase gets inactivated by PKA (protein kinase A) dependent phosphorylation (Funayama et al., 1980). In a final step, the enzyme is degraded by the ubiquitin-proteasome-system (UPS) (Schork et al., 1994, Schork et al., 1995). So far, the process of catabolite degradation is described in *S. cerevisiae* only, however there is evidence for its existence in the human liver as well (Bertinat et al., 2011).

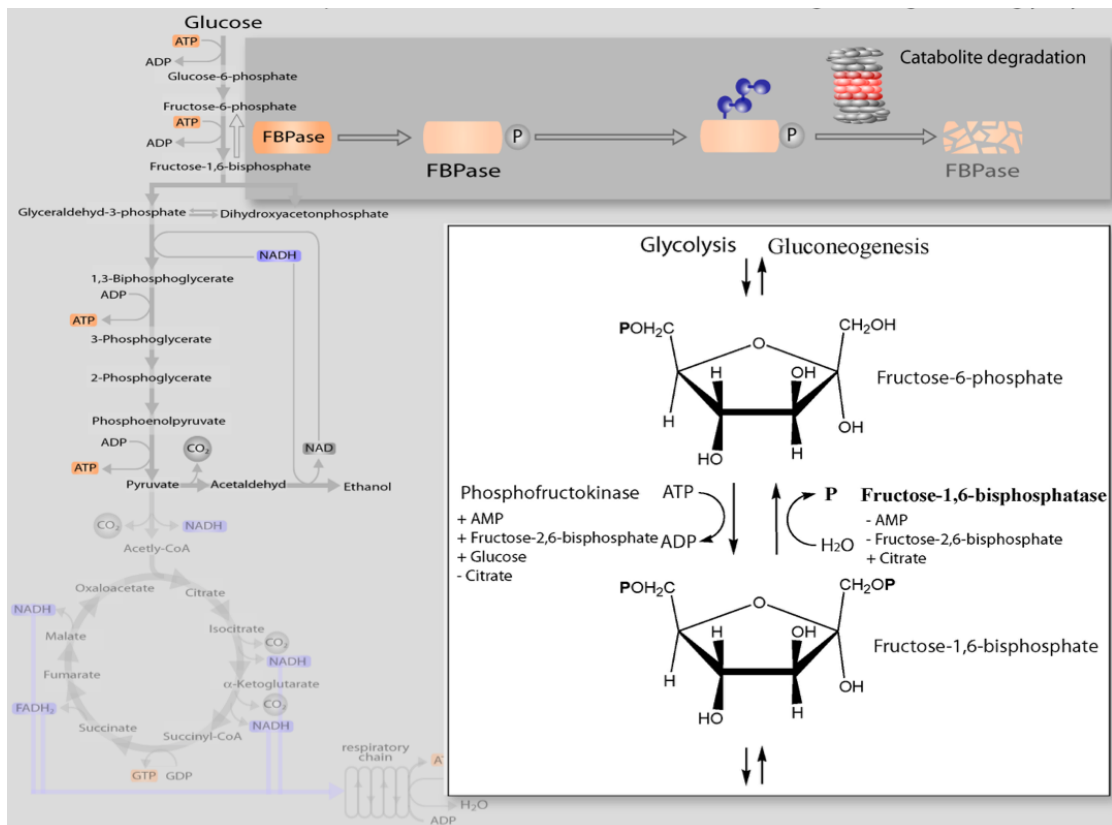


Figure 6: Catabolite degradation of fructose-1,6-bisphosphatase (FBPase). FBPase is a key gluconeogenic enzyme. It catalyzes the dephosphorylation of the sugar fructose-1,6-bisphosphate to fructose-6-phosphate. Addition of glucose to gluconeogenic yeast cells leads to FBPase inactivation by phosphorylation with subsequent polyubiquitination and degradation by the 26S proteasome. This process is called catabolite degradation and is the major switch from anabolic gluconeogenesis to catabolic glycolysis in *Saccharomyces cerevisiae*.

4.3.1 The Yeast GID Complex, a Novel Ubiquitin Ligase (E3) Involved in the Regulation of Carbohydrate Metabolism

In *Saccharomyces cerevisiae* we discovered nine GID-genes (glucose induced degradation deficient) essential for UPS dependent glucose induced degradation of fructose-1,6-bisphosphatase (FBPase), a key gluconeogenic enzyme. This process regulates the metabolic switch from gluconeogenesis to glycolysis (Regelmann et al., 2003). Among them *Gid6* turned out to be the ubiquitin specific protease *Ubp14* (Eisele et al., 2006) and *Gid3* turned out to be *Ubc8*, a ubiquitin-conjugating enzyme (Schule et al., 2000). At the start of my PhD thesis in the lab of Prof. Wolf we had the hypothesis, that the remaining seven *Gid*-proteins could be part of a novel ubiquitin-ligase complex. At the time, several proteomics studies in yeast discovered the *Gid*-proteins *Gid1*, *Gid2*, *Gid4*, *Gid5*, *Gid7*, *Gid8* and *Gid9* to be part of a protein complex (Ho et al., 2002). However, our effort to detect E3-typical RING domains in *Gid*-subunits with regular search algorithms failed. Canonical RING-finger containing ubiquitin ligases contain seven cysteine residues and one histidine residue that coordinate two Zn^{2+} -ions. The

RING domain in ubiquitin-ligases is important for structural integrity and binds the corresponding ubiquitin-conjugating enzyme in the ternary complex (Lorick et al., 1999). Together with Dr. Hoffmann, a bio-informatician working for Miltenyi-biotech at the time, we could show that both *Gid2* and *Gid9* contained non-canonical rudimentary RING domains. This finding set the base for the upcoming story and supported our prior hypothesis that the *Gid* complex is a novel E3 ubiquitin ligase complex (Braun et al., 2011a, Santt et al., 2008).

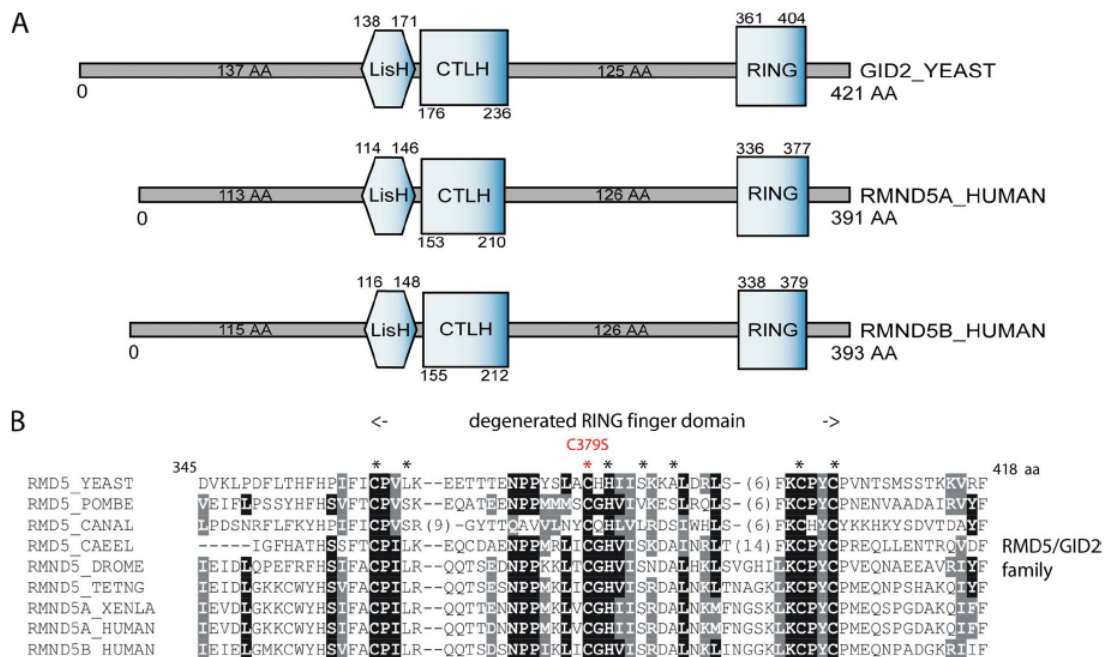


Figure 7: Comparative representation of orthologous *Gid2/Rmd5* proteins.

(A) *Gid2/Rmd5* protein domains from *S. cerevisiae* (upper panel) and *RMND5A/B* from *homo sapiens* (lower panels). (B) Alignment of the RING domains found in the *Gid2/Rmd5* protein family and classic RING-finger proteins. Positions with invariant or conservatively replaced residues in at least 50% of the sequences are printed on black or grey background, respectively. The leftmost column describes the sequence name and contains the species abbreviation: YEAST, *S. cerevisiae*; POMBE, *S. pombe*; CANAL, *Candida albicans*; HUMAN, *H. sapiens*; XENLA, *Xenopus laevis*; DROME, *Drosophila melanogaster*; CAEEL, *Caenorhabditis elegans*; TETNG, *Tetraodon nigroviridis* (taken from (Santt et al., 2008)).

Gid2 and *Gid9* both contain non-canonical rudimentary RING domains essential for glucose induced polyubiquitination and subsequent degradation of gluconeogenic key enzymes such as *FBPase* and *phosphoenolpyruvat-carboxykinase (PEPCK)*. Interestingly, *Gid* proteins of eukaryotic cells are highly conserved (Table 1) (Santt et al., 2008) and are part of a protein complex in humans and in *Arabidopsis thaliana* (Kobayashi et al., 2007, Tomastikova et al., 2012). The domain distribution of the yeast *Gid2* protein and two human orthologous proteins *RMND5A* and *RMND5B* are depicted in the upper panel (Figure 7A). Not only the order of domains is highly conserved (see *LisH* and *CTLH* domain), but also the sequence of the individual

domains and the overall sequence of Gid2. The RING domain of Gid2 in (Figure 7B) is non-canonical, however contains several of the zinc complexing cysteine and histidine residues present in the canonical RING domain. This suggests an important function of the RING domain for catabolite degradation of FBPase in yeast. We started out to rigorously test the possibility that the Gid-complex could be a novel type of RING-ubiquitin ligase. Some key experiments will be shown in the following section.

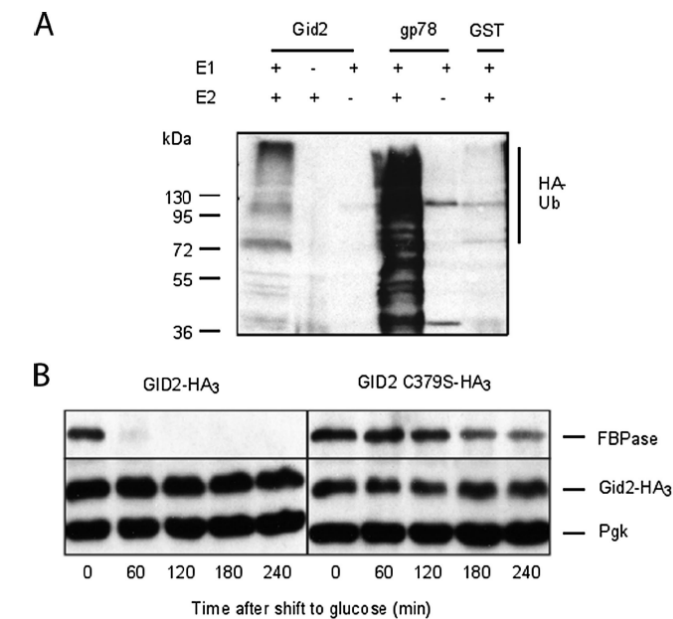


Figure 8: Gid2/Rmd5 shows E3 activity.

(A) Gid2/Rmd5 ubiquitinates protein *in vitro*. Lysates of *E. coli* expressing either Gid2/Rmd5 or the mammalian RING-finger protein gp78 as a positive control and GST as a negative control were incubated with E1, E2 (UbcH5b), ATP and HA-ubiquitin for 2 h at 30°C. To assess the specificity of the reaction, same lysates were incubated without E1 or E2. Polyubiquitination was detected using monoclonal HA antibody. (B) GID2-HA₃ and its mutated C379S counterpart-expressing cells were grown 16 h in YPethanol at 25°C and shifted to YPD. Samples were taken at indicated time points and FBPase degradation was monitored by immunoblotting. Pgk, 3-phosphoglycerate kinase, loading control. fbp1: FBPase deletion. Presence of FBPase in the immunoprecipitates was controlled by immunoblotting with FBPase antibody (taken from (Santt et al., 2008)).

Figure 8 shows a standard experiment to test whether a RING domain containing protein is a ubiquitin ligase. The rationale behind the setup is that RING-ubiquitin ligases or the RING domain alone polyubiquitinate themselves *in vitro* in the presence of purified E3, E2 (UbcH5b), E1 and HA-ubiquitin. To test whether yeast Gid2 protein is a subunit of a ubiquitin ligase, purified Gid2 was incubated together with E1, E2 and HA-Ub and subjected to Western blot analysis. Decoration with antibodies directed against the HA-epitope reveals a signal typical for polyubiquitination (left lane), which is absent in the control sample without E1. The E3 GP78 was used as a positive control, while GST was subjected as a negative control (lane 3 and 6, respectively). As a result derived from the polyubiquitin smear present in the Gid2 sample we conclude that Gid2 polyubiquitinates itself *in vitro* and thus is part of a ubiquitin ligase. In Figure 8B we have tested the importance of the RING domain for catabolite degradation of FBPase. We constructed a Gid2 variant containing a C379S mutation in the conserved region of the RING domain. As highlighted in B this cysteine residue is most probably a zinc complexing residue and is critical for function. After chromosomal insertion into the

native locus we compared glucose induced catabolite degradation of both wild type and C379S mutant strains. In a representative Western blot, Figure 8 shows a rapid glucose induced degradation of FBPase in the control strain (left panel) and 60 minutes after glucose addition FBPase is entirely degraded. The C379S mutant strain however is severely impaired in the catabolite degradation process, reflecting the importance of the RING domain for this process. Together these experiments suggest, that the Gid-complex is a novel ubiquitin ligase complex.

An unusual subunit of the Gid-complex is Gid4/Vid24. It is the only Gid subunit that is either not present under de-repressing growth conditions or expressed in very low amounts and turned over immediately. Nevertheless, as seen in Figure 9A, yeast extracts from cells grown on YP-ethanol do not show a measurable Gid4 signal by Western blot analysis. Already 5 minutes after glucose supplementation a signal appears and peaks around 30 minutes after glucose addition. Gid4 protein levels negatively correlate with FBPase degradation, suggesting a Gid4 function in recruiting FBPase and other substrates to the Gid-complex for polyubiquitination and subsequent degradation. The addition of the translation-inhibitor cycloheximide (CHX) inhibits Gid4 translation and thus FBPase degradation is blocked as a result. All other Gid-complex subunits are expressed and are part of the complex under several growth conditions (see Santt et al., 2008). This suggests, that a core Gid-complex is always present and the differential expression of Gid4 regulates substrate stability. Indeed, the ectopic expression of Gid4 under de-repressing conditions can induce FBPase degradation (Figure 9B). This data indicates a function of the Gid4/Vid24 protein in substrate recognition and recruitment to the Gid-complex for polyubiquitination and subsequent degradation. In a recent report Gid4 is described as a novel N-recogin that specifically binds N-terminal proline residues for recruitment to the Gid-complex (Chen et al., 2017). This finding suggests that more than the prior described gluconeogenic N-terminal proline bearing enzymes are substrates of the Gid-complex.

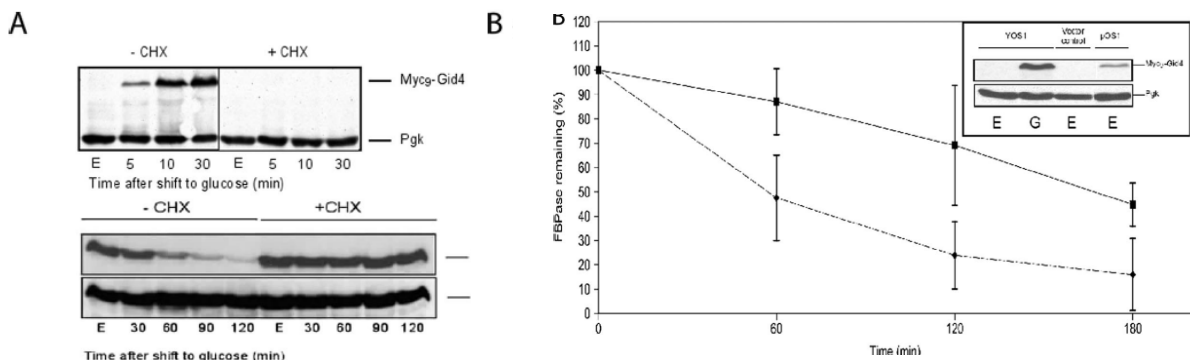


Figure 9: Gid4 expression regulates FB Pase degradation. (A) *De novo* protein synthesis is necessary for FB Pase degradation and Myc9-Gid4 expression. Wild-type cells were grown 16h in YPethanol (E) and shifted to YPD with (CHX) or without (CHX) cycloheximide (100 g/ml). FB Pase and Myc9-Gid4 levels were monitored at indicated times via immunoblotting with anti-FB Pase or anti-Myc antibodies, respectively. (B) Gid4/Vid24 expression triggers FB Pase degradation. Myc9-GID4 was cloned under a TetR promoter and expressed in cells growing on YPethanol. Pulse-chase analysis of FB Pase in cells bearing either the Myc9-GID4 expressing plasmid or the respective vector control (f) was carried out (means of three independent experiments, confidence interval, 0.05). Inset, immunoblot showing the steady-state levels of Myc9-Gid4 in glucose inactivated cells (30 min, YOS1, G) and in ethanol grown cells (pOS1, E) (taken from (Santt et al., 2008)).

In a next step we started out to test the function of a second Gid-subunit with a rudimentary non-canonical RING domain. Similar to Gid2 also Gid9 contains an unusual RING domain (Braun et al., 2011). Analogous to experiments shown above, Gid9 polyubiquitinates itself *in vitro* and conserved cysteine residues within the non-canonical RING domain are critical for the glucose-induced degradation of FB Pase and other gluconeogenic key enzymes.

In conclusion, the Gid-complex is a novel ubiquitin ligase that regulates the metabolic switch from anabolic gluconeogenesis to metabolic glycolysis in yeast by targeting the key gluconeogenic enzymes FB Pase, PEPCK, Mdh2 and Icl1 for proteasomal degradation. It contains two subunits with non-canonical RING domains. Both domains are essential for FB Pase polyubiquitination and subsequent catabolite degradation. It is very likely, that both RING domains are essential binding partners of the respective ubiquitin-conjugating enzyme (E2) and thus recruit Ubc8 to the ternary complex consisting of the substrate, Ubc8 and the Gid-complex. A mechanism in which two non-canonical RING domains in subunits of an E3-complex bind the corresponding E2 is unique to the Gid/CTLH complex. Another unusual feature of the Gid-complex is the controlled substrate degradation by regulated production of a substrate recognition- and recruiting-factor like the subunit Gid4. The high evolutionary conservation of the Gid/CTLH complex suggests similar functions in higher vertebrates and will be discussed in the following chapter.

5 Chapter II - The vertebrate Gid/CTLH ubiquitin ligase complex in development and disease

5.1 Introduction

5.1.1 Structure and function of the vertebrate Gid/CTLH complex

In the Institute of Physiology at the Martin-Luther University it was of our prime interest to understand the function of the vertebrate Gid/CTLH complex. The model system used in the lab of Prof. Hollemann turned out to be an ideal tool for this purpose. The clawed African frog, *Xenopus laevis*, is a good model to study organismal development with many advantages compared to other organisms like e.g. *Mus musculus*. For example, the *ex utero* fertilisation does allow to fertilize 100–1000 of eggs at the same time. Fertilized eggs are synchronized resulting in tadpoles at comparable developmental stages, which allows direct comparison of the tadpoles and thus increases statistical relevance. The size of the eggs allows relatively easy injection of synthetic RNA, for ectopic expression of genes or the targeted knock-down of protein synthesis by synthetic antisense oligonucleotides (morpholinos) for reverse genetics studies. Another advantage is the well-organized scientific community, with a vivid exchange of novel methods and techniques that can be found e.g. on the community website (<http://www.xenbase.org/other/static/xenopusIntro.jsp>). Some very unexpected results concerning the Gid/CTLH complex that we obtained by using *Xenopus laevis* will be re- and previewed in this chapter.

As mentioned earlier, the Gid/CTLH protein complex is a highly evolutionary conserved ubiquitin ligase complex (Francis et al., 2013, Pfirrmann et al., 2015, Santt et al., 2008, Tomastikova et al., 2012). Individual subunits of the yeast Gid/CTLH-complex are conserved throughout the eukaryotic kingdom and Gid1, Gid2, Gid4, Gid5, Gid7, Gid8 and Gid9 have their closest human relatives in RANBP9, RMND5, C17ORF39, ARMC8, MKLN1, C20ORF11 (aka Twa1) and MAEA respectively. All these subunits are part of the human Gid/CTLH-complex (Texier et al., 2014) (see table 1). While function, topology and several substrates of the yeast Gid-complex are found in the literature, the vertebrate counterpart requires more detailed analysis of its cellular, organismal function as well as of its substrates. Most of the components, except ARMC8, possess a Lissencephaly type-1-like homology (LisH)/CTLH motif, which is present in proteins involved in microtubule dynamics, cell migration, nucleokinesis, and

chromosome segregation (Gerlitz et al., 2005). The latter is often associated with syndromes involving malformations of the central nervous system, e.g. the ciliopathy oral-facial-digital syndrome type1 (OCD), Treacher Collins syndrome or lissencephaly (Emes and Ponting, 2001). The mammalian CTLH/LisH subunit MKLN1, the ortholog of yeast *Gid7* (Kobayashi et al., 2007, Santt et al., 2008), is expressed in the hippocampus and the cerebellum (Tagnaouti et al., 2007) and was recently described to be involved in dynein dependent GABA_A- receptor transport along actin filaments and microtubuli (Heisler et al., 2011). The LisH-domain of MKLN1 seems to be crucial for oligomerization and its intracellular localization (Delto et al., 2015). Similar to the yeast *Gid2* protein, RMND5A also contains a CTLH/LisH- and the ubiquitin-ligase typical RING-domain (Santt et al., 2008).

Due to the crucial function of the RING domain in ubiquitin ligase complexes we decided to further study the function of the *Gid*/CTLH complex with RMND5A as a representative subunit of the whole complex. It is very likely, that other subunits will show similar phenotypic variances due to the fact that a complete CTLH-complex is required to ubiquitinate the same substrates.

Table 1: The *Gid*/CTLH complex with accession numbers and protein domains

Gid-complex	Accession Nr.	H. sapiens ortholog	Domains	Accession Nr.
Gid1	NP_011287.1	RANBP10, <u>RANBP9</u>	SPRY, LisH, CTLH, CR	NM_005493
Gid2/Rmd5	NP_010541.3	<u>RMND5A/ RMND5b</u>	LisH, CTLH, RING	NM_022780
Gid4	NP_009663.1	<u>C17ORF39</u>	-	NM_024052
Gid5	NP_012247.3	<u>ARMC8</u>	ARM	NM_213654
Gid7	NP_009891.1	<u>MKLN1</u>	LisH, CTLH, WD40	NM_013225
Gid8	NP_013854.1	<u>C20orf11/Twa1</u>	LisH, CTLH, CRA	NM_017896
Gid9	NP_012169.1	<u>MAEA</u>	LisH, CTLH	BC001225

5.1.2 Primary cilia and ciliated cells of the skin

The primary cilium consists of a ciliary axoneme build-up of a nine-duplet microtubular filament ring that arises from the basal body and is surrounded by the ciliary membrane. These organelles are involved in diverse cellular functions, such as cell proliferation, differentiation and polarity and act as signaling hubs for extracellular signals (Berbari et al., 2009, Goetz and Anderson, 2010). For instance, primary cilia are critical for Sonic-hedgehog (SHH) signaling and thus defects in ciliogenesis cause major brain

malformations e.g. splitting failure of cerebral hemispheres (holoprosencephaly 3 [MIM# 142945]) or cerebral clefts (schizencephaly [MIM# 269160]) (Hehr et al., 2010, Roessler et al., 1996, Schell-Apacik et al., 2009).

Interestingly, the formation of the primary cilium is induced by nutrient limitation such as FCS-depletion and is thus connected to the cell cycle. It is formed when cells are in G1 phase or reside in G0 phase. Before mitosis it gets disassembled when the cell needs the centrosome/basal body for proper cell division (Izawa et al., 2015, Phua et al., 2017, Quarmby and Parker, 2005). Proteins required for cilia formation are synthesised in the cytosol and are subsequently transported to the cilium. Within the cilium, a special protein transport machinery transports lipids and proteins to the tip of the cilium and back again. The intimate control of both anterograde and retrograde transport regulates e.g. cilia length and cilia function. The anterograde IFT-B transport system delivers proteins kinesin-dependent from the base of the cilium to the tip, while the dynein-dependent IFT-A transporter regulates retrograde transport (Lehtreck, 2015, Scholey, 2008, Pedersen et al., 2008, Rosenbaum and Witman, 2002) (see Figure 16A). Cilia play a major role in different hereditary organ-specific or syndromic diseases, summarized as ciliopathies, among them Leber congenital amaurosis [LCA1; MIM#204000], polycystic kidney disease [PKD1; MIM#173900], primary ciliary dyskinesia [CILD1; MIM#244400], Meckel-Gruber-syndrome [MKS1; MIM#249000], Joubert-syndrome [JBTS1; MIM#213300], Bardet-Biedl-syndrome [BBS1; MIM# 209900] and many more (Braun and Hildebrandt, 2017, den Hollander et al., 2007, Fliegauf et al., 2007, Tobin and Beales, 2009, Waters and Beales, 2011). The genetic causes are heterogeneous, but they all manifest in disturbed ciliogenesis or cilia dysfunction.

A structurally similar type of cilium is the motile cilium that can be found in several organs, e.g. the olfactory system, respiratory system, ventricles of the brain and the skin of *X. laevis*. Motile cilia contain an additional central pair of microtubules besides the nine-duplet filaments. Their function is to generate fluid flow to move molecules over a certain surface that is achieved by two rows of dynein motor units. The dynein motor units are able to move along microtubule doublet by an ATP-dependent process and are thereby bending the cilium (Brooks and Wallingford, 2014, Meunier and Azimzadeh, 2016, Zhou and Roy, 2015). These motile cilia generate a unidirectional fluid flow from the anterior site of the *Xenopus laevis* embryo to the posterior and thereby continuously replenish oxygenated water and distribute mucus

(Walentek and Quigley, 2017). We use the mouse fibroblast cell line NIH-3T3 to study primary cilia function. *Xenopus laevis* is used to study ciliopathy-like phenotypes and multi-ciliated cells of the skin (MCCs).

A very recent system biology approach tries to define the entire protein-protein network within the primary cilium and finds the Gid/CTLH-complex as a core component situated in proximity to the basal body of the primary cilium (Boldt et al., 2016). This data suggests the intriguing hypothesis that the CTLH-complex functions during ciliogenesis or is important for cilia function. Our data indeed supports such a hypothesis and suggests that a yet unknown regulator of ciliogenesis or cilia function is a substrate of the Gid/CTLH complex and regulates cilia length and function. The following chapters focus on novel unpublished results that support this hypothesis.

5.2 The Gid/CTLH ubiquitin ligase complex is associated with ciliopathies in Humans and *Xenopus laevis*

Our previous studies show early developmental expression of the CTLH-subunit *rmnd5a* in the eyes and the prosencephalon of *Xenopus laevis* (Pfaffmann et al., 2015). Whole mount in situ Hybridization (WMISH) reveals *rmnd5a* expression particularly in the eyes, the prosencephalon (pe) and the branchial arches (ba). While *rmnd5a* expression in the prosencephalon is mostly restricted to dorsal areas, with a strong signal periventricular, in the eyes, it is restricted to the ciliary marginal zone (cmz) and the retina. Additionally, a strong expression appears in the otic vesicles (ot) and in the pronephric tubule (kd). These observations are particularly interesting because these organs require functional cilia for proper development and are often misdeveloped in patients with ciliopathies (see table 2). A probe directed against an additional subunit of the CTLH-complex, *mkln1*, shows a similar expression pattern and underpins the notion that probably all CTLH subunits behave similar in terms of expression patterns and molecular function (Figure 10, unpublished results).

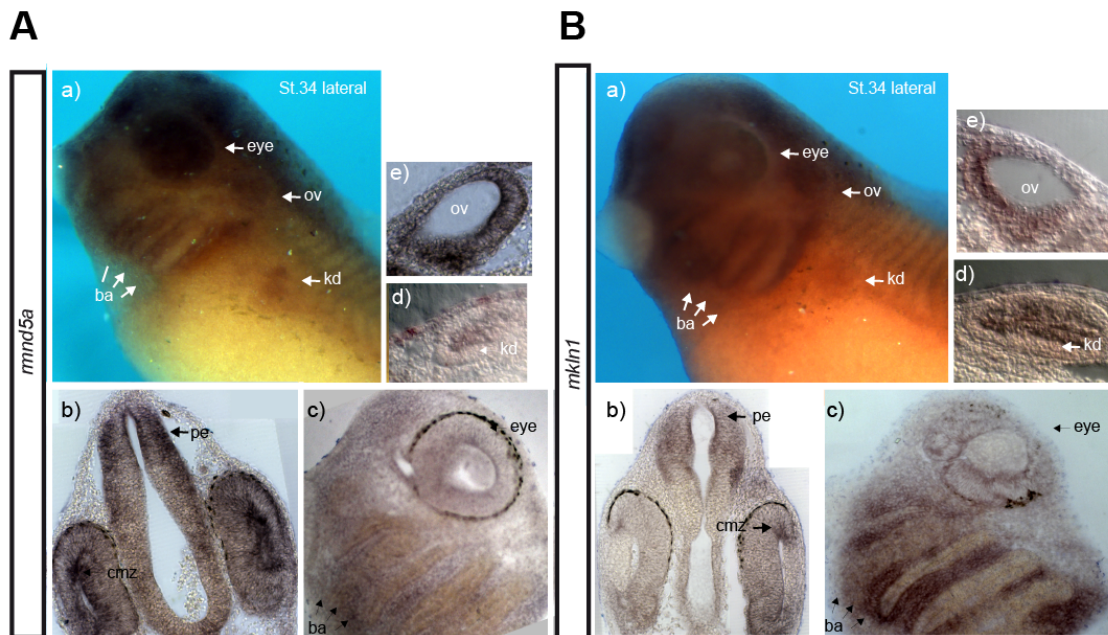


Figure 10: Spatial analysis of *rmnd5* (A) and *mkl1* (B) expression. Whole mount *in situ* hybridisation (Wmish) of wild type *Xenopus laevis* embryos at developmental stage 34 (A, a and B, a) and the corresponding transverse (b, e, d) and sagittal (c) sections. Abbreviations: proencephalon (pe), otic vesicle (ov), branchial arches (ba), pronephric kidney (kd), ciliary marginal zone (cmz) and eyes (eye).

Developmental defects, commonly associated with ciliopathies include kidney cysts, hydrocephalus, mispatterning of the left-right body axis and defects in craniofacial cartilage. The severity of symptoms ranges from relatively mild symptoms, e.g. a restriction to retinitis pigmentosa in Leber Congenital Amaurosis, to severe embryonic lethal symptoms like combined polydactyly, *situs inversus*, cognitive impairments, hepatic disease (polycystic kidneys), as well as skeletal malformation and defects in the formation of the brain in the Meckel-Gruber-Syndrome (see table 2). To test whether *RMND5A* knock-down causes ciliopathy-typical phenotypes we suppressed the function of *RMND5A* with antisense oligonucleotides (morpholino, *RMND5A*-mo), blocking translation of *RMND5A*. The microinjection of *RMND5A*-morpholinos but not of control-morpholinos in one blastomere at two-cell stage leads to a subset of phenotypic alterations summarized in table 2. Taken together the ventricular system in our morphants is characterized by developmental defects in the dorsal prosencephalon reminding of encephaloceles in *homo sapiens*. The ocular anlagen appear to be smaller in size and the stratification of the retina looks disorganized (see Figure 12 and Pfirmann et al., 2015). *RMND5A* morphants still form Meckel's cartilage, ceratohyal cartilage, branchial cartilage and palatoquadral cartilage on the *rmnd5a*-MO injected body site. However, the depletion of *rmnd5a* alters the formation of the craniofacial skeleton, specifically, Meckel's-, ceratohyal- and branchial-cartilage are severely shortened and the palatoquadrate cartilage appears to be decreased in size (not shown).

This probably reflects the skeletal affection known in ciliopathies, e.g. orofacial digital syndrome (ODC) or Meckel-Gruber-Syndrome. We also performed WMISH with a subset of different kidney marker genes, specifically labeling the individual segments of the pronephric kidney during *Xenopus laevis* development. The *rmnd5a*-morpholino injected side of the kidneys is not largely affected in the development of individual segments; all areas of the proximal tubule (PT1, PT2, PT3), the intermediate tubule (IT1, IT2), the distal tubule (DT1) and the duct are fully developed. However, segments appear to be enlarged with diffused margins in comparison to the non-injected side and the renal tubular epithelial cells appear disorganized and increased in number (Figure 11, c' and g').

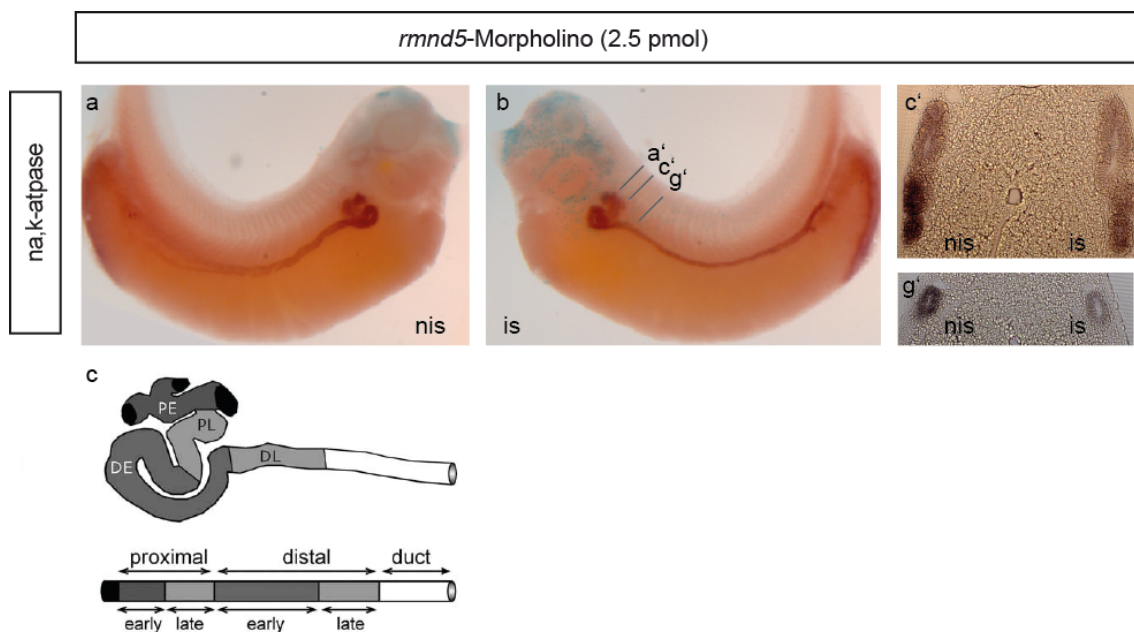


Figure 11: *rmnd5a* loss of function results in morphological changes of the pronephric kidney in *Xenopus laevis*. Na,K-ATPase whole mount *in situ* hybridisation (Wmish) of embryos injected with antisense oligonucleotides directed against *rmnd5a*. Knock down of *rmnd5* does not largely effect the segmentation of the pronephric kidney; segments are divided into early proximal (PE), late proximal (PL), early distal (DE) late distal (DL) pronephric tubule and the duct (see C); injected side (is) non-injected side (nis). (C' and G') Sections of embryos show segments that appear larger on the injected side with diffused margins

Table 2 Phenotypic comparison of different ciliopathies and models.

Main features	Patient	Xenopus	MKS	BBS	JBS	OFD	LCA
CNS							
Occipital encephalocele							
Cerebellar hypoplasia							
Eye							
Microphthalmia							
Retinopathy							
Craniofacial							
Microcephaly							
Cleft palate							
Micrognathia							
Cardiovascular							

Septal defects							
Coarctation of aorta							
Patent ductus arteriosus							
Kidneys							
Polycystic kidneys							
Renal agenesis							
Skeleton							
Postaxial polydactyly							
Gene			MKS1-14				

Some of the main phenotypic features (left column) typical for the ciliopathies Meckel-Gruber-syndrome [MKS; MIM#249000], Bardet-Biedel-syndrome [BBS; MIM# 209900], Joubert syndrome [JBS; MIM#213300], Oral-Facial-Digital syndrome [OFD; MIM#311200] and Leber-congenital amaurosis [LCA; MIM#204000] are compared to phenotypes that appear in a *Xenopus laevis* *rmnd5a* LoF model and a patient with a RMND5A duplication described in Figure 13 and Vogel et al., 2012. *Grey*: phenotype present; *White*: phenotype not present

Next we wanted to directly test a potential effect of *rmnd5a* knock-down on ciliogenesis. A suitable way to study ciliogenesis in *Xenopus laevis* is to study the function and structure of multi-ciliated cells of the skin (MCCs). These motile cilia generate a unidirectional fluid flow from the anterior site of the *Xenopus laevis* embryo to the posterior and thereby continuously replenish oxygenated water and distribute mucus (Walentek and Quigley, 2017). Cilia generated fluid-flow can be measured by time-lapse fluorescent microscopy of labeled beads and thus give a first impression of MCC functionality. To do so we injected synthetic GFP m-RNA into both blastomeres of a two-cell stage embryo together with either standard morpholino (Strd-MO) or morpholino directed against *rmnd5a* (*rmnd5a*-MO) and measured fluid-flow by addition of labeled microbeads. Particles were subsequently tracked using particle-tracking software. As expected, a fluid flow from the anterior to the posterior of the embryo uniformly accelerates fluorescent particles moving on top of the embryo (Figure 12, Standard). Particles on top of the *rmnd5a*-MO injected embryos still move over the embryo, however the trajectory of the particles does not follow a uniform straight line and acceleration of the particles is significantly reduced (Figure 12, *rmnd5a* LoF). We reason, that cilia formation and/or synchronized beating of the cilia is affected in *rmnd5a* knock down embryos. To test this hypothesis, we injected embryos with synthetic RNA coding for the protein clamp-RFP and centrin-CFP together with *rmnd5a* morpholinos or standard morpholinos, respectively. At stage 30 the embryos were fixed and cilia were visualized by immunostaining with antibodies directed against acetylated-tubulin and subsequent confocal-microscopy imaging. The co-injection of *rmnd5a*-MO leads to defects in ciliogenesis, more specifically MCCs injected with morpholino have severely shortened or no cilia at all. Strd-MO injected embryos and non-injected cells show normal cilia and basal body orientation. Similar results can be observed by environmental scanning electron microscopy (ESEM) (Figure 12C).

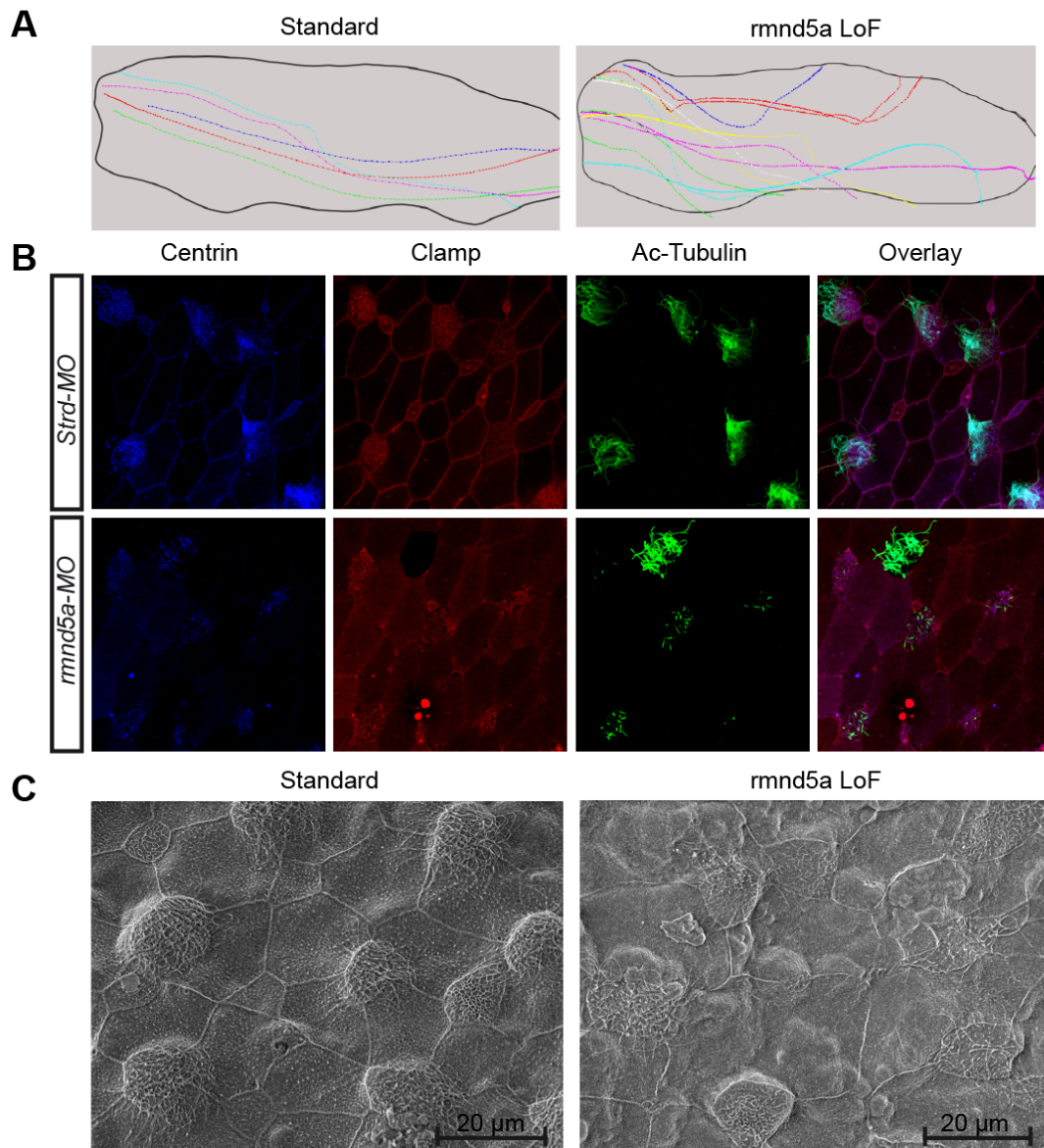


Figure 12: *rmnd5a* knock down alters ciliogenesis of multi-ciliated cells of the skin (MCCs) in *Xenopus laevis*. (A) Cilia generated fluid-flow measured by time-lapse microscopy of fluorescent beads. Synthetic GFP m-RNA was injected into both blastomeres of a two-cell stage embryo together with either standard morpholino (Standard) or morpholino directed against *rmnd5a* (*rmnd5a*-LoF). Fluid-flow was measured by addition of labeled microbeads to the embryos and subsequent particle tracking. Colored dots correspond to particles at certain time points. (B) Immunostaining of embryos injected with standard morpholino (Strd-MO) or morpholino directed against *rmnd5* (*rmnd5a*-MO). Embryos were injected with synthetic Clamp-RFP RNA to visualize basal bodies (CLAMP, red); cilia of multi-ciliated cells were stained with antibodies against acetylated Tubulin (Ac-Tubulin, green) and merged (overlay). (C) Similar to A, embryos were injected with either standard morpholino (Standard) or morpholino directed against *rmnd5a* (*rmnd5a*-LoF). After fixation embryos were subjected to environmental scanning microscopy (ESEM) to visualize skin cells. Scale bar; 20 μ m. (unpublished).

Taken together, all *rmnd5* loss of function phenotypes in *Xenopus laevis* resemble those of classical ciliopathies, including eye defects, skeletal malformations, brain defects similar to encephaloceles and disturbed kidney development (table 2). We observe strong phenotypic overlap of *rmnd5a* LoF tadpoles and ciliopathies of the more severe spectrum, e.g. MKS and JBS.

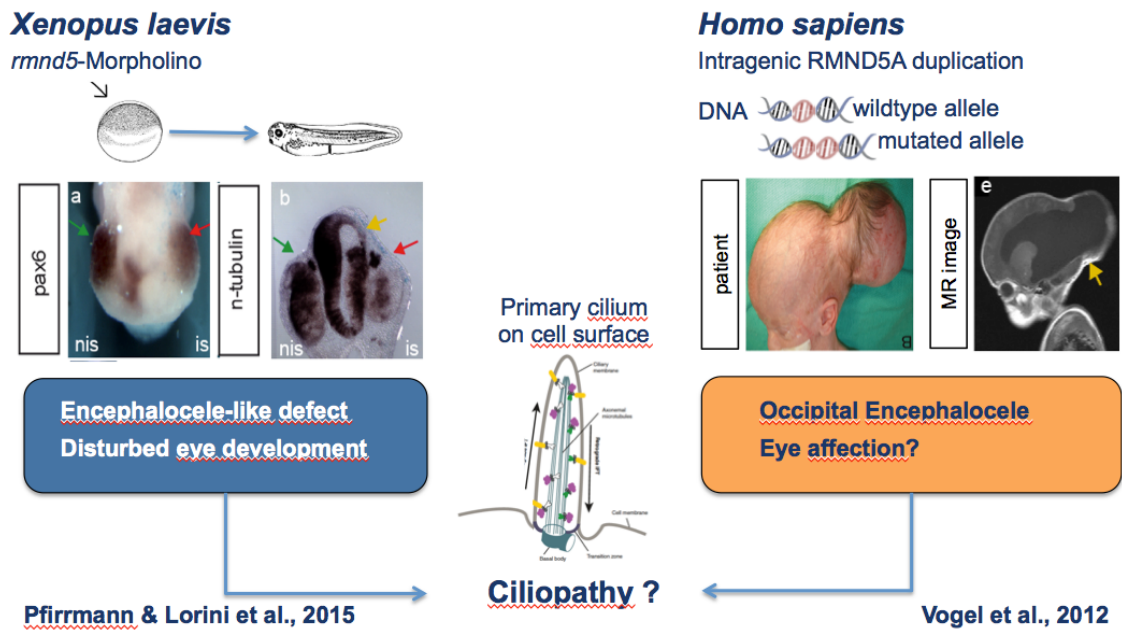


Figure 13: Ciliopathy typical phenotypic features in RMND5a LoF *Xenopus laevis* and a patient with a partial RMND5a duplication. (left) the injection of antisense oligonucleotides directed against *rmnd5a* into one blastomere of the two cell stage of development results in defects in the periventricular region of the prosencephalon and disturbed eye development on the injected side (is) but not on the non-injected side (nis). A patient with an intragenic partial duplication of the RMND5a gene shows similar ciliopathy-typical phenotypes including an occipital encephalocele (Vogel et al., 2012).

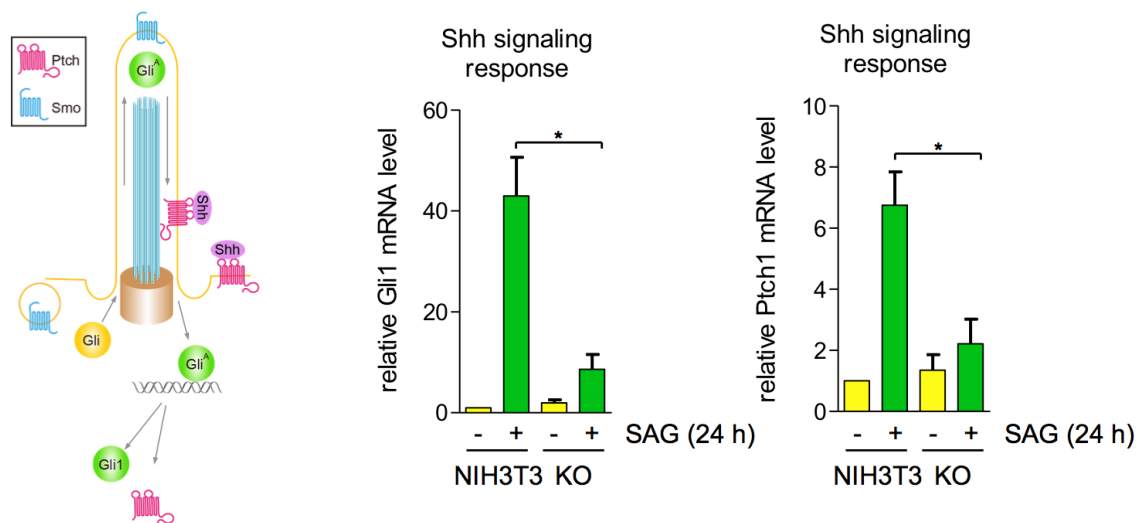


Figure 14: RMND5a loss-of-function alters primary cilia dependent sonic hedgehog signaling in NIH3T3 cells. (left) schematic representation of primary cilium dependent sonic hedgehog (SHH) signaling in the “on state”. Binding of SHH to PTCH relieves SMO inhibition and activates the pathway by processing GLI1 into an active transcription factor GLI^A upregulating transcription of GLI1 and PTCH; PTCH, Patched1; SMO, Smoothened; GLI1, GLI1 repressor; GLI^A, GLI1 active form. (right) Quantitative PCR of GLI1 and PTCH1 in NIH3T3 and RMND5a knock out (KO) cells with (+) or without (-) 24h SAG treatment. Relative GLI1/PTCH1 levels of three independent experiments with error bars are depicted on the y-axes (unpublished).

To study RMND5a dependent effects on primary cilia formation and function, we CrispR/Cas9-generated a RMND5a loss of function NIH-3T3 cell line. Loss of SHH-signaling is often used to measure primary cilia function and is the most significant molecular reason for developmental alterations in ciliopathies. Treatment of NIH3T3 cells with SAG activates the Sonic Hedgehog signaling pathway and induces a strong

transcriptional upregulation of GLI1 and PTCH1 (Figure 14, compare NIH3T3 -, +). However, SAG treatment of the RMND5a loss-of-function cell line (KO) reduces sonic hedgehog response (Figure 14, compare NIH3T3 + and KO +). This result strongly suggests that RMND5a plays a vital role in primary ciliogenesis or –function. Supporting this idea, we find RMND5a localizing to the basal body of the primary cilium (Figure 15).

In conclusion, our results strongly suggest that RMND5a is a subunit of a basal body associated E3 ubiquitin-ligase with a function in cilia dependent SHH signaling. In short, RMND5a and most probably all other members of the CTLH complex comprise a novel class of ciliopathy diagnostic marker genes.

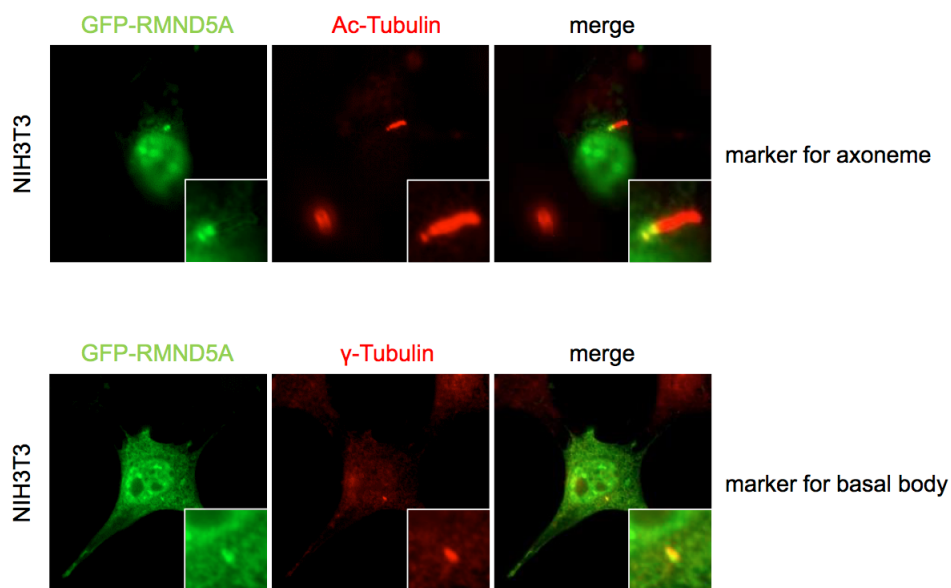


Figure 15: Co-localization of RMND5a with the basal body of the primary cilia in NIH3T3 cells. NIH3T3 cells were transfected with a plasmid expressing GFP-RMND5a. 24h after transfection cells were grown in medium with 0.5% FCS to induce ciliogenesis. After fixation cells were either stained with antibodies directed against acetylated tubulin (ac-Tubulin, upper panel to visualize primary cilia or with antibodies directed against γ -tubulin (lower panel) to visualize the basal body (unpublished).

6 Outlook and future perspectives

One of our primary goals is to understand the molecular details of the CTLH-complex function in cilia. An intriguing hypothesis is a function of the vertebrate CTLH complex similar to the yeast Gid-complex in glucose sensing and energy homeostasis. Newer studies suggest that the primary cilium also regulates the response to extracellular nutrients e.g. glucose (Boehlke et al., 2010) and functions as a sensor to maintain energy homeostasis in the cell. For example AMPK is phosphorylated at the basal body of the primary cilium and thus links the primary cilium to cellular energy homeostasis. From there it regulates mTOR activity and thus autophagy (Boehlke et al., 2010, Pampliega et al., 2013). Defects in cilia function are therefore often associated with metabolic disorders (reviewed in Lee et al., 2015). This raises the fundamental question if the function of the vertebrate Gid/CTLH complex is partially related to the yeast complex and regulates glucose metabolism and energy homeostasis in vertebrates as well. Several observations support this hypothesis. First, Bardet-Biedl-syndrome and Almström-syndrome are both ciliopathies that are accompanied with obesity of patients and an increased risk of developing type II diabetes (Lee et al., 2015). Other publications link primary cilia in β -cells of the pancreas to insulin secretion (Gerdes et al., 2014). Second, a direct connection to primary cilia and energy homeostasis comes from a study performed in the group around Prof. Walz in Freiburg. According to their study, LKB1 is a ciliary kinase that directly phosphorylates AMPK in order to activate it during times of energy deprivation (Boehlke et al., 2010). This kinase is regulated by the AMP/ATP ratio within the cell and regulates downstream events such as mTOR signaling, cell size and autophagy. Our preliminary results support a function around AMPK, because we find a reduction in mTOR signaling in the RMND5a LoF cell line. Further experiments are planned to find CTLH complex targets upstream of the mTOR pathway. We are specifically planning to measure AMPK phosphorylation and LKB1 levels in the LoF cells. In an intriguing model that can explain most phenotypic alterations described above, LKB1 is polyubiquitinated by the CTLH complex and subsequently degraded at the basal body to regulate AMPK activation. Prior studies show, that LKB1 is degraded by the 26S proteasome, however ubiquitin ligases involved in this process are currently unknown (Nony et al., 2003).

Another major future challenge will be the discovery of novel Gid/CTLH complex substrates. Several unbiased screens in order to find substrates in yeast and *homo*

sapiens are planned. A finding that the group of Prof. Wolf published in 1998 sets the basis for a recent Science article: An N-end rule pathway that recognizes proline and destroys gluconeogenic enzymes (Chen et al., 2017, Hammerle et al., 1998). The group around Prof. Varshavsky shows in a series of experiments that the Gid-complex in yeast is most probably a novel so called N-recognin. N-recognins are E3 ubiquitin-ligases that recognize N-terminal destabilizing amino acids in order to polyubiquitinate them for subsequent 26S proteasomal destruction. The Gid/CTLH complex subunit Gid4 specifically binds proline residues at position two in the primary substrate-sequence of three gluconeogenic key enzymes in yeast. The detailed description of the yeast Gid4 substrate recognition motif enables the *in silico* screen for novel substrates. Together with Dr. Dissmeyer we have developed an algorithm that enables to search any organismal protein database for proteins that match the N-terminal consensus sequence shown in Figure 16. Among these proteins that match the consensus sequence we find several interesting candidates. One protein sedoheptulose-1,7-bisphosphatase is involved in the regulation of a process called riboneogenesis (Clasquin et al., 2011). Two other surprising candidates coming up in the list are the transcription factors Stp1 and Stp2 (see chapter 4) that are both proteasomal substrates with unknown E3 ubiquitin ligases (see Figure 2). It is very likely, that both transcription factors are constantly turned over by the Gid-complex in the absence of activating aminoacids to prevent a cytosolic overflow and thus transcriptional activation under non-inducing conditions. In future it is planned to experimentally address a potential function of the Gid/CTLH complex in the degradation of these potential novel yeast substrates in collaboration with Prof. Wolf and Prof. Ljungdahl.

We will also address the question, if the N-terminal consensus sequences of Gid/CTLH substrates are conserved in vertebrates. This information will enable to find eukaryotic substrates by *in silico* search algorithms as well. To be able to develop a similar search algorithm for vertebrates, several key experiments must be performed. At first it is important to analyse the hsGID4 substrate binding sequence for substrates in human cell lines. It is planned to perform a yeast-2-hybrid assay with human GID4 protein as bait. From the following interacting proteins it will be possible to isolate proteins with common consensus sequences that can later be used for *in silico* analysis of potential CTLH/Gid-complex subunits. In a second approach in the lab of Dr. Dissmeyer we will use a peptide-binding array together with recombinant purified human-GID4 to search for short peptides capable of binding the CTLH/Gid recruiting factor. From these two

approaches we will be able to deduce a consensus sequence, to detect and subsequently characterize novel substrates.

Most probably caused by gene duplication, mammals encode for two *GID2* orthologous genes called *RMND5A* and *RMND5B*. Not much is known about the function of the two isoforms. Nevertheless, *RMND5B* associates with several ubiquitin-conjugating enzymes (van Wijk et al., 2009) and thus it is likely that both proteins function as ubiquitin-ligase subunits. An intriguing hypothesis includes *RMND5A* and *RMND5B* as exchangeable subunits of the CTLH-complex. Such a mechanism would exemplify yet another possibility of the cell to broaden substrate specificity of a core ubiquitin ligase complex, by recruiting different ubiquitin conjugating enzymes to the ternary complex.

In summary, it is very likely that the yeast *Gid*-complex is not only structurally conserved, but also functionally plays a role in regulating energy homeostasis at the basal body of the primary cilium similar to yeast. A yet unknown negative regulator of the mTOR pathway and autophagy might be the first substrate of the homo sapiens *Gid*/CTLH complex to be discovered.

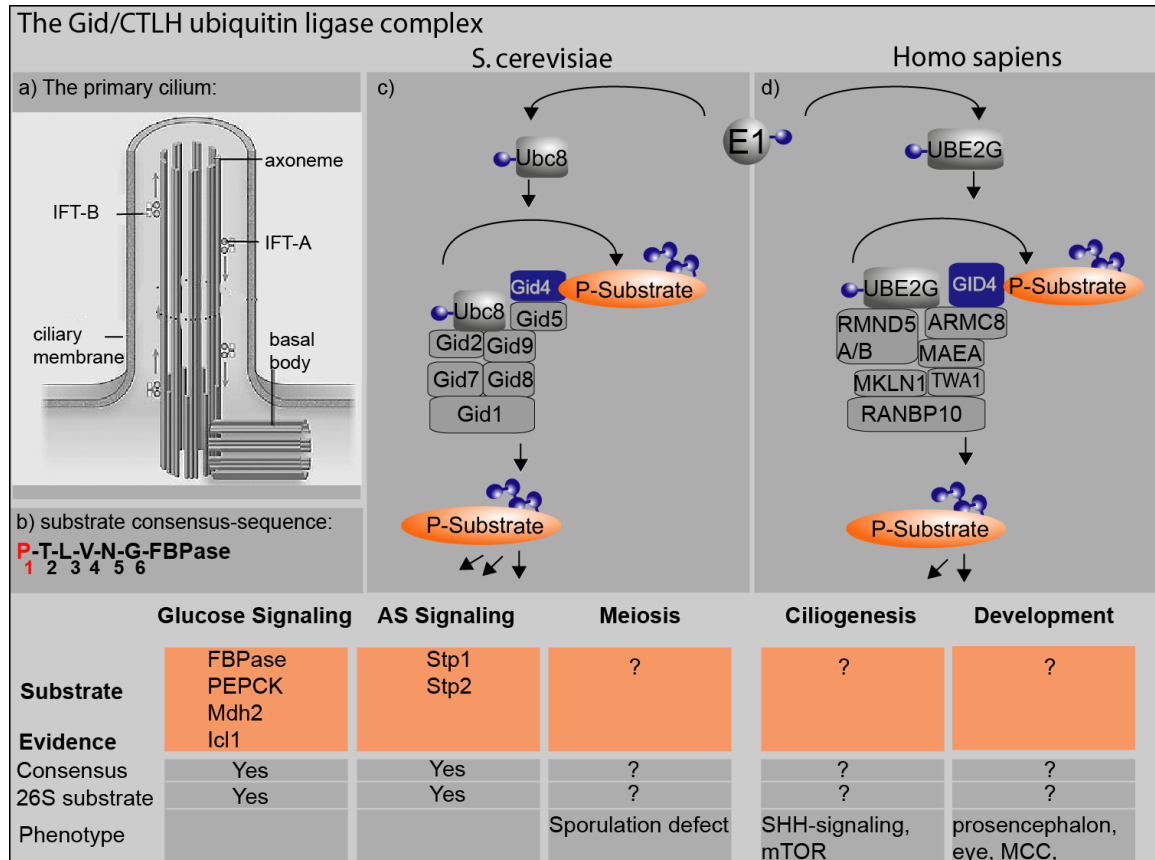


Figure 16: The *Gid*/ CTLH ubiquitin ligase complex in yeast and homo sapiens. A) Diagram of a primary cilium. The primary cilium consists of a ciliary axoneme build-up of a nine-duplet microtubular filament ring that

arises from the basal body and is surrounded by the ciliary membrane. The IFT-A transport machinery is responsible for anterograde transport from the basal body to the ciliary tip, IFT-B is the transport machinery for retrograde transport. The vertebrate Gid/CTLH complex localizes to the basal body of the primary cilium. Taken and modified from <http://www.ciliopathyalliance.org/cilia/structure-and-function-of-cilia.html>. **B) Substrate consensus sequence of the yeast Gid-complex.** In yeast the Gid complex is a novel N-recognin, substrates with N-terminal proline residues (FBPase, Mdh2, Icl1) bind the subunit Gid4 and recruit them to the Gid complex for polyubiquitination and subsequent degradation (Chen et al., 2017, Hammerle et al., 1998). **C and D) Diagram of the yeast (C) and human (D) Gid/CTLH subunit composition, function, phenotype and substrates.** A possible subunit composition of the yeast Gid complex inspired by (Menssen et al., 2012) and the human CTLH complex inspired by (Boldt et al., 2016).

7 Literature

1. Abdel-Sater, F., El Bakkoury, M., Urrestarazu, A., Vissers, S., and André, B. (2004) Amino acid signaling in yeast: casein kinase I and the Ssy5 endoprotease are key determinants of endoproteolytic activation of the membrane-bound Stp1 transcription factor. *Mol Cell Biol* 24, 9771-9785.
2. Abdel-Sater, F., Jean, C., Merhi, A., Vissers, S., and André, B. (2011) Amino-acid signalling in yeast: activation of the Ssy5 protease is associated with its phosphorylation-induced ubiquitylation. *J Biol Chem* 286, 12006-12015.
3. Andréasson, C., Heessen, S., and Ljungdahl, P.O. (2006) Regulation of transcription factor latency by receptor-activated proteolysis. *Genes Dev* 20, 1563-1568.
4. Andréasson, C. and Ljungdahl, P.O. (2002) Receptor-mediated endoproteolytic activation of two transcription factors in yeast. *Genes Dev* 16, 3158-3172.
5. Baker, D., Shiau, A.K., and Agard, D.A. (1993) The role of pro regions in protein folding. *Curr Opin Cell Biol* 5, 966-970.
6. Baker, D., Silen, J.L., and Agard, D.A. (1992) Protease pro region required for folding is a potent inhibitor of the mature enzyme. *Proteins* 12, 339-344.
7. Barrett, A.J. and Rawlings, N.D. (1995) Families and clans of serine peptidases. *Arch Biochem Biophys* 318, 247-250.
8. Berbari, N.F., O'Connor, A.K., Haycraft, C.J., and Yoder, B.K. (2009) The primary cilium as a complex signaling center. *Curr Biol* 19, R526-535.
9. Bernard, F. and André, B. (2001) Ubiquitin and the SCF^{Grr1} ubiquitin ligase complex are involved in the signalling pathway activated by external amino acids in *Saccharomyces cerevisiae*. *FEBS Lett* 496, 81-85.
10. Bertinat, R., Pontigo, J.P., Perez, M., Concha, II, Martin, R.S., Guinovart, J.J., . . . Yanez, A.J. (2011) Nuclear accumulation of fructose 1,6-bisphosphatase is impaired in diabetic rat liver. *J Cell Biochem* 113, 848-856.
11. Boehlke, C., Kotsis, F., Patel, V., Braeg, S., Voelker, H., Bredt, S., . . . Kuehn, E.W. (2010) Primary cilia regulate mTORC1 activity and cell size through Lkb1. *Nat Cell Biol* 12, 1115-1122.
12. Boldt, K., van Reeuwijk, J., Lu, Q., Koutroumpas, K., Nguyen, T.M., Texier, Y., . . . Group, U.K.R.D. (2016) An organelle-specific protein landscape identifies novel diseases and molecular mechanisms. *Nat Commun* 7, 11491.

13. Braun, B., Pfirrmann, T., Menssen, R., Hofmann, K., Scheel, H., and Wolf, D.H. (2011) Gid9, a second RING finger protein contributes to the ubiquitin ligase activity of the Gid complex required for catabolite degradation. *FEBS Lett* 585, 3856-3861.
14. Braun, B., Pfirrmann, T., Menssen, R., Hofmann, K., Scheel, H., and Wolf, D.H. (2011) Gid9, a second RING finger protein contributes to the ubiquitin ligase activity of the Gid complex required for catabolite degradation. *FEBS Lett*.
15. Braun, D.A. and Hildebrandt, F. (2017) Ciliopathies. *Cold Spring Harbor perspectives in biology* 9.
16. Brivanlou, A.H. and Darnell, J.E., Jr. (2002) Signal transduction and the control of gene expression. *Science* 295, 813-818.
17. Brooks, E.R. and Wallingford, J.B. (2014) Multiciliated cells. *Curr Biol* 24, R973-982.
18. Brown, M.S., Ye, J., Rawson, R.B., and Goldstein, J.L. (2000) Regulated intramembrane proteolysis: a control mechanism conserved from bacteria to humans. *Cell* 100, 391-398.
19. Celenza, J.L., Marshall-Carlson, L., and Carlson, M. (1988) The yeast SNF3 gene encodes a glucose transporter homologous to the mammalian protein. *Proc Natl Acad Sci U S A* 85, 2130-2134.
20. Chen, S.J., Wu, X., Wadas, B., Oh, J.H., and Varshavsky, A. (2017) An N-end rule pathway that recognizes proline and destroys gluconeogenic enzymes. *Science* 355.
21. Clasquin, M.F., Melamud, E., Singer, A., Gooding, J.R., Xu, X., Dong, A., . . . Caudy, A.A. (2011) Riboneogenesis in yeast. *Cell* 145, 969-980.
22. Cunningham, E.L. and Agard, D.A. (2003) Interdependent folding of the N- and C-terminal domains defines the cooperative folding of alpha-lytic protease. *Biochemistry* 42, 13212-13219.
23. Delto, C.F., Heisler, F.F., Kuper, J., Sander, B., Kneussel, M., and Schindelin, H. (2015) The LisH motif of muskelin is crucial for oligomerization and governs intracellular localization. *Structure* 23, 364-373.
24. den Hollander, A.I., Koenekoop, R.K., Mohamed, M.D., Arts, H.H., Boldt, K., Towns, K.V., . . . Roepman, R. (2007) Mutations in LCA5, encoding the ciliary protein lebercilin, cause Leber congenital amaurosis. *Nat Genet* 39, 889-895.

25. Dohmen, R.J., Wu, P., and Varshavsky, A. (1994) Heat-inducible degron: a method for constructing temperature-sensitive mutants. *Science* 263, 1273-1276.
26. Eisele, F., Braun, B., Pfirrmann, T., and Wolf, D.H. (2006) Mutants of the deubiquitinating enzyme Ubp14 decipher pathway diversity of ubiquitin-proteasome linked protein degradation. *Biochem Biophys Res Commun* 350, 329-333.
27. Emes, R.D. and Ponting, C.P. (2001) A new sequence motif linking lissencephaly, Treacher Collins and oral-facial-digital type 1 syndromes, microtubule dynamics and cell migration. *Human molecular genetics* 10, 2813-2820.
28. Fliegauf, M., Benzing, T., and Omran, H. (2007) When cilia go bad: cilia defects and ciliopathies. *Nature reviews* 8, 880-893.
29. Forsberg, H. and Ljungdahl, P.O. (2001) Genetic and biochemical analysis of the yeast plasma membrane Ssy1p-Ptr3p-Ssy5p sensor of extracellular amino acids. *Mol Cell Biol* 21, 814-826.
30. Francis, O., Han, F., and Adams, J.C. (2013) Molecular phylogeny of a RING E3 ubiquitin ligase, conserved in eukaryotic cells and dominated by homologous components, the muskelin/RanBPM/CTLH complex. *PLoS One* 8, e75217.
31. Funayama, S., Gancedo, J.M., and Gancedo, C. (1980) Turnover of yeast fructose-bisphosphatase in different metabolic conditions. *Eur J Biochem* 109, 61-66.
32. Gerdes, J.M., Christou-Savina, S., Xiong, Y., Moede, T., Moruzzi, N., Karlsson-Edlund, P., . . . Berggren, P.O. (2014) Ciliary dysfunction impairs beta-cell insulin secretion and promotes development of type 2 diabetes in rodents. *Nat Commun* 5, 5308.
33. Gerlitz, G., Darhin, E., Giorgio, G., Franco, B., and Reiner, O. (2005) Novel functional features of the Lis-H domain: role in protein dimerization, half-life and cellular localization. *Cell cycle (Georgetown, Tex)* 4, 1632-1640.
34. Goetz, S.C. and Anderson, K.V. (2010) The primary cilium: a signalling centre during vertebrate development. *Nature reviews. Genetics* 11, 331-344.
35. Hammerle, M., Bauer, J., Rose, M., Szallies, A., Thumm, M., Dusterhus, S., . . . Wolf, D.H. (1998) Proteins of newly isolated mutants and the amino-terminal proline are essential for ubiquitin-proteasome-catalyzed catabolite degradation

- of fructose-1,6-bisphosphatase of *Saccharomyces cerevisiae*. *J Biol Chem* 273, 25000-25005.
36. Hehr, U., Pineda-Alvarez, D.E., Uyanik, G., Hu, P., Zhou, N., Hehr, A., . . . Muenke, M. (2010) Heterozygous mutations in SIX3 and SHH are associated with schizencephaly and further expand the clinical spectrum of holoprosencephaly. *Hum Genet* 127, 555-561.
 37. Heisler, F.F., Loebrich, S., Pechmann, Y., Maier, N., Zivkovic, A.R., Tokito, M., . . . Kneussel, M. (2011) Muskelein regulates actin filament- and microtubule-based GABA(A) receptor transport in neurons. *Neuron* 70, 66-81.
 38. Ho, Y., Gruhler, A., Heilbut, A., Bader, G.D., Moore, L., Adams, S.L., . . . Tyers, M. (2002) Systematic identification of protein complexes in *Saccharomyces cerevisiae* by mass spectrometry. *Nature* 415, 180-183.
 39. Hoppe, T., Rape, M., and Jentsch, S. (2001) Membrane-bound transcription factors: regulated release by RIP or RUP. *Curr Opin Cell Biol* 13, 344-348.
 40. Izawa, I., Goto, H., Kasahara, K., and Inagaki, M. (2015) Current topics of functional links between primary cilia and cell cycle. *Cilia* 4, 12.
 41. Jonkers, W. and Rep, M. (2009) Lessons from fungal F-box proteins. *Eukaryot Cell* 8, 677-695.
 42. Klein, C.J., Olsson, L., and Nielsen, J. (1998) Glucose control in *Saccharomyces cerevisiae*: the role of Mig1 in metabolic functions. *Microbiology* 144 (Pt 1), 13-24.
 43. Kobayashi, N., Yang, J., Ueda, A., Suzuki, T., Tomaru, K., Takeno, M., . . . Ishigatsubo, Y. (2007) RanBPM, Muskelein, p48EMLP, p44CTLH, and the armadillo-repeat proteins ARMC8alpha and ARMC8beta are components of the CTLH complex. *Gene* 396, 236-247.
 44. Lechtreck, K.F. (2015) IFT-Cargo Interactions and Protein Transport in Cilia. *Trends Biochem Sci* 40, 765-778.
 45. Lee, H., Song, J., Jung, J.H., and Ko, H.W. (2015) Primary cilia in energy balance signaling and metabolic disorder. *BMB Rep* 48, 647-654.
 46. Lorick, K.L., Jensen, J.P., Fang, S., Ong, A.M., Hatakeyama, S., and Weissman, A.M. (1999) RING fingers mediate ubiquitin-conjugating enzyme (E2)-dependent ubiquitination. *Proc Natl Acad Sci U S A* 96, 11364-11369.
 47. Menssen, R., Schweiggert, J., Schreiner, J., Kusevic, D., Reuther, J., Braun, B., and Wolf, D.H. (2012) Exploring the Topology of the Gid Complex, the E3

- Ubiquitin Ligase Involved in Catabolite-induced Degradation of Gluconeogenic Enzymes. *J Biol Chem* 287, 25602-25614.
48. Meunier, A. and Azimzadeh, J. (2016) Multiciliated Cells in Animals. *Cold Spring Harbor perspectives in biology* 8.
 49. Moriya, H. and Johnston, M. (2004) Glucose sensing and signaling in *Saccharomyces cerevisiae* through the Rgt2 glucose sensor and casein kinase I. *Proc Natl Acad Sci U S A* 101, 1572-1577.
 50. Nony, P., Gaude, H., Rossel, M., Fournier, L., Rouault, J.P., and Billaud, M. (2003) Stability of the Peutz-Jeghers syndrome kinase LKB1 requires its binding to the molecular chaperones Hsp90/Cdc37. *Oncogene* 22, 9165-9175.
 51. Omnus, D.J., Pfirrmann, T., Andreasson, C., and Ljungdahl, P.O. (2011) A phosphodegron controls nutrient-induced proteasomal activation of the signaling protease Ssy5. *Mol Biol Cell* 22, 2754-2765.
 52. Ozcan, S., Dover, J., Rosenwald, A.G., Wolf, S., and Johnston, M. (1996) Two glucose transporters in *Saccharomyces cerevisiae* are glucose sensors that generate a signal for induction of gene expression. *Proc Natl Acad Sci U S A* 93, 12428-12432.
 53. Pampliega, O., Orhon, I., Patel, B., Sridhar, S., Diaz-Carretero, A., Beau, I., . . . Cuervo, A.M. (2013) Functional interaction between autophagy and ciliogenesis. *Nature* 502, 194-200.
 54. Pavri, R., Zhu, B., Li, G., Trojer, P., Mandal, S., Shilatifard, A., and Reinberg, D. (2006) Histone H2B monoubiquitination functions cooperatively with FACT to regulate elongation by RNA polymerase II. *Cell* 125, 703-717.
 55. Pedersen, L.B., Veland, I.R., Schroder, J.M., and Christensen, S.T. (2008) Assembly of primary cilia. *Dev Dyn* 237, 1993-2006.
 56. Pfirrmann, T., Heessen, S., Omnus, D.J., Andreasson, C., and Ljungdahl, P.O. (2010) The prodomain of Ssy5 protease controls receptor-activated proteolysis of transcription factor Stp1. *Molecular and cellular biology* 30, 3299-3309.
 57. Pfirrmann, T., Villavicencio-Lorini, P., Subudhi, A.K., Menssen, R., Wolf, D.H., and Hollemann, T. (2015) RMND5 from *Xenopus laevis* Is an E3 Ubiquitin-Ligase and Functions in Early Embryonic Forebrain Development. *PLoS One* 10, e0120342.

58. Pfirrmann, T., Ljungdahl, P. (2012) Chapter 685 – Ssy5 Peptidase: A Chymotrypsin-Like Signaling Protease in Yeast. Handbook of proteolytic enzymes DOI: <http://dx.doi.org/10.1016/B978-0-12-382219-2.00685-2>, .
59. Phua, S.C., Chiba, S., Suzuki, M., Su, E., Roberson, E.C., Pusapati, G.V., . . . Inoue, T. (2017) Dynamic Remodeling of Membrane Composition Drives Cell Cycle through Primary Cilia Excision. *Cell* 168, 264-279 e215.
60. Pickart, C.M. and Eddins, M.J. (2004) Ubiquitin: structures, functions, mechanisms. *Biochim Biophys Acta* 1695, 55-72.
61. Poulsen, P., Lo Leggio, L., and Kielland-Brandt, M.C. (2006) Mapping of an internal protease cleavage site in the Ssy5p component of the amino acid sensor of *Saccharomyces cerevisiae* and functional characterization of the resulting pro- and protease domains by gain-of-function genetics. *Eukaryot Cell* 5, 601-608.
62. Purwin, C., Leidig, F., and Holzer, H. (1982) Cyclic AMP-dependent phosphorylation of fructose-1,6-bisphosphatase in yeast. *Biochem Biophys Res Commun* 107, 1482-1489.
63. Quarumby, L.M. and Parker, J.D. (2005) Cilia and the cell cycle? *J Cell Biol* 169, 707-710.
64. Regelman, J., Schule, T., Josupeit, F.S., Horak, J., Rose, M., Entian, K.D., . . . Wolf, D.H. (2003) Catabolite degradation of fructose-1,6-bisphosphatase in the yeast *Saccharomyces cerevisiae*: a genome-wide screen identifies eight novel GID genes and indicates the existence of two degradation pathways. *Mol Biol Cell* 14, 1652-1663.
65. Roessler, E., Belloni, E., Gaudenz, K., Jay, P., Berta, P., Scherer, S.W., . . . Muenke, M. (1996) Mutations in the human Sonic Hedgehog gene cause holoprosencephaly. *Nat Genet* 14, 357-360.
66. Rolland, F., Winderickx, J., and Thevelein, J.M. (2002) Glucose-sensing and -signalling mechanisms in yeast. *FEMS Yeast Res* 2, 183-201.
67. Rosenbaum, J.L. and Witman, G.B. (2002) Intraflagellar transport. *Nature reviews* 3, 813-825.
68. Sadowski, M., Suryadinata, R., Tan, A.R., Roesley, S.N., and Sarcevic, B. (2012) Protein monoubiquitination and polyubiquitination generate structural diversity to control distinct biological processes. *IUBMB Life* 64, 136-142.
69. Santt, O., Pfirrmann, T., Braun, B., Juretschke, J., Kimmig, P., Scheel, H., . . . Wolf, D.H. (2008) The yeast GID complex, a novel ubiquitin ligase (E3)

- involved in the regulation of carbohydrate metabolism. *Mol Biol Cell* 19, 3323-3333.
70. Schell-Apacik, C.C., Ertl-Wagner, B., Panzel, A., Klausener, K., Rausch, G., Muenke, M., . . . Hehr, U. (2009) Maternally inherited heterozygous sequence change in the sonic hedgehog gene in a male patient with bilateral closed-lip schizencephaly and partial absence of the corpus callosum. *Am J Med Genet A* 149A, 1592-1594.
71. Scholey, J.M. (2008) Intraflagellar transport motors in cilia: moving along the cell's antenna. *J Cell Biol* 180, 23-29.
72. Schork, S.M., Bee, G., Thumm, M., and Wolf, D.H. (1994) Site of catabolite inactivation. *Nature* 369, 283-284.
73. Schork, S.M., Thumm, M., and Wolf, D.H. (1995) Catabolite inactivation of fructose-1,6-bisphosphatase of *Saccharomyces cerevisiae*. Degradation occurs via the ubiquitin pathway. *J Biol Chem* 270, 26446-26450.
74. Schule, T., Rose, M., Entian, K.D., Thumm, M., and Wolf, D.H. (2000) Ubc8p functions in catabolite degradation of fructose-1, 6-bisphosphatase in yeast. *EMBO J* 19, 2161-2167.
75. Sha, Z. and Goldberg, A.L. (2014) Proteasome-mediated processing of Nrf1 is essential for coordinate induction of all proteasome subunits and p97. *Curr Biol* 24, 1573-1583.
76. Spielwoy, N., Flick, K., Kalashnikova, T.I., Walker, J.R., and Wittenberg, C. (2004) Regulation and recognition of SCF^{Grr1} targets in the glucose and amino acid signaling pathways. *Mol Cell Biol* 24, 8994-9005.
77. Tagnaouti, N., Loeblich, S., Heisler, F., Pechmann, Y., Fehr, S., De Arcangelis, A., . . . Kneussel, M. (2007) Neuronal expression of muskelin in the rodent central nervous system. *BMC neuroscience* 8, 28.
78. Texier, Y., Toedt, G., Gorza, M., Mans, D.A., van Reeuwijk, J., Horn, N., . . . Boldt, K. (2014) Elution profile analysis of SDS-induced subcomplexes by quantitative mass spectrometry. *Mol Cell Proteomics* 13, 1382-1391.
79. Tobin, J.L. and Beales, P.L. (2009) The nonmotile ciliopathies. *Genetics in medicine : official journal of the American College of Medical Genetics* 11, 386-402.
80. Tomastikova, E., Cenklova, V., Kohoutova, L., Petrovska, B., Vachova, L., Halada, P., . . . Binarova, P. (2012) Interactions of an Arabidopsis RanBPM

- homologue with LisH-CTLH domain proteins revealed high conservation of CTLH complexes in eukaryotes. *BMC plant biology* 12, 83.
81. van Wijk, S.J., de Vries, S.J., Kemmeren, P., Huang, A., Boelens, R., Bonvin, A.M., and Timmers, H.T. (2009) A comprehensive framework of E2-RING E3 interactions of the human ubiquitin-proteasome system. *Mol Syst Biol* 5, 295.
 82. Vangala, J.R., Sotzny, F., Kruger, E., Deshaies, R.J., and Radhakrishnan, S.K. (2016) Nrf1 can be processed and activated in a proteasome-independent manner. *Curr Biol* 26, R834-835.
 83. Vogel, T.W., Manjila, S., and Cohen, A.R. (2012) Novel neurodevelopmental disorder in the case of a giant occipitoparietal meningoencephalocele. *Journal of neurosurgery. Pediatrics* 10, 25-29.
 84. Walentek, P. and Quigley, I.K. (2017) What we can learn from a tadpole about ciliopathies and airway diseases: Using systems biology in *Xenopus* to study cilia and mucociliary epithelia. *Genesis* 55.
 85. Waters, A.M. and Beales, P.L. (2011) Ciliopathies: an expanding disease spectrum. *Pediatr Nephrol* 26, 1039-1056.
 86. Wiborg, O., Pedersen, M.S., Wind, A., Berglund, L.E., Marcker, K.A., and Vuust, J. (1985) The human ubiquitin multigene family: some genes contain multiple directly repeated ubiquitin coding sequences. *EMBO J* 4, 755-759.
 87. Woelk, T., Oldrini, B., Maspero, E., Confalonieri, S., Cavallaro, E., Di Fiore, P.P., and Polo, S. (2006) Molecular mechanisms of coupled monoubiquitination. *Nat Cell Biol* 8, 1246-1254.
 88. Wolf, D.H., Sommer, T., and Hilt, W. (2004) Death gives birth to life: the essential role of the ubiquitin-proteasome system in biology. *Biochim Biophys Acta* 1695, 1-2.
 89. Yanez, A.J., Bertinat, R., Spichiger, C., Carcamo, J.G., de Los Angeles Garcia, M., Concha, II, . . . Slebe, J.C. (2005) Novel expression of liver FBPase in Langerhans islets of human and rat pancreas. *J Cell Physiol* 205, 19-24.
 90. Zhou, F. and Roy, S. (2015) SnapShot: Motile Cilia. *Cell* 162, 224-224 e221.

8 Published articles relevant for this work*

- Pfirkmann, T.**, Heessen, S., Omnus, D.J., Andreasson, C., and Ljungdahl, P.O. (2010) The prodomain of Ssy5 protease controls receptor-activated proteolysis of transcription factor Stp1. *Molecular and cellular biology* 30, 3299-3309.
- Omnus, D.J., **Pfirkmann, T.**, Andreasson, C., and Ljungdahl, P.O. (2011) A phosphodegron controls nutrient-induced proteasomal activation of the signaling protease Ssy5. *Mol Biol Cell* 22, 2754-2765 (shared first authorship).
- Pfirkmann, T.**, Ljungdahl, P. (2012) Chapter 685 – Ssy5 Peptidase: A Chymotrypsin-Like Signaling Protease in Yeast. Handbook of proteolytic enzymes DOI: <http://dx.doi.org/10.1016/B978-0-12-382219-2.00685-2>, .
- Braun, B., **Pfirkmann, T.**, Menssen, R., Hofmann, K., Scheel, H., and Wolf, D.H. (2011) Gid9, a second RING finger protein contributes to the ubiquitin ligase activity of the Gid complex required for catabolite degradation. *FEBS Lett* 585, 3856-3861.
- Santt, O., **Pfirkmann, T.**, Braun, B., Juretschke, J., Kimmig, P., Scheel, H., . . . Wolf, D.H. (2008) The yeast GID complex, a novel ubiquitin ligase (E3) involved in the regulation of carbohydrate metabolism. *Mol Biol Cell* 19, 3323-3333 (shared first authorship).
- Pfirkmann, T.**, Villavicencio-Lorini, P., Subudhi, A.K., Menssen, R., Wolf, D.H., and Hollemann, T. (2015) RMND5 from *Xenopus laevis* Is an E3 Ubiquitin-Ligase and Functions in Early Embryonic Forebrain Development. *PLoS One* 10, e0120342.

* With the exception of Pfirkmann and Ljungdahl, 2012 all manuscripts can be found in the appendix of this work or can be downloaded from PubMed.

9 Theses

1. All cells and organisms possess highly specialized nutrient sensing and signaling pathways in order to adapt to changing nutrient supply. This enables cellular and organismal survival.
2. *Saccharomyces cerevisiae* is a single cell eukaryotic organism particularly suitable to study nutrient sensing and signaling pathways. The power of yeast genetics is legendary and the availability of elaborated tools like the Euroscarf deletion library enables to screen for novel genes involved in different signaling pathways.
3. The SPS-signaling pathway is a yeast specific pathway that reacts to extracellular aminoacids in order to take them up to utilize them for metabolic or anabolic purposes. The SPS component Ssy5 is a chymotrypsin-like protease, that activates latent transcription factor Stp1 by cleavage of an N-terminal cytosolic retention signal. Active Stp1 enters the nucleus in order to activate transcription of amino acid permease genes.
4. Ssy5 is activated by the ubiquitin proteasome system by targeting the inhibitory Pro-domain for degradation. The Pro-domain is polyubiquitinated by the SCF^{Grr1}-complex upon Yck1/2 dependent phosphorylation of the Pro-domain to activate the protease. This activation mechanism was dubbed receptor-activated-proteolysis (RAP).
5. Glucose serves as a high-energy carbon source and its availability is constantly monitored. Glucose sensing- and signaling-systems are extremely advanced and sensitive. During glycolysis glucose is metabolized to pyruvate under aerobic conditions or to ethanol under anaerobic conditions in yeast. Gluconeogenesis is the antagonistic reciprocally controlled pathway that is required to synthesize glucose *de novo* from precursor molecules.
6. The yeast Gid-complex is a novel ubiquitin ligase complex that functions in the glucose dependent metabolic switch from gluconeogenesis and glycolysis.

Degradation of fructose-1,6-bisphosphatase (FBPase) and other gluconeogenic key enzymes irreversibly shuts off the pathway and constitutes a major regulatory path to switch off gluconeogenesis.

7. The subunit *Gid4* functions as a mediator that binds substrates of the *Gid* complex in yeast and recruits them for subsequent polyubiquitination and degradation. Ectopic expression of *Gid4* leads to FBPase degradation under derepressing conditions.
8. Subunits of the *Gid/CTLH* complex are evolutionary conserved and a similar complex is present in all eukaryotic organisms. The human *Gid/CTLH* complex is also a ubiquitin ligase with important functions for embryonic development. *Rmnd5a* loss of function leads to developmental defects in the prosencephalon, the eyes, the kidney and the facial structure.
9. Ciliopathies are severe developmental disorders that manifest due to defects in ciliogenesis or cilia function. These organelles are involved in diverse cellular functions, such as cell proliferation, differentiation and polarity and act as signaling hubs for extracellular signals like sonic hedgehog signaling. A structurally similar type of cilium is the motile cilium that can be found in several organs, e.g. the olfactory system, respiratory system, ventricles of the brain and the skin of *X. laevis*. Motile cilia contain an additional central pair of microtubules besides the nine-duplet filaments.
10. *CTLH* complex subunits localize to the basal body of the primary cilium. Loss of *Rmnd5a* function leads to disturbed ciliogenesis and cilia function, e.g. cilia of multiciliated cells of the skin are severely damaged and the sonic hedgehog signaling response is altered.
11. The *CTLH* complex regulates mTOR activity in NIH-3T3 cells suggesting a function as a regulator of energy homeostasis in the primary cilium of the cell.

10 Eidesstattliche Erklärung

Hiermit erkläre ich an Eides statt, dass ich die hier vorliegende Habilitationsschrift selbständig und nur unter Verwendung der angegebenen Literatur und Hilfsmittel angefertigt habe. Ein Habilitationsverfahren wurde an keiner anderen Universität eröffnet oder beantragt. Frühere Habilitationsversuche sind nicht unternommen worden. Halle (Saale), den 29.06.2017

gez. Dr. rer. nat. Thorsten Pfirrmann

11 Curriculum vitae

Dr. rer. nat. Thorsten Pfirrmann

NameThorsten Pfirrmann
Date of birth8th December 1974
Place of birthHeidelberg, Germany
NationalityGerman
Home address.....Rheinsbergerstr. 64, 10115 Berlin, Germany
Phone.....+49-163-3845331
Institutional addressInstitute for Physiological Chemistry,
Faculty of Medicine Halle (Saale), Hollystr. 1,
06114 Halle, Germany
Phone.....+49-(0)345-557 3849
Fax+49-(0)345-557 3811
E-mail.....thorsten.pfirrmann@medizin.uni-halle.de



1. Curriculum Vitae

Education and academic degrees

1995-2001 Study of Technical Biology at the University of Stuttgart
2001 Diploma (~ M.A.), Biology (with technical focus), University of Stuttgart
2001-2002 Master thesis (Diplomarbeit), John Curtin School of Medical Research,
Canberra, Australia
2006 Dr. rer. nat. (~ PhD in Biology), University of Stuttgart
2006-2008 Postdoctoral studies, Karolinska Institute, Stockholm, Sweden (Network
of excellence fellow)

Civil service

1994-1995 Medical assistance in Heidelberg

Regular academic positions and professional employment

1998-1999 Scientific assistant, Fraunhofer Institute, Stuttgart
2008-2011 Project leader, Wenner-Gren Institute, Stockholm, Sweden
2011 Research and Development at ILBC GmbH, Potsdam
Since 2011 Group leader at the Martin-Luther University Halle-Wittenberg

Further functions

Member of the following academic associations

Interdisziplinäres Zentrum für Altern Halle: Biologie-Medizin-Gesellschaft
(IZAH)
German Society of Molecular Biology and Biochemistry
Gesellschaft für Entwicklungsbiologie

Grants and fellowships

2006 FP6, Network of Excellence fellow: Role of Ubiquitin and Ubiquitin-like

	Modifiers in Cellular Regulation
2012-2013	Fonds der chemischen Industrie: Regulation of gluconeogenic key enzyme homeostasis by a novel ubiquitin ligase complex
2013-2014	Wilhelm-Roux: The function of RMD5 during neurogenesis
2014-2016	Wilhelm-Roux: OTUD3: function and clinical defects in ubiquitin dependent signaling
2015-2020	ProMoAge (GRK2155): The role of protein glycation on proteostasis

Courses

2007	Proteomics course, SILAC, Max Planck Institute, Munich, Germany
2004	Proteomics course, Rudolph Virchow Center, Würzburg, Germany
2009	Introductory Akta Training, GE Healthcare, Uppsala, Sweden

Languages

German (mother language), English (fluent), Swedish (fluent), French (basic)

Scientific training of junior researchers (since 2009)

PhD theses

Huaize Liu: The role of protein glycation on proteostasis (since 2016)

Carolin Mai: OTUD3: function and clinical defects in ubiquitin dependent signalling (since 2014)

MD theses

Abinash Kumar Subudhi: Functional Characterization of *Xenopus laevis* RMND5a (2014)

Konstantin Schmidt: Analysing the function of RMND5a in mammalian cells (2015)

Selected talks and posters

2016	EMBO meeting, Amsterdam, Netherlands Cilia 2016. Poster
2015	EMBO meeting, Cavtat, Croatia Ubiquitin and ubiquitin-like modifiers: From molecular mechanisms to human diseases. Poster
2012	Nasa Ames, Mountain View, California Amino acid sensing and signaling in yeast: The role of the Ubiquitin Proteasome system in the activation of a novel type of Protease. Invited speaker (online seminar)
2010	Yeast genetics and molecular biology meeting, Vancouver, Canada Intramolecular control of the Ssy5 protease by its Pro-domain accounts for regulated Receptor Activated Proteolysis of transcription factor Stp1. Poster
2009	4th Intracellular proteolysis meeting, Barcelona, Spain The Gid-E3 and Cdc48 machines are central components in ubiquitin proteasome triggered regulation of carbohydrate metabolism in yeast. Poster
2008	Rubicon network of excellence plenary and scientific review meeting, Rome, Italy Regulation of cell adhesion and migration by UCH-L1. Speaker

Ten most relevant publications

1. **Pfirkmann T**, Jandt E, Ranft S, Lokapally A, Neuhaus, H, Perron M, Hollemann T. Hh-dependent E3-Ligase Mid1 regulates ubiquitin-mediated proteasomal degradation of Pax6 during visual system development. PNAS. **2016**
2. **Pfirkmann T**, Emmerich D, Ruokonen P, Quandt D, Buchen R, Fischer-Zirnsak B, Hecht J, Krawitz P, Meyer P, Klopocki E, Stricker S, Lausch E, **Seliger B**, Hollemann T, Reinhard T, Auw-Haedrich C, Zabel B, **Hoffmann K**, Villavicencio-Lorini P. Molecular mechanism of CHRDL1-mediated X-linked megalocornea in humans and in Xenopus model. Human molecular genetics. **2015**.
3. **Pfirkmann T**, Villavicencio-Lorini P, Subudhi AK, Menssen R, Wolf DH, Hollemann T. RMND5 from Xenopus laevis Is an E3 Ubiquitin-Ligase and Functions in Early Embryonic Forebrain Development. PloS one. **2015**;10(3):e0120342. (*corresponding and senior author*).
4. **Pfirkmann T**, Lokapally A, Andreasson C, Ljungdahl P, Hollemann T. SOMA: a single oligonucleotide mutagenesis and cloning approach. PloS one. **2013**;8(6):e64870. (*corresponding and senior author*).
5. Zhao B, Velasco K, Sompallae R, **Pfirkmann T**, Masucci MG, Lindsten K. The ubiquitin specific protease-4 (USP4) interacts with the S9/Rpn6 subunit of the proteasome. Biochemical and biophysical research communications. **2012**;427(3):490-6.
6. Braun B, **Pfirkmann T**, Menssen R, Hofmann K, Scheel H, Wolf DH. Gid9, a second RING finger protein contributes to the ubiquitin ligase activity of the Gid complex required for catabolite degradation. FEBS letters. **2011**;585(24):3856-61.
7. Omnus DJ*, **Pfirkmann T***, Andreasson C, Ljungdahl PO. A phosphodegron controls nutrient-induced proteasomal activation of the signaling protease Ssy5. Molecular biology of the cell. **2011**;22(15):2754-65. (*shared first authorship*).
8. **Pfirkmann T**, Heessen S, Omnus DJ, Andreasson C, Ljungdahl PO. The prodomain of Ssy5 protease controls receptor-activated proteolysis of transcription factor Stp1. Molecular and cellular biology. **2010**;30(13):3299-309.
9. Basseres E, Coppotelli G, **Pfirkmann T**, Andersen JB, Masucci M, Frisan T. The ubiquitin C-terminal hydrolase UCH-L1 promotes bacterial invasion by altering the dynamics of the actin cytoskeleton. Cellular microbiology. **2010**;12(11):1622-33.
10. Santt O*, **Pfirkmann T***, Braun B, Juretschke J, Kimmig P, Scheel H, et al. The yeast GID complex, a novel ubiquitin ligase (E3) involved in the regulation of carbohydrate metabolism. Molecular biology of the cell. **2008**;19(8):3323-33. (*shared first authorship*).

12 Appendix

The Prodomain of Ssy5 Protease Controls Receptor-Activated Proteolysis of Transcription Factor Stp1[∇]

Thorsten Pfirrmann, Stijn Heessen, Deike J. Omnus, Claes Andréasson, and Per O. Ljungdahl*

Wenner-Gren Institute, Department of Cell Biology, Stockholm University, S-106 91 Stockholm, Sweden

Received 19 March 2010/Returned for modification 14 April 2010/Accepted 19 April 2010

Extracellular amino acids induce the yeast SPS sensor to endoproteolytically cleave transcription factors Stp1 and Stp2 in a process termed receptor-activated proteolysis (RAP). Ssy5, the activating endoprotease, is synthesized with a large N-terminal prodomain and a C-terminal chymotrypsin-like catalytic (Cat) domain. During biogenesis, Ssy5 cleaves itself and the prodomain and Cat domain remain associated, forming an inactive primed protease. Here we show that the prodomain is a potent inhibitor of Cat domain activity and that its inactivation is a requisite for RAP. Accordingly, amino acid-induced signals trigger proteasome-dependent degradation of the prodomain. A mutation that stabilizes the prodomain prevents Stp1 processing, whereas destabilizing mutations lead to constitutive RAP-independent Stp1 processing. We fused a conditional degron to the prodomain to synthetically reprogram the amino acid-responsive SPS signaling pathway, placing it under temperature control. Our results define a regulatory mechanism that is novel for eukaryotic proteases functioning within cells.

Proteolytic processing is a mechanism used by eukaryotes to control the activity of latent transcription factors (9). For example, regulated intramembrane proteolysis (RIP) and ubiquitin/proteasome-dependent processing (RUP) are two mechanisms that employ proteolysis-dependent activation of latent membrane-anchored transcription factors (24). RIP is catalyzed by membrane-bound proteases that cleave inactive precursor molecules to release active transcription factors from their membrane anchor (10). In the RUP mechanism, a polyubiquitylated membrane-anchored precursor is partially degraded by the 26S proteasome, resulting in the release of an active transcription factor (23). Both RIP and RUP rely on constitutively active proteases that process substrate transcription factors when they become available and bind the protease. Control of substrate availability is achieved by altering the intracellular compartmentalization of the substrate (RIP) or by covalent modification to target the substrate to an enclosed protease compartment (RUP). Consequently, in these pathways, the regulation of signal transduction occurs at the level of substrate availability and not by direct regulation of the proteolytic activity of the processing protease.

By studying the mechanism responsible for amino acid-induced gene expression in the yeast *Saccharomyces cerevisiae*, we have found that transcription factor activity can be regulated by directly controlling the enzymatic activity of an intracellular protease (3). We have termed this mechanism receptor-activated proteolysis (RAP) to signify the critical involvement of a plasma membrane receptor. RAP is distinguished from the previously described protease-based signaling mechanisms, RIP and RUP, in that it does not rely on the modulation of substrate accessibility.

RAP enables yeast cells to respond to amino acids in the growth medium by increasing the expression of amino acid

permeases, leading to an enhanced capacity to take up these nutrients. The signal transduction pathway governing this transcriptional response is known as the SPS sensing pathway. Signaling requires a functional Ssy1-Ptr3-Ssy5 (SPS) sensor, the SCF^{Grr1} ubiquitin ligase complex, casein kinase-dependent phosphorylation, and two homologous transcription factors, Stp1 and Stp2 (1, 17, 19, 27, 29, 34, 35). In the absence of SPS sensor signaling, Stp1 and Stp2 exhibit latent characteristics and are excluded from the nucleus by the presence of N-terminal negative regulatory domains (4, 5). Upon induction by extracellular amino acids, the primary amino acid receptor Ssy1 initiates signals (48) that, via hyperphosphorylation of Ptr3 (28), result in activation of the Ssy5 protease, leading to the endoproteolytic processing of Stp1 and Stp2, which enter the nucleus and activate the transcription of amino acid permease genes (4).

The core SPS sensor component Ssy5 is the RAP-controlled protease (1, 3, 34). Ssy5 exhibits homology to chymotrypsin-like serine proteases and is expressed as a zymogen that cleaves itself into an N-terminal prodomain and a C-terminal catalytic (Cat) domain. The Cat domain contains a conserved catalytic triad with a predicted active-site serine (S640) that is required for function (1, 2). N-terminal sequencing of the Cat domain identified alanine 382 as the first residue, consistent with the notion that autoprocessing takes place between prodomain residue 381 and Cat domain residue 382 (34).

The mechanism of RAP-dependent activation of Stp1 and Stp2 is not well understood, but several observations point to an important regulatory role for the Ssy5 Pro domain. First, in comparison to the size of characterized serine proteases, the prodomain of Ssy5 is unusually large, suggesting a more complex regulatory function. Further, after autolytic processing, the prodomain and Cat domain remain associated, forming a primed protease that associates with Stp1 and, although catalytically competent, does not process its substrate (3). Last, Stp1 cleavage correlates in time with the downregulation of prodomain levels. These observations led us to propose that

* Corresponding author. Mailing address: Stockholm University, Wenner-Gren Institute, S-106 91 Stockholm, Sweden. Phone: 46 8 16 41 01. Fax: 46 8 15 98 37. E-mail: plju@wgi.su.se.

[∇] Published ahead of print on 26 April 2010.

TABLE 1. Yeast strains used in this study

Strain	Genotype	Reference
AA255/PLY115-derived strains		
CAY265	<i>MATa ura3-52 ssy5Δ2::hisG gap1Δ::PAGP1-lacZ</i>	3
CAY276	<i>MATa lys2Δ201 ura3-52 ssy5Δ2::hisG grr1Δ50::hphMX4</i>	This work
CAY285	<i>MATa lys2Δ201 ura3-52 ptr3Δ15::hisG ssy1Δ13::hisG ssy5Δ2::hisG</i>	3
HKY77	<i>MATa lys2Δ201 ura3-52 ssy5Δ2::hisG</i>	19
HKY84	<i>MATa lys2Δ201 ura3-52 ssy1Δ13::hisG ssy5Δ2::hisG</i>	19
HKY85	<i>MATa lys2Δ201 ura3-52 ptr3Δ15::hisG ssy5Δ2::hisG</i>	19
TPY101	<i>MATa lys2Δ201 ura3-52 ssy1Δ13::hisG ssy5Δ2::hisG ubr1Δ::natMX</i>	This work
W303-1B-derived strains		
CAY220	<i>MATα ura3-52 leu2Δ1 ssd1 RPT6 (CIM3)</i>	4
CMY763	<i>MATα ura3-52 leu2Δ1 ssd1 rpt6 (cim3-1)</i>	21

after assembling into a primed protease, the prodomain inhibits the Cat domain and dissociates before substrate processing (3).

In this study, we examined the role of the Ssy5 prodomain in controlling the endoproteolytic Stp1-processing activity of the Cat domain. We found that the prodomain undergoes proteasomal degradation as a consequence of SPS sensor signaling. Mutations in *SSY5* that induce prodomain degradation result in constitutive protease activity, whereas deletion of the N-terminal 90 amino acids abolishes Stp1 processing without affecting autolysis or Stp1 binding. These results strongly suggest that the prodomain functions as a potent inhibitor of the Cat domain. We have critically tested this model by synthetically targeting the prodomain for regulated proteasomal degradation and found that proteasomal degradation of the prodomain is sufficient to fully induce Cat domain-dependent Stp1 processing. The regulatory mechanism described here represents a novel way of controlling an intracellular eukaryotic protease.

MATERIALS AND METHODS

Media. Standard media, including yeast extract-peptone-dextrose (YPD) medium, ammonia-based synthetic minimal dextrose (SD) medium, supplemented as required to enable the growth of auxotrophic strains, and ammonia-based synthetic complete dextrose (SC) were prepared as described previously (4). When needed, L-leucine was added at a concentration of 1.3 mM to induce SPS sensor signaling. Sensitivity to 2-[[[(4-methoxy-6-methyl)-1,3,5-triazin-2-yl]amino]carbonyl]amino]-sulfonyl]-benzoic acid (MM; 450 μg/ml) on complex medium is described elsewhere (5). Sensitivity to 1 mM azetidine-2-carboxylic acid (AzC) was tested on solid SD medium.

Strains and plasmids. The *S. cerevisiae* strains used in this study (Table 1) are isogenic descendants of S288C-derived strain AA255/PLY115 (6) or W303-1B (43), as indicated. The plasmids used in this work are listed in Table 2. Plasmids pSH105 and pSH106 were obtained by recombination of a Pro-HA-SSY5₄₁₋₃₂₆ PCR fragment amplified from pFL005 and AatII-restricted pCA174. Plasmids pSH119 and pSH120 were created identically to pSH105 and pSH106 but with different primer pairs. A fragment containing a temperature-regulated degron was amplified from plasmid pKLL187 (36) and recombined into BamHI-linearized pHK48 (19), after which the 1,791-bp AatII/NotI fragment from this plasmid was recombined into PmeI-linearized pSH120, creating plasmid pTP110. A PCR-generated fragment with the critical arginine (R_{ds}) replaced with alanine (A_s) was recombined into SacII-linearized pTP110, creating pTP111. Plasmids

TABLE 2. Plasmids used in this study

Plasmid	Description	Reference
pCA030	pRS317 (<i>LYS2</i>) containing <i>PAGP1-lacZ</i>	5
pCA047	pRS316 (<i>URA3</i>) containing <i>STP1-3HA</i>	4
pCA122	pRS317 (<i>LYS2</i>) containing <i>STP1-3HA</i>	5
pCA177	pRS316 (<i>URA3</i>) containing <i>SSY5-HA-KITRP1</i>	3
pCA195	pRS316 (<i>URA3</i>) containing <i>HA-SSY5</i>	3
pCA204	pRS317 (<i>LYS2</i>) containing <i>STP1-MYC-kanMX</i>	3
pFL001	pRS316 (<i>URA3</i>) containing <i>SSY5</i>	3
pSH105	pRS316 (<i>URA3</i>) containing <i>HA_i-SSY5₄₁₋₆₉₉-GST</i>	This work
pSH106	pRS316 (<i>URA3</i>) containing <i>HA_i-SSY5₆₁₋₆₉₉-GST</i>	This work
pSH119	pRS316 (<i>URA3</i>) containing <i>HA_i-SSY5₉₁₋₆₉₉-GST</i>	This work
pSH120	pRS316 (<i>URA3</i>) containing <i>HA_i-SSY5₁₋₆₉₉-GST</i>	This work
pHK048	pRS316 (<i>URA3</i>) containing <i>SSY5-myc</i>	19
pTP110	pRS316 (<i>URA3</i>) containing <i>Ubi-R_{ds}-tsDHRF-HA_i-SSY5₁₋₆₉₉-GST</i>	This work
pTP111	pRS316 (<i>URA3</i>) containing <i>Ubi-A_s-tsDHRF-HA_i-SSY5₁₋₆₉₉-GST</i>	This work
pTP112	pRS316 (<i>URA3</i>) containing <i>HA_i-SSY5₁₋₆₉₉-GST (L126S V129A E131A)</i>	This work
pTP113	pRS316 (<i>URA3</i>) containing <i>HA_i-SSY5₁₋₆₉₉-GST (L126S E131A)</i>	This work
pTP114	pRS316 (<i>URA3</i>) containing <i>HA_i-SSY5₁₋₆₉₉-GST (L126S V129A)</i>	This work
pTP115	pRS316 (<i>URA3</i>) containing <i>HA_i-SSY5₁₋₆₉₉-GST (E131A)</i>	This work
pTP116	pRS316 (<i>URA3</i>) containing <i>HA_i-SSY5₁₋₆₉₉-GST (E131V)</i>	This work
pTP117	pRS316 (<i>URA3</i>) containing <i>HA_i-SSY5₁₋₆₉₉-GST (V129A)</i>	This work
pTP118	pRS316 (<i>URA3</i>) containing <i>HA_i-SSY5₁₋₆₉₉-GST (V129D)</i>	This work
pTP119	pRS316 (<i>URA3</i>) containing <i>HA_i-SSY5₁₋₆₉₉-GST (V129G)</i>	This work
pTP120	pRS316 (<i>URA3</i>) containing <i>HA_i-SSY5₁₋₆₉₉-GST (L126W)</i>	This work
pTP121	pRS316 (<i>URA3</i>) containing <i>HA_i-SSY5₁₋₆₉₉-GST (L126S)</i>	This work

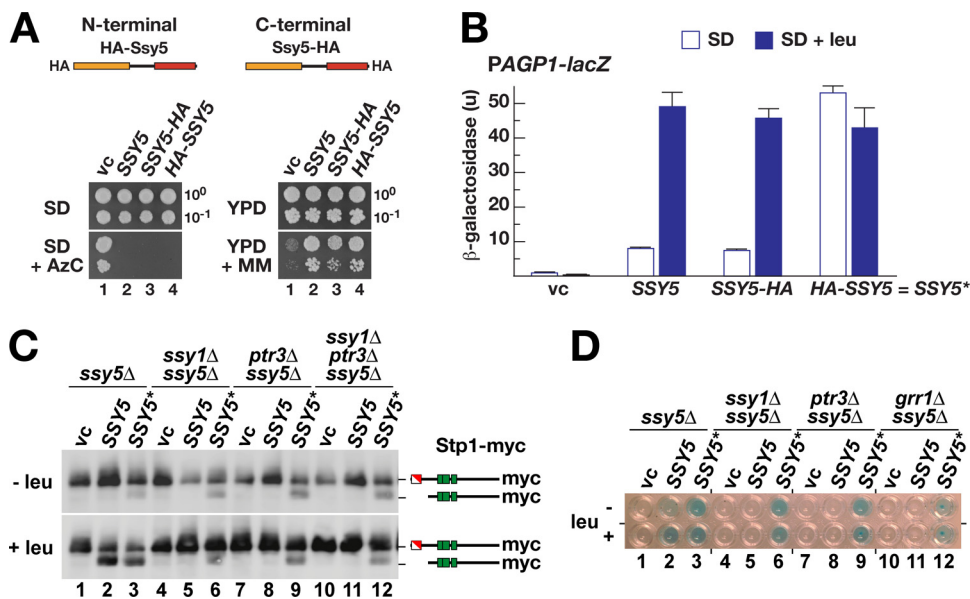


FIG. 1. Stp1 is constitutively processed in strains expressing N-terminally HA-tagged Ssy5 (Ssy5*). (A) Schematic diagram and functional analysis of N- and C-terminally HA-tagged Ssy5. The empty vector pRS316 (vc), pFL001 (Ssy5), pCA177 (Ssy5-HA), and pCA195 (HA-Ssy5) were individually introduced into *ssy5* Δ mutant strain CAY265. Dilutions of cultures grown in SD were spotted onto SD, SD with AzC (SD + AzC), YPD, and YPD with MM (YPD + MM). Plates were incubated for 2 to 3 days at 30°C. (B) β -Galactosidase activity in *ssy5* Δ mutant strain HKY77 [pCA030 (*PAGP1-lacZ*)] carrying pRS316 (vc), pFL001 (SSY5), pCA177 (SSY5-HA), or pCA195 (HA-SSY5) and grown in SD or SD supplemented with leucine (SD + leu). Error bars indicate 95% confidence intervals based on assays carried out using four independent transformants. The constitutive HA-SSY5 allele is designated SSY5*. (C) Immunoblot analysis of extracts prepared from strains HKY77 (*ssy5* Δ), HKY84 (*ssy5* Δ *ssy1* Δ), HKY85 (*ssy5* Δ *ptr3* Δ), and CAY285 (*ssy5* Δ *ptr3* Δ *ssy1* Δ) carrying pCA204 (Stp1-myc) and pRS316 (vc), pFL001 (SSY5), or pCA195 (SSY5*) and grown in SD (- leu) and 30 min after induction with leucine (+ leu). (D) β -Galactosidase activity from *PAGP1-lacZ* (pCA030) expressed in HKY77 (*ssy5* Δ), HKY84 (*ssy5* Δ *ssy1* Δ), HKY85 (*ssy5* Δ *ptr3* Δ), and CAY276 (*ssy5* Δ *grr1* Δ) carrying pRS316 (vc), pFL001 (SSY5), pCA177 (SSY5-HA), or pCA195 (SSY5*). The strains were grown in SD or SD supplemented with leucine (+ leu) as indicated. β -Galactosidase activity was detected by 5-bromo-4-chloro-3-indolyl- β -D-galactopyranoside (X-Gal) staining (blue precipitate).

pTP112, pTP113, pTP114, pTP115, pTP116, pTP117, pTP118, pTP119, pTP120, and pTP121, encoding mutant alleles affecting Pro domain function, were obtained by recombination of PCR fragments carrying the indicated mismatch mutations and a silent mutation eliminating a diagnostic BamHI site. The sequences of the mutagenic oligonucleotides and PCR primers used are available upon request.

β -Galactosidase activity assays. Semiquantitative β -galactosidase activity was measured in *N*-lauroylsarcosine-permeabilized cells as described elsewhere (5).

Immunoblot analysis. Whole-cell extracts were prepared under denaturing conditions using NaOH and trichloroacetic acid as described previously (39). Primary antibodies were diluted as follows: 12CA5 ascites fluid (antihemagglutinin [anti-HA] monoclonal antibody), 1:1,000; purified rabbit polyclonal anti-glutathione *S*-transferase (anti-GST) antibody, 1:5,000; anti-myc monoclonal antibody (Roche Applied Science), 1:1,000; horseradish peroxidase (HRP)-conjugated 3F10 anti-HA monoclonal antibody (Roche Applied Science), 1:5,000; anti-GST 3-4C monoclonal antibody (Zymed Laboratories Inc.), 1:500; anti-myc-HRP 9E10 monoclonal antibody (Roche Applied Science), 1:1,000; anti-FLAG polyclonal antibody (Sigma), 1:5,000; anti-Pgk1 antibody (Molecular Probes), 1:5,000. Immunoreactive bands were visualized by chemiluminescence detection (SuperSignal West Dura Extended-Duration Substrate; Pierce) and quantified using a LAS1000 system (Fuji Photo Film Co., Ltd.).

CHX chase. Cells were inoculated at an optical density at 600 nm of 0.5 and grown at 30°C for 3 h. Cycloheximide (CHX) was added to the cells at a concentration of 100 μ g/ml, and where indicated, leucine was added to a concentration of 1.3 mM (+ leu). Extracts were prepared from samples taken at the time points indicated and analyzed by immunoblotting. Cells harboring temperature-sensitive alleles were treated similarly but were pregrown at 25°C for 4 h, after which the culture was shifted to 37°C for 30 min prior to CHX addition.

PCR mutagenesis. Prodomain-encoding sequences were amplified using error-prone PCR (47) in the presence of 1.25 mM dCTP and TTP, 0.025 mM dATP and dGTP, 3.5 mM MgCl₂, and 0.125 mM MnCl₂. The resulting PCR products and AatII-linearized pSH120 were introduced together into strain HKY84 (*ssy5* Δ *ssy1* Δ), and Ura⁺ transformants with recombinant plasmids were selected on SC

medium lacking uracil. Cells carrying plasmids expressing constitutively active alleles of SSY5 were selected on YPD containing MM.

RESULTS

SSY5* encodes a constitutively active protease that functions independently of other SPS sensor components. We set out to critically test whether the prodomain is responsible for the proper regulation of the Ssy5 protease. Previously, we reported that fusion of a 6HA tag to the N terminus of Ssy5 results in constitutive Stp1 processing in the absence of inducing amino acids. Also, we found that N-terminally HA-tagged Ssy5 cleaves Stp1 when these proteins are heterologously expressed in *Schizosaccharomyces pombe*, a yeast that lacks an identifiable SPS sensing pathway (3). In contrast to our results, Liu et al. (28) recently reported that the insertion of a similar HA tag at the N terminus of Ssy5 did not result in constitutive Stp1 processing. This apparent discrepancy prompted us to fully characterize the functional properties of N- and C-terminally HA-tagged Ssy5 alleles.

SSY5 alleles encoding HA tags at either the N or the C terminus are functional and complement *ssy5* Δ -encoded phenotypes (Fig. 1A); i.e., they complement SPS sensor-dependent uptake of a toxic proline analogue (AzC) (5) and branched-chain amino acid uptake in the presence of MM (MM is a sulfonylurea analogue that inhibits branched-chain amino acid synthesis) (25). In order to quantify the extent of

SPS sensor-induced transcriptional activation and to detect possible constitutive behavior of HA-tagged Ssy5, we monitored the ability of epitope-tagged Ssy5 to restore SPS sensor-induced gene expression in an *ssy5Δ* strain by monitoring *AGPI* promoter activity of a *PAGPI-lacZ* reporter gene integrated chromosomally (3). Interestingly, while cells carrying wild-type or C-terminally HA-tagged Ssy5 responded normally to SPS sensor signaling (Fig. 1B, *SSY5* and *SSY5-HA*), cells with N-terminally HA-tagged Ssy5 exhibited constitutively high levels of β-galactosidase activity, even in medium lacking the SPS sensor inducer leucine (Fig. 1B, *HA-SSY5*). Hence, the insertion of the 6HA tag at the N terminus of Ssy5 clearly creates an artificially activated species, here designated Ssy5*.

Ssy5* may represent a protease that is hyperresponsive to basal (noninduced) SPS sensor signaling, retaining its dependency on the presence of the other SPS sensor components. Alternatively, Ssy5* may function in a fully uncontrolled manner that is independent of the other signaling components. We tested these possibilities by monitoring Stp1 processing in *ssy1Δ*, *ptr3Δ*, and *ssy1Δ ptr3Δ* mutant strains harboring the *SSY5** allele (Fig. 1C). *SSY5**-induced Stp1 processing was observed in all of the strains, both in the absence and in the presence of leucine in the growth medium, although processing was more effective in leucine-induced cells with a functional SPS sensor (Fig. 1C, lane 3). To test if processing of Stp1 resulted in promoter activation in these experiments, we monitored β-galactosidase expression from the *AGPI* promoter. Indeed, *SSY5** facilitated expression from the *AGPI* promoter in all SPS sensor-deficient strains, including a *grr1Δ* mutant strain (Fig. 1D). Together, these observations indicate that Ssy5* is able to process Stp1 without the participation of the other SPS sensor components. It is likely that the fusion of an HA tag to the N terminus affects the conformation of the Pro domain in a manner that favors Cat domain-mediated Stp1 processing.

26S proteasome-dependent prodomain degradation correlates with Stp1 processing. We have previously reported that prodomain levels rapidly decrease upon SPS sensor induction by amino acids in a manner that correlates in time with Stp1 processing (3, 19). These findings led us to propose that the dissociation of the prodomain from the Cat domain, or a conformational change in the prodomain, changes its stability and may be the key regulatory step in Ssy5 activation (3). However, the relevance of reduced prodomain levels and the correlation with Ssy5 activity have recently been questioned (28), which required us to examine the amino acid-induced downregulation of the prodomain in more detail.

First, we addressed the potential experimental artifact that prodomain downregulation was a consequence of the insertion of an N-terminal HA tag. Leucine-induced downregulation was apparent when either an N-terminal myc tag (19) or an internal HA tag (HA_i) inserted after amino acid position 216 (3) was used to tag the prodomain (Fig. 2A, upper panels). Importantly, both of these epitope-tagged Ssy5 constructs exhibit fully regulated activity, judging by their ability to rapidly induce Stp1 processing in response to leucine addition (Fig. 2A, lower panels). These results indicate that prodomain downregulation is independent of the epitope tag used to detect it.

Next, we directly tested whether downregulation of the prodomain is the result of altered rates of degradation or

synthesis. We repeated the time course experiments in the presence of the translation inhibitor CHX and extended the analysis by simultaneously monitoring Cat domain levels using a C-terminal GST tag (Fig. 2B). In the absence of amino acid induction, the prodomain is relatively stable and was readily detected over the entire 45-min time course (Fig. 2B, lanes 1 to 4). In contrast, leucine induction rapidly reduced prodomain levels (Fig. 2B, lanes 5 to 8); levels were already significantly reduced 15 min postinduction and were barely detectable by the 30-min time point. Consequently, amino acid induction enhances prodomain degradation. Again, the reduced prodomain levels correlated with Stp1 processing. Both full-length and processed forms of Stp1 have a high turnover rate (half-life, ≤ 10 min) (5); consequently, the processed form of Stp1 is most abundant at the 15-min time point. The levels of the Cat domain were stable, as were the levels of the protein loading control Pgk1 (38).

Finally, to investigate whether the 26S proteasome is involved in prodomain downregulation, we assayed amino acid-induced degradation in strains carrying a temperature-sensitive mutation in *RPT6* (*cim3-1*), which encodes one of the ATPases of the 19S regulatory particle of the proteasome. Proteasomal substrates are stabilized at nonpermissive temperatures in strains carrying *cim3-1* (21, 37). We found that the prodomain was stabilized under both noninducing (no leu) and inducing (+leu) conditions in cells harboring the *cim3-1* mutation relative to the isogenic wild-type strain (Fig. 2C, upper panels). Apparently, both basal and SPS sensor-induced degradation of the prodomain is mediated by the 26S proteasome. Similarly, we found *cim3-1*-induced stabilization of full-length Stp1 under both noninducing (no leu) and inducing (+leu) conditions compared to the isogenic wild-type strain (Fig. 2C, lower panel). As shown previously, Stp1 is processed even when proteasomal activity is impaired (1, 4).

Progressive deletions within the first 90 amino acids of the Ssy5 prodomain define negative- and positive-acting sequences required for proper Stp1 processing. Based on the observation that manipulation of the prodomain with an N-terminal HA epitope results in constitutively active Ssy5 (Fig. 1), we focused on the possibility that the prodomain possesses autoregulatory activity. We created a series of N-terminal deletion mutations in the context of the functional *SSY5* allele with an internal HA tag (HA_i) and a C-terminal GST tag (Fig. 3A, left panel). This HA_i -Ssy5-GST allele (*SSY5*) fully complements the *ssy5Δ* mutation and correctly responds to amino acid induction (Fig. 3B). Consistently, the N- and C-terminal tags do not affect autolytic cleavage into separate pro- and Cat domains (Fig. 3A, right panel, lane 2) or proteasome-dependent degradation (Fig. 2B).

Three N-terminal truncation mutant proteins in which the first 40, 60, and 90 amino acids ($\Delta 40$, $\Delta 60$ and $\Delta 90$), respectively, were removed were evaluated for their effects on Ssy5 maturation into processed pro- and Cat domains. All of the truncated proteins were processed, indicating that deletion of up to the first 90 amino acids does not impair the catalytic activity of the Cat domain (Fig. 3A, right panels). Next, we assessed the functionality of the truncated proteins using a growth-based assay and analyzed their ability to induce the *PAGPI-lacZ* reporter (Fig. 3B). Whereas the $\Delta 40$ allele behaved like wild-type *SSY5* (Fig. 3B, dilution 3), the $\Delta 60$ allele

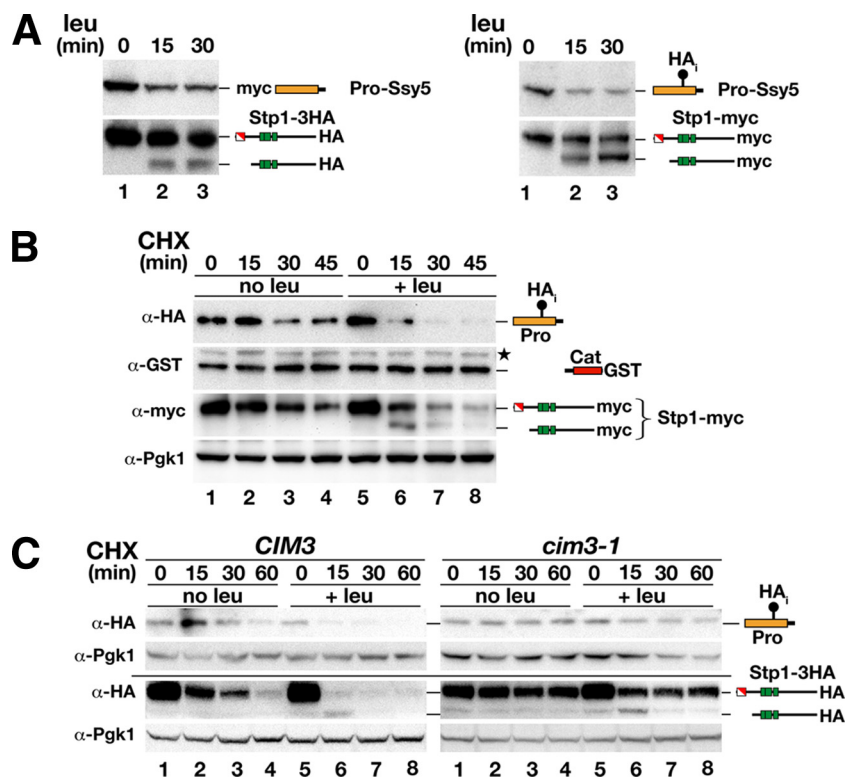


FIG. 2. Amino acid-induced proteasomal degradation of the Ssy5 prodomain correlates with Stp1 processing. (A) SD-grown cultures of *ssy5Δ* mutant strain HKY77 carrying plasmids pHK048 (myc-Ssy5) and pCA122 (Stp1-HA) (left panel) or pSH120 (HA₁-Ssy5-GST) and pCA204 (Stp1-myc) (right panel) were induced with leucine. Immunoblot analysis of cell extracts prepared from subsamples of each culture removed at the indicated time after leucine addition. (B) Immunoblot analysis of cell extracts from strain HKY77 carrying pSH120 (HA₁-Ssy5-GST) and pCA204 (Stp1-myc) treated with CHX. Cells were pregrown in SD, the culture was split into two equal volumes at $t = 0$, and the subcultures received an aliquot of CHX (final concentration equal to 100 mg/ml) and leucine as indicated. (C) Immunoblot analysis of cell extracts from *CIM3* (CAY220) and *cim3-1* (CMY763) mutant strains carrying pRS315 (*LEU2*) and pSH120 (HA₁-Ssy5-GST) or pCA047 (Stp1-HA). Cells were pregrown in SD at 25°C, and cultures were split into two equal volumes and incubated at 37°C for 30 min prior to the addition of CHX and leucine as indicated. Samples were taken at the indicated time points after CHX addition. The immunoreactive forms of the Ssy5 Pro domain and Stp1 are schematically represented at their corresponding positions of migration. Levels of Pgk1 served as an internal control for protein loading.

induced constitutive activation of the *PAG1-lacZ* reporter (Fig. 3B, dilution 4). The latter result prompted us to test whether the $\Delta 60$ allele, like the *SSY5** allele, bypassed the requirement of the other SPS sensor components (Fig. 3C). When the $\Delta 60$ allele was introduced into an *ssy1Δ ptr3Δ ssy5Δ* mutant strain, *PAG1-lacZ* was expressed independently of amino acid induction, indicating that the allele encodes a constitutively active species. In contrast, the $\Delta 90$ allele lacked Stp1-processing activity since the *ssy5Δ* mutant host strain remained MM sensitive and *PAG1-lacZ* expression was not induced by leucine (Fig. 3B, dilution 5). Thus, the $\Delta 90$ allele encodes a protein that is catalytically competent (i.e., prodomain and Cat domain autolysis occurs normally) but is unable to process Stp1.

Based on the previously observed correlation between prodomain degradation and Stp1 processing (Fig. 2), we postulated that cells with the constitutive $\Delta 60$ allele would have lower, constitutively downregulated levels of the prodomain. Similarly, we predicted that cells with the nonresponsive $\Delta 90$ allele would fail to downregulate the prodomain in response to amino acid induction. These predictions were tested by measuring the levels of the prodomain and Cat domain and the state of Stp1 processing in cells before and after leucine in-

duction. Cells with wild-type *SSY5* (HA₁-*SSY5-GST*) responded to leucine induction with a 30% ($\pm 10\%$) reduction of the prodomain signal and accompanying Stp1 processing (Fig. 3D, lanes 1 and 2). Uninduced cells harboring a $\Delta 60$ allele also exhibited a 35% ($\pm 10\%$) reduction in prodomain levels relative to uninduced wild-type *SSY5*, and no further reduction was observed upon leucine induction (Fig. 3D, lanes 3 and 4). Cells harboring the $\Delta 90$ allele exhibited constant prodomain levels and no Stp1 processing (Fig. 3D, lanes 5 and 6).

Taken together, these results show that, in all instances, the prodomain levels inversely correlate with Stp1-processing activity; i.e., at high prodomain levels, no Stp1 processing is observed, and at low prodomain levels, Stp1 processing is observed. Presumably, deletion of the first 60 residues of the prodomain results in the constitutive activation of Ssy5 as a consequence of increased prodomain turnover. The larger deletion that removes the N-terminal 90 residues results in a protein that is unable to respond to amino acid induction, the likely consequence of the removal of sequences required for signal-induced degradation of the prodomain.

Constitutive activating mutations cluster in a conserved region of the Ssy5 prodomain. To critically test whether consti-

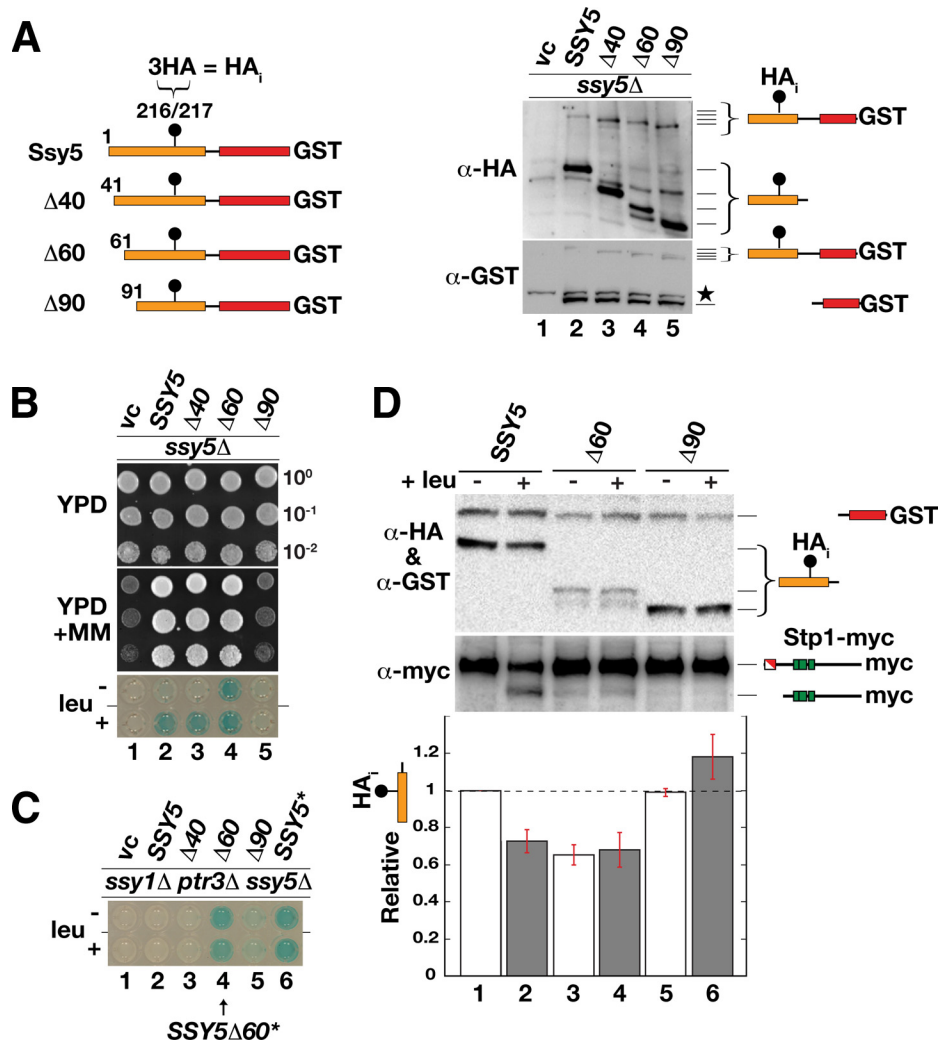


FIG. 3. Deletion analysis of the prodomain yields constitutive and nonresponsive Ssy5 alleles. (A) Schematic representation of the N-terminal deletion constructs analyzed. The positions of the N-terminal residues, each preceded by an initiator methionine, are indicated (left panel). Each construct is expressed with an internal $3 \times$ HA tag (HA₁) and a C-terminal GST fusion protein. Shown is an immunoblot analysis of protein extracts from an *ssy5Δ* mutant strain (CAY265) carrying pRS316 (vc), pSH120 (SSY5), pSH105 (Δ40), pSH106 (Δ60), or pSH119 (Δ90) (right panel); extracts were prepared from cells grown in SD. The immunoreactive forms of Ssy5 are schematically depicted at their corresponding positions of migration. A star marks the position of an unrelated cross-reacting protein. (B) Dilution series of cell suspensions from strains as in panel A carrying pCA030 (*PAG1-lacZ*) were pregrown in SD and spotted onto YPD and YPD plus MM. Expression of β-galactosidase from *PAG1-lacZ* was detected by X-Gal staining of cells grown in SD without or with leucine as indicated. (C) Strain CAY285 (*ssy1Δ ptr3Δ ssy5Δ*) carrying pCA030 (*PAG1-lacZ*) and pRS316 (vc), pSH120 (SSY5), pSH105 (Δ40), pSH106 (Δ60), pSH119 (Δ90), or pCA205 (6HA-SSY5) was grown with or without leucine as indicated, and the levels of X-Gal staining were assessed in permeabilized cells (lower panel). (D) Immunoblot analysis of protein extracts from an *ssy5Δ* mutant strain (HKY77) carrying pCA204 (Stp1-myc) and pSH120 (SSY5), pSH106 (Δ60), or pSH119 (Δ90). Extracts were prepared from cells grown in SD and from cells harvested 30 min after induction by leucine as indicated. The immunoreactive forms of Ssy5 and Stp1 are schematically depicted at their corresponding positions of migration. The signal intensity of the immunoreactive bands corresponding to the HA-tagged prodomain and the GST-tagged Cat domain were quantified; the prodomain/Cat domain ratios were determined and normalized to the ratio of Ssy5 in uninduced cells (lane 1), and mean values were plotted. Error bars show standard errors ($n = 3$).

tutive activity is linked to prodomain degradation, we screened for point mutations in prodomain-encoding sequences of *SSY5* that result in constitutive protease activity (see Materials and Methods). Briefly, a plasmid library with mutations specifically localized to sequences encoding the prodomain was generated by error-prone PCR. This library was introduced into a *ssy5Δ ssy1Δ* double-mutant yeast strain, and out of 2×10^6 transformants, 100 reproducibly scored positive for growth on YPD plus MM, a phenotype that is diagnostic for constitutive SPS

sensor-regulated gene expression. Sixteen plasmids carrying constitutive alleles were further analyzed, and their inserts were sequenced; see Table 3 for a summary of the genetic selection and resulting mutations. Most of the inserts contained multiple mutations; however, we noted that several mutations affected three specific codons clustered within a conserved region (amino acids 126 to 131). Specifically, nine inserts carried mutations in codon 131, coding for glutamate; the mutations resulted in the substitution of alanine, valine,

TABLE 3. Summary of PCR-generated *SSY5* constitutive alleles^a

Amino acid codon affected in plasmid insert and resulting change	No. of times isolated
E131	
V.....	4
A.....	3
G.....	1
K.....	1
V129	
D.....	3
G.....	1
A.....	1
L126	
S.....	1
W.....	1

^a Analyzed were 2×10^6 transformants, 300 MM^r colonies in a primary selection, and 100 MM^r colonies in a rescreening, and the sequences of inserts of 16 plasmids were analyzed.

lysine, or glycine at this residue. Of the remaining inserts, five carried mutations in valine codon 129; here, the mutations resulted in the substitution of aspartate, alanine, or glycine at this residue. The last two inserts carried mutations resulting in the replacement of leucine residue 126 with either tryptophan or serine.

Since the inserts contained several mutations in addition to the ones just described, we introduced each of the mutations affecting these three conserved amino acid residues, both individually and in combination, into the fully functional and doubly tagged *HA_r-SSY5-GST* allele. These new mutant alleles, presumably affecting Pro domain function, were subjected to further analysis. First, the mutant alleles were tested for the ability to complement a *ssy5Δ* mutation, and as expected, all fully complemented growth phenotypes in a manner indistinguishable from that of wild-type *SSY5* (data not shown). Next, the constitutive activity of the mutant alleles was examined in an *ssy5Δ ssy1Δ* double-mutant strain using a growth-based assay on YPD plus MM (Fig. 4, upper panels). The growth characteristics enabled the single mutations to be classified into three groups. Group I mutations, E131A/V (dilutions 6 and 7) and V129D/G (dilutions 9 and 10), supported robust growth indicative of a high degree of constitutive activity. Group II mutations, V129A and L126W (dilutions 8 and 11), resulted in visibly weaker growth than group I mutations in the presence of MM. The single group III mutation, L126S, conferred poor growth on both YPD plus MM and YPD, which made it difficult to assess its constitutive activity. However, in combination with the weak group II V129A mutation, the L126S mutation had an enhancing effect that markedly improved growth on MM (Fig. 4, compare dilution 5 with dilution 8). The latter finding likely explains our ability to isolate mutations affecting this residue.

The status of Stp1 processing was examined in the cells carrying the constitutive alleles (Fig. 4, lower middle panel). Consistent with the growth phenotypes, the expression of group I alleles induced readily detectable levels of Stp1 processing, whereas Stp1 processing was barely or not detectable in cells expressing group II and group III mutations. Hence,

the YPD-plus-MM growth phenotype provides a more sensitive assay of constitutive Ssy5 activity than immunoblot analysis of Stp1 processing. The higher sensitivity of growth-based assays is expected since both chromosomal copies of wild-type *STP1* and *STP2* are present in our strains; our analysis does not detect the processing of these native factors. Also, it has been reported that Ssy5-dependent processing of Stp2 occurs at lower levels of SPS sensor signaling (46). Thus, the weaker constitutive group II alleles may preferentially result in Stp2 processing.

Finally, we directly tested the possibility that the mutant alleles possess constitutively reduced prodomain levels. Indeed, we found a striking correlation between constitutive activity and prodomain downregulation (Fig. 4, upper middle and lower panels). The strong group I mutations reduced prodomain levels to between 30 and 40% of the

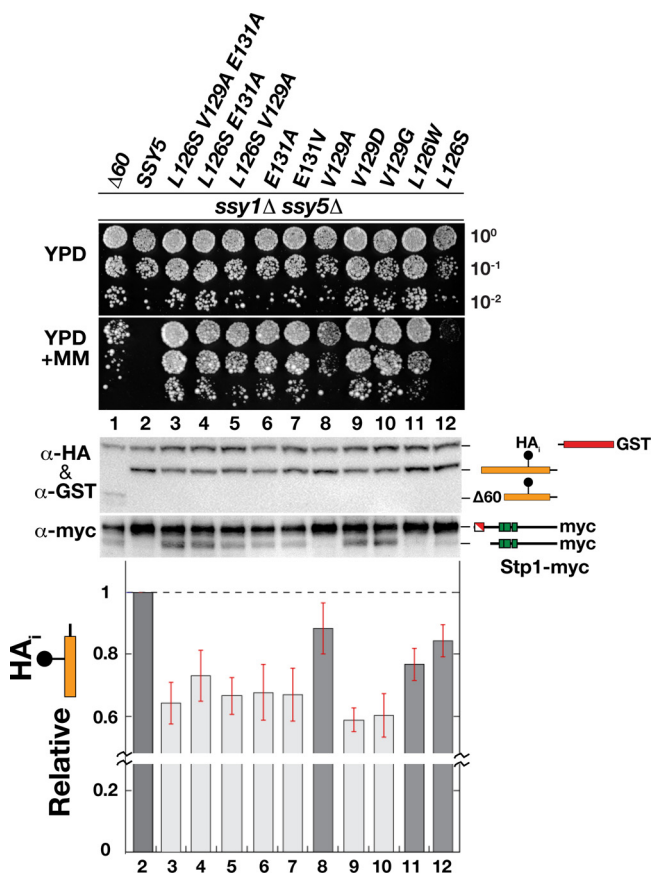


FIG. 4. Mutations decreasing prodomain levels lead to constitutive Stp1 processing. Growth of HKY84 (*ssy5Δ ssy1Δ*) carrying pCA204 (Stp1-myc) and plasmid pSH106 ($\Delta 60$), pSH120 (HA_r-Ssy5-GST), or pTP112-pTP121 expressing the indicated *SSY5* alleles. Dilutions prepared from cells pregrown in SD were spotted onto YPD and YPD plus MM. Shown is an immunoblot analysis of protein extracts prepared from the strains grown in SD. The immunoreactive forms of Ssy5 and Stp1 are schematically depicted at their corresponding positions of migration. The signal intensities of the immunoreactive bands corresponding to the HA-tagged prodomain and the GST-tagged Cat domain were quantified; the prodomain/Cat domain ratios were determined and normalized to the ratio in Ssy5 (lane 2), and mean values were plotted. Error bars show standard errors ($n = 5$). Note the break in the y axis.

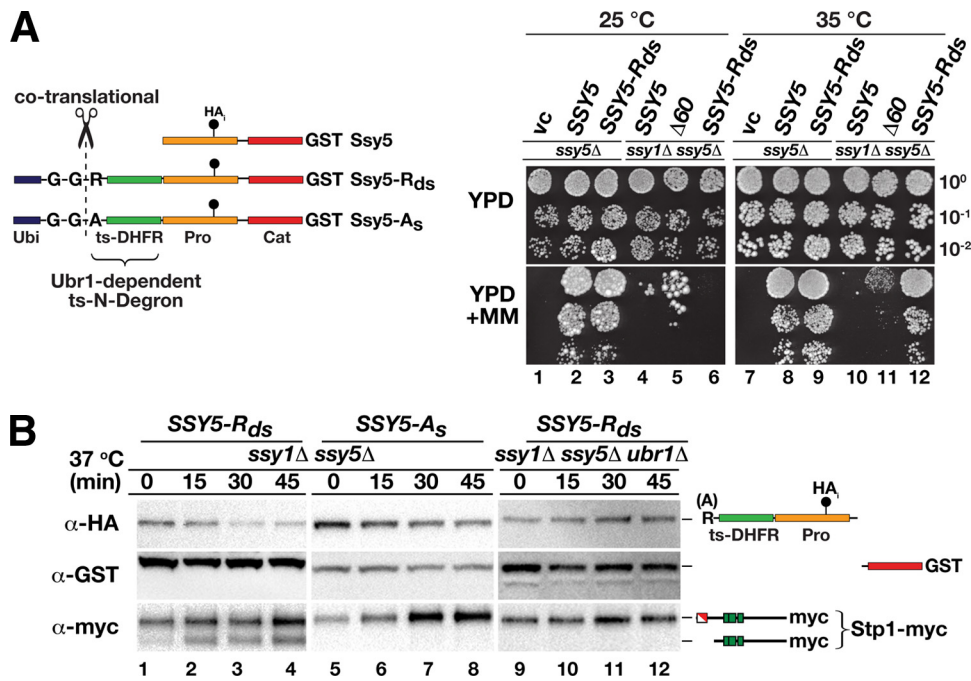


FIG. 5. Synthetic N-degron-regulated prodomain degradation results in temperature-controlled Stp1 processing. (A) Ssy5 N-degron constructs are schematically represented. The constructs have an N-terminal ubiquitin moiety (Ubi), a destabilizing arginine (R) or a stabilizing alanine (A_s) residue, and a temperature-sensitive dihydrofolate reductase (ts-DHFR) linker fused at the N terminus of Ssy5 with an internal prodomain HA epitope (HA_i) and a C-terminal GST tag. The ubiquitin is cotranslationally cleaved (scissors) following the diglycine (G-G) residues, resulting in proteins with an N-terminal arginine or alanine residue. Arginine, but not alanine, is an N-end rule substrate recognized by Ubr1. Growth of HKY77 (*ssy5 Δ) and HKY84 (*ssy5 Δ *ssy1 Δ) carrying a vector control (vc), pSH120 (SSY5), pSH106 ($\Delta 60$), or pTP110 (SSY5- R_{ds}) is shown. Cells were pregrown in SD, dilutions were prepared and spotted onto YPD and YPD plus MM, and the plates were incubated at 25 or 35°C for 6 or 3 days, respectively. pSH106 ($\Delta 60$) was used as a positive constitutive control (right panel). (B) Immunoblot analysis of protein extracts from HKY84 (*ssy5 Δ *ssy1 Δ) carrying pCA204 (Stp1-myc) and pTP110 (SSY5- R_{ds} , lanes 1 to 4) or pTP111 (SSY5- A_s , lanes 5 to 8) and from TPY101 (*ssy5 Δ *ssy1 Δ *ubr1 Δ) carrying pCA204 (Stp1-myc) and pTP110 (SSY5- R_{ds} , lanes 9 to 12). Cells were grown in SD at 25°C, cultures were shifted to 37°C at $t = 0$, and extracts were prepared from equivalent numbers of cells harvested at the indicated time points.********

wild-type level, while the weaker group II mutations reduced levels between 10 and 20%. Taken together, these results show that all constitutive mutations induce signal-independent degradation of the prodomain, and importantly, the endoproteolytic Stp1-processing activity of the Ssy5 protease is detected when low prodomain levels are observed.

Synthetically induced degradation of the prodomain is sufficient to activate Ssy5. The results of all previous experiments are consistent with the prodomain functioning as an inhibitor of Stp1-processing activity of the Cat domain after assisting its correct folding. We directly tested this notion by asking if posttranslational removal of the prodomain would suffice to activate Ssy5 protease activity. To accomplish this, we fused a temperature-regulated N-degron (15, 16, 26, 36) to the N terminus of the Ssy5 prodomain (Fig. 5A, left panel, Ssy5- R_{ds}). This N-degron is latent at 25°C but induces rapid, proteasome-dependent degradation at elevated temperatures (35 to 37°C). Importantly, the N-degron relies on the presence of a destabilizing N-terminal arginine residue (R_{ds}) that is created by cotranslational processing of appropriately fused ubiquitin. At elevated temperatures, this residue is exposed due to a temperature-induced conformational change in the linking temperature-sensitive dihydrofolate reductase moiety. The residue is then recognized by the N-end rule ubiquitin ligase Ubr1,

which leads to polyubiquitylation and proteasomal degradation (44, 49). The replacement of the N-terminal arginine with a stabilizing alanine residue (A_s), which is not recognized by Ubr1, is expected to yield a stable protein (44, 49).

When the SSY5- R_{ds} allele was introduced into an *ssy5 Δ mutant strain, it fully complemented the MM mutant growth phenotype at both 25 and 35°C (Fig. 5A, compare dilution 2 with dilution 3 and dilution 8 with dilution 9). Thus, the N-degron-containing prodomain is functional and capable of operating in the context of the other SPS sensor components. Importantly, when the SSY5- R_{ds} allele was introduced into an *ssy1 Δ *ssy5 Δ double-mutant strain, the cells did not grow at 25°C, indicating that the presence of the N-degron does not constitutively activate Stp1 processing. However, when these cells were incubated at 35°C, a temperature predicted to trigger N-degron-dependent prodomain degradation, robust growth was observed (Fig. 5A, compare dilution 6 with dilution 12). Clearly, the activity of this novel SSY5 allele is temperature regulated and functions independently of a functional SPS sensor.***

To directly test if the SSY5- R_{ds} growth phenotype was a result of temperature-induced prodomain degradation, we measured the stability of the prodomain encoded by SSY5- R_{ds} in *ssy1 Δ *ssy5 Δ double-mutant cells after shifting the temperature from 25 to 37°C by immunoblot analysis (Fig. 5B). The**

stability of the prodomain was severely reduced at the elevated temperature, and the prodomain was rapidly degraded, whereas the Cat domain remained stable (Fig. 5B, lanes 1 to 4). The reduced level of the prodomain correlated precisely with Stp1 processing. The temperature-induced degradation and Cat domain activation were fully dependent on the regulated N-degron since substitution of the destabilizing N-terminal arginine residue with the stabilizing alanine residue (Fig. 5B, lanes 5 to 8) or deletion of *UBR1* (Fig. 5B, lanes 9 to 12) prevented both prodomain degradation and Stp1 processing. These experiments unambiguously demonstrate that the prodomain functions as a potent inhibitor of the Cat domain and its degradation is sufficient for the endoproteolytic cleavage of Stp1.

DISCUSSION

According to our current understanding of RAP, the Ssy5 endoprotease is expressed as a zymogen. During biogenesis, the prodomain assists the folding of the Cat domain. Once active, the Cat domain autolytically cleaves Ssy5 between the two domains and the noncovalently associated domains remain attached, forming an inactive but primed protease that binds its substrates, Stp1 and Stp2 (3). After amino acid induction of the SPS sensor, the prodomain is degraded by the ubiquitin proteasome system, presumably as a consequence of a conformational change. Once released from its inhibitory interaction with the prodomain, the Cat domain endoproteolytically processes Stp1 and Stp2. Hence, the prodomain is required for maturation of the protease and subsequently functions as a potent inhibitor that prevents Ssy5 proteolytic activity in the absence of signaling.

Consistent with an inhibitory function, we found a tight correlation between reduced prodomain levels and Stp1 processing. This observation can be accounted for by a model in which the prodomain attains two alternative conformations, a stable inhibitory conformation and an unstable noninhibitory conformation. According to this model, the conformational switch from the inhibitory to the noninhibitory conformation is triggered by amino acid-induced signals and leads to the degradation of the prodomain by the 26S proteasome. This model predicts that the constitutive mutant alleles that result in unregulated processing of Stp1 (*SSY5**, *SSY5Δ60*, and substitution mutations in codons 126, 129, and 131) encode prodomains with properties that mimic or favor the unstable noninhibitory conformation. Indeed, the constitutive nature of these alleles was traced to one common attribute; i.e., they all exhibited decreased prodomain levels (Fig. 3 and 4). In contrast, the enhanced stability of the nonsignaling *ssy5Δ90* truncated prodomain (Fig. 3) can be explained by its being trapped in the inhibitory conformation. Hence, sequence elements responsible for the induced conformational switch of the prodomain reside N terminally of residue 90, while the basic inhibitory function of the Pro domain resides C terminally of this residue. This mapping is consistent with the observation that our isolated constitutive mutations cluster at positions 126, 129, and 131. In summary, the proposed conformational model of the activation of primed Ssy5 accounts for both the normal and the mutant behavior of this regulated protease.

The mechanisms underlying the amino acid-induced switch

of the Ssy5 prodomain from its stable inhibitory to unstable noninhibitory conformation remains elusive. Posttranslational modifications, including phosphorylation and ubiquitylation, are given candidates to function as the trigger. Notably, the casein kinase Yck1 or Yck2 (Yck1/2) is required for SPS sensor signaling. These rather promiscuous kinases have been shown to constitutively phosphorylate Stp1 and to phosphorylate Ptr3 in an amino acid-induced manner (1, 28). Hence, given the involvement of these kinases in both upstream and downstream signaling events, Ssy5 might also be a substrate during SPS sensor signaling. In several instances, Yck1/2-catalyzed phosphorylation has been shown to lead to Grr1-dependent polyubiquitylation and subsequent degradation of the modified substrates by the 26S proteasome (30, 40). Grr1 is an F-box protein of the SCF E3 ubiquitin ligase complex, which is required for transducing SPS sensor-mediated signals (5, 8). Consequently, the possibility that Yck1/2-dependent phosphorylation and Grr1-mediated ubiquitylation govern the conformation of the Pro domain, and hence its inhibitory activity, needs to be investigated.

To unambiguously test the inhibitory role of the prodomain, we synthetically reprogrammed the SPS sensing pathway by placing the degradation of the prodomain under temperature control (Fig. 5). Two experimental aspects require comment. First, at 25°C, the N-degron-containing prodomain is fully functional and capable of operating in the context of the other SPS sensor components. Thus, the presence of the N-degron does not interfere with SPS sensor function, but more importantly, the stability of the N-degron-containing prodomain remains controlled by amino acid-induced and SPS sensor-mediated signaling events. Presumably, Stp1 processing at 25°C is the result of the same conformational switch affecting the stability of the wild-type prodomain. Second, at the elevated inducing temperature, the presence of the synthetic N-degron leads to efficient Stp1 processing in the absence of a functional SPS sensor, a situation normally incompatible with Stp1 processing. Thus, similar to the constitutive active mutations that affect Pro domain stability, direct targeting of the prodomain for degradation, independently of upstream signaling events, suffices to liberate a fully competent Cat domain that processes its substrate. This result demonstrates that the critical event in the activation of primed Ssy5 is liberation of the Cat domain from prodomain inhibition.

Although N-degron-induced prodomain degradation suffices to activate the Cat domain, it remains to be elucidated whether prodomain degradation is required for Stp1 processing in the context of SPS sensor signaling. We raise this issue based on our finding that amino acid-induced processing occurs in the temperature-sensitive proteasomal *cim3-1* mutant under conditions where the prodomain exhibits clearly enhanced stability (Fig. 2C). This result, consistent with previous reports (1, 4), opens the possibility that the unstable noninhibitory Pro domain conformation has a decreased affinity for the Cat domain; its dissociation may relieve inhibition. However, rigorous interpretation of the apparent Cat domain activation in the absence of prodomain degradation is confounded by the experimental setup. Specifically, in no instance do the experimental conditions used here or in previously published work (1, 4) result in complete inhibition of the proteasome. Thus, residual proteasomal activity may still account for the observed Stp1

processing. Consequently, at this time it is impossible to evaluate the importance of direct proteasomal involvement in signaling. Regardless, in cells with a fully active ubiquitin proteasome system, amino acid-induced signaling results in reduced prodomain levels, indicating that signaling and degradation are normally coupled events.

An important characteristic of RAP is that Ssy5 autolysis, which occurs concomitantly with its biogenesis, is not sufficient to trigger Stp1 processing (3). In this respect, Ssy5 differs from classical chymotrypsin-like proteases that are most commonly activated by intermolecular proteolytic processing of an inactive zymogen precursor (32). The processing of the prodomain within the zymogen is frequently associated with a conformational change that suffices to fully activate the protease (18, 41, 45). In contrast to this established concept, Ssy5 requires a second signal-mediated activation step.

Although, to our knowledge, the mode of Ssy5 activation that we document here is unique among eukaryotic proteases, similar two-step mechanisms have been described for secreted bacterial serine proteases, e.g., the secreted bacterial protease alpha-lytic protease, a distant relative of Ssy5 (2, 34). Alpha-lytic protease is expressed with a prodomain that functions as an effective catalyst of Cat domain folding (13, 14). Similar to Ssy5, alpha-lytic protease undergoes autolysis upon Cat domain maturation. The cleaved prodomain and Cat domain of alpha-lytic protease remain strongly associated, forming a complex in which the C-shaped prodomain surrounds the beta barrel of the folded Cat domain, sterically blocking the active site. The active Cat domain is liberated from the prodomain by proteolysis in the extracellular milieu (7, 12, 20). Despite the obvious similarities between the two-step activation of Ssy5 and that of alpha-lytic protease, there is one striking difference; i.e., the Ssy5 prodomain requires a signal transduced by a plasma membrane-localized receptor complex to initiate a conformational change that triggers its degradation.

Serine proteases are involved in a variety of important physiological processes in metazoan organisms, e.g., food digestion, blood coagulation, immune response, and signal transduction. Dysregulation of the proteolytic activity of several of these proteases is linked to disease states in humans (11, 22, 31, 33, 45). A thorough understanding of the full repertoire of regulatory processes governing the function of this class of proteases, including the RAP mechanism described here, is a requisite for the development of new approaches to the beneficial modulation of protease functions. Interestingly, with respect to the central regulatory role of the prodomain of Ssy5 in RAP, the potential of targeting prodomains to engineer proteases with unique catalytic properties has been recognized (42). In line with this, we emphasize that we were able to successfully reprogram Ssy5 to control its activity by temperature. In light of the modularity and transferability of the Ssy5 recognition and cleavage site (5), such a protease is an ideal signal input device to engineer synthetic temperature-regulated signaling pathways.

ACKNOWLEDGMENTS

We thank members of the Ljungdahl laboratory for constructive comments throughout the course of this work.

This research was supported by the Swedish Research Council (P.O.L.). The Ludwig Institute for Cancer Research is gratefully acknowledged for support during the initial stages of this work.

REFERENCES

1. Abdel-Sater, F., M. El Bakkoury, A. Urrestarazu, S. Vissers, and B. André. 2004. Amino acid signaling in yeast: casein kinase I and the Ssy5 endoprotease are key determinants of endoproteolytic activation of the membrane-bound Stp1 transcription factor. *Mol. Cell. Biol.* **24**:9771–9785.
2. Andréasson, C. 2004. Ligand-activated proteolysis in nutrient signaling. Ph.D. thesis. Karolinska Institute, Stockholm, Sweden.
3. Andréasson, C., S. Heessen, and P. O. Ljungdahl. 2006. Regulation of transcription factor latency by receptor-activated proteolysis. *Genes Dev.* **20**:1563–1568.
4. Andréasson, C., and P. O. Ljungdahl. 2002. Receptor-mediated endoproteolytic activation of two transcription factors in yeast. *Genes Dev.* **16**:3158–3172.
5. Andréasson, C., and P. O. Ljungdahl. 2004. The N-terminal regulatory domain of Stp1p is modular and, fused to an artificial transcription factor, confers full Ssy1p-Ptr3p-Ssy5p sensor control. *Mol. Cell. Biol.* **24**:7503–7513.
6. Antebi, A., and G. R. Fink. 1992. The yeast Ca(2+)-ATPase homologue, PMR1, is required for normal Golgi function and localizes in a novel Golgi-like distribution. *Mol. Biol. Cell.* **3**:633–654.
7. Baker, D., J. L. Silen, and D. A. Agard. 1992. Protease pro region required for folding is a potent inhibitor of the mature enzyme. *Proteins* **12**:339–344.
8. Bernard, F., and B. André. 2001. Ubiquitin and the SCF(Grr1) ubiquitin ligase complex are involved in the signalling pathway activated by external amino acids in *Saccharomyces cerevisiae*. *FEBS Lett.* **496**:81–85.
9. Brivanlou, A. H., and J. E. Darnell, Jr. 2002. Signal transduction and the control of gene expression. *Science* **295**:813–818.
10. Brown, M. S., J. Ye, R. B. Rawson, and J. L. Goldstein. 2000. Regulated intramembrane proteolysis: a control mechanism conserved from bacteria to humans. *Cell* **100**:391–398.
11. Coughlin, S. R. 2000. Thrombin signalling and protease-activated receptors. *Nature* **407**:258–264.
12. Cunningham, E. L., and D. A. Agard. 2004. Disabling the folding catalyst is the last critical step in alpha-lytic protease folding. *Protein Sci.* **13**:325–331.
13. Cunningham, E. L., and D. A. Agard. 2003. Interdependent folding of the N- and C-terminal domains defines the cooperative folding of alpha-lytic protease. *Biochemistry* **42**:13212–13219.
14. Cunningham, E. L., T. Mau, S. M. Truhlar, and D. A. Agard. 2002. The pro region N-terminal domain provides specific interactions required for catalysis of alpha-lytic protease folding. *Biochemistry* **41**:8860–8867.
15. Dohmen, R. J., and A. Varshavsky. 2005. Heat-inducible degron and the making of conditional mutants. *Methods Enzymol.* **399**:799–822.
16. Dohmen, R. J., P. Wu, and A. Varshavsky. 1994. Heat-inducible degron: a method for constructing temperature-sensitive mutants. *Science* **263**:1273–1276.
17. Eckert-Boulet, N., B. Regenber, and J. Nielsen. 2005. Grr1p is required for transcriptional induction of amino acid permease genes and proper transcriptional regulation of genes in carbon metabolism of *Saccharomyces cerevisiae*. *Curr. Genet.* **47**:139–149.
18. Eder, J., and A. R. Fersht. 1995. Pro-sequence-assisted protein folding. *Mol. Microbiol.* **16**:609–614.
19. Forsberg, H., and P. O. Ljungdahl. 2001. Genetic and biochemical analysis of the yeast plasma membrane Ssy1p-Ptr3p-Ssy5p sensor of extracellular amino acids. *Mol. Cell. Biol.* **21**:814–826.
20. Fuhrmann, C. N., B. A. Kelch, N. Ota, and D. A. Agard. 2004. The 0.83 Å resolution crystal structure of alpha-lytic protease reveals the detailed structure of the active site and identifies a source of conformational strain. *J. Mol. Biol.* **338**:999–1013.
21. Ghislain, M., A. Udvardy, and C. Mann. 1993. *S. cerevisiae* 26S protease mutants arrest cell division in G₂/metaphase. *Nature* **366**:358–362.
22. Hedstrom, L. 2002. An overview of serine proteases. *Curr. Protoc. Protein Sci.* Chapter 21:Unit 11.10.
23. Hoppe, T., K. Matuschewski, M. Rape, S. Schlenker, H. D. Ulrich, and S. Jentsch. 2000. Activation of a membrane-bound transcription factor by regulated ubiquitin/proteasome-dependent processing. *Cell* **102**:577–586.
24. Hoppe, T., M. Rape, and S. Jentsch. 2001. Membrane-bound transcription factors: regulated release by RIP or RUP. *Curr. Opin. Cell Biol.* **13**:344–348.
25. Jørgensen, M. U., M. B. Bruun, T. Didion, and M. C. Kielland-Brandt. 1998. Mutations in five loci affecting GAPI-independent uptake of neutral amino acids in yeast. *Yeast* **14**:103–114.
26. Kanemaki, M., A. Sanchez-Diaz, A. Gambus, and K. Labib. 2003. Functional proteomic identification of DNA replication proteins by induced proteolysis in vivo. *Nature* **423**:720–724.
27. Klasson, H., G. R. Fink, and P. O. Ljungdahl. 1999. Ssy1p and Ptr3p are plasma membrane components of a yeast system that senses extracellular amino acids. *Mol. Cell. Biol.* **19**:5405–5416.
28. Liu, Z., J. Thornton, M. Spirek, and R. A. Butow. 2008. Activation of the SPS amino acid-sensing pathway in *Saccharomyces cerevisiae* correlates with the

- phosphorylation state of a sensor component, *Ptr3*. *Mol. Cell. Biol.* **28**:551–563.
29. **Ljungdahl, P. O.** 2009. Amino-acid-induced signalling via the SPS-sensing pathway in yeast. *Biochem. Soc. Trans.* **37**:242–247.
 30. **Moriya, H., and M. Johnston.** 2004. Glucose sensing and signaling in *Saccharomyces cerevisiae* through the Rgt2 glucose sensor and casein kinase I. *Proc. Natl. Acad. Sci. U. S. A.* **101**:1572–1577.
 31. **Neurath, H.** 1984. Evolution of proteolytic enzymes. *Science* **224**:350–357.
 32. **Neurath, H., and G. H. Dixon.** 1957. Structure and activation of trypsinogen and chymotrypsinogen. *Fed. Proc.* **16**:791–801.
 33. **Page, M. J., R. T. Macgillivray, and E. Di Cera.** 2005. Determinants of specificity in coagulation proteases. *J. Thromb. Haemost.* **3**:2401–2408.
 34. **Poulsen, P., L. Lo Leggio, and M. C. Kielland-Brandt.** 2006. Mapping of an internal protease cleavage site in the Ssy5p component of the amino acid sensor of *Saccharomyces cerevisiae* and functional characterization of the resulting pro- and protease domains by gain-of-function genetics. *Eukaryot. Cell* **5**:601–608.
 35. **Poulsen, P., B. Wu, R. F. Gaber, K. Ottow, H. A. Andersen, and M. C. Kielland-Brandt.** 2005. Amino acid sensing by Ssy1. *Biochem. Soc. Trans.* **33**:261–264.
 36. **Sanchez-Diaz, A., M. Kanemaki, V. Marchesi, and K. Labib.** 2004. Rapid depletion of budding yeast proteins by fusion to a heat-inducible degron. *Sci. STKE* **2004**:PL8.
 37. **Schork, S. M., M. Thumm, and D. H. Wolf.** 1995. Catabolite inactivation of fructose-1,6-bisphosphatase of *Saccharomyces cerevisiae*. Degradation occurs via the ubiquitin pathway. *J. Biol. Chem.* **270**:26446–26450.
 38. **Schüle, T., M. Rose, K. D. Entian, M. Thumm, and D. H. Wolf.** 2000. Ubc8p functions in catabolite degradation of fructose-1,6-bisphosphatase in yeast. *EMBO J.* **19**:2161–2167.
 39. **Silve, S., C. Volland, C. Garnier, R. Jund, M. R. Chevallier, and R. Haguenaue-Tsapis.** 1991. Membrane insertion of uracil permease, a polytopic yeast plasma membrane protein. *Mol. Cell. Biol.* **11**:1114–1124.
 40. **Spielewoy, N., K. Flick, T. I. Kalashnikova, J. R. Walker, and C. Wittenberg.** 2004. Regulation and recognition of SCFGrr1 targets in the glucose and amino acid signaling pathways. *Mol. Cell. Biol.* **24**:8994–9005.
 41. **Stroud, R. M., A. A. Kossiakoff, and J. L. Chambers.** 1977. Mechanisms of zymogen activation. *Annu. Rev. Biophys. Bioeng.* **6**:177–193.
 42. **Takagi, H., and M. Takahashi.** 2003. A new approach for alteration of protease functions: pro-sequence engineering. *Appl. Microbiol. Biotechnol.* **63**:1–9.
 43. **Thomas, B. J., and R. Rothstein.** 1989. Elevated recombination rates in transcriptionally active DNA. *Cell* **56**:619–630.
 44. **Varshavsky, A.** 2008. The N-end rule at atomic resolution. *Nat. Struct. Mol. Biol.* **15**:1238–1240.
 45. **Whitcomb, D. C., and M. E. Lowe.** 2007. Human pancreatic digestive enzymes. *Dig. Dis. Sci.* **52**:1–17.
 46. **Wielemans, K., C. Jean, S. Vissers, and B. André.** 2010. Amino acid signaling in yeast: post-genome duplication divergence of the Stp1 and Stp2 transcription factors. *J. Biol. Chem.* **285**:855–865.
 47. **Wilson, D. S., and A. D. Keefe.** 2001. Random mutagenesis by PCR. *Curr. Protoc. Mol. Biol.* **Chapter 8**:Unit 8.3.
 48. **Wu, B., K. Ottow, P. Poulsen, R. F. Gaber, E. Albers, and M. C. Kielland-Brandt.** 2006. Competitive intra- and extracellular nutrient sensing by the transporter homologue Ssy1p. *J. Cell Biol.* **173**:327–331.
 49. **Xia, Z., A. Webster, F. Du, K. Piatkov, M. Ghislain, and A. Varshavsky.** 2008. Substrate-binding sites of UBR1, the ubiquitin ligase of the N-end rule pathway. *J. Biol. Chem.* **283**:24011–24028.

A phosphodegron controls nutrient-induced proteasomal activation of the signaling protease Ssy5

Deike J. Omnus*, Thorsten Pfirrmann*, Claes Andréasson, and Per O. Ljungdahl

Wenner-Gren Institute, Stockholm University, S-106 91 Stockholm, Sweden

ABSTRACT Regulated proteolysis serves as a mechanism to control cellular processes. The SPS (Ssy1-Ptr3-Ssy5) sensor in yeast responds to extracellular amino acids by endoproteolytically activating transcription factors Stp1 and Stp2 (Stp1/2). The processing endoprotease Ssy5 is regulated via proteasomal degradation of its noncovalently associated N-terminal prodomain. We find that degradation of the prodomain requires a conserved phosphodegron comprising phosphoacceptor sites and ubiquitin-accepting lysine residues. Upon amino acid induction, the phosphodegron is modified in a series of linked events by a set of general regulatory factors involved in diverse signaling pathways. First, an amino acid-induced conformational change triggers phosphodegron phosphorylation by the constitutively active plasma membrane-localized casein kinase I (Yck1/2). Next the prodomain becomes a substrate for polyubiquitylation by the Skp1/Cullin/Grr1 E3 ubiquitin ligase complex (SCF^{Grr1}). Finally, the modified prodomain is concomitantly degraded by the 26S proteasome. These integrated events are requisite for unfettering the Ssy5 endoprotease, and thus Stp1/2 processing. The Ssy5 phosphoacceptor motif resembles the Yck1/2- and Grr1-dependent degrons of regulators in the Snf3/Rgt2 glucose-sensing pathway. Our work defines a novel proteolytic activation cascade that regulates an intracellular signaling protease and illustrates how general signaling components are recruited to distinct pathways that achieve conditional and specific signaling outputs.

Monitoring Editor
Thomas D. Fox
Cornell University

Received: Apr 1, 2011
Revised: May 24, 2011
Accepted: May 28, 2011

INTRODUCTION

Regulated proteolysis serves as an important mechanism used to control many cellular processes, including the separation of chromosomes during cell division and modulation of gene expression in response to environmentally induced signals (Brivanlou and Darnell,

2002; Nasmyth, 2005). Proteolysis can result in the complete degradation of proteins, and site-specific endoproteolytic processing events can generate proteolytic fragments with altered biological activities. Paradoxically, protein degradation can have activating functions. For example, degradation of an autoinhibitory domain or regulatory inhibitory subunit within a protein complex can liberate an intrinsic catalytic activity. Understanding the mechanisms governing regulated proteolysis is an important task in cell biology.

The SPS (Ssy1-Ptr3-Ssy5) signaling pathway enables yeast cells to respond to the presence of extracellular amino acids and induce their uptake (Forsberg and Ljungdahl, 2001). By studying this signal transduction pathway, we and others have unraveled a proteolytic mechanism responsible for the activation of the two homologous transcription factors Stp1 and Stp2 by receptor-activated proteolysis (RAP) (Andréasson and Ljungdahl, 2002; Andréasson *et al.*, 2006; Pfirrmann *et al.*, 2010). According to our current understanding of RAP and the signaling events carried out by the SPS sensor, extracellular amino acids are detected at the plasma membrane by the receptor Ssy1. Amino acid binding stabilizes a conformation of Ssy1

This article was published online ahead of print in MBoc in Press (<http://www.molbiolcell.org/cgi/doi/10.1091/mbc.E11-04-0282>) on June 8, 2011.

*These authors contributed equally to the work.

Address correspondence to: Per O. Ljungdahl (plju@wgi.su.se).

Abbreviations used: CHX, cycloheximide; HA, hemagglutinin; HRP, horseradish peroxidase; MM, (2-(((4-methoxy-6-methyl)-1,3,5-triazin-2-yl)-amino)carbonyl)amino-]-sulfonyl)-benzoic acid; RAP, receptor-activated proteolysis; SC, synthetic complete dextrose; SCF, Skp1/Cdc53/F-box protein; SD, synthetic minimal dextrose; SPS, Ssy1-Ptr3-Ssy5; TCA, trichloroacetic acid; WT, wild type; YPD, yeast extract-peptone-dextrose.

© 2011 Omnus *et al.* This article is distributed by The American Society for Cell Biology under license from the author(s). Two months after publication it is available to the public under an Attribution-Noncommercial-Share Alike 3.0 Unported Creative Commons License (<http://creativecommons.org/licenses/by-nc-sa/3.0>). "ASCB®," "The American Society for Cell Biology®," and "Molecular Biology of the Cell®" are registered trademarks of The American Society of Cell Biology.

that, together with the peripheral membrane protein Ptr3, activates the Ssy5 endoprotease (Klasson *et al.*, 1999; Abdel-Sater *et al.*, 2004; Andréasson *et al.*, 2006; Wu *et al.*, 2006). On activation, Ssy5 processes transcription factors Stp1 and Stp2, resulting in the removal of N-terminal sequences required for cytoplasmic retention. Consequently, processed Stp1 and Stp2 can enter the nucleus, bind promoters of genes encoding a set of broad specificity amino acid permeases, and activate transcription (Andréasson and Ljungdahl, 2002, 2004; Wielemans *et al.*, 2010; Tumusiime *et al.*, 2011). The molecular mechanisms underlying RAP, and therefore the activation of the Ssy5 endoprotease activation, are under intense study.

The RAP-activated endoprotease Ssy5 exhibits homology to chymotrypsin-like serine proteases and is expressed as an inactive precursor in the form of a zymogen. Directly after translation and folding, Ssy5 cleaves itself into an N-terminal prodomain and a C-terminal catalytic (Cat)-domain. Strikingly, the N-terminal prodomain remains associated with the Cat-domain forming a primed but inactive protease subcomplex of the SPS sensor that is associated with Stp1 and Stp2 (Andréasson *et al.*, 2006; Poulsen *et al.*, 2006). On amino acid induction, the prodomain is degraded by the 26S proteasome and the Cat-domain is able to process Stp1 and Stp2. Removal of the prodomain by synthetically inducing its proteasomal degradation activates the protease in a manner that bypasses the requirement of the other SPS sensor components. These findings unambiguously demonstrate that the prodomain functions as an inhibitory subunit of the SPS sensor (Pfirrmann *et al.*, 2010).

Consistent with an inhibitory function of the prodomain, a tight inverse correlation exists between prodomain levels and Stp1 processing. We have previously proposed a model in which the prodomain attains two alternative conformations, a stable inhibitory conformation and an unstable noninhibitory conformation. According to this model, extracellular amino acids trigger events leading to a conformational switch from the inhibitory to the noninhibitory conformation. The first 130 amino acids of the N-terminal prodomain are essential for proper regulation of this conformational switch. Several mutations in this region destabilize the prodomain independent of Ssy1 and constitutively activate Stp1 processing. Conversely, even though the intrinsic activity of the Cat-domain remains intact, mutations that interfere with prodomain degradation prevent Stp1 processing. Together these observations suggest that the crucial event of the RAP mechanism is the proteasomal degradation of the prodomain (Pfirrmann *et al.*, 2010).

Canonical 26S proteasomal degradation relies on polyubiquitylation of target lysine residues in the substrate that labels the protein for proteolysis. In this process a set of enzymes is required to generally activate (E1), conjugate (E2), and specifically ligate (E3) the ubiquitin modifier to the substrate or its growing polyubiquitin chain (Wolf, 2004). Hence, proteasomal degradation of the Ssy5 prodomain likely involves a specific E3 ubiquitin ligase that mediates polyubiquitylation of the prodomain in response to SPS signaling. A candidate is the general Skp1/Cdc53/F-box protein (SCF) complex, an E3 ubiquitin ligase that is required for Ssy5 activation (Iraqi *et al.*, 1999; Bernard and André, 2001; Abdel-Sater *et al.*, 2004, 2011; Andréasson *et al.*, 2006). SCF complexes achieve substrate specificity through association with exchangeable F-box proteins that enable specific binding and subsequent polyubiquitylation of target proteins (Jonkers and Rep, 2009). Grr1 is one of the best-characterized F-box proteins in yeast, and Grr1 is known to recognize and bind phosphorylated substrates. Notably, several proteins have been found to be inducibly phosphorylated by casein kinase I, Yck1, or Yck2, leading to their SCF^{Grr1}-dependent proteasomal degradation (Moriya and Johnston, 2004; Spielewoy *et al.*, 2010). Both

Yck1/2 and SCF^{Grr1} are required for SPS sensor signaling (Abdel-Sater *et al.*, 2004, 2011; Spielewoy *et al.*, 2004), and importantly, Grr1 is required for prodomain down-regulation (Andréasson *et al.*, 2006; Abdel-Sater *et al.*, 2011).

Recently, Abdel-Sater *et al.* proposed that Yck1/2- and SCF^{Grr1}-dependent polyubiquitylation of the Ssy5 prodomain induces a conformational change that activates Ssy5. According to their model, the degradation of the Ssy5 prodomain is not the activating step, but a secondary event (Abdel-Sater *et al.*, 2011). Discrepancies between this hypothesis and our RAP model, in which proteasomal degradation of the prodomain is crucial, required that we independently evaluate the role of the general signaling components Yck1/2 and SCF^{Grr1} and their function in facilitating signaling. In contrast to the Abdel-Sater hypothesis, our results delineate a novel proteolytic activation cascade that ultimately transduces amino acid-induced signals through the proteasomal degradation of the inhibitory prodomain. At the heart of this mechanism is the activation of an intrinsic phosphodegron, which strikingly resembles the Yck1/2- and Grr1-dependent degrons required for the degradation of transcriptional regulators in the Snf3/Rgt2 glucose-sensing pathway (Moriya and Johnston, 2004). Our work provides a paradigm illustration of how general signaling factors are recruited to distinct pathways that achieve conditional and specific signaling outputs.

RESULTS

Casein kinase I activity is required for amino acid-induced degradation of the Ssy5 prodomain

Casein kinase I (Yck1/2) function is required for Ssy5 activation and prodomain phosphorylation (Abdel-Sater *et al.*, 2011). According to our RAP model, amino acid-induced protease activation is triggered by prodomain degradation (Andréasson *et al.*, 2006; Pfirrmann *et al.*, 2010). Consequently, we set out to test if Yck1/2 activity is required for degradation of the Ssy5 prodomain. We compared prodomain levels in amino acid (leucine)-induced wild-type (WT) cells and in *yck1Δ yck2-1* cells with conditional temperature-sensitive casein kinase I activity. Consistent with our previous findings, in WT cells, leucine induced the degradation of the well-characterized and fully functional HA-tagged prodomain (Ssy5-HA_i) (Pfirrmann *et al.*, 2010). A clear reduction in prodomain levels was observed already 15 min after induction, which strictly correlated in time with Stp1 processing (Figure 1A, lanes 1–4). In contrast, in *yck1Δ yck2-1* cells, induction with leucine did not lead to reduced prodomain levels or Stp1 processing (Figure 1A, lanes 5–8). Our results indicate that Yck1/2 act upstream of Ssy5 in the SPS signaling pathway, possibly by directly phosphorylating the prodomain for the induction of its degradation.

SCF^{Grr1} mediates the degradation of phosphorylated prodomain

On SPS sensor induction, Ssy5 prodomain accumulates as a phosphorylated form in *grr1Δ* cells (Abdel-Sater *et al.*, 2011). To test whether this posttranslational modification is linked to prodomain degradation, we examined prodomain levels after leucine addition in a time-course experiment in the presence of the translation inhibitor cycloheximide (CHX). In contrast to WT cells, the prodomain levels were stable in *grr1Δ* cells, and no Stp1 processing was evident (Figure 1B). In extracts prepared from *grr1Δ* cells, a higher-molecular-weight species of the prodomain was detected. The modified prodomain was not detected in extracts from WT cells, indicating that it is rapidly degraded. Formation of the modified prodomain was dependent on SPS sensor signaling because it did not appear in *ssy1Δ grr1Δ* cells, which lack the amino acid receptor

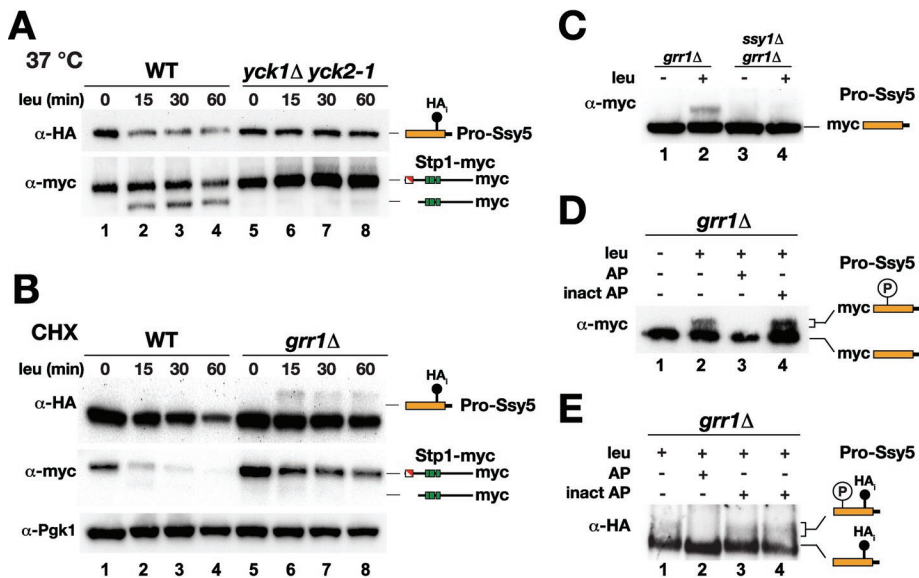


FIGURE 1: Casein kinase I and Grr1 are required for amino acid-induced degradation of the Ssy5 prodomain. (A) Immunoblot analysis of cell extracts from HKY77 (*ssy5Δ YCK1 YCK2*) (WT) and CAY320 (*yck1Δ yck2-1*) carrying pSH120 (HA₃-SSY5-GST) and pCA204 (STP1-MYC). Cells were pregrown in SD medium at room temperature and incubated at 37°C for 30 min, then samples were taken at the indicated time points after leucine addition. (B) Immunoblot analysis of cell extracts from HKY77 (*ssy5Δ*) and CAY276 (*ssy5Δ grr1Δ*) carrying plasmids as in (A); extracts were prepared from cells grown in SD medium after the addition of CHX and leucine at the indicated time points. (C) Immunoblot analysis of extracts from CAY86 (*grr1Δ*) and CAY267 (*ssy1Δ grr1Δ*) carrying pHK048 (MYC-SSY5) with (+) or without (–) leucine induction. (D) Immunoblot analysis of immunoprecipitated prodomain from extracts from cultures of CAY276 (*ssy5Δ grr1Δ*) carrying pHK048 (MYC-SSY5) and pRS317 induced with leucine as indicated. Immunoprecipitated material was incubated with active (AP) or heat-inactivated (inact AP) alkaline phosphatase as indicated. (E) Immunoblot analysis of immunoprecipitated prodomain from extracts obtained from CAY276 (*ssy5Δ grr1Δ*) carrying pSH120 (HA₃-SSY5-GST) and pCA204 (STP1-MYC). Immunoprecipitated material was treated with active (AP), heat (lane 3), or EDTA (lane 4) inactivated alkaline phosphatase (inact AP). Immunoreactive forms of phosphorylated and dephosphorylated Ssy5 prodomain and Stp1 are schematically represented at their corresponding positions of migration.

component of the SPS sensor (Figure 1C). We tested whether the modified prodomain was phosphorylated. Functional HA₃- and myc-epitope-tagged Ssy5 were immunoprecipitated from extracts prepared from leucine-induced *grr1Δ* cells. Incubation with protein phosphatase resulted in the disappearance of the slower migrating species, indicating that the aberrant migration induced by leucine was indeed due to phosphorylation (Figure 1, D and E).

Importantly, under no circumstances did we detect phosphorylated prodomain in extracts prepared from WT cells. Thus the accumulation of phosphorylated prodomain appears to be restricted to *grr1Δ* cells, suggesting that SCF^{Grr1} is involved in degradation of the phosphorylated prodomain upon signaling. This experimental evidence, and the fact that Yck1/2 are required for prodomain degradation, led us to predict two coupled and amino acid-induced events: first, Yck1/2 directly phosphorylate the prodomain, and second, Grr1 specifically and physically interacts with the phosphorylated prodomain to catalyze its ubiquitylation, creating a signal for prodomain degradation.

Spatial proximity of Yck1 to Ssy5 constitutively activates the protease

We set out to test our first prediction that Yck1/2 directly phosphorylate the prodomain. We reasoned that the spatial proximity of the kinase to its potential substrate Ssy5 might positively modulate pathway activation, and we investigated the effect of fusing Yck1 to

the C terminus of Ssy5. A chimeric Ssy5-Yck1 protein lacking the two C-terminal cysteine residues of Yck1 was constructed; these cysteines normally serve as sites for palmitoylation that anchors the kinase to the plasma membrane (Vancura et al., 1994). To test whether Ssy5-Yck1 bypasses the requirement of upstream signaling components, and thus exhibits constitutive signaling characteristics, the chimera was expressed in an *ssy1Δ ptr3Δ ssy5Δ* strain. This strain lacks a functional SPS pathway and therefore has a severe defect in amino acid uptake and cannot grow on yeast extract-peptone-dextrose (YPD) medium containing MM (2-[[[[(4-methoxy-6-methyl)-1,3,5-triazin-2-yl]amino]carbonyl]amino]-sulfonyl]-benzoic acid), an inhibitor of branched-chain amino acid synthesis (Jørgensen et al., 1998). Whereas cells expressing WT SSY5 did not grow, we found that cells expressing SSY5-YCK1 grew robustly and similar to cells expressing SSY5*, encoding a well-characterized constitutively active form of Ssy5 (Figure 2A, compare lanes 1, 2, and 3) (Andréasson et al., 2006; Pfirrmann et al., 2010). The constitutive activity of Ssy5-Yck1 was dependent on the kinase activity of the chimeric protein, because a kinase-inactivating K98R mutation (SSY5-yck1) in the ATP binding domain of Yck1 (Wang et al., 1992; Moriya and Johnston, 2004) abolished growth on YPD+MM (Figure 2A, lane 4). Importantly, in the context of an intact SPS sensor, the Ssy5 protease moiety encoded by the kinase-defective SSY5-yck1 allele was fully capable

of mediating SPS pathway signaling (Figure 2A, lane 5), which indicates that the K98R mutation does not generally impair Ssy5 function.

To elucidate the mechanism underlying the constitutive activity of Ssy5-Yck1, we monitored Stp1 processing and prodomain levels in *ssy1Δ ptr3Δ ssy5Δ* cells expressing Ssy5-Yck1. As expected, the constitutive activity of Ssy5-Yck1 correlated with Stp1 processing. Remarkably, the prodomain levels in these cells were so low that the signal was below the detection limit (Figure 2B, lanes 3 and 4). The absence of detectable prodomain was dependent on the kinase activity of the fusion protein; readily detectable levels of prodomain were obtained in extracts from cells expressing the SSY5-yck1 allele (Figure 2B, lanes 5 and 6).

These results show that the mere placement of Yck1 kinase activity in physical proximity to Ssy5 triggers efficient degradation of the prodomain, resulting in constitutive Stp1 processing. This finding suggests that, on SPS sensor induction, Yck1/2 directly phosphorylate the Ssy5 prodomain, triggering its degradation and thus protease activation.

Constitutively phosphorylated Ssy5 requires Grr1 for its activity

The fact that phosphorylated prodomain of Ssy5-Yck1 was efficiently degraded led us to examine whether the constitutive activity of this chimera was dependent on SCF^{Grr1} ubiquitylation. If so, we

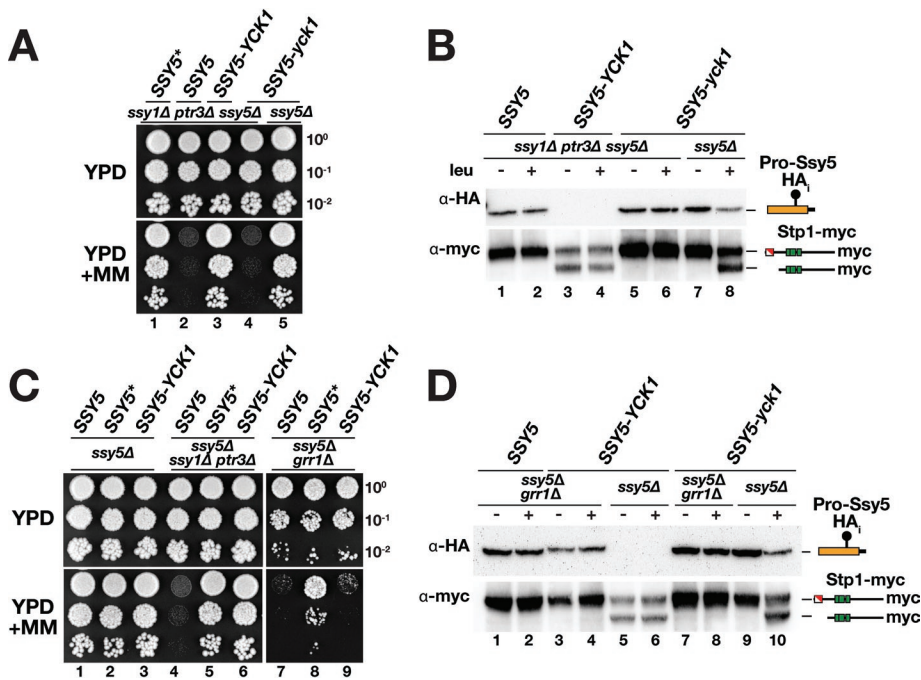


FIGURE 2: Fusion of Yck1 to the C terminus of Ssy5 constitutively activates the protease. (A) Plasmids pCA195 (SSY5*), pSH120 (SSY5), pDO100 (SSY5-YCK1), and pDO099 (SSY5-yck1) were introduced into CAY285 (*ssy1Δ ptr3Δ ssy5Δ*) or HKY77 (*ssy5Δ*) together with pCA204 (STP1-MYC). Dilutions of cultures were spotted onto YPD and YPD+MM, then plates were incubated at 30°C for 2–3 d and photographed. (B) Immunoblot analysis of cell extracts from strains in (A) induced with leucine as indicated. (C) Plasmids pSH120 (SSY5), pCA195 (SSY5*), and pDO100 (SSY5-YCK1) were introduced into HKY77 (*ssy5Δ*), CAY285 (*ssy1Δ ptr3Δ ssy5Δ*), and CAY276 (*ssy5Δ grr1Δ*) together with pCA204 (STP1-MYC). Dilutions of cultures were spotted onto YPD and YPD+MM. (D) Immunoblot analysis of cell extracts from strains in (C) and strains HKY77 (*ssy5Δ*) and CAY276 (*ssy5Δ grr1Δ*) carrying pDO099 (SSY5-yck1) and pCA204 (STP1-MYC) induced with leucine as indicated. The immunoreactive forms of the Ssy5 prodomain and Stp1 are schematically depicted at their corresponding positions of migration.

expected that the constitutive activity of the Ssy5-Yck1 chimera would require *GRR1*. This notion was tested by monitoring SPS sensor-dependent growth of *grr1Δ ssy5Δ* cells expressing the SSY5, SSY5*, or SSY5-YCK1 allele. In contrast to cells expressing the fully constitutive and *GRR1*-independent Ssy5*, cells expressing Ssy5-Yck1 did not grow on YPD+MM (Figure 2C, dilution series 8 and 9). Subsequent immunoblot analysis revealed that the prodomain was stable and readily detected in *grr1Δ* cells (Figure 2D, lanes 3 and 4). Consistent with an inhibitory function of the prodomain, Stp1 was not processed in these cells (Figure 2D, lanes 3 and 4). These findings indicate that SCF^{Grr1} is required for activation of Ssy5-Yck1, presumably by targeting the prodomain for rapid degradation by a mechanism that relies on ubiquitylation of the phosphorylated prodomain. Our results clearly place Grr1 downstream of Ssy1-, Ptr3-, and Yck1/2-dependent phosphorylation of Ssy5 in the SPS signaling pathway.

Grr1 physically interacts with induced Ssy5 and catalyzes prodomain polyubiquitylation

Grr1 is required for amino acid-induced prodomain degradation (Andréasson *et al.*, 2006), and it has recently been shown that the prodomain undergoes *GRR1*-dependent polyubiquitylation upon SPS sensor induction (Abdel-Sater *et al.*, 2011). Based on this knowledge, we posited and tested the possibility that Grr1 directly mediates SCF^{Grr1}-complex-dependent polyubiquitylation and degradation of the phosphorylated prodomain. First, using our strains and

characterized epitope-tagged Ssy5 proteins, we confirmed that the prodomain was polyubiquitylated in an amino acid-induced and *GRR1*-dependent manner (Figure 3A). Next we sought evidence for the requisite physical interaction between Ssy5 and Grr1. We used a directed yeast two-hybrid approach to overcome limitations associated with coimmunoprecipitation approaches (i.e., difficulties to detect low abundance Grr1 and Ssy5) and the anticipated transient nature of their interaction. We examined the ability of WT Ssy5 and Ssy5-L126S V129A E131A, a mutant protein that exhibits Ssy1-independent constitutive signaling properties (Pfirrmann *et al.*, 2010), to interact with Grr1. Although Grr1 did not interact with WT Ssy5, we found that constitutively active Ssy5-L126S V129A E131A interacted efficiently with Grr1, as scored by the robust growth on medium selective for expression of the two-hybrid interaction reporters (Figure 3C). These findings suggest that Grr1 binds directly to an induced form of Ssy5, mediating its polyubiquitylation.

SPS sensor induction triggers the prodomain to switch to a signaling conformation that undergoes phosphorylation-dependent proteasomal degradation

Our ability to detect a direct physical interaction between Ssy5-L126S V129A E131A and Grr1, and the fact that this mutant protein exhibits constitutively down-regulated levels of its prodomain (Pfirrmann *et al.*, 2010), led us to hypothesize that this constitutive Ssy5 mutant adopts a prodomain conformation that attracts Yck1/2 phosphorylation and subsequent SCF^{Grr1}-dependent ubiquitylation. We examined whether the constitutive activity of Ssy5-L126S V129A E131A was SCF^{Grr1}-dependent by monitoring growth on YPD+MM of *grr1Δ ssy5Δ* cells expressing this mutant protein. We found a strict requirement for Grr1 activity for growth and Stp1 processing (Figure 3D, compare dilution series/lanes 5 and 8). In contrast, control cells expressing the *GRR1*-independent and constitutive SSY5* allele exhibited robust growth in the presence of MM, and, accordingly, Stp1 processing was observed.

The requirement for an intact SCF^{Grr1} ubiquitin ligase complex raised the possibility that the activity of constitutive Ssy5 mutant proteins require Yck1/2 function in an event that would obligatorily precede ubiquitylation. We have previously described the isolation of several constitutive mutant alleles affecting the prodomain of SSY5, all carrying mutations in a sequence stretch coding for a short conserved motif around amino acid residue 130 (Figure 3B) (Pfirrmann *et al.*, 2010). The constitutive single point mutant SSY5-E131A allele that exhibits *GRR1*-dependent growth in the presence of MM (Figure 3E) was used to examine Yck1/2 involvement. The constitutive Stp1 processing activity of the Ssy5-E131A mutant was dependent on Yck1/2 activity (Figure 3G). Taken together, our findings indicate that a single point mutation in a conserved residue of the prodomain activates the Ssy5 protease independently of amino acid-induced signals and upstream SPS sensor component Ssy1,

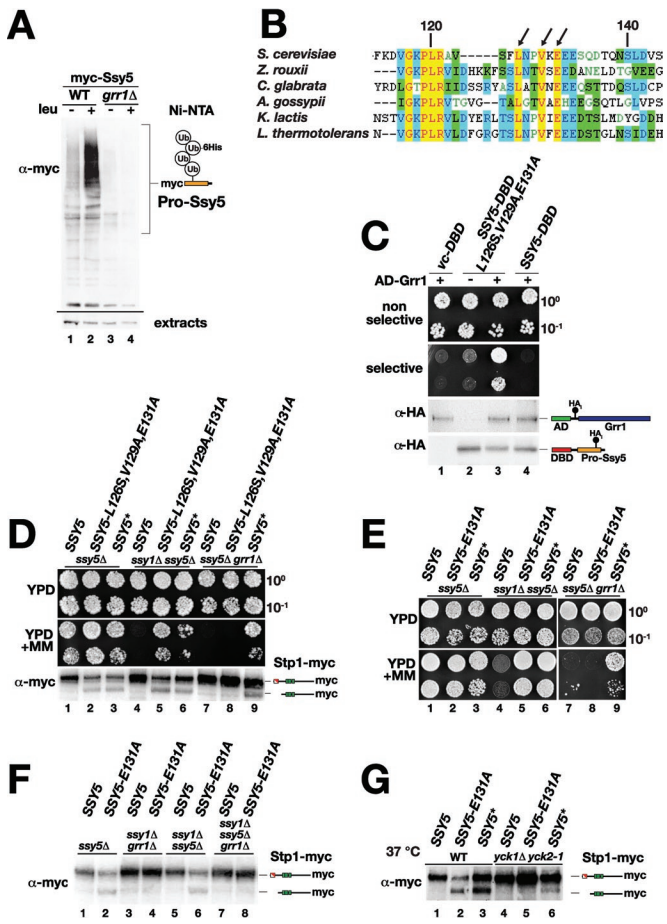


FIGURE 3: Grr1 physically interacts with Ssy5 and catalyzes its polyubiquitylation. (A) Immunoblot analysis of polyubiquitylated prodomain present in extracts from strains TPY116 (WT) and TPY117 (*grr1Δ*) carrying plasmids pHK048 (MYC-SSY5) and pTP156 (PCUP1-6His-UBI) induced with leucine as indicated. The immunoreactive forms of polyubiquitylated prodomain are schematically represented at their corresponding position of migration. The levels of a nonspecific immunoreactive band serves as an input control (extracts). (B) Amino acid residues 113–144 of the Ssy5 prodomain (*S. cerevisiae*) and fungal orthologues were aligned using Clustal X; conserved (yellow) and similar (blue, green) residues are highlighted, and the conserved residues, L126, V129, and E131, are indicated with arrows. (C) Directed two-hybrid analysis of Ssy5 and Grr1 interactions. Plasmids pCA146 (vc-DBD), pTP133 (DBD-SSY5-L126S,V129A,E131A), or pTP134 (DBD-SSY5) were introduced together with pTP122 (AD-GRR1, +) or pJG4-5 (–) into strain CAY235. Growth of transformants was assessed on SC (-His, -Trp) (nonselective) or SC-Gal (-His, -Trp, -Leu, -Lys) (selective), and expression of DNA-binding domain (DBD) and activation domain (AD) constructs were analyzed by immunoblotting. (D) Growth of HKY77 (*ssy5Δ*), HKY84 (*ssy5Δ ssy1Δ*), and CAY276 (*ssy5Δ grr1Δ*) carrying pCA204 (STP1-MYC) and pSH120 (SSY5), pTP112 (SSY5-L126S, V129S, E131A), or pCA195 (SSY5*) on YPD and YPD+MM. Immunoblot analysis of protein extracts from strains grown in SD medium. (E) Growth of HKY77 (*ssy5Δ*), HKY84 (*ssy5Δ ssy1Δ*), and CAY276 (*ssy5Δ grr1Δ*) carrying pCA204 (STP1-MYC) and pSH120 (SSY5), pTP112 (SSY5-E131A), or pCA195 (SSY5*) on YPD and YPD+MM. (F) Immunoblot analysis of extracts from HKY77 (*ssy5Δ*), CAY276 (*ssy5Δ grr1Δ*), HKY84 (*ssy5Δ ssy1Δ*), and TPY120 (*ssy5Δ ssy1Δ grr1Δ*) carrying pCA204 (STP1-MYC) and pSH120 (SSY5) or pTP115 (SSY5-E131A) grown on SMD. (G) Immunoblot analysis of extracts from HKY77 (*ssy5Δ YCK1 YCK2*) (WT) and CAY320 (*yck1Δ yck2-1*) carrying pCA204 (STP1-MYC) and pSH120 (SSY5), pTP115 (SSY5-E131A), or pCA195 (SSY5*). Cells were pregrown in SD at room

but still retains a requirement for phosphorylation and ubiquitylation for its activity. The data support a model that amino acids induce a conformational change of the Ssy5 prodomain that facilitates subsequent phosphorylation and ubiquitylation-dependent degradation. The switch of the prodomain to the signaling conformation can be mimicked by substitutions close to amino acid residue 130.

A conserved phosphoacceptor motif defines a phosphodegron in the prodomain

Having established that SPS signaling functions via induced phosphorylation of the prodomain as a trigger for its Grr1-dependent proteasomal degradation, we sought to identify the phosphorylation and ubiquitylation acceptor residues within the prodomain. Alignment of the prodomain sequences of Ssy5 orthologues revealed a conserved sequence motif rich in serine residues potentially serving as phosphoacceptor sites (Figure 4A). We have previously found that the region containing this motif, amino acids 60–90 of the prodomain, is required for signal-induced degradation of the prodomain (Pfirrmann et al., 2010). Consistently, mutation of seven potential phosphoacceptor sites in this motif abolishes phosphorylation and protease activation (Abdel-Sater et al., 2011). We tested whether the first 90 amino acids of the prodomain are important for SPS sensor-induced phosphorylation and found that the prodomain of *ssy5Δ90* does not undergo phosphorylation in *grr1Δ* cells upon leucine induction (Figure 4B, lane 4).

This finding prompted us to further investigate the role of the conserved serine residues between amino acids 60 and 90 as potential acceptor sites for phosphorylation and prodomain degradation. We focused our efforts on three highly conserved serine residues (residues 67, 70, and 72) that we found to meet the criteria for Yck1/2 consensus sites (Flotow et al., 1990; Knippschild et al., 2005) or were predicted to be phosphorylated (Ingrell et al., 2007). We replaced these serine residues with either alanine residues (*ssy5-62*, 3S-A) or with more structurally related cysteine residues (*ssy5-67*, 3S-C) and assessed the impact of the mutations on prodomain stability and Stp1-processing activity. Both mutant proteins displayed normal autoprocessing, indicating that the mutations did not induce gross protein folding defects affecting the catalytic potential of the Ssy5 protease (Figure 4C, top panel, lanes 3–6). Importantly, the mutant prodomains were stable and were not degraded in response to SPS-sensor induction (Figure 4C, compare lanes 1 and 2 with lanes 3–6). Consistently, Stp1 processing activity was not detected (Figure 4C, lanes 4 and 6), nor did the mutant proteins support growth in the presence of MM (Figure 4D, dilutions 2 and 3). Taken together, our data indicate that Ser-67, -70, and -72 are required for induced prodomain degradation, likely due to their function as acceptor sites for phosphorylation.

Next we asked how the introduction of negatively charged amino acids at these positions would influence Ssy5 activation. The SSY5-63 (3S-D) allele encodes a mutant protein in which the three serine residues are replaced with aspartate residues. This allele fully complemented the *ssy5Δ* mutation; similar to WT Ssy5, Ssy5-63 exhibited leucine-induced prodomain degradation and Stp1-processing activity, and supported growth on YPD+MM (Figure 4C, lanes 7 and 8 and 4D, lane 4). This finding raised the possibility that residues with negative charges at putative phosphorylation sites are

temperature, and extracts were prepared 30 min after cultures were shifted to 37°C. Immunoreactive forms of Stp1 are schematically depicted at their corresponding positions of migration.

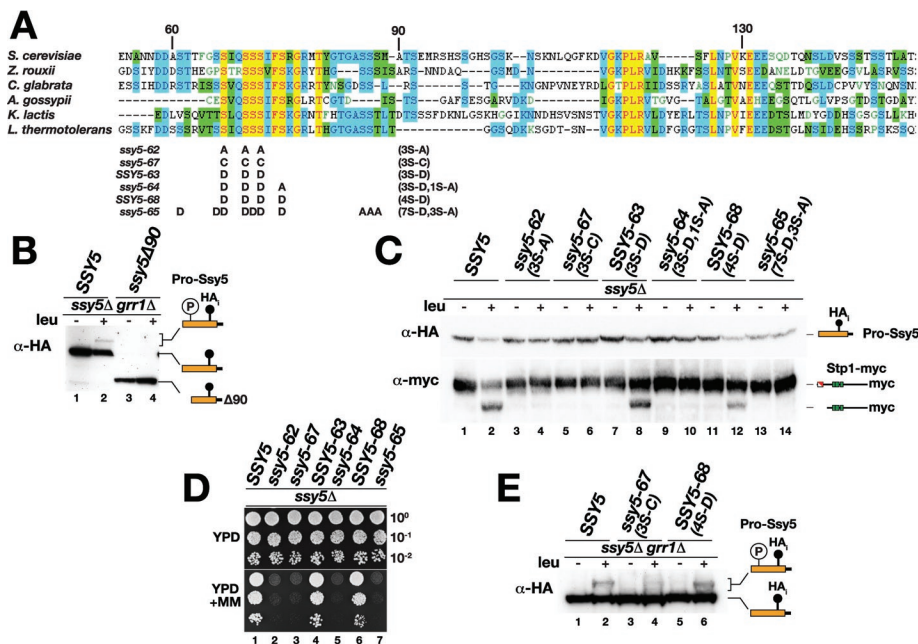


FIGURE 4: A conserved phosphoacceptor motif in the prodomain is required for its degradation and Stp1 processing. (A) Amino acid residues 53–153 of the Ssy5 prodomain (*S. cerevisiae*) and fungal orthologues were aligned by using Clustal X; conserved (yellow) and similar (blue, green) residues are highlighted. The serine substitution alleles *ssy5-62*, *-64*, *-65*, *-67* and *SSY5-63* and *-68* are shown. (B) Immunoblot analysis of extracts from CAY276 (*ssy5Δ grr1Δ*) carrying pCA204 (*STP1-MYC*) and pSH120 (*SSY5*) or pSH119 (*ssy5Δ90*) induced with leucine as indicated. (C) Immunoblot analysis of extracts from strain HKY77 (*ssy5Δ*) carrying pCA204 (*STP1-MYC*) and pSH120 (*SSY5*), pDO067 (*ssy5-62*), pDO082 (*ssy5-67*), pDO068 (*SSY5-63*), pDO069 (*ssy5-64*), pDO083 (*SSY5-68*), or pDO072 (*ssy5-65*) induced with leucine as indicated. (D) Strains in (C) were spotted onto YPD and YPD+MM medium; plates were incubated at 30°C for 2–3 d and photographed. (E) Immunoblot analysis of extracts from strain CAY276 (*ssy5Δ grr1Δ*) carrying pCA204 (*STP1-MYC*) and pSH120 (*SSY5*), pDO082 (*SSY5-67*), or pDO083 (*SSY5-68*) induced with leucine as indicated. Immunoreactive forms of Stp1 and Ssy5 prodomain are schematically depicted at their corresponding positions of migration.

more compatible with Ssy5 activation than are neutral ones. We tested this notion by creating alleles with different charge profiles; *ssy5-64* (3S-D 1S-A) carries an additional serine-to-alanine substitution, and *SSY5-68* (4S-D) carries aspartate residues at all four positions. Functional tests showed that *ssy5-64* expressed an inactive protein, whereas *SSY5-68* expressed a functional one (Figure 4C, compare lanes 9–12, and 4D, dilution series 5 and 6). Apparently, the introduction of negative charges at the putative phosphorylation sites is indeed more compatible with Ssy5 activation.

To examine whether the introduction of a greater number of negatively charged aspartate residues could activate the protease, perhaps independently of phosphorylation, we constructed the *ssy5-65* (7S-D 3S-A) allele encoding a protein with seven serine residues replaced with aspartate and three additional serine residues replaced with alanine, eliminating all possible serine phosphoacceptor sites. Although the *ssy5-65* allele expressed a protein that was correctly folded, as indicated by proper autolytic processing into Pro- and Cat-domain (Figure 4C, lanes 13 and 14), it did not complement the *ssy5Δ* mutation (Figure 4D, dilution series 7). This result suggests that negative charges at potential phosphorylation sites cannot substitute for the required phosphorylation in this region of the prodomain as the trigger for protease activation.

We directly assessed the phosphorylation status of the prodomains carrying cysteine (*ssy5-67*, 3S-C) or aspartate (*SSY5-68*, 4S-D) substitutions in *grr1Δ* cells. Compared to WT Ssy5, we reproducibly observed lower levels of induced phosphorylation of the inactive

Ssy5-67 prodomain (Figure 4E, compare lanes 4 and 2). The remaining phosphorylation indicates that this mutant still harbors residual functional phosphorylation sites. Apparently, the residual phosphorylation is not sufficient to trigger SCF^{Grr1} recognition and protease activation. In contrast, the functional Ssy5-68 mutant prodomain displayed induced phosphorylation to the same extent as WT Ssy5. The phosphorylated forms of Ssy5-68 prodomain migrated faster than the corresponding modified WT prodomain, suggesting that fewer phosphogroups were attached to the remaining serine residues (Figure 4E, compare lanes 6 and 2). In context of the negative charges contributed by the aspartate side chains, this residual phosphorylation apparently suffices for downstream signaling events that activate Ssy5.

Taken together, the mutational analysis demonstrates that multisite phosphorylation, and in part the overall negative charge, in the region of amino acid residues 60–90 triggers the degradation of the prodomain. We therefore propose that the prodomain contains a phosphodegron comprising this region, which functions as a recognition module for SCF^{Grr1}, and is therefore required for Ssy5 activation in response to extracellular amino acids.

Ubiquitin acceptor sites in the prodomain are required for activation of Ssy5

To define the complete phosphodegron in the prodomain, we sought to identify the SCF^{Grr1} ubiquitylation acceptor lysine residues required for proteasomal degradation. First, we examined whether the lysine residues in the prodomain are required for activation of the protease (Figure 5). We replaced all potential ubiquitin acceptor lysine residues in the prodomain with arginine residues, with the exception of residues K379 and K380 (Figure 5A), which are directly adjacent to the autolytic cleavage site (381/382), to avoid interfering with protease maturation (Poulsen et al., 2006). We found that, although autolytic processing occurred, albeit at reduced levels, the Ssy5-K1-22R mutant protein was non-functional (Figure 5B, dilution series 1–3). Accordingly, we could not detect Stp1 processing (Figure 5C, lanes 5 and 6). To rigorously test the catalytic competency of Ssy5-K1-22R, we artificially induced the degradation of its prodomain by fusing a temperature-regulated N degron to the N terminus (Ssy5-R_{de}-K1-22R) (Figure 5D). We have previously established that this degron can artificially activate WT Ssy5 even in the absence of other SPS sensor components (Pfirrmann et al., 2010). We found that, at 35°C, a temperature that triggers N degron-mediated degradation of the prodomain, Ssy5-K1-22R was activated, and its activity bypassed the requirement of *SSY1* or *PTR3* (Figure 5D, dilution series 3, 6, and 9). Thus *ssy5K1-22R* encodes a protease that is fully capable of processing Stp1 but cannot be activated by amino acid-induced signals.

We investigated the underlying cause of the blocked activation of Ssy5-K1-22R, considering that an impaired polyubiquitylation of the prodomain is predicted to exert a stabilizing effect during SPS

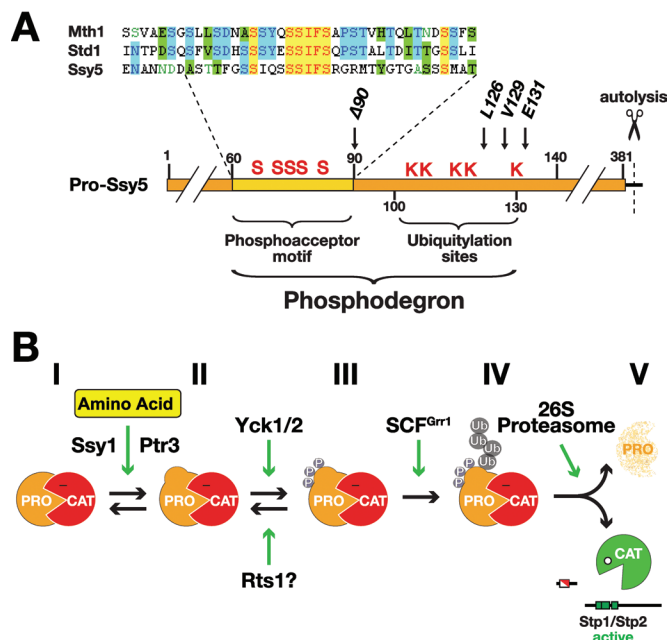


FIGURE 6: The phosphodegron in the prodomain controls the activation of Ssy5. (A) Schematic diagram of the Ssy5 prodomain (residues 1–381; scissors indicate the autolytic cleavage site); the phosphodegron (residues 60–130) contains the phosphoacceptor motif (conserved serine residues, S, in the region amino acids 60–90) and the ubiquitylation sites (K). The positions of the conserved L126, V129, and E131 residues and the *ssy5*Δ90 allele are indicated. The similarity of the phosphoacceptor motif and sequences in Mth1 (amino acids 111–149) and Std1 (amino acids 122–160) are displayed in expanded form; identical (yellow) and similar (blue, green) residues are highlighted. (B) Diagram of the five (I–V) experimentally determined Ssy5 prodomain states leading to SPS sensor–induced Stp1/Stp2-processing activity of the Ssy5 Cat-domain.

by the SPS sensor. Specifically, the intrinsic sequence determinants reside in the N terminus of the inhibitory prodomain (amino acid residues 60–130) and function as an inducible phosphodegron (Figure 6A). The phosphodegron consists of a conserved, positively acting sequence motif comprising several phosphoacceptor residues and a cluster of five lysine residues that likely serve as sites for ubiquitylation. On signaling, the phosphodegron becomes activated, resulting in its phosphorylation converting it into a substrate for ubiquitylation that targets the entire prodomain for degradation by the proteasome. The outcome of this chain of rapid and linked events is the liberation of active Cat-domain that processes the downstream transcription factors Stp1 and Stp2.

The integrated chain of events that activates the phosphodegron on SPS sensor induction can be summarized in a simple model with five prodomain states (Figure 6B). Accordingly, the catalytic activity of the Ssy5 protease is inhibited by the noncovalently associated prodomain in its inhibitory state (I). On amino acid induction, the prodomain receives signals from upstream SPS sensor components Ssy1 and Ptr3, and switches to a signaling conformation (II). Adoption of the signaling conformation exposes the phosphodegron leading to Yck1/2-mediated phosphorylation on multiple sites within the phosphoacceptor motif (III). Phosphorylation is presumably counteracted by phosphatase PP2A with its regulatory subunit Rts1 (Eckert-Boulet *et al.*, 2006; Liu *et al.*, 2008), which, under non-signaling conditions, may maintain the prodomain in the hypophosphorylated state (II). The shift in the balance between phosphoryla-

tion and dephosphorylation rates serves as a switchlike trigger for recognition by the ubiquitin E3 ligase complex SCF^{Grr1}, which recognizes the hyperphosphorylated phosphodegron and directly ubiquitylates at least one of the lysine residues (IV). Concomitantly, the polyubiquitylated prodomain (V) is degraded by the 26S proteasome, unfettering the catalytic activity of the Ssy5 Cat-domain.

The biological significance of the proposed model is based on several lines of key experimental evidence. We have physical evidence for four of five prodomain states (I, III–V) and have genetic evidence to infer the existence of the state II conformation. First, the inhibitory Ssy5 prodomain state I can be detected in extracts from noninduced cells (Abdel-Sater *et al.*, 2004; Andréasson *et al.*, 2006; Poulsen *et al.*, 2006). The stable phosphorylated and ubiquitylated prodomain states, III and IV, can be purified from induced cells carrying downstream blocking mutations (i.e., *grr1*Δ cells and proteasome inhibited cells, respectively) (Figure 1 and Figure 3; Abdel-Sater *et al.*, 2011). Similarly, upon amino acid induction, we can observe rapid prodomain degradation (V) and stable Cat-domain levels (Andréasson *et al.*, 2006; Pfirrmann *et al.*, 2010). Second, the existence of an unmodified signaling conformation of the prodomain (II) is based on finding that specific mutations in the prodomain constitutively activate the protease (Pfirrmann *et al.*, 2010). Importantly, these mutations bypass the upstream component Ssy1, but not the downstream activity of Yck1/2 and Grr1 (Figure 3); hence, the mutant prodomains must adopt an intermediate signaling conformation (II) that is distinct from state I. Third, we have evidence for direct physical interactions between the required signaling factors, i.e., Yck1 and Grr1, and the Ssy5 prodomain (Figures 2 and 3). Finally, mutations affecting the phosphoacceptor sites or the adjacent lysine residues within the phosphodegron impair prodomain degradation, and consequently prevent amino acid–induced and SPS sensor–mediated gene expression (Figures 4 and 5).

According to our model, the phosphodegron of Ssy5 is the recognition determinant for the general signaling factors Yck1/2 and SCF^{Grr1}, raising the possibility that other inducible proteasomal substrates carry similar modules. Strikingly, we find that the phosphoacceptor motif in the phosphodegron of Ssy5 exhibits sequence similarity to the regulatory degron sequences found in the two transcriptional repressors Mth1 and Std1 (Figure 6A, sequence alignment). Mth1 and Std1 are the effector components of the yeast Snf3/Rgt2 glucose-sensing pathway. On glucose induction, Std1 and Mth1 undergo SCF^{Grr1}-dependent degradation, resulting in derepression of glucose transporter gene expression (Flick *et al.*, 2003; Lakshmanan *et al.*, 2003). Although functionally and mechanistically distinct from the SPS signaling pathway, the Snf3/Rgt2 glucose-sensing pathway shares certain characteristics, including primary transporter-like sensors and a requirement for Yck1/2 and SCF^{Grr1} (Johnston and Kim, 2005). The sequence similarity to the regulatory motifs comprising Yck1/2 consensus phosphorylation acceptor serines in Ssy5, Mth1, and Std1 (Moriya and Johnston, 2004) provides an explanation for how these discrete pathways interact with the same signaling factors. Accordingly, casein kinase I and SCF^{Grr1}, which are known to participate as constitutively active signaling components in a variety of cellular processes (Gross and Anderson, 1998; Willems *et al.*, 2004; Knippschild *et al.*, 2005; Jonkers and Rep, 2009), are recruited to distinct signaling pathways by their recognition of inducible and regulated phosphodegrons. This concept raises the possibility that we have identified a phosphodegron that, in a context-dependent manner, can be controlled by several different pathways that generate highly distinct signaling outputs.

All our data are consistent with the model that proteasomal degradation of the prodomain activates the Ssy5 protease. However,

the direct involvement of the 26S proteasome in the activation of Ssy5 has recently been questioned. In a recent study, Abdel-Sater *et al.* propose that prodomain ubiquitylation (state IV) rather than its degradation (state V) is the Ssy5-activating step (Abdel-Sater *et al.*, 2011). This alternative model is based on two observations: Stp1 processing appears to precede prodomain degradation, and Stp1 processing occurs in cells with inhibited proteasome function. We note, however, that neither of these two observations exclude the notion of a critical involvement of the proteasome in Ssy5 activation. First, Stp1 processing activity of the Cat-domain is catalytic (i.e., a small amount of prodomain degradation can generate a substantial amount of processed Stp1). Accordingly, the level of processed Stp1 is predicted to increase before substantial down-regulation of the prodomain. Second, residual proteolytic activity is known to persist in all experimental setups used to decrease proteasome function (i.e., mutational inactivation and MG132 inhibition; Ghislain *et al.*, 1993; Hoppe *et al.*, 2000; Andréasson and Ljungdahl, 2002). As discussed in a previous report, the residual proteasome activity can readily account for the observed Stp1-processing activity (Pfirmsmann *et al.*, 2010). Moreover, both unprocessed and processed forms of Stp1 are proteasomal substrates (Pfirmsmann *et al.*, 2010; Tumusiime *et al.*, 2011). Consequently, under conditions where the proteasome is inhibited, both forms of Stp1 accumulate. Thus the fact that processed Stp1 accumulates can misleadingly provide the basis for overestimating Ssy5 activity. In summary, although our data do not formally exclude the possibility that polyubiquitylation of the prodomain can suffice to initiate downstream signaling, all available experimental evidence support a model of Ssy5 activation requiring proteasomal degradation of the prodomain.

Pathways involving multiple proteases are frequently organized in cascades (i.e., upstream proteases endoproteolytically activate downstream proteases in a sequential manner). Prominent examples are the blood-clotting cascade (Page *et al.*, 2005), caspases in apoptosis (Boatright and Salvesen, 2003), and proteases in digestion (Stroud *et al.*, 1977). In this study we have defined a novel proteolytic activation cascade with the ubiquitin proteasome system as a central component. To our knowledge, the finding that phosphorylation-dependent proteolysis by the proteasome activates an intracellular signaling protease is novel. A predicating example of the ubiquitin proteasome system activating an intracellular protease, however, is the protease separase (Esp1). Separase is inhibited by its binding to securin (Pds1). Ubiquitylation of securin by the anaphase-promoting complex APC-Cdc20 triggers its subsequent degradation by the proteasome. The degradation of securin liberates separase activity, leading to the degradation of cohesin that links sister chromatids during cell division (Ciosk *et al.*, 1998; Uhlmann *et al.*, 1999; Nasmyth, 2005). Aberrant regulation of separase activity is connected to missegregation and increased loss of chromosomes, a phenomenon frequently found in cancer cells (Nasmyth, 2002). The crucial involvement of proteases in fundamental regulatory events in eukaryotes underlines the importance of studying the general principles of their activation mechanisms.

MATERIALS AND METHODS

Strains and plasmids

The *Saccharomyces cerevisiae* strains and plasmids used in this work are listed in Table 1 and Table 2, respectively. The yeast strains are isogenic descendants of the S288C-derived strain AA255/PLY115 (Antebi and Fink, 1992), with the exception of the two-hybrid strain CAY235. The sequences of mutagenic oligonucleotides and PCR primers for homologous recombination are available upon request.

Media

Standard media, including YPD medium; ammonia-based synthetic minimal dextrose (SD) medium, supplemented as required to enable growth of auxotrophic strains; and ammonia-based synthetic complete dextrose (SC) were prepared as described (Andréasson and Ljungdahl, 2002). When needed, L-leucine was added at a concentration of 1.3 mM for 30 min to induce SPS sensor signaling. Sensitivity to MM (100 µg/ml) was monitored on complex medium as described (Andréasson and Ljungdahl, 2004).

Immunoblot analysis

Whole-cell extracts were prepared under denaturing conditions using NaOH and trichloroacetic acid (TCA) as described previously (Silve *et al.*, 1991). Primary antibodies were diluted (vol:vol) as follows: 3F10 anti-HA-horseradish peroxidase (HRP) (Roche Applied Science, Basel, Switzerland), 1:5000; anti-myc-HRP 9E10 mAb (Roche Applied Science), 1:1000; anti-Pgk1 (Molecular Probes, Eugene, OR), 1:5000; anti Penta-His-HRP, 1:1000 (Qiagen, Chatsworth, CA). Immunoreactive bands were visualized by chemiluminescence detection (SuperSignal West Dura Extended-Duration Substrate; Pierce, Rockford, IL) and quantified using an LAS1000 system (Fuji Photo Film Co., Tokyo, Japan).

Dephosphorylation assay

Proteins were immunoprecipitated (Anti-c-Myc-Agarose Affinity Gel; Sigma, St. Louis, MO) from extracts obtained using glass bead lysis in IP-1 buffer (50 mM Tris-HCl, pH 7.5; 250 mM NaCl) containing PhosSTOP (Roche) and Complete Mini EDTA free (Roche). Beads were washed twice with IP-1 buffer and once with dephosphorylation buffer (10 mM Tris-HCl pH 8; 5 mM MgCl₂; 0.1 M KCl; 0.02% Triton X-100). Alternatively, cells were lysed in 5% TCA and neutralized with Tris (1 M), and precipitated material was resolubilized in four volumes of IP-2 buffer (50 mM Tris, pH 7.5; 100 mM NaCl; 2 mM EDTA; 1.2% Triton X-100; 1 mM iodoacetic acid) containing PhosSTOP and Complete Mini EDTA free. Immunopurification of HA-tagged Ssy5 was carried out using HA Affinity Matrix (Roche), beads were washed twice with 10 ml of wash buffer (20 mM Tris, pH 7.5; 1 M NaCl), and bound material was eluted by incubating beads two times at 37°C for 15 min in the presence of 250 µl of elution buffer (20 mM Tris, pH 7.5; 0.1 M NaCl) containing 1 mg/ml HA peptide (Roche). Dephosphorylation reactions were performed in 100 µl of dephosphorylation buffer without bovine serum albumin with 10 µl of phosphatase (FastAP, Fermentas Sweden, Helsingborg, Sweden).

CHX chase

Cells were grown to log phase, and CHX was added to the culture at a concentration of 100 µg/ml. Where indicated, leucine was added to a concentration of 1.3 mM (+ leu). Extracts were prepared from samples taken at the time points indicated and were analyzed by immunoblotting.

Directed yeast two-hybrid assay

Two-hybrid interactions between LexA fused to full length Ssy5 variants (pTP133 and pTP134) and an activation domain (AD) fused to full-length Grr1 (pTP122) were tested in strain CAY235. Interactions were assayed for growth on SCD plates lacking tryptophan, histidine, leucine, and lysine, and containing 2% galactose and 1% raffinose as carbon sources.

Strain	Genotype	Reference
CAY86	MATa <i>ura3-52 grr1Δ50::hphMX4</i>	Andréasson and Ljungdahl, 2002
CAY235	MATα <i>his3 trp1-100 ura3-52 leu2Δ::6×lexAOp-LEU2 lys2Δ::URA3-p8×lexAOp-LYS2-GAL1 GAL2</i>	This work
CAY267	MATa <i>ura3-52 ssy1Δ13::hisG grr1Δ50::hphMX4</i>	This work
CAY276	MATa <i>lys2Δ201 ura3-52 ssy5Δ2::hisG grr1Δ50::hphMX4</i>	This work
CAY285	MATa <i>lys2Δ201 ura3-52 ptr3Δ15::hisG ssy1Δ13::hisG ssy5Δ2::hisG</i>	Andréasson et al., 2006
CAY320	MATa <i>lys2Δ201 ura3-52 yck1Δ::hphMX4 yck2-1</i>	This work
HKY77	MATa <i>lys2Δ201 ura3-52 ssy5Δ2::hisG</i>	Forsberg and Ljungdahl, 2001
HKY84	MATa <i>lys2Δ201 ura3-52 ssy1Δ13::hisG ssy5Δ2::hisG</i>	Forsberg and Ljungdahl, 2001
HKY85	MATa <i>lys2Δ201 ura3-52 ptr3Δ15::hisG ssy5Δ2::hisG</i>	Forsberg and Ljungdahl, 2001
TPY116	MATa <i>lys2Δ201 ura3-52 ssy5Δ2::hisG pdr5Δ3</i>	This work
TPY117	MATa <i>lys2Δ201 ura3-52 ssy5Δ2::hisG grr1Δ pdr5Δ3</i>	This work
TPY120	MATa <i>lys2Δ201 ura3-52 ssy1Δ13::hisG ssy5Δ2::hisG grr1::hphMX4</i>	This work

TABLE 1: Yeast strains used in this study.

Plasmid	Description	Reference
pCA146	2μm <i>HIS3 Km^R G418^R</i> containing <i>PADH-LexA</i>	This work
pCA195	pRS316 (<i>URA3</i>) containing <i>HA-SSY5</i>	Andréasson et al., 2006
pCA204	pRS317 (<i>LYS2</i>) containing <i>STP1-MYC-kanMX</i>	Andréasson et al., 2006
pDO067	pRS316 (<i>URA3</i>) containing <i>HA_i-ssy5-62-GST</i>	This work
pDO068	pRS316 (<i>URA3</i>) containing <i>HA_i-SSY5-63-GST</i>	This work
pDO069	pRS316 (<i>URA3</i>) containing <i>HA_i-ssy5-64-GST</i>	This work
pDO072	pRS316 (<i>URA3</i>) containing <i>HA_i-ssy5-65-GST</i>	This work
pDO082	pRS316 (<i>URA3</i>) containing <i>HA_i-ssy5-67-GST</i>	This work
pDO083	pRS316 (<i>URA3</i>) containing <i>HA_i-SSY5-68-GST</i>	This work
pDO099	pRS316 (<i>URA3</i>) containing <i>HA_i-SSY5-yck1₂₋₅₂₇K98R</i>	This work
pDO100	pRS316 (<i>URA3</i>) containing <i>HA_i-SSY5-YCK1₂₋₅₂₇</i>	This work
pHK048	pRS316 (<i>URA3</i>) containing <i>MYC-SSY5</i>	Forsberg and Ljungdahl, 2001
pJG4-5	yeast two hybrid prey vector (<i>TRP1</i>)	Gyuris et al., 1993
pSH119	pRS316 (<i>URA3</i>) containing <i>HA_i-SSY5₉₁₋₆₉₉-GST</i>	Pfirrmann et al., 2010
pSH120	pRS316 (<i>URA3</i>) containing <i>HA_i-SSY5-GST</i>	Pfirrmann et al., 2010
pTP110	pRS316 (<i>URA3</i>) containing <i>Ubi-R_{ds}-tsDHFR-HA_i-SSY5-GST</i>	Pfirrmann et al., 2010
pTP112	pRS316 (<i>URA3</i>) containing <i>HA_i-SSY5-L126S,V129A,E131A-GST</i>	Pfirrmann et al., 2010
pTP115	pRS316 (<i>URA3</i>) containing <i>HA_i-SSY5-E131A-GST</i>	Pfirrmann et al., 2010
pTP122	pJG4-5 (<i>TRP1</i>) containing <i>PGAL1-AD-HA-GRR1₂₋₁₁₅₂</i>	This work
pTP133	2μm <i>HIS3 Km^R G418^R</i> containing <i>PADH-LexA-SSY5-L126S,V129A,E131A</i>	This work
pTP134	2μm <i>HIS3 Km^R G418^R</i> containing <i>PADH-LexA-SSY5</i>	This work
pTP135	pRS316 (<i>URA3</i>) containing <i>HA_i-SSY5-K9R-GST</i>	This work
pTP140	pRS316 (<i>URA3</i>) containing <i>HA_i-SSY5-K5-8R,K10-22R-GST</i>	This work
pTP142	pRS316 (<i>URA3</i>) containing <i>HA_i-SSY5-K1-8R,K10-22R-GST</i>	This work
pTP143	pRS316 (<i>URA3</i>) containing <i>HA_i-ssy5-K5-22R-GST</i>	This work
pTP144	pRS316 (<i>URA3</i>) containing <i>HA_i-ssy5-K1-22R- GST</i>	This work
pTP145	pRS316 (<i>URA3</i>) containing <i>HA_i-ssy5-K5-9R-GST</i>	This work
pTP149	pRS316 (<i>URA3</i>) containing <i>Ubi-R_{ds}-tsDHFR-HA_i-SSY5-K1-22R-GST</i>	This work
pTP156	YEp195 based (<i>URA3</i> replaced with <i>LYS2</i>) containing <i>PCUP1-6HIS-UBI</i>	This work

TABLE 2: Plasmids used in this study.

In vivo polyubiquitylation assay

Ubiquitylated prodomain was affinity purified and detected as described previously (Iglesias *et al.*, 2010). Briefly, 80 OD₆₀₀ of cells per sample were incubated (30 min) in the presence of 100 μM MG132 (Sigma-Aldrich, St. Louis, MO). Cells were lysed in 10% TCA using glass beads. Precipitated protein was washed with 1 M Tris, resuspended in 1 ml of Buffer A (6 M guanidium HCl; 20 mM Tris, pH 8; 100 mM K₂HPO₄, 20 mM imidazole, 100 mM NaCl, 0.1% Triton X-100), resolubilized for 1 h (room temperature), then ubiquitylated proteins were purified using 100 μl of NiNTA beads (Qiagen). Beads were washed three times with Buffer A, three times with wash buffer 1 (20 mM Tris, pH 8; 100 mM K₂HPO₄, 20 mM imidazole, 100 mM NaCl, 0.1% Triton X-100), and three times with wash buffer 2 (20 mM Tris, pH 8; 100 mM K₂HPO₄, 10 mM imidazole, 1 M NaCl, 0.1% Triton X-100). Bound material was eluted three times with 200 μl of elution buffer (20 mM Tris, pH 8; 100 mM K₂HPO₄, 500 mM imidazole, 100 mM NaCl) for 10 min.

ACKNOWLEDGMENTS

We thank the members of the Ljungdahl laboratory for constructive comments throughout the course of this work and D.H. Wolf (University of Stuttgart, Germany) for plasmids. Nicole Meseberg is gratefully acknowledged for experimental assistance. This research was supported by the Center for Biomembrane Research, Stockholm University (to C.A. and P.O.L.) and by funding from the Swedish Research Council (to P.O.L.).

REFERENCES

- Abdel-Sater F, El Bakkoury M, Urrestarazu A, Vissers S, André B (2004). Amino acid signaling in yeast: casein kinase I and the Ssy5 endoprotease are key determinants of endoproteolytic activation of the membrane-bound Stp1 transcription factor. *Mol Cell Biol* 24, 9771–9785.
- Abdel-Sater F, Jean C, Merhi A, Vissers S, André B (2011). Amino-acid signalling in yeast: activation of the Ssy5 protease is associated with its phosphorylation-induced ubiquitylation. *J Biol Chem* 286, 12006–12015.
- Andréasson C, Heessen S, Ljungdahl PO (2006). Regulation of transcription factor latency by receptor-activated proteolysis. *Genes Dev* 20, 1563–1568.
- Andréasson C, Ljungdahl PO (2002). Receptor-mediated endoproteolytic activation of two transcription factors in yeast. *Genes Dev* 16, 3158–3172.
- Andréasson C, Ljungdahl PO (2004). The N-terminal regulatory domain of Stp1p is modular and, fused to an artificial transcription factor, confers full Ssy1p-Ptr3p-Ssy5p sensor control. *Mol Cell Biol* 24, 7503–7513.
- Antebi A, Fink GR (1992). The yeast Ca²⁺-ATPase homologue, PMR1, is required for normal Golgi function and localizes in a novel Golgi-like distribution. *Mol Biol Cell* 3, 633–654.
- Bernard F, André B (2001). Ubiquitin and the SCF^{Grr1} ubiquitin ligase complex are involved in the signalling pathway activated by external amino acids in *Saccharomyces cerevisiae*. *FEBS Lett* 496, 81–85.
- Boatright KM, Salvesen GS (2003). Mechanisms of caspase activation. *Curr Opin Cell Biol* 15, 725–731.
- Brivanlou AH, Darnell JE, Jr (2002). Signal transduction and the control of gene expression. *Science* 295, 813–818.
- Ciosk R, Zachariae W, Michaelis C, Shevchenko A, Mann M, Nasmyth K (1998). An ESP1/PDS1 complex regulates loss of sister chromatid cohesion at the metaphase to anaphase transition in yeast. *Cell* 93, 1067–1076.
- Eckert-Boulet N, Larsson K, Wu B, Poulsen P, Regenbreg B, Nielsen J, Kielland-Brandt MC (2006). Deletion of *RTS1*, encoding a regulatory subunit of protein phosphatase 2A, results in constitutive amino acid signaling via increased Stp1p processing. *Eukaryot Cell* 5, 174–179.
- Flick KM, Spielowoy N, Kalashnikova TI, Guaderrama M, Zhu Q, Chang HC, Wittenberg C (2003). Grr1-dependent inactivation of Mth1 mediates glucose-induced dissociation of Rgt1 from *HXT* gene promoters. *Mol Biol Cell* 14, 3230–3241.
- Flotow H, Graves PR, Wang AQ, Fiol CJ, Roeske RW, Roach PJ (1990). Phosphate groups as substrate determinants for casein kinase I action. *J Biol Chem* 265, 14264–14269.
- Forsberg H, Ljungdahl PO (2001). Genetic and biochemical analysis of the yeast plasma membrane Ssy1p-Ptr3p-Ssy5p sensor of extracellular amino acids. *Mol Cell Biol* 21, 814–826.
- Ghislain M, Udvardy A, Mann C (1993). *S. cerevisiae* 26S protease mutants arrest cell division in G2/metaphase. *Nature* 366, 358–362.
- Gross SD, Anderson RA (1998). Casein kinase I: spatial organization and positioning of a multifunctional protein kinase family. *Cell Signal* 10, 699–711.
- Gyuris J, Golemis E, Chertkov H, Brent R (1993). Cdi1, a human G1 and S phase protein phosphatase that associates with Cdk2. *Cell* 75, 791–803.
- Hoppe T, Matuschewski K, Rape M, Schlenker S, Ulrich HD, Jentsch S (2000). Activation of a membrane-bound transcription factor by regulated ubiquitin/proteasome-dependent processing. *Cell* 102, 577–586.
- Iglesias N, Tutucci E, Gwizdek C, Vinciguerra P, Von Dach E, Corbett AH, Dargemont C, Stutz F (2010). Ubiquitin-mediated mRNP dynamics and surveillance prior to budding yeast mRNA export. *Genes Dev* 24, 1927–1938.
- Ingrell CR, Miller ML, Jensen ON, Blom N (2007). NetPhosYeast: prediction of protein phosphorylation sites in yeast. *Bioinformatics* 23, 895–897.
- Iraqi I, Vissers S, Bernard F, de Craene JO, Boles E, Urrestarazu A, André B (1999). Amino acid signaling in *Saccharomyces cerevisiae*: a permease-like sensor of external amino acids and F-Box protein Grr1p are required for transcriptional induction of the *AGP1* gene, which encodes a broad-specificity amino acid permease. *Mol Cell Biol* 19, 989–1001.
- Johnston M, Kim JH (2005). Glucose as a hormone: receptor-mediated glucose sensing in the yeast *Saccharomyces cerevisiae*. *Biochem Soc Trans* 33, 247–252.
- Jonkers W, Rep M (2009). Lessons from fungal F-box proteins. *Eukaryot Cell* 8, 677–695.
- Jørgensen MU, Bruun MB, Didion T, Kielland-Brandt MC (1998). Mutations in five loci affecting *GAP1*-independent uptake of neutral amino acids in yeast. *Yeast* 14, 103–114.
- Klasson H, Fink GR, Ljungdahl PO (1999). Ssy1p and Ptr3p are plasma membrane components of a yeast system that senses extracellular amino acids. *Mol Cell Biol* 19, 5405–5416.
- Knippschild U, Gocht A, Wolff S, Huber N, Lohler J, Stoter M (2005). The casein kinase 1 family: participation in multiple cellular processes in eukaryotes. *Cell Signal* 17, 675–689.
- Lakshmanan J, Mosley AL, Özcan S (2003). Repression of transcription by Rgt1 in the absence of glucose requires Std1 and Mth1. *Curr Genet* 44, 19–25.
- Liu Z, Thornton J, Spirek M, Butow RA (2008). Activation of the SPS amino acid-sensing pathway in *Saccharomyces cerevisiae* correlates with the phosphorylation state of a sensor component, Ptr3. *Mol Cell Biol* 28, 551–563.
- Moriya H, Johnston M (2004). Glucose sensing and signaling in *Saccharomyces cerevisiae* through the Rgt2 glucose sensor and casein kinase I. *Proc Natl Acad Sci USA* 101, 1572–1577.
- Nasmyth K (2002). Segregating sister genomes: the molecular biology of chromosome separation. *Science* 297, 559–565.
- Nasmyth K (2005). How do so few control so many?. *Cell* 120, 739–746.
- Page MJ, Macgillivray RT, Di Cera E (2005). Determinants of specificity in coagulation proteases. *J Thromb Haemost* 3, 2401–2408.
- Pfirrmann T, Heessen S, Omrus DJ, Andréasson C, Ljungdahl PO (2010). The prodomain of Ssy5 protease controls receptor-activated proteolysis of transcription factor Stp1. *Mol Cell Biol* 30, 3299–3309.
- Poulsen P, Lo Leggio L, Kielland-Brandt MC (2006). Mapping of an internal protease cleavage site in the Ssy5p component of the amino acid sensor of *Saccharomyces cerevisiae* and functional characterization of the resulting pro- and protease domains by gain-of-function genetics. *Eukaryot Cell* 5, 601–608.
- Silve S, Volland C, Garnier C, Jund R, Chevallier MR, Haguenaer-Tsapis R (1991). Membrane insertion of uracil permease, a polytopic yeast plasma membrane protein. *Mol Cell Biol* 11, 1114–1124.
- Spielowoy N, Flick K, Kalashnikova TI, Walker JR, Wittenberg C (2004). Regulation and recognition of SCF^{Grr1} targets in the glucose and amino acid signaling pathways. *Mol Cell Biol* 24, 8994–9005.
- Spielowoy N, Guaderrama M, Wohlschlegel JA, Ashe M, Yates JR, 3rd, Wittenberg C (2010). Npr2, yeast homolog of the human tumor suppressor NPRL2, is a target of Grr1 required for adaptation to growth on diverse nitrogen sources. *Eukaryot Cell* 9, 592–601.
- Stroud RM, Kossiakoff AA, Chambers JL (1977). Mechanisms of zymogen activation. *Annu Rev Biophys Bioeng* 6, 177–193.

- Tumusiime S, Zhang C, Overstreet MS, Liu Z (2011). Differential regulation of transcription factors Stp1 and Stp2 in the Ssy1-Ptr3-Ssy5 amino acid sensing pathway. *J Biol Chem* 286, 4620–4631.
- Uhlmann F, Lottspeich F, Nasmyth K (1999). Sister-chromatid separation at anaphase onset is promoted by cleavage of the cohesin subunit Scc1. *Nature* 400, 37–42.
- Vancura A, Sessler A, Leichus B, Kuret J (1994). A prenylation motif is required for plasma membrane localization and biochemical function of casein kinase I in budding yeast. *J Biol Chem* 269, 19271–19278.
- Wang PC, Vancura A, Mitcheson TG, Kuret J (1992). Two genes in *Saccharomyces cerevisiae* encode a membrane-bound form of casein kinase-1. *Mol Biol Cell* 3, 275–286.
- Wielemans K, Jean C, Vissers S, Andre B (2010). Amino acid signaling in yeast: post-genome duplication divergence of the Stp1 and Stp2 transcription factors. *J Biol Chem* 285, 855–865.
- Willems AR, Schwab M, Tyers M (2004). A hitchhiker's guide to the cul-
lin ubiquitin ligases: SCF and its kin. *Biochim Biophys Acta* 1695, 133–170.
- Wolf DH (2004). From lysosome to proteasome: the power of yeast in the dissection of proteinase function in cellular regulation and waste disposal. *Cell Mol Life Sci* 61, 1601–1614.
- Wu B, Ottow K, Poulsen P, Gaber RF, Albers E, Kielland-Brandt MC (2006). Competitive intra- and extracellular nutrient sensing by the transporter homologue Ssy1p. *J Cell Biol* 173, 327–331.



Gid9, a second RING finger protein contributes to the ubiquitin ligase activity of the Gid complex required for catabolite degradation

Bernhard Braun^a, Thorsten Pfirrmann^b, Ruth Menssen^a, Kay Hofmann^c, Hartmut Scheel^c, Dieter H. Wolf^{a,*}

^a Institut für Biochemie, Universität Stuttgart, 70569 Stuttgart, Germany

^b Stockholm University, Wenner-Gren Institute, S-106 91 Stockholm, Sweden

^c Miltenyi Biotec, 51429 Bergisch-Gladbach, Germany

ARTICLE INFO

Article history:

Received 9 September 2011

Revised 20 October 2011

Accepted 23 October 2011

Available online 29 October 2011

Edited by Noboru Mizushima

Keywords:

Catabolite degradation

Gid ubiquitin ligase

RING finger

Glycolysis

Gluconeogenesis

Fructose-1,6-bisphosphatase

ABSTRACT

The two major antagonistic pathways of carbon metabolism in cells, glycolysis and gluconeogenesis, are tightly regulated. In the eukaryotic model organism *Saccharomyces cerevisiae* the switch from gluconeogenesis to glycolysis is brought about by proteasomal degradation of the gluconeogenic enzyme fructose-1,6-bisphosphatase. The ubiquitin ligase responsible for polyubiquitylation of fructose-1,6-bisphosphatase is the Gid complex. This complex consists of seven subunits of which subunit Gid2/Rmd5 contains a RING finger domain providing E3 ligase activity. Here we identify an additional subunit containing a degenerated RING finger, Gid9/Fyv10. This subunit binds to Gid2/Rmd5. A mutation in the degenerated RING finger of Gid9/Fyv10 abolishes polyubiquitylation and degradation of three enzymes specific for gluconeogenesis.

Structured summary of protein interactions:

Gid2 physically interacts with **Gid9** by anti tag coimmunoprecipitation (View interaction)

© 2011 Federation of European Biochemical Societies. Published by Elsevier B.V. All rights reserved.

1. Introduction

Glucose is the most prominent carbon and energy source for many cells, being essential for mammals. Glucose is metabolized by the catabolic glycolysis pathway. When it is not available glucose must be synthesized by the anabolic pathway gluconeogenesis, which is in part a reversal of the glycolytic pathway. Irreversible and main regulatory catalytic steps of glycolysis are circumvented in gluconeogenesis by various enzymes. These steps are phosphorylation of glucose by hexokinase (glycolysis) and dephosphorylation of glucose-6-phosphate by glucose-6-phosphatase (gluconeogenesis), phosphorylation of fructose-6-phosphate by phosphofructokinase (glycolysis) and dephosphorylation of fructose-1,6-bisphosphate by fructose-1,6-bisphosphatase (FBPase) (gluconeogenesis), synthesis of pyruvate and ATP from phosphoenolpyruvate by pyruvate kinase (glycolysis) and synthesis of phosphoenolpyruvate by cytoplasmic malate dehydrogenase (c-MDH) and phosphoenolpyruvate carboxykinase (PEPCK) [1]. Malregulation of these two central antagonistic pathways in humans leads to type 2 diabetes [2]. When yeast cells are grown

* Corresponding author. Address: Universität Stuttgart, Institut für Biochemie, Pfaffenwaldring 55, 70569 Stuttgart, Germany. Fax: +49 711 68564392.

E-mail address: dieter.wolf@ibc.uni-stuttgart.de (D.H. Wolf).

on a non-fermentable carbon source such as ethanol, gluconeogenesis is turned on and specific gluconeogenic enzymes such as FBPase, c-MDH and PEPCK are synthesized. Transfer of cells to glucose containing medium leads to rapid inactivation of these enzymes. The fate of FBPase has been studied best up to now. In a process called catabolite inactivation the *FBP1* gene is repressed, the enzyme is allosterically inhibited by fructose-2,6-bisphosphate and AMP and finally phosphorylated and degraded [3–10]. Two different mechanisms were published for the degradation step [11]. After glucose addition of cells grown and starved for 48 h on acetate as non-fermentable carbon source a vacuolar degradation of FBPase was reported. This process is dependent on the uptake of FBPase into vesicles and requires so-called Vid proteins [12–14]. In contrast, glucose addition to cells grown on ethanol for 16–18 h results in rapid degradation of the enzyme by the ubiquitin proteasome pathway (UPS) called catabolite degradation [7,11,15–20]. Likewise, degradation of PEPCK was shown to follow the proteasomal degradation route [20]. In addition, proteasomal degradation of FBPase and PEPCK requires the Hsp70 chaperone Ssa1 as well as the Cdc48-Ufd1-Npl4 motor complex [21–23]. Ubiquitin triggered degradation of a protein is initiated by a polyubiquitin chain linked to a lysine residue or the amino terminus of the respective protein [24]. This requires activation of the 76 amino acid ubiquitin by an ubiquitin activating enzyme

Table 1
Strains used in this study.

Strain	Genotype	Source
YWO0903	W303-1B MATalpha, <i>ade2 leu2-3, 112 his3 trp1 ura3</i>	H.L. Chiang
YWO0986	W303 MATalpha, <i>ade2 leu2-3, 112 his3 trp1 ura3 GID9-HA₃::HIS5^{S.pombe}</i>	T. Pfirrmann
Y31488	MATalpha, <i>his3Δ1/his3Δ1 leu2Δ0/leu2Δ0 MET15/met15Δ0 lys2Δ0/LYS2 ura3Δ0/ura3Δ0 gid9Δ::KANMX4/gid9Δ::KANMX4</i>	EUROSCARF
YRM49b	W303-1B <i>gid1Δ::loxP gid2Δ::loxP gid4Δ::loxP gid5Δ::loxP gid7Δ::loxP gid8Δ::loxP gid9Δ::loxP</i>	R. Menssen
YWO1850	W303-1B <i>gid1Δ::loxP gid2Δ::GID2-V5-HIS3^{S.pombe} gid4Δ::loxP gid5Δ::loxP gid7Δ::loxP gid8Δ::loxP gid9Δ::loxP</i>	J. Schweiggert
YWO1978	W303-1B <i>gid1Δ::loxP gid2Δ::GID2ΔCTLH-V5-HIS3^{S.pombe} gid4Δ::loxP gid5Δ::loxP gid7Δ::loxP gid8Δ::loxP gid9Δ::loxP</i>	This study
YWO1979	W303-1B <i>gid1Δ::loxP gid2Δ::GID2ΔLisH-V5-HIS3^{S.pombe} gid4Δ::loxP gid5Δ::loxP gid7Δ::loxP gid8Δ::loxP gid9Δ::loxP</i>	This study
YWO1255	W303-1B <i>gid9Δ::KANMX4</i>	M. Lehmann

Table 2
Plasmids used in this study.

Plasmid	Characteristics	Backbone	Source
PWO0747	3.2kbp DNA fragment containing Gid9 with its native promoter and terminator	pRS316	T. Pfirrmann, B. Braun
PWO1315	3.2kbp DNA fragment containing Gid9C434S with its native promoter and terminator	pRS316	This study
pJD421	His ₆ -Ubiquitin inserted between P _{CUP1} and T _{CYC1}	YEplac181	J. Dohmen
PWO1283	Gid2-V5, genomic promoter, ADH1 terminator	pRS303	J. Schweiggert
PWO1313	<i>gid2Δ216-229CTLH-V5</i>	pRS303	This study
PWO1314	<i>gid2Δ138-171LisH-V5</i>	pRS303	This study
PWO1153	Gid2-HA ₃ , native promoter, ADH1 terminator	pRS316	L. Barbin
PWO1316	<i>gid2Δ216-229CTLH-HA₃</i>	pRS316	This study with help of E. Diler
PWO1317	<i>gid2Δ138-171LisH-HA₃</i>	pRS316	This study

Table 3
Primers used in this study.

Primers	
Gid9fwd	aaagaattcgaagcgaagatataca
Gid9rev	aaaaactcgagaactaatcaagggaagg
Gid9 RING fwd	cgctacattcactaaaaggaagaattctcccgtttgcagtgagac
Swa1-Pme1	gctataaaaaataatagtttaacttttaataataatata
ED 3	ctaaccatacggctttatctcgaagcatggaatccggtagag
ED 4	ctctaccggatttccttgagcagataaagccgatggttag
ED 9	Aaaatcgatttcgccccgactaccacgggttccctaacca
ED 10	gtcagtcgacgtttatccctagcggatct
Gid2 LisHfwd	gagacaattggaatgttaataaaaagaatctactgaattttatgagatg
Gid2 LisHrev	catctcaataaattcagtagattcaattcattaatttccattgtctc
RM83	tatagtcgaccgctacagagatggaccg
RM84	tatagcggcgcactacaaaaagcaccaggcc

(E1) resulting in a thioester bond between the C-terminal glycine of ubiquitin and a cysteine residue of the E1. Transfer of ubiquitin to an ubiquitin conjugating enzyme (E2) follows. Subsequently ubiquitin is transferred to the target protein in a concerted action of the E2 and ubiquitin ligases (E3's). While HECT domain E3 ligases first receive the ubiquitin from the E2 and then transfer it to the protein to be degraded, RING domain E3 ligases bind the E2 as well as the substrate and catalyse the direct transfer of the ubiquitin from the E2 to the substrate [25]. The responsible ubiquitin ligase for FBPase degradation, the Gid (glucose induced degradation deficient) complex, was discovered [18]. This E3 ligase complex is composed of 7 subunits of which Gid2 contains a RING finger domain, which confers ubiquitin ligase activity to the complex *in vitro* and *in vivo* [20]. In addition, the two other

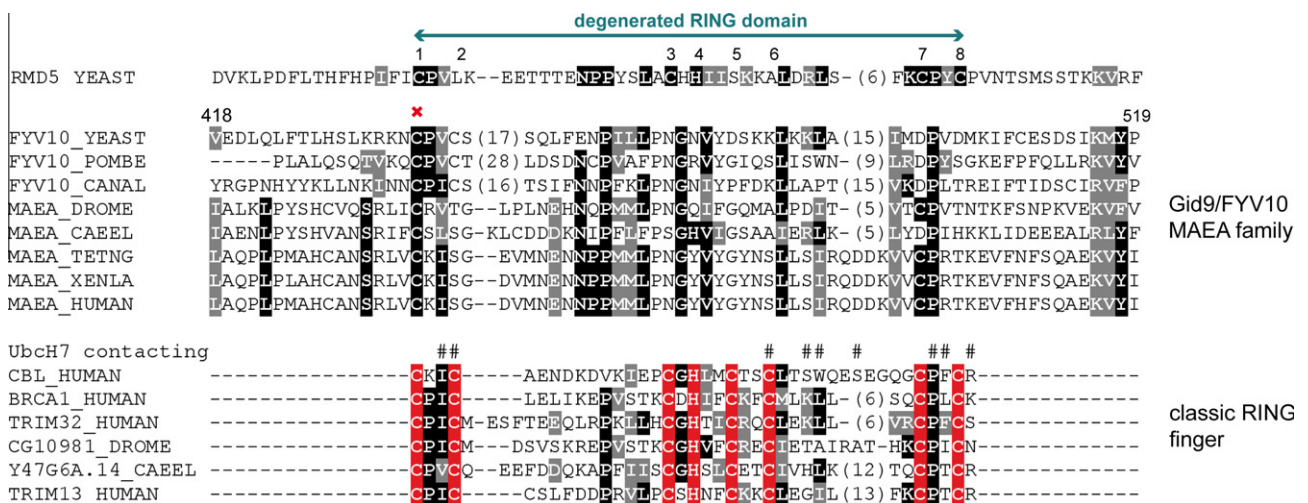


Fig. 1. RING domain alignment of the Gid9 protein family with Gid2 and classic RING-finger proteins. Black or grey background labels amino acid positions with invariant or conservatively replaced residues in at least 50% of the sequences. Numbers (1–8) of the alignment show positions homologous to zinc binding residues in classic RING finger proteins. A red cross marks the position of a point mutation introduced into the degenerated RING domain of Gid9 (C434S). # marks the residues essential for interaction between Cbl and UbcH7 [44]. MAEA: macrophage erythroblast attacher. Species abbreviation: YEAST, *S. cerevisiae*; POMBE, *S. pombe*; CANAL, *Candida albicans*; DROME, *Drosophila melanogaster*; CAEEL, *Caenorhabditis elegans*; TETNG, *Tetraodon nigroviridis*; XENLA, *Xenopus laevis*; HUMAN, *H. sapiens*.

gluconeogenic enzymes PEPCK and c-MDH are also targets of the E3 complex [20, this paper]. So far, no other proteins than the gluconeogenic enzymes have been found to be ubiquitylated by the Gid complex. A similar complex, the so called CTLH complex, of mainly unknown function was found in mammalian cells [20,26]. Interestingly, some of the Gid proteins were also identified as Vid proteins required for vesicle and vacuole dependent degradation of FBPase under harsh starvation conditions on acetate. However, no specific biochemical function has been assigned to these proteins in this process [27,28]. Here we show that besides Gid2 a second subunit of the Gid complex, Gid9, contains a degenerated RING finger domain. When this domain is mutated, the three gluconeogenic enzymes FBPase, PEPCK and c-MDH fail to be ubiquitylated and degraded. Gid9 binds to Gid2 in the absence of other Gid proteins. The two subunits seem to form the heterodimeric E3 ligase unit of the Gid complex.

2. Materials and methods

2.1. Yeast strains, plasmids and media

Previously described standard methods were used for media preparation and genetic and molecular biological techniques [29]. Yeast strains were grown at 30 °C. Precultures were grown 16 h in YPD or CM medium containing 2% glucose, diluted 1:12.5 into YPD or CM and grown for additional 6–7 h. Thereafter, cells were resuspended in YPethanol or CM (2% ethanol) and grown for 16 h to allow FBPase synthesis (final OD₆₀₀ 1–2). For induction of FBPase degradation cells were shifted to YPD or CM medium containing 2% glucose.

For construction of strain YTP12 see [20]. Strain Y31488 (Δ *gid9*) was obtained from the EUROSCARF collection.

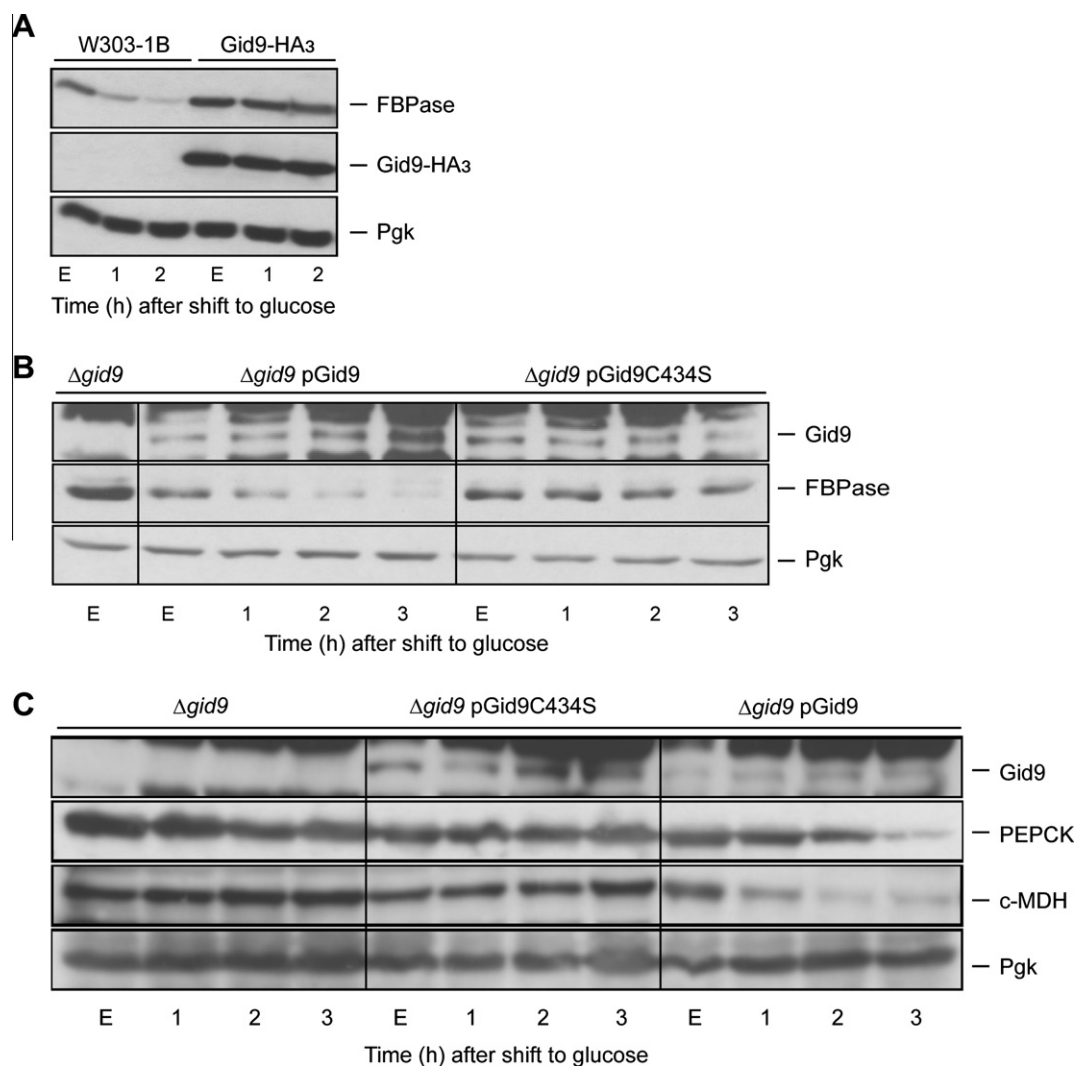


Fig. 2. (A) A C-terminal HA₃ tag renders Gid9 inactive. Cells were grown 16 h at 30 °C in YPethanol and then shifted into YPD medium. Cell samples were taken at the indicated time points, lysed and after SDS PAGE proteins were visualized via immunoblotting. Loading control: Pgk, 3-phosphoglycerate kinase. (B) A mutation in the putative RING domain of Gid9 (Gid9C434S) leads to inactivation of the protein with respect to FBPase degradation. Gid9 and its mutated C434S counterpart were expressed in a Δ *gid9* strain from plasmid pRS316. Cells were grown 16 h at 30 °C in CM medium with ethanol as carbon source without uracil and shifted to the same medium containing glucose instead of ethanol. At the indicated time points 1.5 OD of cells were harvested and after cell lysis and SDS PAGE proteins were monitored by immunoblotting. Loading control: Pgk, 3-phosphoglycerate kinase. (C) A mutation in the putative RING domain of Gid9 (Gid9C434S) leads to inactivation of the protein with respect to degradation of PEPCK and c-MDH. Gid9 and its mutated C434S counterpart were expressed in a Δ *gid9* strain from plasmid pRS316. Cells were grown 16 h at 30 °C in CM medium with ethanol as carbon source without uracil and shifted to the same medium containing glucose instead of ethanol. At the indicated time points 1.5 OD of cells were harvested, lysed and after SDS PAGE and proteins were monitored by immunoblotting. Loading control: Pgk, 3-phosphoglycerate kinase.

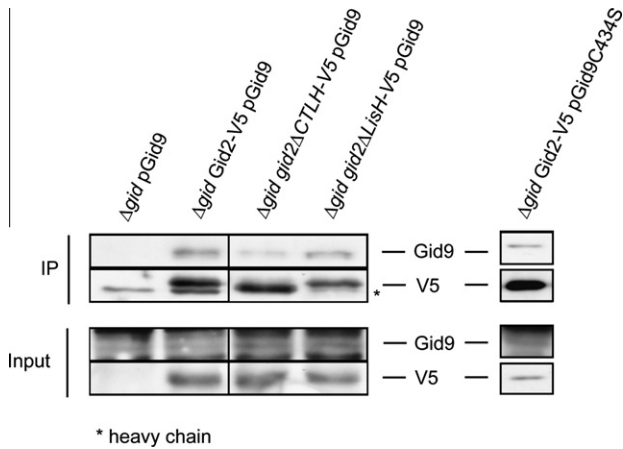


Fig. 3. Gid2 and Gid9 interact. A strain, Δ gid, deleted in all Gid subunits (*GID1*, *GID2*, *GID4*, *GID5*, *GID7*, *GID8* and *GID9*) and chromosomally expressing *GID2-V5*, *gid2 Δ 216-229CTLH-V5* or *gid2 Δ 138-171LisH-V5* respectively, was transformed with plasmid pWO 0747 expressing *GID9*. Cells were grown 16 h on CM medium with ethanol as carbon source and without uracil. Samples were taken and immunoprecipitation was performed with V5 antibody. Proteins were visualized by immunodetection with V5 and Gid9 antibodies.

Strain YRM49b (Δ gid, deletion of *GID1,2,4,5,7,8,9*) was generated using the technique described (R. Menssen, in preparation); [30]. Δ gid *GID2-V5*, Δ gid *gid2 Δ 216-229CTLH-V5* and Δ gid *gid2 Δ 138-171LisH-V5* strains were generated by integration of Sfo1 digested plasmids pWO1283, pWO1313 and pWO1314 into YRM49b.

The plasmids expressing wildtype Gid9 or RING finger mutated Gid9C434S were constructed by insertion of a *GID9* PCR-fragment (primers Gid9fwd, Gid9rev) with its endogenous promoter and terminator regions in a Xho1/EcoR1 digested pRS316 plasmid [31]. Point mutation of the preserved Cys residue 434 of Gid9 was performed using the Transformer site-directed mutagenesis kit (Clontech, Mountain View, CA) (primers Gid9*RING fwd, Swa1-Pme1). The plasmid JD421 expressing poly-histidine-tagged Ub was obtained from Dohmen et al. [32]. PWO1153 [33] was used as template plasmid for construction of CTLH domain deleted pWO1316 (primers ED3, ED4, ED9, ED10) and LisH domain deleted pWO1317 (primers Gid2*LisHfwd, Gid2*LisHrev, ED9, ED10). A cloned PCR fragment from strain YWO1850 obtained with primers RM83 and RM84 was inserted into Sal1/Not1 digested pRS303 resulting in plasmid pWO1283. Tables 1–3 list the yeast strains, plasmids and primers used.

2.2. FBPase/c-MDH/PEPCK ubiquitylation analysis

Ubiquitylation assays were performed by growing cells with a plasmid encoding poly-histidine-tagged ubiquitin (pJD421). Expression of His₆-Ub was induced by adding CuSO₄ to a final concentration 0.2 mM. Cells were grown 16–22 h in CM medium with ethanol as carbon source without uracil and leucine to allow derepression of FBPase. Thereafter, 150 OD₆₀₀ of yeast cells were harvested before and 30 min after addition of 2% glucose. After washing in 1 ml of water, cells were frozen in liquid N₂ and stored at -80 °C. Cells were then further processed as described in [34].

2.3. Western blotting

Western blotting was carried out as described in ref. [17] and [20]. Antibodies used were obtained from BABCO (Richmond, CA) (hemagglutinin [HA], clone 16B12); Sigma Aldrich (Schnellendorf), (V5). FBPase, PEPCK and c-MDH polyclonal antibodies were pro-

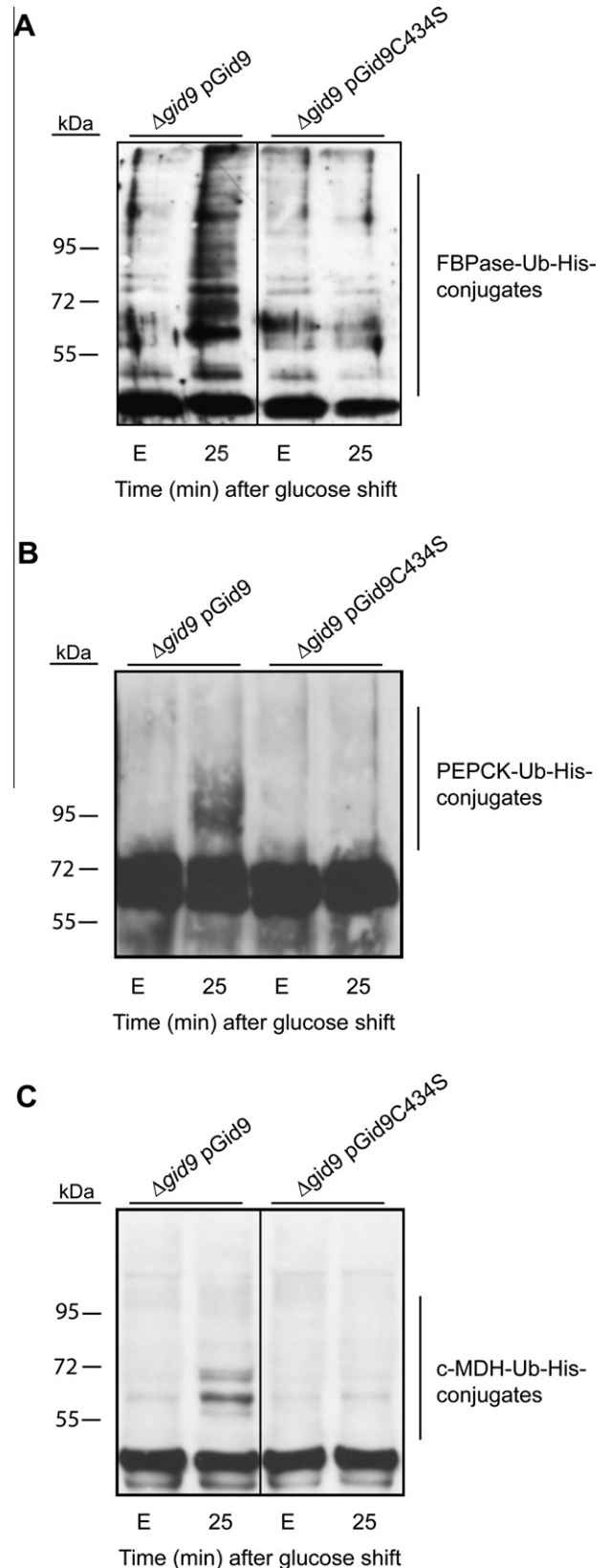


Fig. 4. Polyubiquitylation of gluconeogenic enzymes is abolished in strains expressing Gid9C434S. A Δ gid9 strain expressing plasmid encoded wild-type Gid9 or mutant Gid9C434S as well as poly-histidine-tagged ubiquitin were grown for 16–22 h in CM medium without uracil and leucine, 2% ethanol as carbon source and shifted onto the same medium with 2% glucose instead of ethanol. Samples were taken at indicated time points and poly-histidine tagged ubiquitin was precipitated with Ni-NTA-Sepharose beads. Polyubiquitylation was detected using specific antibody against (A) FBPase, (B) PEPCK and (C) c-MDH.

duced by immunization of rabbits using a purified FBPase-/PEPCK-/c-MDH-glutathione transferase (GST). Gid9 antibody was produced by immunization of rabbits using a Gid9 peptide (amino acid 471 to 486 of the Gid9 sequence; Charles River).

2.4. Co-immunoprecipitation

For immunoprecipitations (IPs) cells were cultivated as described above and samples were taken at the indicated time points. Cells (50–70 OD₆₀₀) were harvested, washed with water and resuspended in 600 µl of phosphate-buffered saline (PBS) buffer pH 7.4 (137 mM NaCl, 1.25 g/l Na₂HPO₄, and 0.35 g/l NaH₂PO₄) containing protease inhibitors (ProteoBlock PIC, Thermo Scientific, Fermentas Molecular Biology Tools; 1.1 mM phenylmethyl-sulfonyl-fluoride (PMSF), 0.1–0.2% Triton-X-100) and lysed at 8 °C with glass beads for 15 min. After centrifugation, 500 µl of the supernatant were transferred to a new test tube. 0.8 µl V5-antibody was added and the samples were gently agitated end over end for 2 h at 8 °C. Immunoprecipitates were collected by adding 50 µl of 6% (wt/vol) protein A-Sepharose CL-4B (GE Healthcare, Little Chalfont, United Kingdom) and further incubated for 1.5 h. For IP the Sepharose beads were centrifuged and washed five times with ice-cold PBS buffer. Proteins were released from Sepharose by boiling in 50 µl of urea buffer.

Bioinformatic sequence analysis was performed as indicated in [20].

3. Results and discussion

Recently, Gid2 was identified as a RING finger protein providing ubiquitin ligase activity to the seven subunit containing Gid complex. In several cases it has been shown that RING finger E3 ligases exert their optimum activity in a dimeric state whereby homodimers and heterodimers have been found [25,35–42]. We therefore searched whether the Gid-ubiquitin ligase complex harbors a second subunit which besides Gid2 contains a RING-finger motif.

When aligning the amino acid sequences of yeast Gid proteins with the sequence of yeast Gid2, the sequences of the MAEA protein family, formerly found to be mammalian orthologues of Gid9 [20], as well as classical RING finger proteins, Gid9 emerges carrying a degenerated RING finger domain with two conserved residues (Fig. 1). For analysis of the function of Gid9 in the Gid complex we fused a triple HA tag onto the C-terminus of Gid9. However, the Gid9-HA₃ fusion proved to be not functional: the protein failed to trigger degradation of FBPase when cells were transferred from gluconeogenic to glycolytic growth conditions. Obviously HA-tagging of Gid9 results in a biochemically inactive Gid9 mutant (Fig. 2A). The outcome of the experiment indicated a central function for a structurally intact Gid9 protein in the Gid-complex. We therefore raised antibodies against Gid9 in rabbits to follow its expression and to monitor the interaction of Gid9 with Gid2, which had been shown to exhibit ubiquitin ligase activity [20]. For this monitoring purpose we tagged Gid2 with the V5 tag. The fusion protein is active *in vivo* (not shown). For monitoring an interaction of Gid9 with Gid2-V5 we expressed both proteins in a strain deleted in all seven Gid proteins, which is fully viable but fails to degrade the gluconeogenic enzymes. As can be seen in Fig. 3, when precipitating Gid2 with V5 antibodies, Gid9 co-precipitates. Clearly, Gid2 and Gid9 interact in the Gid complex. In addition to its RING domain Gid2 contains a CTLH and a LisH domain [20]. Deletion of these domains slows down FBPase degradation (not shown). We asked whether any of these domains were involved in the binding to Gid9. When expressing Gid2-V5 deleted in its CTLH domain or in its LisH domain together with Gid9 in the strain devoid of all other Gid proteins, both Gid2 domain mutant proteins co-precipitated with Gid9 upon application of V5 antibodies. This indicates that these domains are not essential for the Gid2-Gid9 interaction even though the interaction was somehow less pronounced when the CTLH domain in Gid2 was deleted (Fig. 3). The fact that tagging of Gid9 results in stabilization of FBPase indicates that Gid9 has a crucial function in the degradation process (Fig. 2A). We therefore introduced a mutation into the

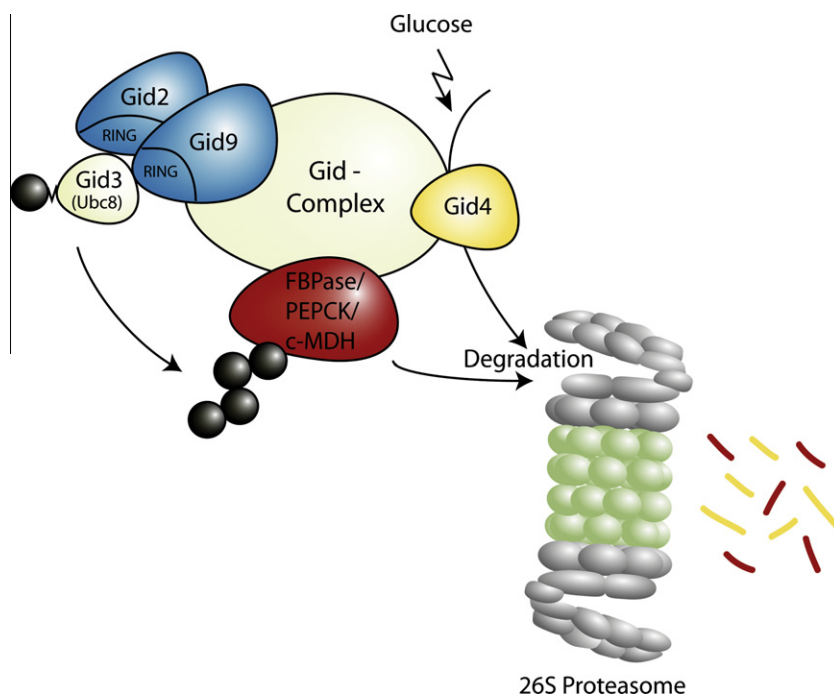


Fig. 5. The Gid complex triggers polyubiquitylation and subsequent proteasomal degradation of the gluconeogenic enzymes FBPase, PEPCK and c-MDH. After addition of glucose, Gid4 appears and activates the Gid E3 ligase. The Gid2 and Gid9 dimer together with Gid3, the ubiquitin conjugating enzyme Ubc8, polyubiquitylate the substrate proteins and by this trigger their degradation by the proteasome. (modified from [20]).

degenerated RING finger domain of Gid9 by changing the conserved cysteine residue 434 to serine to inactivate the RING domain [20,43]. When testing the consequence of the Gid9C434S mutation on the catabolite degradation of FBPase, it was obvious that degradation of the enzyme is blocked (Fig. 2B). Also catabolite degradation of the gluconeogenic enzymes PEPCK and c-MDH is abrogated by the mutation (Fig. 2C). As the Gid-complex acts as the ubiquitin ligase in the proteasome catalyzed degradation process of these three enzymes, we expected that ubiquitylation is disturbed by the C434S mutation in Gid9. This is indeed the case: expression of the mutated Gid9C434S protein in a strain otherwise deleted for *GID9* leads to a lack in polyubiquitylation of FBPase (Fig. 4A), PEPCK (Fig. 4B) and c-MDH (Fig. 4C), when cells are shifted from gluconeogenic to glycolytic conditions, by this preventing subsequent proteasomal degradation (Fig. 2B and C). We were not able to show any Gid9 ligase activity *in vitro* (not shown). Interestingly the C434S mutation in Gid9 does not disturb binding of the protein to Gid2 (Fig. 3). This excludes a defective complex formation between Gid2 and Gid9 as the cause of failure of the Gid-complex harboring Gid9C434S to polyubiquitylate and degrade FBPase, PEPCK and c-MDH. Clearly, an intact Gid9 protein has an important impact on the polyubiquitylating activity of the Gid-ubiquitin ligase complex. A model proposing the sequence of events of the catabolite degradation process is depicted in Fig. 5.

Acknowledgments

We thank J. Dohmen, L. Barbin, J. Schweiggert and E. Diler for plasmids, J. Juretschke for FBPase antibodies and M. Ziegler for PEPCK and c-MDH antibodies. This work was supported by the Deutsche Forschungsgemeinschaft, Bonn.

References

- [1] Berg, J.M., Tymoczko, J.L. and Stryer, L. (2006) Biochemistry, W. H. Freeman and Company, New York.
- [2] Wahren, J. and Ekberg, K. (2007) Splanchnic regulation of glucose production. *Annu. Rev. Nutr.* 27, 329–345.
- [3] Holzer, H. (1976) Catabolite inactivation in yeast. *Trends Biochem. Sci.* 1, 178–181.
- [4] von Herrath, M. and Holzer, H. (1988) Sensitivity of fructose-1,6-bisphosphatase from yeast, liver and skeletal muscle to fructose-2,6-bisphosphate and 5'-adenosine monophosphate. *Z. Lebensm. Unters. Forsch.* 186, 427–430.
- [5] Mazón, M.J., Gancedo, J.M. and Gancedo, C. (1982) Inactivation of yeast fructose-1,6-bisphosphatase. *In vivo* phosphorylation of the enzyme. *J. Biol. Chem.* 257, 1128–1130.
- [6] Marcus, F. et al. (1988) Yeast (*Saccharomyces cerevisiae*) fructose-1,6-bisphosphatase. Properties of phospho and dephospho forms and of two mutants in which serine 11 has been changed by site-directed mutagenesis. *J. Biol. Chem.* 263, 6058–6062.
- [7] Hämmerle, M. et al. (1998) Proteins of newly isolated mutants and the amino-terminal proline are essential for ubiquitin-proteasome-catalyzed catabolite degradation of fructose-1,6-bisphosphatase of *Saccharomyces cerevisiae*. *J. Biol. Chem.* 273, 25000–25005.
- [8] Müller, D. and Holzer, H. (1981) Regulation of fructose-1,6-bisphosphatase in yeast by phosphorylation/dephosphorylation. *Biochem. Biophys. Res. Commun.* 103, 926–933.
- [9] Gancedo, C. (1971) Inactivation of fructose-1,6-diphosphatase by glucose in yeast. *J. Bacteriol.* 107, 401–405.
- [10] Funayama, S., Gancedo, J.M. and Gancedo, C. (1980) Turnover of yeast fructose-bisphosphatase in different metabolic conditions. *Eur. J. Biochem.* 109, 61–66.
- [11] Wolf, D.H. (2004) From lysosome to proteasome: the power of yeast in the dissection of proteinase function in cellular regulation and waste disposal. *Cell. Mol. Life Sci.* 61, 1601–1614.
- [12] Chiang, M.C. and Chiang, H.L. (1998) Vid24p, a novel protein localized to the fructose-1,6-bisphosphatase-containing vesicles, regulates targeting of fructose-1,6-bisphosphatase from the vesicles to the vacuole for degradation. *J. Cell Biol.* 140, 1347–1356.
- [13] Chiang, H.L. and Schekman, R. (1991) Regulated import and degradation of a cytosolic protein in the yeast vacuole. *Nature* 350, 313–318.
- [14] Huang, P.H. and Chiang, H.L. (1997) Identification of novel vesicles in the cytosol to vacuole protein degradation pathway. *J. Cell Biol.* 136, 803–810.
- [15] Schork, S.M., Bee, G., Thumm, M. and Wolf, D.H. (1994) Catabolite inactivation of fructose-1,6-bisphosphatase in yeast is mediated by the proteasome. *FEBS Lett.* 349, 270–274.
- [16] Schork, S.M., Bee, G., Thumm, M. and Wolf, D.H. (1994) Site of catabolite inactivation. *Nature* 369, 283–284.
- [17] Schork, S.M., Thumm, M. and Wolf, D.H. (1995) Catabolite inactivation of fructose-1,6-bisphosphatase of *Saccharomyces cerevisiae*. Degradation occurs via the ubiquitin pathway. *J. Biol. Chem.* 270, 26446–26450.
- [18] Regelmann, J. et al. (2003) Catabolite degradation of fructose-1,6-bisphosphatase in the yeast *Saccharomyces cerevisiae*: a genome-wide screen identifies eight novel GID genes and indicates the existence of two degradation pathways. *Mol. Biol. Cell* 14, 1652–1663.
- [19] Schüle, T., Rose, M., Entian, K.D., Thumm, M. and Wolf, D.H. (2000) Ubc8p functions in catabolite degradation of fructose-1,6-bisphosphatase in yeast. *EMBO J.* 19, 2161–2167.
- [20] Santt, O. et al. (2008) The yeast GID complex, a novel ubiquitin ligase (E3) involved in the regulation of carbohydrate metabolism. *Mol. Biol. Cell* 19, 3323–3333.
- [21] Juretschke, J., Menssen, R., Sickmann, A. and Wolf, D.H. (2010) The Hsp70 chaperone Ssa1 is essential for catabolite induced degradation of the gluconeogenic enzyme fructose-1,6-bisphosphatase. *Biochem. Biophys. Res. Commun.* 397, 447–452.
- [22] Barbin, L., Eisele, F., Santt, O. and Wolf, D.H. (2010) The Cdc48-Ufd1-Npl4 complex is central in ubiquitin-proteasome triggered catabolite degradation of fructose-1,6-bisphosphatase. *Biochem. Biophys. Res. Commun.* 394, 335–341.
- [23] Stolz, A., Hilt, W., Buchberger, A. and Wolf, D.H. (2011) Cdc48: a power machine in protein degradation. *Trends Biochem. Sci.* 36, 515–523.
- [24] Wolf, D.H. (2011) The ubiquitin clan: A protein family essential for life. *FEBS Lett.* 585, 2769–2771.
- [25] Deshaies, R.J. and Joazeiro, C.A.P. (2009) RING domain E3 ubiquitin ligases. *Annu. Rev. Biochem.* 78, 399–434.
- [26] Kobayashi, N. et al. (2007) RanBPM, Muskelein, p48EMLP, p44CTLH, and the armadillo-repeat proteins ARMC8alpha and ARMC8beta are components of the CTLH complex. *Gene* 396, 236–247.
- [27] Brown, C.R., Dunton, D. and Chiang, H.-L. (2010) The vacuole import and degradation pathway utilizes early steps of endocytosis and actin polymerization to deliver cargo proteins to the vacuole for degradation. *J. Biol. Chem.* 285, 1516–1528.
- [28] Brown, C.R., McCann, J.A., Hung, G.G.-C., Elco, C.P. and Chiang, H.-L. (2002) Vid22p, a novel plasma membrane protein, is required for the fructose-1,6-bisphosphatase degradation pathway. *J. Cell Sci.* 115, 655–666.
- [29] Guthrie, C. and Fink, G.R. (1991) Methods in Enzymology, Volume 194: Guide to Yeast Genetics and Molecular Biology, Academic Press Inc.
- [30] Guldener, U., Heinisch, J., Koehler, G.J., Voss, D. and Hegemann, J.H. (2002) A second set of loxP marker cassettes for Cre-mediated multiple gene knockouts in budding yeast. *Nucleic Acids Res.* 30, e23.
- [31] Sikorski, R.S. and Hieter, P. (1989) A system of shuttle vectors and yeast host strains designed for efficient manipulation of DNA in *Saccharomyces cerevisiae*. *Genetics* 122, 19–27.
- [32] Dohmen, R.J. et al. (1995) An essential yeast gene encoding a homolog of ubiquitin-activating enzyme. *J. Biol. Chem.* 270, 18099–18109.
- [33] Barbin, L. (2009) Ubiquitin-proteasome dependent catabolite degradation of fructose-1,6-bisphosphatase: localization and involvement of novel components, Universität Stuttgart, Stuttgart.
- [34] Geng, F. and Tansey, W.P. (2008) Polyubiquitylation of histone H2B. *Mol. Biol. Cell* 19, 3616–3624.
- [35] Hashizume, R. et al. (2001) The RING heterodimer BRCA1-BARD1 is a ubiquitin ligase inactivated by a breast cancer-derived mutation. *J. Biol. Chem.* 276, 14537–14540.
- [36] Brzovic, P.S. et al. (2003) Binding and recognition in the assembly of an active BRCA1/BARD1 ubiquitin-ligase complex. *Proc. Natl. Acad. Sci. USA* 100, 5646–5651.
- [37] Linares, L.K., Hengstermann, A., Ciechanover, A., Müller, S. and Scheffner, M. (2003) HdmX stimulates Hdm2-mediated ubiquitination and degradation of p53. *Proc. Natl. Acad. Sci. USA* 100, 12009–12014.
- [38] Wang, H. et al. (2004) Role of histone H2A ubiquitination in Polycomb silencing. *Nature* 431, 873–878.
- [39] Park, Y.C., Burkitt, V., Villa, A.R., Tong, L. and Wu, H. (1999) Structural basis for self-association and receptor recognition of human TRAF2. *Nature* 398, 533–538.
- [40] Polekhina, G. et al. (2002) Siah ubiquitin ligase is structurally related to TRAF and modulates TNF-alpha signaling. *Nat. Struct. Biol.* 9, 68–75.
- [41] Kozlov, G. et al. (2007) Structural basis for UBA-mediated dimerization of c-bis-ubiquitin ligase. *J. Biol. Chem.* 282, 27547–27555.
- [42] Mace, P.D. et al. (2008) Structures of the cIAP2 RING domain reveal conformational changes associated with ubiquitin-conjugating enzyme (E2) recruitment. *J. Biol. Chem.* 283, 31633–31640.
- [43] Itahana, K. et al. (2007) Targeted inactivation of Mdm2 RING finger E3 ubiquitin ligase activity in the mouse reveals mechanistic insights into p53 regulation. *Cancer Cell* 12, 355–366.
- [44] Zheng, N., Wang, P., Jeffrey, P.D. and Pavletich, N.P. (2000) Structure of a c-Cbl-UbcH7 complex: RING domain function in ubiquitin-protein ligases. *Cell* 102, 533–539.

The Yeast GID Complex, a Novel Ubiquitin Ligase (E3) Involved in the Regulation of Carbohydrate Metabolism

Olivier Santt,^{*†} Thorsten Pfirrmann,^{*†‡} Bernhard Braun,^{*§} Jeannette Juretschke,^{*§} Philipp Kimmig,^{*§} Hartmut Scheel,[§] Kay Hofmann,[§] Michael Thumm,^{*||} and Dieter H. Wolf^{*}

^{*}Institut für Biochemie, Universität Stuttgart, 70569 Stuttgart, Germany; and [§]Miltenyi Biotec GmbH, 50829 Köln, Germany

Submitted March 28, 2008; Revised May 13, 2008; Accepted May 19, 2008
Monitoring Editor: Thomas Sommer

Glucose-dependent regulation of carbon metabolism is a subject of intensive studies. We have previously shown that the switch from gluconeogenesis to glycolysis is associated with ubiquitin-proteasome linked elimination of the key enzyme fructose-1,6-bisphosphatase. Seven glucose induced degradation deficient (Gid)-proteins found previously in a genomic screen were shown to form a complex that binds FBPase. One of the subunits, Gid2/Rmd5, contains a degenerated RING finger domain. In an in vitro assay, heterologous expression of GST-Gid2 leads to polyubiquitination of proteins. In addition, we show that a mutation in the degenerated RING domain of Gid2/Rmd5 abolishes fructose-1,6-bisphosphatase polyubiquitination and elimination in vivo. Six Gid proteins are present in gluconeogenic cells. A seventh protein, Gid4/Vid24, occurs upon glucose addition to gluconeogenic cells and is afterwards eliminated. Forcing abnormal expression of Gid4/Vid24 in gluconeogenic cells leads to fructose-1,6-bisphosphatase degradation. This suggests that Gid4/Vid24 initiates fructose-1,6-bisphosphatase polyubiquitination by the Gid complex and its subsequent elimination by the proteasome. We also show that an additional gluconeogenic enzyme, phosphoenolpyruvate carboxykinase, is subject to Gid complex-dependent degradation. Our study uncovers a new type of ubiquitin ligase complex composed of novel subunits involved in carbohydrate metabolism and identifies Gid4/Vid24 as a major regulator of this E3.

INTRODUCTION

Glucose is the main carbon source of many cells, providing energy and building blocks for a variety of essential cellular components. Glucose also has a pivotal role in cellular regulation. Its consumption via glycolysis and its regeneration via gluconeogenesis are central pathways of carbohydrate metabolism in many organisms. Regulation of both pathways occurs at three steps catalyzed by different reciprocally acting enzymes. In glycolysis, these steps include the phosphorylation of glucose by hexokinase, the phosphorylation of fructose-6-phosphate by phosphofructokinase, and the synthesis of pyruvate and ATP from phosphoenolpyruvate by pyruvate kinase. In gluconeogenesis, these steps are circumvented by pyruvate carboxylase and phosphoenolpyruvate carboxykinase (PEPCK), fructose-1,6-bisphosphatase

(FBPase), and glucose-6-phosphatase. Dysregulation of these antagonistic pathways in humans leads to type 2 diabetes (Wahren and Ekberg, 2007).

In the yeast *Saccharomyces cerevisiae*, major regulation events occur when cells previously grown in a glucose-deprived medium are supplied with this sugar. These events include gene expression and repression, alterations in the stability of certain mRNAs, and posttranslational modification of many gene products (Gancedo, 1998; Vaultont *et al.*, 2000). FBPase is expressed when yeast cells are growing in media without a fermentable carbon source (growth on ethanol [EtOH] or acetate). After glucose addition, catabolite inactivation and degradation of FBPase occur (Gancedo, 1971; Holzer, 1976; Marcus *et al.*, 1988; Hämmerle *et al.*, 1998; Wolf, 2004). Catabolite inactivation encompasses repression of the *FBP1* gene, decrease of the enzyme activity upon phosphorylation, and allosteric inhibition by fructose-2,6-bisphosphate and AMP (Mazon *et al.*, 1982; von Herrath and Holzer, 1988). Subsequently, FBPase undergoes rapid degradation (Holzer, 1989). Similar mechanisms are described for PEPCK, cytosolic malate dehydrogenase, and isocitrate lyase (Holzer, 1976; Hämmerle *et al.*, 1998). Degradation of FBPase blocks gluconeogenesis and prevents an otherwise ongoing futile cycle of ATP hydrolysis (Schork *et al.*, 1994a,b, 1995; Wolf, 2004).

In addition to the previously identified *GID1/VID30*, *GID2/RMD5*, and *GID3* genes, a genome-wide screen for FBPase stabilization upon glucose shift allowed the discovery of six further so-called glucose induced degradation deficient (*GID*) genes termed *GID4* to *GID9* (Regelmann *et al.*, 2003). Among those genes, *GID3* and *GID6* were shown to encode the ubiquitin-conjugating enzyme Ubc8 and the

This article was published online ahead of print in *MBC in Press* (<http://www.molbiolcell.org/cgi/doi/10.1091/mbc.E08-03-0328>) on May 28, 2008.

[†] These authors contributed equally to this work.

Present addresses: [†] University of Stockholm, Wenner-Gren Institute, Svante Arrheniusväg 16-18, 10691 Stockholm, Sweden; ^{||} Institut für Biochemie und Molekulare Zellbiologie, Universität Göttingen, Heinrich-Dueker-Weg 12, 37073 Göttingen, Germany.

Address correspondence to: Dieter H. Wolf (dieter.wolf@ibc.uni-stuttgart.de).

Abbreviations used: CTLH, C-terminal to LisH motif; FBPase, fructose-1,6-bisphosphatase; GST, Glutathione transferase; LisH, Lissencephaly type-1-like homology motif; ORF, Open reading frame; PEPCK, phospho-enol-pyruvate carboxykinase.

deubiquitinating enzyme Ubp14 (Schüle *et al.*, 2000; Regelmann *et al.*, 2003). Gid1, Gid4, and Gid5 had previously been identified as Vid30, Vid24, and Vid28, respectively. They were implicated in a glucose-induced vesicular targeting of FBPase for vacuolar degradation observed when yeast cells were starved >48 h in media containing acetate as a nonfermentable carbon source (Hoffman and Chiang, 1996; Chiang and Chiang, 1998; Hung *et al.*, 2004). Proteasome-dependent degradation of FBPase was obtained using different conditions: yeast cells were grown overnight in ethanol-containing media before glucose addition (Schüle *et al.*, 2000; Regelmann *et al.*, 2003; Hung *et al.*, 2004). Detailed characterization of Gid2/Rmd5 demonstrated that it is not present as a monomeric protein within the cell. In a glycerol step gradient, it sediments at ~600 kDa, suggesting that it is part of a soluble protein complex called Gid complex (Regelmann *et al.*, 2003). Proteomic interaction studies demonstrated that seven of the Gid proteins belong to one and the same complex (Ho *et al.*, 2002; Krogan *et al.*, 2006; Pitre *et al.*, 2006). A similar complex, constituted from protein homologues to the Gid proteins, has been found in mammals, in which one of its subunits has been shown to be involved in proteasome-dependent degradation of α -catenin (Kobayashi *et al.*, 2007; Suzuki *et al.*, 2008). Except for Gid3/Ubc8, which is not integral to the complex, and Gid2/Rmd5, no function in proteasome-dependent catabolite degradation of FBPase has been described for the newly discovered Gid proteins (Regelmann *et al.*, 2003).

Here, we further characterize the contribution of Gid2/Rmd5 to proteasomal degradation of FBPase, and we show that it confers E3 activity to the Gid complex. In addition, we show that degradation of PEPCCK is dependent on Gid2/Rmd5. Moreover, we uncover Gid4/Vid24 as a key regulator of FBPase degradation by the proteasome.

MATERIALS AND METHODS

Yeast Strains and Media

Previously described standard methods were used for media preparation and genetic and molecular biological techniques (Guthrie and Fink, 1991; Ausubel *et al.*, 1992). The *S. cerevisiae* strains used in these studies are summarized in Supplemental Table 1. Unless otherwise stated, all yeast strains were grown at 30°C. Precultures were grown 16 h in YPD medium containing 2% glucose, diluted 1:12.5 into YPD, and grown for additional 6–7 h. Thereafter, cells were resuspended in YPethanol (2%) and grown for 16 h to allow FBPase synthesis. For induction of FBPase degradation, cells were shifted onto YPD medium containing 2% glucose.

Construction of Epitope-tagged Gid Proteins and Plasmids

Gid1/Vid30, Gid5/Vid28, Gid6/Ubp14, Gid7, Gid8, and Gid9/Fyv10 were C-terminally labeled with a 3xHA-tag. Strain YJR12 (*GID1-HA₃*) was constructed by chromosomal integration of a 1.6-kb polymerase chain reaction (PCR) fragment consisting of a 3xHA-tag and a *Schizosaccharomyces pombe* HIS5 marker (Cottarel, 1995) into W303-1B cells. The PCR fragment was generated using oligonucleotides YJR12fwd, YJR12rev and plasmid p3xHA-HIS5 (S. Munro, Cambridge, United Kingdom) as template. Strains YTP10 (*GID7-HA₃*), YTP11 (*GID5-HA₃*), YTP12 (*GID9-HA₃*), YSA1 (*GID8-HA₃*), and YBB1 (*GID6-HA₃*) were generated by chromosomal integration of a 1.75-kb PCR fragment. Plasmid pFA6a-3HA-His3MX6 was described previously (Longtine *et al.*, 1998). Gid4/Vid24 was N-terminally Myc₃ tagged according to Gauss *et al.* (2005). For URA3 marker rescue with pSH63, instead of 1% raffinose and 1% galactose, the medium contained 2% galactose. The integration cassette was amplified from pOM22 (Gauss *et al.*, 2005) by using primer YOS1fwd and YOS1rev and transformed into strain W303-1B. Correct integration was confirmed by Southern blot analysis or PCR. *GID2-HA₃* construction is described in Regelmann *et al.* (2003). The pOS2 plasmid was constructed by insertion of a *Myc₃-GID4* fragment in a StuI/SbfI-digested pCM184 plasmid (Euroscarf, Frankfurt, Germany). All oligonucleotides used are listed in Supplemental Table 2. The construction of FBPase C-terminal TAP fusion was conducted as described previously based on the homologous recombination of a PCR product at a specific gene locus on the chromosome (Puig *et al.*, 2001). The plasmid expressing the FBPase-TAP fusion protein was

obtained using a gap-repair strategy. Plasmid pRG6 (de la Guerra *et al.*, 1988), which contains the *FBP1* gene and its genomic flanking regions was digested with NcoI. The plasmid, lacking the 800 base pair NcoI fragment was then transformed in a yeast strain expressing a chromosomally C-terminally tagged FBPase. Cells able to survive on complete minimal (CM) media lacking uracil were selected, plasmid rescue was performed, and the obtained plasmids were analyzed for the presence of an FBPase-TAP coding sequence, under the native FBPase promoter.

To construct the plasmid pFBPase, a genomic fragment encompassing the *FBP1* gene together with 1000 base pairs of its upstream and 200 base pairs of its downstream sequences was amplified by PCR with primers pFBPase-fwd and pFBPase-rev (Supplemental Table 2) and inserted into a SpeI/ClaI-digested pRS316 plasmid (Sikorski and Hieter, 1989). The resulting plasmid was verified by enzymatic restriction and sequencing. The plasmid-expressed FBPase is functional and undergoes degradation as the chromosomally expressed enzyme.

Mutation of the Degenerated RING Domain of GID2/RMD5

A point mutation in the conserved Cys residue 379 of Gid2/Rmd5 was performed using the Transformer site-directed mutagenesis kit (Clontech, Mountain View, CA). The template plasmid was generated by digesting a YCP50 plasmid (Rose *et al.*, 1987) using BamHI and Sall. The resulting fragment, bearing the *GID2/RMD5* ORF with its endogenous promoter and terminator regions was inserted in pRS316. Oligonucleotides are listed in Supplemental Table 2. The mutated *GID2/RMD5* was integrated in pRS306 digested with BamHI and Sall. Genomic integration was carried out by transforming the resulting plasmid in YTS3 yeast cells. Chromosomal DNA of colonies that lost the ability to grow on 5-fluorouracil containing medium was extracted, and the *GID2/RMD5* gene was sequenced.

Western Blotting

Western blotting was performed as described in Schork *et al.* (1995). Extracts were prepared via alkaline lysis (Yaffe and Schatz, 1984) and finally resuspended in urea buffer (200 mM Tris-HCl pH 6.8, 8 M urea, 5% SDS, 0.1 mM EDTA, 1% 2-mercaptoethanol, and 0.05% bromophenol blue). We used 3 OD₆₀₀ of cells for each sample. Antibodies used were obtained from BABCO (Richmond, CA) (hemagglutinin [HA], clone 16B12) and Calbiochem (San Diego, CA) (Myc, clone 9E10); FBPase polyclonal antibody was obtained from K. D. Entian (Goethe Universität, Frankfurt, Germany) or was produced by rabbit immunization using a purified FBPase-glutathione transferase (GST).

Immunoprecipitation

For immunoprecipitations (IPs) cells were cultivated as described above for FBPase turnover assays and samples were withdrawn at the indicated time points. Cells (30 OD₆₀₀) were harvested, washed with water, and resuspended in 600 μ l of phosphate-buffered saline (PBS) buffer pH 7.4 (137 mM NaCl, 1.25g/l Na₂HPO₄, and 0.35g/l NaH₂PO₄) containing protease inhibitors (Complete; Roche Diagnostics, Mannheim, Germany; 1.1 mM phenylmethylsulfonyl fluoride [PMSF]; 1 μ g/ml each of antipain, pepstatin A, chymostatin, and leupeptin) and lysed at 4°C with glass beads for 20 min. After centrifugation, 500 μ l of the supernatant was transferred to a new test tube. FBPase antibody was added, and the samples were gently agitated end over end for 2 h at 4°C. Immunoprecipitates were collected by adding 50 μ l of 5% (wt/vol) protein A-Sepharose CL-4B (GE Healthcare, Little Chalfont, United Kingdom) and further incubated for 1.5 h. For IP, the Sepharose beads were centrifuged and washed five times with ice-cold PBS buffer. Proteins were released from Sepharose by boiling in 50 μ l of urea buffer.

Glycerol Density Gradient Fractionation

Yeast cells were grown for 16 h in YPethanol. For analysis in gluconeogenic cells, 50 OD₆₀₀ of cells were harvested; for analysis in glycolytic cells, cells were shifted on YPD for 20 min before 50 OD₆₀₀ of cells were harvested. Cells were resuspended in 600 μ l of 0.1 M KH₂PO₄ pH 7.0, in the presence of Complete, 1.1 mM PMSF, and protease inhibitors; lysed with glass beads (20 min; 4°C); and centrifuged at 10,000 \times g for 15 min. Then, 200 μ l aliquots of the resulting cell extracts were layered on top of a glycerol step gradient [450 μ l each of 50%, 40%, 30%, 20 and 10% of glycerol in 20 mM piperazine-N,N'-bis(2-ethanesulfonic acid) buffer pH 6.8] and centrifuged at 55,000 rpm and 15°C for 4 h in a TLS-55 rotor. Thereafter, 200 μ l fractions were collected, precipitated with trichloroacetic acid (10%), solubilized in urea buffer, and analyzed by Western blotting.

Polyubiquitination of FBPase

Polyubiquitination was assessed either by growing the cells containing the FBPase-tandem affinity purification (TAP)-tag encoding plasmid on CM medium without uracil, 2% glucose or growing the *GID2-HA₃* and *GID2C379S-HA₃* strains on YPD to OD₆₀₀ 3–4. After harvesting (500 \times g; 5 min), cells were resuspended in the same medium containing 2% ethanol and left to grow for 6 h to allow derepression of FBPase. Then, 50 OD₆₀₀ of yeast were harvested

before and 25 min after addition of 2% glucose. After washing in 1 ml of water containing 20 mM N-ethylmaleimide, 20 mM Na₂S₂O₈, and 1 mM PMSF, cells were pelleted at 500 × *g* for 4 min at 4°C and resuspended in 600 μl of ice-cold PBS buffer containing protease inhibitors and lysed at 4°C with glass beads (300 μl; 0.4–0.6 mm in diameter) during 20 min. IP of FBPase was performed as described above, and the pellet was washed five times with PBS buffer containing 0.2% Triton X-100. Alternatively, FBPase-TAP was pulled down using 80 μl of 50% (vol/vol) immunoglobulin G (IgG)-Sepharose beads. After 3 h of incubation at room temperature, beads were washed four times with PBS added with 150 mM NaCl and 1% (vol/vol) Triton X-100. In both cases, beads were resuspended in 50 μl of urea buffer, boiled for 5 min at 95°C and used for immunoblotting with monoclonal anti-ubiquitin antibody (clone P4G7; Covance Research Products, Princeton, NJ).

In Vitro Polyubiquitination Assay

A GST-fusion protein of Gid2/Rmd5, and, as a positive control, the mammalian RING protein gp78 (309–643-amino acid fragment) were expressed in the *Escherichia coli* BL21 strain. Bacteria were grown to OD₆₀₀ 0.8–1 in 2× yeast tryptone containing 100 μg/ml ampicillin, and expression of the extrinsic protein was induced at 16°C with 0.5 mM isopropyl β-D-thiogalactoside during 6–12 h. Cells were harvested, resuspended in buffer A (50 mM Tris-HCl, pH 7.5, 250 mM NaCl, 5 mM dithiothreitol (DTT), 2 mM PMSF, and 1% Triton-X 100) and lysed with a French press. A typical 20 μl ubiquitination reaction was carried out by adding 0.25 μg of E1 (yeast), 0.6 μg of UbcH5b, 10 μg of HA-ubiquitin, 1 μl of energy regeneration solution (all BostonBiochem, Cambridge, MA), 2 μl of 10× ubiquitin reaction buffer (500 mM Tris-HCl, pH 7.5, 500 mM NaCl, 100 mM MgCl₂, 10 mM DTT, and 250 μM ZnCl₂), and 8 μl of Gid2/Rmd5 or gp78 cell lysate. The reactions were incubated at 30°C for 2 h, and ubiquitination of proteins was monitored by Western blotting using monoclonal anti-HA antibody.

Gid4/Vid24 Expression in Gluconeogenic Cells

gid4Δ/vid24Δ yeast cells were transformed with the pOS2 plasmid encoding Gid4/Vid24 under control of the Tet^R promoter or the corresponding control vector. After 16 h of growth on CM-Trp media containing 2% glucose and 40 μg/ml doxycycline, cells were transferred into the same medium lacking cysteine and methionine for 16-h growth. Five OD₆₀₀ of yeast were pelleted washed once with distilled water and resuspended in 2% EtOH-CM-Trp medium without cysteine and methionine, but containing 40 μg/ml doxycycline. After 3 h of incubation; radiolabeling was achieved by addition of 9.25 MBq of [³⁵S]methionine and a further 2 h of incubation time (pulse). Consecutively, cells were centrifuged, washed with water and resuspended in 6.5 ml of CM-Trp-EtOH (2%) containing 10 mM nonradioactive methionine (chase). Samples were harvested every hour during 3 h. After FBPase immunoprecipitation and 10% SDS-polyacrylamide gel electrophoresis, gels were overlaid with Phosphor screen and scanned with Storm 860 (GE Healthcare) for protein quantification.

Degradation of Gid4/Vid24

To monitor Gid4/Vid24 degradation, cells were grown as described above for FBPase turnover assays. After 16 h of growth on YPethanol (2%); cells were shifted onto YPD for 30 min to induce *GID4/VID24* expression. Cells were then shifted onto fresh YPD with 100 μg/ml cycloheximide. For the proteasome inhibition experiment, along with cycloheximide treatment, 60 μM MG-132 were added 30 min ahead of harvesting. This treatment was repeated every 30 min to ensure a proper proteasome inhibition. To monitor Gid4/Vid24 stability; 1.5 OD₆₀₀ of cells were taken at each time point and analyzed by immunoblotting.

Sequence Analysis

Sequence database searches were carried out with a nonredundant data set assembled from current releases of Uniprot and GenPept (Benton, 1990; Bairoch and Apweiler, 1997). Multiple alignments were calculated by MUSCLE (Edgar, 2004), using excised domains instead of the entire protein sequences. Generalized profile construction (Bucher *et al.*, 1996), and searches were run locally using the pftools package, version 2.1. Generalized profiles were constructed using the BLOSUM45 substitution matrix (Henikoff and Henikoff, 1992) and default penalties of 2.1 for gap opening and 0.2 for gap extension. Profile matches were analyzed for statistical significance by means of the score distribution of a randomized database (Hofmann, 2000). Only sequence matches that were detected with a probability *p* lower than 0.01 were included in subsequent rounds of iterative profile refinement.

RESULTS

Expression Profiles and Sedimentation Pattern of Gid Proteins

In a genomic screen, the previously discovered *GID1/VID30*, *GID2/RMD5*, and *GID3/UBC8* genes were identified along

with six additional *GID* genes to be necessary for glucose-induced FBPase degradation (Schork *et al.*, 1995; Hämmerle *et al.*, 1998; Schüle *et al.*, 2000; Regelman *et al.*, 2003). Further characterization of Gid2/Rmd5 suggested that it is part of a complex of at least 600 kDa (Regelman *et al.*, 2003). Mass spectrometry analyses of proteins interacting with either Gid7 or Gid1/Vid30 uncovered the Gid proteins as subunits of the same complex (Ho *et al.*, 2002; Krogan *et al.*, 2006; Pitre *et al.*, 2006).

To be able to detect the Gid proteins immunologically, their genes were chromosomally tagged with either 3xHA or 9xMYC coding sequences. The resulting strains were tested for their ability to degrade FBPase. Except for cells expressing the Gid9-HA₃ protein, all strains displayed wild-type FBPase degradation kinetics (data not shown). The expression of the Gid proteins was monitored in ethanol-growing cells and up to 120 min after shift to glucose-containing media. Besides Gid2/Rmd5 (Regelman *et al.*, 2003), five additional Gid proteins (Gid1/Vid30, Gid5/Vid28, Gid7, Gid8, and Gid9/Fyv10) were already present in ethanol-grown (gluconeogenic conditions) cells, and their levels remained constant over 120 min after shift to glucose (Figure 1A). An additional Gid protein, Gid4/Vid24 was undetectable when cells were grown in ethanol-containing medium. However, as soon as cells were transferred to glucose-containing medium, the Gid4/Vid24 protein rapidly occurred, its levels culminating ~30 min after shift. Thereafter, Gid4/Vid24 levels decreased in parallel with those of FBPase (Figure 1A). Gid4/Vid24 synthesis upon glucose addition to cells growing on a nonfermentable carbon source had already been described, whereas no subsequent degradation of the protein had been observed under the inactivation conditions used (Chiang and Chiang, 1998).

Using glycerol step gradient analysis, Regelman *et al.* (2003) found that Gid2/Rmd5 exists in a complex of ~600 kDa. As shown in Regelman *et al.* (2003) for the Gid2/Rmd5 protein, the other six Gid proteins (Gid1/Vid30, Gid4/Vid24, Gid5/Vid28, Gid7, Gid8, and Gid9/Fyv10) also sediment at high molecular mass (data not shown). Indeed, mass spectrometry analyses identified a complex in which the seven Gid proteins reside (Ho *et al.*, 2002; Krogan *et al.*, 2006; Pitre *et al.*, 2006). All these analyses were performed in glucose-containing media. Because Gid4/Vid24 is absent under gluconeogenic conditions, we tested its requirement for the formation of a high molecular mass Gid complex. Glycerol step gradients were performed to observe the sedimentation patterns of Gid1-HA₃ and Gid7-HA₃ in gluconeogenic conditions (Gid4/Vid24 absent; Figure 1A), and 20 min after shift to glucose, where Gid4/Vid24 is present (Figure 1A). As shown in Figure 1B, no significant differences in the sedimentation patterns of Gid1-HA₃ (116 kDa) and Gid7-HA₃ (92 kDa) before (*T* = 0) and 20 min (*T* = 20) after glucose shift could be seen: both proteins sediment with molecular masses in the range of 600 kDa, as shown by their cofractionation with the 600 kDa aminopeptidase I homodimer complex (Ape1). Although it cannot be completely excluded that the binding partners within the Gid-complex vary between ethanol- and glucose-grown cells, this experiment suggests that the tested Gid proteins are already present in a complex when cells grow on a nonfermentable carbon source and do not dissociate to their respective monomers when Gid4/Vid24 is absent from the cell.

Gid1/Vid30 Interacts with FBPase

A direct involvement of the Gid complex in FBPase degradation requires binding of FBPase to Gid proteins. We therefore examined whether Gid1-HA₃, as an example,

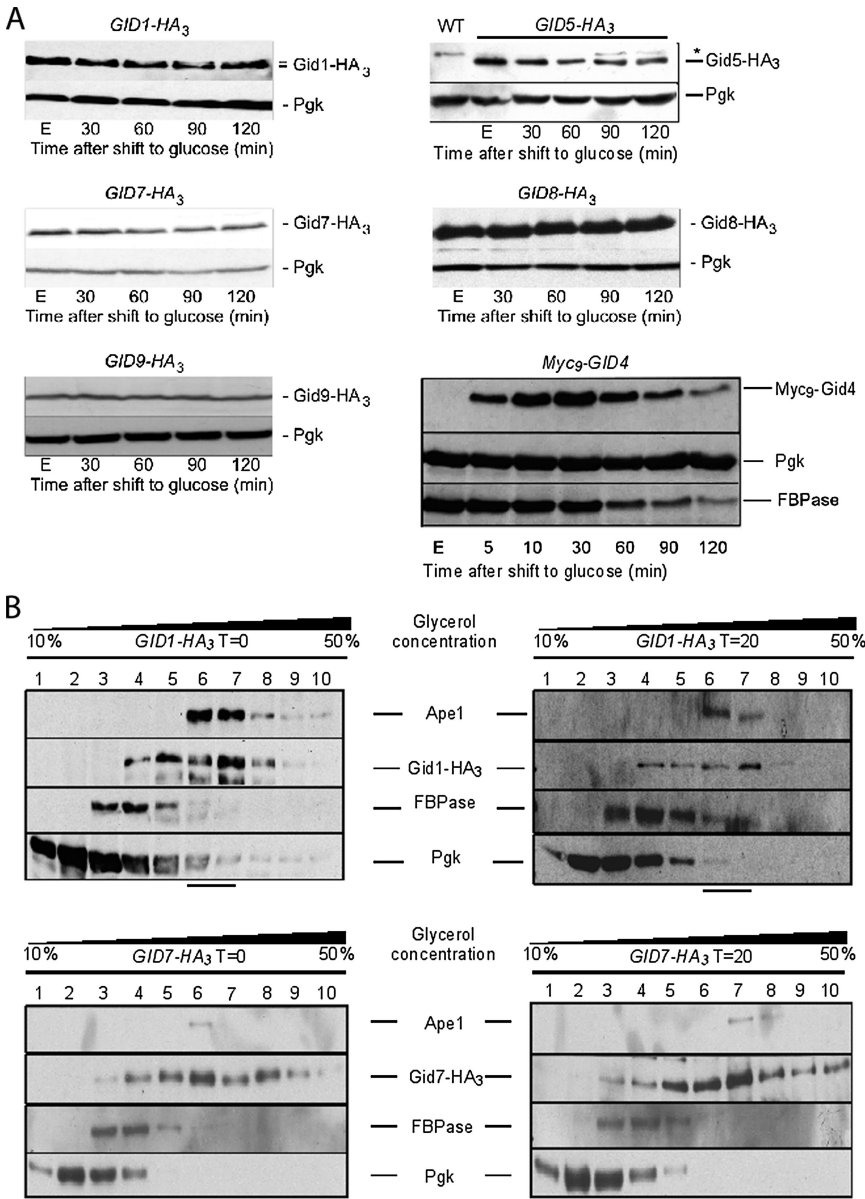


Figure 1. Gid complex subunits are present in gluconeogenic cells. (A) Strains expressing chromosomally tagged Gid proteins with the HA or Myc epitope were grown 16 h in YPethanol (E) and thereafter treated with 2% glucose. Samples were taken at the indicated time points and processed as described in *Material and Methods*. Proteins were visualized by immunoblotting. *, cross reaction; WT, wild type, control for cross-reaction. (B) Strains bearing a chromosomally expressed HA-tagged Gid protein (Gid1/Vid30 and Gid7) were grown 16 h in YPethanol. Samples were harvested before (T = 0) or 20 min after shift to glucose (T = 20), and proteins were separated on a glycerol step gradient. Ten fractions were collected, and proteins were visualized by immunoblotting (Pgk, 3-phosphoglycerate kinase; Ape1, aminopeptidase I).

coimmunoprecipitates with FBpase. We used a *GID6-HA₃* strain as a control for the interaction of FBpase with the Gid complex. *GID6* was shown previously to encode Ubp14 deubiquitinating enzyme, its deletion prevents the cleavage of polyubiquitin chains released from proteasome substrates into single ubiquitin moieties. This deletion leads to competition between uncleaved polyubiquitin chains and polyubiquitinated proteins for the proteasome (Amerik *et al.*, 1997), which has been shown to impair proteasomal degradation of FBpase (Eisele *et al.*, 2006). Thus, the effect of *GID6* deletion on FBpase degradation is unspecific. Moreover, Gid6/Ubp14 was not detected as being part of the Gid complex (Ho *et al.*, 2002; Krogan *et al.*, 2006; Pitre *et al.*, 2006). YJJ9 (*GID1-HA₃*, *fbp1Δ*) and YBB1 (*GID6-HA₃*) strains were transformed with a plasmid expressing a wild-type FBpase (pFBpase) or pRS316 as a vector control. YJJ9 strain transformed with pFBpase and YBB1 strain transformed with pRS316 were grown in YPethanol and shifted to YPD. The YJJ9

strain transformed with pRS316, for which the endogenous FBpase is not replaced by a plasmid-encoded enzyme, is unable to grow on nonfermentable carbon sources and was therefore grown on YPD only. Samples were withdrawn at the indicated time points, and FBpase was precipitated using specific anti-FBpase antibodies (Figure 2). The precipitates were monitored by immunoblotting with FBpase and HA-antibodies. Figure 2 shows that FBpase strongly coimmunoprecipitates with Gid1-HA₃ in YPethanol at the time point “0” and after 20 min of glucose addition to cells. A similar result was obtained when a strain expressing FBpase chromosomally was used for the immunoprecipitation (data not shown). No interaction between FBpase and Gid6-HA₃/Ubp14-HA₃ could be observed, demonstrating that no unspecific interaction occurs between FBpase and the HA-tag. Moreover, Gid1-HA₃ was not immunoprecipitated when no FBpase was present, establishing that the anti-FBpase antibody does not bind unspecifically to Gid1-HA₃.

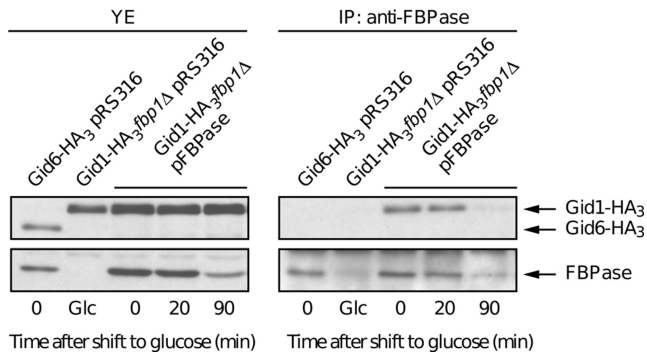


Figure 2. FBPase binds to Gid1/Vid30. Strains expressing HA-tagged Gid proteins (Gid1/Vid30 and Gid6/Ubp14) and transformed with a plasmid expressing a wild-type FBPase (pFBPase) or its corresponding vector control (pRS316) were grown 16 h on YPethanol. Samples were harvested 0, 20, and 90 min after glucose treatment, and proteins were extracted. Coimmunoprecipitation was performed with FBPase antibody. Protein immunoblot was carried out with FBPase and HA antibodies. The noninteracting Gid6/Ubp14 protein serves as a control (YE, extracts; IP, immunoprecipitations). The *FBP1* deletion mutant transformed with the vector control was grown on glucose and provides a control for the specificity of the anti-FBPase antibody.

Gid2/Rmd5 Confers Ubiquitin Ligase (E3) Activity

Gid2/Rmd5 contains a Lissencephaly type-1-like homology motif (LisH), a C-terminal to LisH motif (CTLH), and a degenerated RING finger domain, an organization shared with its human orthologues (Figure 3, A and C). Many ubiquitin ligases contain a RING-finger domain bearing eight Cys/His coordination sites to complex Zn^{2+} ions necessary for activity (Lorick *et al.*, 1999; Fang and Weissman, 2004). A complete cysteine and histidine pattern in a RING domain is not necessarily critical for the E3 function, as the U-box domain family shows. Although the U-box domain still adopts the same structure as the RING domain, it is an extreme example of degeneration of zinc-coordinating residues, where none of them are retained (Ohi *et al.*, 2003). In *Gid2/Rmd5* the degenerated RING domain is characterized by an incomplete series of Zn^{2+} ion-coordinating residues compared with the classic RING finger (Figure 3B, compare top and bottom alignments). The canonical RING domain encompasses eight residues coordinating two Zn cations. The first Zn^{2+} ion is coordinated by the first, second, fifth, and sixth residue; the second by the remaining residues three, four, seven, and eight (Lorick *et al.*, 1999; Fang and Weissman, 2004). In *Gid2/Rmd5* besides the first cysteine, the four residues coordinating the second Zn^{2+} ion are conserved (Figure 3B), which strongly suggests that one ion is retained in this degenerated RING domain. This prompted us to suspect that *Gid2/Rmd5* may bear an ubiquitin ligase activity. The ubiquitin system is present in all eukaryotes but is not found among bacteria. A heterologous expression of a GST-Gid2 fusion protein in *E. coli* led to polyubiquitination of proteins in the bacterial lysate when E1 and E2 enzymes, ATP and HA-ubiquitin were added (Figure 4A). When only the GST protein was expressed, no polyubiquitination could be detected (Figure 4A). We further determined the contribution of the *Gid2/Rmd5* degenerated RING finger to FBPase polyubiquitination in vivo by mutating the conserved cysteine residue at position 379 of the putative *Gid2/Rmd5* RING domain to serine. The HA-tagged version of the mutated gene was introduced into the yeast genome. As can be seen in Figure 4B, degradation of FBPase

is dramatically impaired in cells carrying the *GID2C379S* mutation. The strain expressing the mutant protein is unable to polyubiquitinate FBPase in vivo (Figure 4C). We conclude that *Gid2/Rmd5* bears an E3 activity necessary for degradation of FBPase.

Role of *Gid4/Vid24* in the FBPase Catabolite Degradation

Gid4/Vid24 is necessary for FBPase degradation (Regelmann *et al.*, 2003). The protein is absent in ethanol-growing cells and occurs early after glucose addition to the medium (Figure 1A). Thus, blocking de novo protein synthesis is likely to prevent *Gid4/Vid24* appearance and subsequent FBPase breakdown by the proteasome. To test this hypothesis, cells were treated with the translation inhibitor cycloheximide when they were shifted from gluconeogenic to glycolytic conditions. Indeed, cells that underwent cycloheximide treatment were unable to express *Gid4/Vid24* and therefore to degrade FBPase (Figure 5A). Because *Gid3/Ubc8* and other Gid proteins, except *Gid4/Vid24*, are present in ethanol-growing cells (Figure 1, Regelmann *et al.* (2003)), this result suggests that *Gid4/Vid24* might trigger FBPase degradation. If *Gid4/Vid24* were a switch, initiation of FBPase elimination should take place when *Gid4/Vid24* is expressed in ethanol-growing cells. *FBP1* gene expression is repressed when cells grow on a glucose-containing medium; on the contrary, when grown on a nonfermentable carbon source, yeast cells readily express FBPase (Zaragoza and Gancedo, 2001). Thus, a pulse-chase experiment, where FBPase was radioactively labeled, has been carried out to monitor FBPase degradation when *Gid4/Vid24* expression is forced in ethanol-growing cells. Indeed, expression of *Gid4/Vid24* in YPethanol growing cells lowers the half-life of FBPase by approximately threefold (Figure 5B). Although one cannot exclude that additional modifications are necessary to signal FBPase degradation, this result strongly suggests that *Gid4/Vid24* is the only protein whose de novo synthesis is required to trigger FBPase elimination.

The fact that *Gid4/Vid24* is a molecular switch triggering FBPase degradation even in gluconeogenic conditions led us to ask whether the *Gid2/Rmd5*-dependent polyubiquitination of FBPase would depend on *Gid4/Vid24*. The TAP tag allows to purify proteins (Puig *et al.*, 2001). Because it bears a protein A sequence, it is able to strongly bind the IgG constant fragment. This property allowed us to use the tag to perform IgG-Sepharose pull-downs. Moreover, when fused to an otherwise poorly detectable protein, it easily facilitates protein detection. Immunoprecipitation of FBPase was often complicated by the fact that the enzyme migrates only slightly faster on SDS-polyacrylamide gels than IgGs. Therefore, a plasmid expressing a catalytically active C-terminally TAP-tagged FBPase was transformed in W303 (WT) and *gid4Δ/vid24Δ* strains to ensure a good detection of the enzyme and its polyubiquitinated forms. Pull-down with IgG-Sepharose and subsequent detection with an anti-ubiquitin antibody revealed that *Gid4/Vid24* is indeed necessary for FBPase polyubiquitination (Figure 5C). Together, these results suggest that *Gid4/Vid24* is a switch allowing the polyubiquitination of FBPase before its degradation by the proteasome.

Elimination of *Gid4/Vid24* Depends on the Ubiquitin-Proteasome System and the Gid Complex

As shown in Figure 1A, Myc₉-Gid4 levels increase with time when cells are shifted from YPethanol to YPD. After reaching a maximum at ~30 min after shift to glucose, the Myc₉-Gid4 signal diminishes in parallel with FBPase. To test whether this diminution is dependent on the ubiquitin-

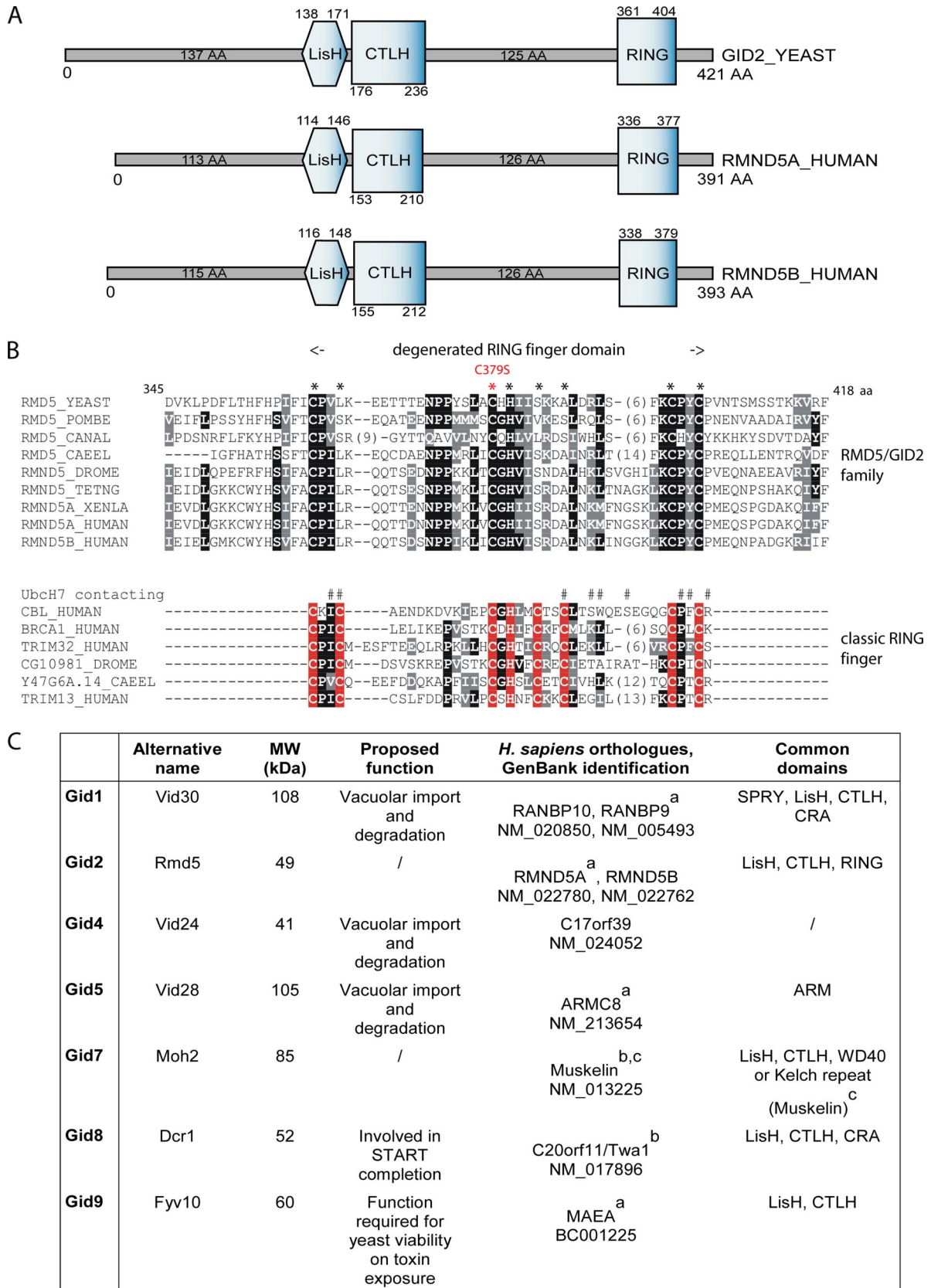


Figure 3. Domain structures of Gid proteins. (A) Structure similarities between the Gid2/Rmd5 (*S. cerevisiae*) and RMND5A/B (*Homo sapiens*) proteins. (B) Alignment of the RING domains found in the Gid2/Rmd5 protein family and classic RING-finger proteins. Positions with invariant or conservatively replaced residues in at least 50% of the sequences are printed on black or gray background, respectively (not all sequences analyzed are shown). The leftmost column describes the sequence name and contains the species abbreviation: YEAST, *S. cerevisiae*;

conjugating enzyme Ubc8, components of the Gid complex, and the proteasome, we deleted *GID2/RMD5*, *UBC8*, and, for proteasome inhibition by the proteasome inhibitor MG-132, *PDR5* in a strain expressing Myc₉-Gid4. *PDR5* encodes an ATP-binding cassette transporter, which prevents accumulation of hydrophobic compounds in the yeast cytosol (Balzi *et al.*, 1994; Bissinger and Kuchler, 1994). Its deletion is thus necessary to prevent inhibitor efflux from the cell. After overnight growth in ethanol-containing medium, the tested strains were shifted to glucose-containing medium for 30 min to allow Myc₉-Gid4 expression before cycloheximide treatment. Samples were collected at the indicated time points after cycloheximide treatment. Figure 6 shows that, similar to elimination of FBPase, degradation of Gid4/Vid24 depends on Ubc8 (E2) and the proteasome. Interestingly, degradation of Gid4/Vid24 also depends on components of the Gid complex because deletion of *GID2/RMD5* stalls its degradation (Figure 6). Elimination of Myc₉-Gid4 is not due to the Myc-tag as native, endogenous Gid4/Vid24 shows identical behavior (Jospeit and Wolf, unpublished).

Catabolite Degradation of PEPCK Requires Subunits of the Gid Complex

The highly exergonic last reaction step in glycolysis, the formation of pyruvate and ATP by pyruvate kinase is circumvented in gluconeogenesis by the action of pyruvate carboxylase and PEPCK. As for FBPase, PEPCK synthesis is repressed by glucose and subjected to catabolite degradation when cells are shifted from gluconeogenic to glycolytic conditions (Holzer, 1976; Muller *et al.*, 1981; Mercado and Gancedo, 1992; Yin *et al.*, 2000). This allowed us to monitor the degradation of PEPCK after shift of cells from YPethanol to YPD. Interestingly, deletions of *GID2/RMD5* or *GID4/VID24* stall degradation of PEPCK, indicating the requirement of the Gid complex for its catabolite degradation (Figure 7). This suggests that the Gid complex plays a general role in catabolite degradation.

DISCUSSION

FBPase is essential for yeast growth on nonfermentable carbon sources such as acetate or ethanol. When a fermentable carbon source becomes available, the *FBP1* gene expression is repressed and the enzyme is inactivated by allosteric inhibition before being degraded (Holzer, 1976; von Herrath and Holzer, 1988). The site of degradation (vacuole or proteasome) has been subject to controversy. Now, it seems rather clear that the type of gluconeogenic conditions influence the degradation pathway (Schork *et al.*, 1994b; Chiang

Figure 3 (cont). POMBE, *S. pombe*; CANAL, *Candida albicans*; HUMAN, *H. sapiens*; XENLA, *Xenopus laevis*; DROME, *Drosophila melanogaster*; CAEEL, *Caenorhabditis elegans*; TETNG, *Tetraodon nigroviridis*. Larger insertions are not shown; the number of omitted residues is indicated in parentheses. Asterisks above the Gid2/Rmd5 family alignment correspond to positions homologous to zinc coordinating residues in classic RING finger domains (red). The mutation introduced in the Gid2/Rmd5 degenerated RING domain is highlighted (C379S, red). Above the classic RING-finger proteins alignment, residues of Cbl in contact with UbcH7 are marked by # (Zheng *et al.*, 2000). (C) Overview of the Gid proteins and their counterparts in *H. sapiens*. The table summarizes the common features in Gid proteins and their human counterparts. ^aOrthologues identified in a CTLH complex by Kobayashi *et al.* (2007); ^bOrthologues found to interact together by Umeda *et al.* (2003). ^cMuskelin bears CTLH and Kelch domains, which makes its overall structure similar to Gid7. Other functions and names, SGD, www.yeastgenome.org.

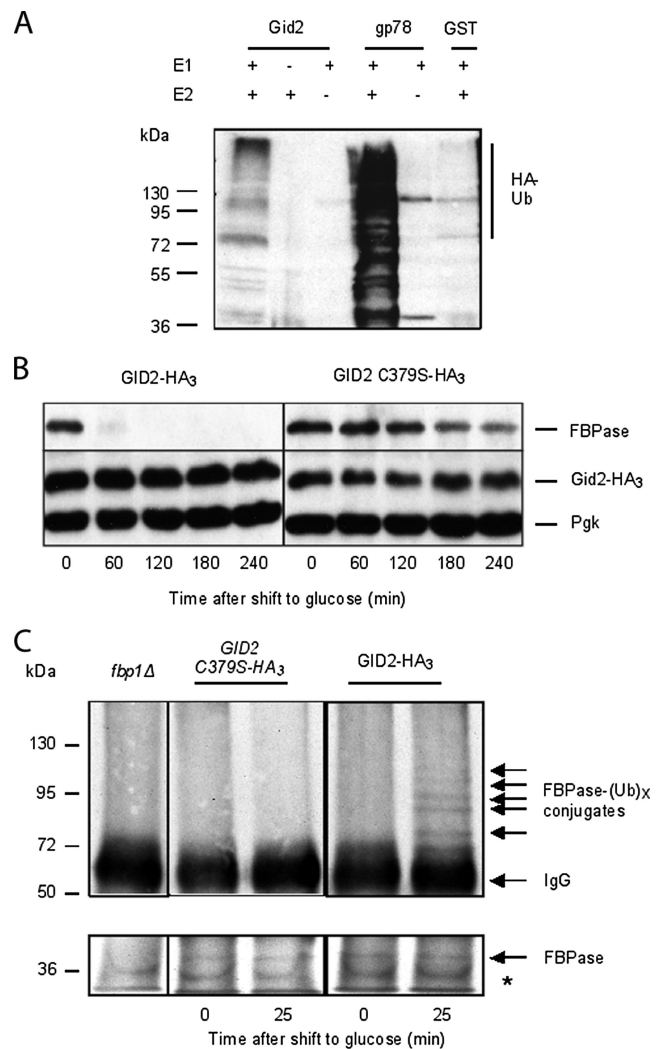


Figure 4. Gid2/Rmd5 shows E3 activity. (A) Gid2/Rmd5 ubiquitinates protein *in vitro*. Lysates of *E. coli* expressing either Gid2/Rmd5 or the mammalian RING-finger protein gp78 as a positive control and GST as a negative control were incubated with E1, E2 (UbcH5b), ATP and HA-ubiquitin for 2 h at 30°C. To assess the specificity of the reaction, same lysates were incubated without E1 or E2. Polyubiquitination was detected using monoclonal HA antibody. (B) *GID2-HA₃* and its mutated C379S counterpart-expressing cells were grown 16 h in YPethanol at 25°C and shifted to YPD. Samples were taken at indicated time points and FBPase degradation was monitored by immunoblotting. Pgk, 3-phosphoglycerate kinase, loading control. (C) Point mutation in the Gid2/Rmd5 degenerated RING domain abolishes FBPase polyubiquitination. Chromosomally tagged *GID2-HA₃*, which shows a wild-type phenotype, and a strain bearing the C379S point mutation in a *GID2-HA₃* strain were grown 16 h in YPethanol at 25°C and shifted to YPD. Samples were taken at indicated time points, and FBPase was immunoprecipitated. Polyubiquitination was detected using monoclonal ubiquitin antibody. *fbp1Δ*: FBPase deletion. Presence of FBPase in the immunoprecipitates was controlled by immunoblotting with FBPase antibody. *, cross-reaction.

and Chiang, 1998; Hämmerle *et al.*, 1998; Hung *et al.*, 2004). Vacuolar import and degradation of FBPase occurs when cells are grown 2–3 d on an acetate-containing medium. Such conditions trigger autophagy, which is not likely to be relieved by the sole addition of glucose to the medium. Thus, one may speculate that yeast cells use the pre-existing

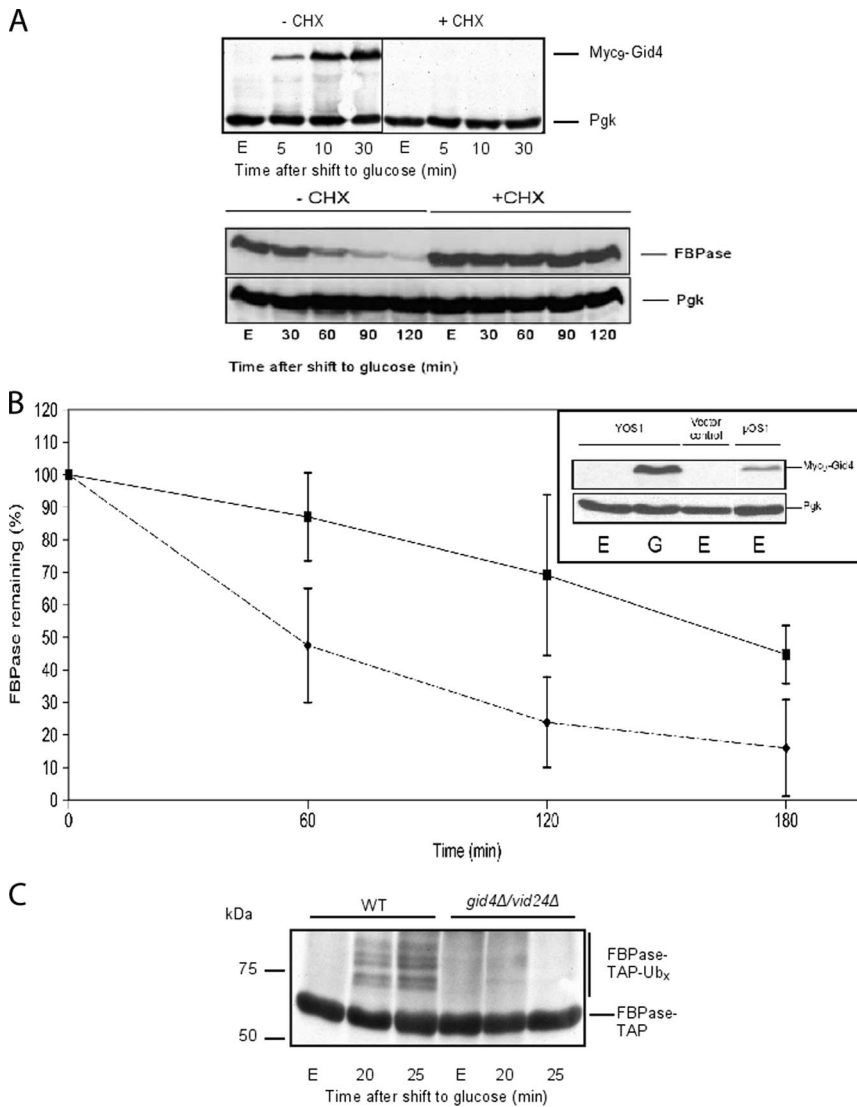


Figure 5. Gid4/Vid24 promotes FBPase degradation. (A) De novo protein synthesis is necessary for FBPase degradation and Myc₉-Gid4 expression. Wild-type cells were grown 16 h in YPethanol (E) and shifted to YPD with (+CHX) or without (−CHX) cycloheximide (100 μg/ml). FBPase and Myc₉-Gid4 levels were monitored at indicated times via immunoblotting with anti-FBPase or anti-Myc antibodies, respectively. (B) Gid4/Vid24 expression triggers FBPase degradation. Myc₉-GID4 was cloned under a Tet^R promoter and expressed in cells growing on YPethanol. Pulse-chase analysis of FBPase in cells bearing either the Myc₉-GID4 expressing plasmid (◆) or the respective vector control (■) was carried out (means of three independent experiments, ± confidence interval, α = 0.05). Inset, immunoblot showing the steady-state levels of Myc₉-Gid4 in glucose-inactivated cells (30 min, YOS1, G) and in ethanol grown cells (pOS1, E). (C) Gid4/Vid24 is necessary for FBPase-TAP polyubiquitination. A plasmid expressing a FBPase-TAP fusion protein was transformed into W303 (WT) and *gid4Δ/vid24Δ* strains. Samples were taken at indicated time points, and FBPase was pulled-down using IgG-Sepharose. Polyubiquitination was detected using monoclonal ubiquitin antibody.

degradation machinery to specifically degrade FBPase when growth conditions favor this autophagic process. On the contrary, overnight growth on ethanol, a nonfermentable but natural carbon source for *S. cerevisiae* triggers FBPase degradation by the proteasome. A genome-wide screen revealed nine genes whose deletion impaired proteasomal-dependent FBPase degradation upon shift to glucose-containing medium (Regelmann *et al.*, 2003). Among these genes, Gid1/Vid30, Gid4/Vid24, Gid5/Vid28 were first implicated in a vacuolar-dependent FBPase degradation (Chiang and Chiang, 1998). Moreover, *GID3* and *GID6* genes were shown to encode Ubc8 and Ubp14, respectively (Schüle *et al.*, 2000; Regelmann *et al.*, 2003). It was demonstrated that Gid2/Rmd5 belongs to a soluble complex of ~600 kDa (Regelmann *et al.*, 2003). Also, Gid1/Vid30, Gid4/Vid24, Gid5/Vid28, Gid7, Gid8, and Gid9/Fyv10 belong to a soluble complex (data not shown). Systematic interaction studies identified those Gid proteins as units of the same complex (Ho *et al.*, 2002; Krogan *et al.*, 2006; Pitre *et al.*, 2006). Epitope tagging allowed us to monitor the expression of the Gid proteins. Interestingly, Gid4/Vid24 is the only Gid protein that cannot be detected in ethanol-growing cells. This led us to suspect that Gid4/Vid24 might be an activator of the Gid

complex. In glycerol step gradient analysis, no differences between the sedimentation patterns of Gid1-HA₃ and Gid7-HA₃ before (Gid4/Vid24 absent) and 20 min after shift to glucose (Gid4/Vid24 present) could be revealed (Figure 1B). Although it cannot be excluded that the binding partners of Gid1/Vid30 or Gid7 differ between gluconeogenic and glycolytic conditions, both proteins remain in a complex even when Gid4/Vid24 is absent, suggesting that this Gid protein has no influence on the assembly of monomeric Gid proteins to a higher molecular mass complex. The Gid proteins are involved in the proteasomal degradation of FBPase. Whether the Gid complex is part of an upstream signaling pathway or whether it is directly involved in FBPase polyubiquitination and degradation remained to be clarified. We show that Gid1/Vid30 interacts with FBPase. As Gid1/Vid30 is part of the Gid complex (Ho *et al.*, 2002; Krogan *et al.*, 2006; Pitre *et al.*, 2006), this result indicates that FBPase and the Gid complex interact.

A *GID2/RMD5* deletion prevents polyubiquitination of FBPase (Regelmann *et al.*, 2003). Alignments of the Gid2/Rmd5 protein sequence with known RING-finger E3s revealed that it bears a so-called degenerated RING-finger where Zn²⁺ coordination residues are missing (Figure 3B).

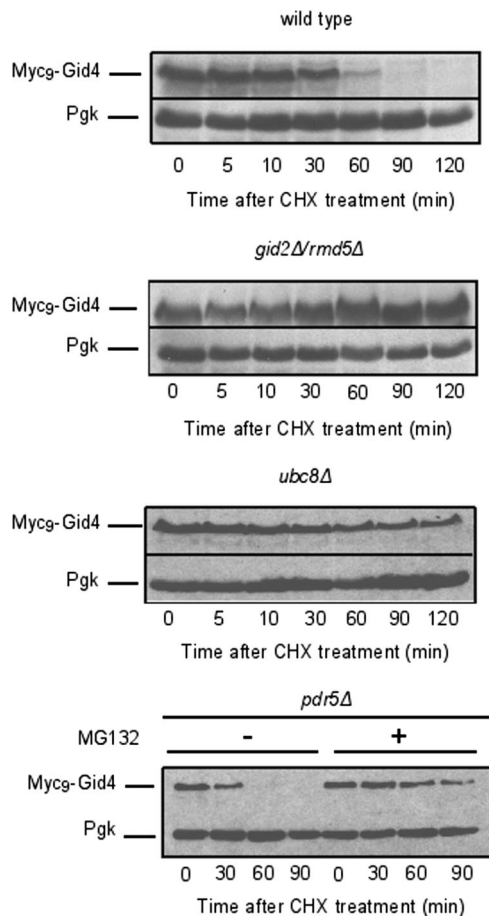


Figure 6. Gid4/Vid24 degradation depends on Gid2/Rmd5, Ubc8 and the proteasome. W303-1B expressing Myc₉-Gid4 was deleted for *UBC8*, *GID2/RMD5*, or *PDR5* (*ubc8Δ*, *gid2Δ*, *pdr5Δ*, respectively). Strains were grown 16 h on YPethanol, shifted to YPD, and expression of Gid4/Vid24 was allowed to proceed during 30 min. Thereafter, cells were treated with cycloheximide and samples were harvested at the indicated times. Proteins were visualized via immunoblotting. Proteasome involvement in Gid4/Vid24 degradation was analyzed in a *pdr5Δ* strain using the proteasome inhibitor MG-132.

Although the U-box domain family lacks all Zn²⁺ coordinating residues, it still polyubiquitinates proteins (Hatakeyama *et al.*, 2001; Ohi *et al.*, 2003). This prompted us to test whether this would also be the case for Gid2/Rmd5. Indeed, Gid2/Rmd5 polyubiquitinates proteins *in vitro*. Moreover, destroying a remaining Zn²⁺ coordination site in Gid2/Rmd5 leads to a failure to polyubiquitinate FBPase *in vivo* (Figure 4). These results imply that the Gid complex is an ubiquitin ligase (E3), whose activity is provided by the Gid2/Rmd5 subunit (Figure 8).

We further characterized the function of the Gid4/Vid24 subunit within the new E3 complex. Gid4/Vid24 had previously been implicated in targeting FBPase from vesicles to the vacuole and was shown to occur only upon glucose addition to acetate-starved cells where it remained stable (Chiang and Chiang, 1998). We here show that also in cells growing on ethanol, a natural carbon source of yeast, Gid4/Vid24 occurs upon glucose shift (Figure 1A). Because Gid4/Vid24 becomes detectable as fast as 5 min after shift of cells from ethanol to glucose, it is unlikely that *GID4/VID24* gene expression depends on transcription followed by translation. Indeed, *GID4/VID24* mRNA levels do not vary signif-

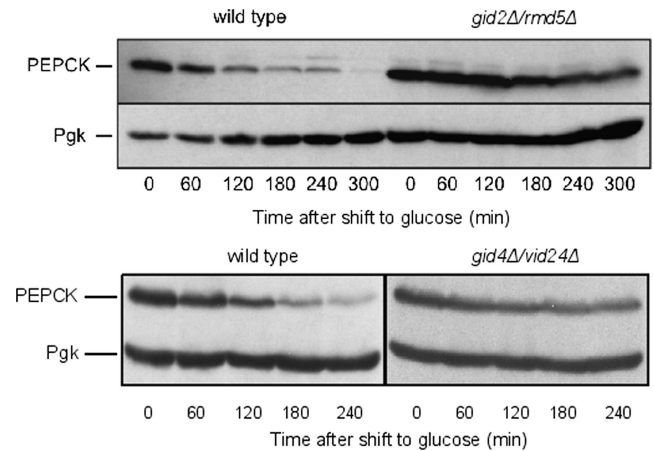


Figure 7. GID deletions impair PEPCK degradation. Wild type, *gid2Δ/rmd5Δ*, or *gid4Δ/vid24Δ* cells were grown 16 h on YPethanol, and thereafter shifted onto YPD. Cells were harvested every hour, and extracts were prepared. Proteins were visualized via immunoblotting. Pgk, 3-phosphoglycerate kinase, loading control.

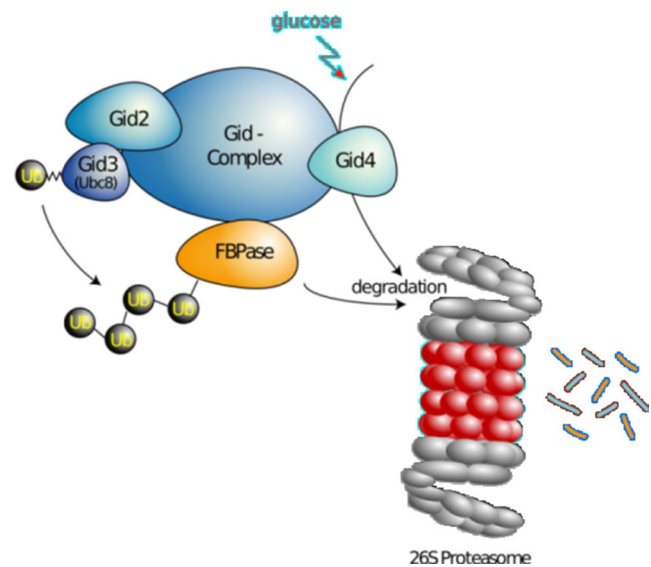


Figure 8. The Gid complex, a novel ubiquitin ligase (E3) required for the degradation of the key gluconeogenic enzyme fructose-1,6-bisphosphatase. The Gid complex binds to FBPase, when *S. cerevisiae* cells are growing on an ethanol-containing medium. On shift of cells to glucose, Gid4/Vid24 occurs and activates the complex, which then polyubiquitinates FBPase before its degradation by the proteasome. Gid4/Vid24 is itself degraded by the proteasome.

icantly when cells grow on these two different media (DeRisi *et al.*, 1997). Thus, the regulation of *GID4/VID24* expression might be carried out at the posttranscriptional level. Hung *et al.* (2004) confirmed our data that Gid4/Vid24 partakes in proteasome-dependent FBPase degradation. The different expression patterns of Gid4/Vid24 observed during the vacuolar degradation process of FBPase in which it remains stable (Chiang and Chiang, 1998) and the proteasomal degradation of the enzyme in which Gid4/Vid24 is degraded might reflect the different requirements of Gid4/Vid24 in these processes. Because Gid4/Vid24 has no influence on sedimentation patterns of two Gid proteins known to be part of the Gid complex (Figure 1B), it seems more likely that Gid4/Vid24 activates the Gid complex rather than stabiliz-

ing it. As shown for acetate-starved cells (Chiang and Chiang, 1998), cycloheximide treatment of cells grown overnight on an ethanol-containing medium prevents Gid4/Vid24 expression on glucose (Figure 5A).

Our result suggests that Gid4/Vid24 might be a switch activating the Gid complex to degrade FBPase. Indeed, forced expression of Gid4/Vid24 under conditions where FBPase is actively expressed and stable, triggered its degradation (Figure 5B). Moreover, lack of Gid4/Vid24 inhibits polyubiquitination of an FBPase-TAP fusion protein (Figure 5C). Together, these results suggest that Gid4/Vid24 activates the Gid complex by promoting Gid2/Rmd5-dependent FBPase polyubiquitination. The mechanism of Gid complex activation by Gid4/Vid24 remains to be elucidated. Because FBPase interacts with the Gid complex already in ethanol-grown cells (Figure 2), Gid4/Vid24 is not likely to recruit FBPase to the complex. Gid4/Vid24 binds to the Gid complex (Ho *et al.*, 2002; Krogan *et al.*, 2006; Pitre *et al.*, 2006); thus, one hypothesis is that it alters the complex conformation to activate it (Figure 8).

Gid4/Vid24 is degraded during elimination of FBPase by the proteasome (Figure 1A). Its degradation depends on the ubiquitin conjugating enzyme Ubc8 and the E3 component Gid2/Rmd5 (Figure 6). Moreover, degradation of Gid4/Vid24 requires the proteasome (Figures 6, 8). Obviously, Gid4/Vid24 undergoes a regulatory loop exerted by components of the Gid complex: it might limit the activity of the Gid complex to a certain type of substrates like FBPase or prepare cells for new growth on nonfermentable carbon sources.

PEPCK, another gluconeogenic enzyme, is also subject to catabolite degradation (Holzer, 1976; Müller *et al.*, 1981). As Figure 7 shows, it is stabilized in *GID2/RMD5* and *GID4/VID24* deleted cells. Thus, Gid complex-dependent degradation is not restricted to FBPase but plays a more general role within the regulation of carbohydrate metabolism.

Gid protein homologues were also found to form a complex in mammals (Kobayashi *et al.*, 2007). Although no function for this CTLH complex has been described, one subunit has been implicated in proteasomal degradation of α -catenin (Suzuki *et al.*, 2008). This suggests that the CTLH complex, like the Gid complex, might also bear E3 activity.

In conclusion (Figure 8), our study shows that the Gid complex is a new ubiquitin ligase with novel types of subunits involved in catabolite degradation of gluconeogenic enzymes in yeast. We also identify Vid24/Gid4 as an important regulator of its ubiquitin ligase activity.

ACKNOWLEDGMENTS

We thank T. Sommer, M. Tyers, S. Munro and A. Weissman for plasmids and K. D. Entian for FBPase antibodies. We also thank Antje Schäfer for invaluable advice and critical reading of the manuscript. The help of E. Tosta during preparation of this manuscript is gratefully acknowledged. This work was supported by the Deutsche Forschungsgemeinschaft, Bonn, SFB 495; and the Fonds der Chemischen Industrie, Frankfurt.

REFERENCES

Amerik, A., Swaminathan, S., Krantz, B. A., Wilkinson, K. D., and Hochstrasser, M. (1997). In vivo disassembly of free polyubiquitin chains by yeast Ubp14 modulates rates of protein degradation by the proteasome. *EMBO J.* 16, 4826–4838.

Ausubel, F. M., Kingston, R. E., Seidman, F. G., Struhl, K., Moore, D. D., Brent, R., and Smith, F. A. (1992). *Current Protocols in Molecular Biology*, New York: Greene.

Bairoch, A., and Apweiler, R. (1997). The SWISS-PROT protein sequence data bank and its supplement TrEMBL. *Nucleic Acids Res.* 25, 31–36.

Balzi, E., Wang, M., Leterme, S., Van Dyck, L., and Goffeau, A. (1994). PDR5, a novel yeast multidrug resistance conferring transporter controlled by the transcription regulator PDR1. *J. Biol. Chem.* 269, 2206–2214.

Benton, D. (1990). Recent changes in the GenBank On-line Service. *Nucleic Acids Res.* 18, 1517–1520.

Bissinger, P. H., and Kuchler, K. (1994). Molecular cloning and expression of the *Saccharomyces cerevisiae* STS1 gene product. A yeast ABC transporter conferring mycotoxin resistance. *J. Biol. Chem.* 269, 4180–4186.

Bucher, P., Karplus, K., Moeri, N., and Hofmann, K. (1996). A flexible motif search technique based on generalized profiles. *Comput. Chem.* 20, 3–23.

Chiang, M. C., and Chiang, H. L. (1998). Vid24p, a novel protein localized to the fructose-1, 6-bisphosphatase-containing vesicles, regulates targeting of fructose-1,6-bisphosphatase from the vesicles to the vacuole for degradation. *J. Cell Biol.* 140, 1347–1356.

Cottarel, G. (1995). The *Saccharomyces cerevisiae* *HIS3* and *LYS2* genes complement the *Schizosaccharomyces pombe* *his5-303* and *lys1-131* mutations, respectively: new selectable markers and new multi-purpose multicopy shuttle vectors, pSP3 and pSP4. *Curr. Genet.* 28, 380–383.

de la Guerra, R., Valdes-Hevia, M. D., and Gancedo, J. M. (1988). Regulation of yeast fructose-1,6-bisphosphatase in strains containing multicopy plasmids coding for this enzyme. *FEBS Lett.* 242, 149–152.

DeRisi, J. L., Iyer, V. R., and Brown, P. O. (1997). Exploring the metabolic and genetic control of gene expression on a genomic scale. *Science* 278, 680–686.

Edgar, R. C. (2004). MUSCLE: multiple sequence alignment with high accuracy and high throughput. *Nucleic Acids Res.* 32, 1792–1797.

Eisele, F., Braun, B., Pfirrmann, T., and Wolf, D. H. (2006). Mutants of the deubiquitinating enzyme Ubp14 decipher pathway diversity of ubiquitin-proteasome linked protein degradation. *Biochem. Biophys. Res. Commun.* 350, 329–333.

Fang, S., and Weissman, A. M. (2004). A field guide to ubiquitylation. *Cell Mol. Life Sci.* 61, 1546–1561.

Gancedo, C. (1971). Inactivation of fructose-1,6-diphosphatase by glucose in yeast. *J. Bacteriol.* 107, 401–405.

Gancedo, J. M. (1998). Yeast carbon catabolite repression. *Microbiol. Mol. Biol. Rev.* 62, 334–361.

Gauss, R., Trautwein, M., Sommer, T., and Spang, A. (2005). New modules for the repeated internal and N-terminal epitope tagging of genes in *Saccharomyces cerevisiae*. *Yeast* 22, 1–12.

Guthrie, C., and Fink, G. R. (1991). *Guide to yeast genetics and molecular biology*. *Methods Enzymol.* 194, 21–37.

Hatakeyama, S., Yada, M., Matsumoto, M., Ishida, N., and Nakayama, K. I. (2001). U box proteins as a new family of ubiquitin-protein ligases. *J. Biol. Chem.* 276, 33111–33120.

Henikoff, S., and Henikoff, J. G. (1992). Amino acid substitution matrices from protein blocks. *Proc. Natl. Acad. Sci. USA* 89, 10915–10919.

Ho, Y. *et al.* (2002). Systematic identification of protein complexes in *Saccharomyces cerevisiae* by mass spectrometry. *Nature* 415, 180–183.

Hoffman, M., and Chiang, H. L. (1996). Isolation of degradation-deficient mutants defective in the targeting of fructose-1,6-bisphosphatase into the vacuole for degradation in *Saccharomyces cerevisiae*. *Genetics* 143, 1555–1566.

Hofmann, K. (2000). Sensitive protein comparisons with profiles and hidden Markov models. *Brief. Bioinform.* 1, 167–178.

Holzer, H. (1976). Catabolite inactivation in yeast. *Trends Biochem. Sci.* 1, 178–181.

Holzer, H. (1989). Proteolytic catabolite inactivation in *Saccharomyces cerevisiae*. *Revis. Biol. Celular* 21, 305–319.

Hung, G. C., Brown, C. R., Wolfe, A. B., Liu, J., and Chiang, H. L. (2004). Degradation of the gluconeogenic enzymes fructose-1,6-bisphosphatase and malate dehydrogenase is mediated by distinct proteolytic pathways and signaling events. *J. Biol. Chem.* 279, 49138–49150.

Hämmerle, M., Bauer, J., Rose, M., Szallies, A., Thumm, M., Dusterhus, S., Mecke, D., Entian, K. D., and Wolf, D. H. (1998). Proteins of newly isolated mutants and the amino-terminal proline are essential for ubiquitin-proteasome-catalyzed catabolite degradation of fructose-1,6-bisphosphatase of *Saccharomyces cerevisiae*. *J. Biol. Chem.* 273, 25000–25005.

Kobayashi, N., Yang, J., Ueda, A., Suzuki, T., Tomaru, K., Takeno, M., Okuda, K., and Ishigatsubo, Y. (2007). RanBPM, Muskelein, p48EMLP, p44CTLH, and the armadillo-repeat proteins ARMC8alpha and ARMC8beta are components of the CTLH complex. *Gene* 396, 236–247.

Krogan, N. J. *et al.* (2006). Global landscape of protein complexes in the yeast *Saccharomyces cerevisiae*. *Nature* 440, 637–643.

- Longtine, M. S., McKenzie, A., 3rd, Demarini, D. J., Shah, N. G., Wach, A., Brachat, A., Philippsen, P., and Pringle, J. R. (1998). Additional modules for versatile and economical PCR-based gene deletion and modification in *Saccharomyces cerevisiae*. *Yeast* *14*, 953–961.
- Lorick, K. L., Jensen, J. P., Fang, S., Ong, A. M., Hatakeyama, S., and Weissman, A. M. (1999). RING fingers mediate ubiquitin-conjugating enzyme (E2)-dependent ubiquitination. *Proc. Natl. Acad. Sci. USA* *96*, 11364–11369.
- Marcus, F., Rittenhouse, J., Moberly, L., Edelstein, I., Hiller, E., and Rogers, D. T. (1988). Yeast (*Saccharomyces cerevisiae*) fructose-1,6-bisphosphatase. Properties of phospho and dephospho forms and of two mutants in which serine 11 has been changed by site-directed mutagenesis. *J. Biol. Chem.* *263*, 6058–6062.
- Mazon, M. J., Gancedo, J. M., and Gancedo, C. (1982). Inactivation of yeast fructose-1,6-bisphosphatase. In vivo phosphorylation of the enzyme. *J. Biol. Chem.* *257*, 1128–1130.
- Mercado, J. J., and Gancedo, J. M. (1992). Regulatory regions in the yeast FBP1 and PCK1 genes. *FEBS Lett.* *311*, 110–114.
- Muller, M., Muller, H., and Holzer, H. (1981). Immunochemical studies on catabolite inactivation of phosphoenolpyruvate carboxykinase in *Saccharomyces cerevisiae*. *J. Biol. Chem.* *256*, 723–727.
- Ohi, M. D., Vander Kooi, C. W., Rosenberg, J. A., Chazin, W. J., and Gould, K. L. (2003). Structural insights into the U-box, a domain associated with multi-ubiquitination. *Nat. Struct. Biol.* *10*, 250–255.
- Pitre, S. *et al.* (2006). PIPE: a protein-protein interaction prediction engine based on the re-occurring short polypeptide sequences between known interacting protein pairs. *BMC Bioinformatics* *7*, 365.
- Puig, O., Caspary, F., Rigaut, G., Rutz, B., Bouveret, E., Bragado-Nilsson, E., Wilm, M., and Seraphin, B. (2001). The tandem affinity purification (TAP) method: a general procedure of protein complex purification. *Methods* *24*, 218–229.
- Regelmann, J., Schüle, T., Josupeit, F. S., Horak, J., Rose, M., Entian, K. D., Thumm, M., and Wolf, D. H. (2003). Catabolite degradation of fructose-1,6-bisphosphatase in the yeast *Saccharomyces cerevisiae*: a genome-wide screen identifies eight novel GID genes and indicates the existence of two degradation pathways. *Mol. Biol. Cell* *14*, 1652–1663.
- Rose, M. D., Novick, P., Thomas, J. H., Botstein, D., and Fink, G. R. (1987). A *Saccharomyces cerevisiae* genomic plasmid bank based on a centromere-containing shuttle vector. *Gene* *60*, 237–243.
- Schork, S., Bee, G., Thumm, M., and Wolf, D. H. (1994a). Catabolite inactivation of fructose-1,6-bisphosphatase in yeast is mediated by the proteasome. *FEBS Lett.* *349*, 270–274.
- Schork, S., Bee, G., Thumm, M., and Wolf, D. H. (1994b). Site of catabolite inactivation. *Nature* *369*, 283–284.
- Schork, S. M., Thumm, M., and Wolf, D. H. (1995). Catabolite inactivation of fructose-1,6-bisphosphatase of *Saccharomyces cerevisiae*. Degradation occurs via the ubiquitin pathway. *J. Biol. Chem.* *270*, 26446–26450.
- Schüle, T., Rose, M., Entian, K. D., Thumm, M., and Wolf, D. H. (2000). Ubc8p functions in catabolite degradation of fructose-1,6-bisphosphatase in yeast. *EMBO J.* *19*, 2161–2167.
- Sikorski, R. S., and Hieter, P. (1989). A system of shuttle vectors and yeast host strains designed for efficient manipulation of DNA in *Saccharomyces cerevisiae*. *Genetics* *122*, 19–27.
- Suzuki, T., Ueda, A., Kobayashi, N., Yang, J., Tomaru, K., Yamamoto, M., Takeno, M., and Ishigatsubo, Y. (2008). Proteasome-dependent degradation of alpha-catenin is regulated by interaction with ARMC8alpha. *Biochem. J.* *411*, 581–591.
- Umeda, M., Nishitani, H., and Nishimoto, T. (2003). A novel nuclear protein, Twa1, and Muskelein comprise a complex with RanBPM. *Gene* *303*, 47–54.
- Vaulont, S., Vasseur-Cognet, M., and Kahn, A. (2000). Glucose regulation of gene transcription. *J. Biol. Chem.* *275*, 31555–31558.
- von Herrath, M., and Holzer, H. (1988). Sensitivity of fructose-1,6-bisphosphatase from yeast, liver and skeletal muscle to fructose-2,6-bisphosphate and 5'-adenosine monophosphate. *Z. Lebensm. Unters. Forsch.* *186*, 427–430.
- Wahren, J., and Ekberg, K. (2007). Splanchnic Regulation of Glucose Production. *Annu. Rev. Nutr.* *27*, 329–345.
- Wolf, D. H. (2004). From lysosome to proteasome: the power of yeast in the dissection of proteinase function in cellular regulation and waste disposal. *Cell Mol. Life Sci.* *61*, 1601–1614.
- Yaffe, M. P., and Schatz, G. (1984). Two nuclear mutations that block mitochondrial protein import in yeast. *Proc. Natl. Acad. Sci. USA* *81*, 4819–4823.
- Yin, Z., Hatton, L., and Brown, A. J. (2000). Differential post-transcriptional regulation of yeast mRNAs in response to high and low glucose concentrations. *Mol. Microbiol.* *35*, 553–565.
- Zaragoza, O., and Gancedo, J. M. (2001). Elements from the cAMP signaling pathway are involved in the control of expression of the yeast gluconeogenic gene FBP1. *FEBS Lett.* *506*, 262–266.
- Zheng, N., Wang, P., Jeffrey, P. D., and Pavletich, N. P. (2000). Structure of a c-Cbl-UbcH7 complex: RING domain function in ubiquitin-protein ligases. *Cell* *102*, 533–539.

RESEARCH ARTICLE

RMND5 from *Xenopus laevis* Is an E3 Ubiquitin-Ligase and Functions in Early Embryonic Forebrain Development

Thorsten Pfirrmann^{1‡*}, Pablo Villavicencio-Lorini², Abinash K. Subudhi¹, Ruth Menssen³, Dieter H. Wolf³, Thomas Hollemann^{1‡}

1 Martin-Luther University Halle-Wittenberg, Institute of Physiological Chemistry, Halle, Germany, **2** Martin Luther University Halle-Wittenberg, Institute of Human Genetics, Halle, Germany, **3** University of Stuttgart, Institute of Biochemistry, Pfaffenwaldring 55, 70569 Stuttgart, Germany

‡ These authors are senior authors on this work.

* thorsten.pfirrmann@medizin.uni-halle.de



OPEN ACCESS

Citation: Pfirrmann T, Villavicencio-Lorini P, Subudhi AK, Menssen R, Wolf DH, Hollemann T (2015) RMND5 from *Xenopus laevis* Is an E3 Ubiquitin-Ligase and Functions in Early Embryonic Forebrain Development. PLoS ONE 10(3): e0120342. doi:10.1371/journal.pone.0120342

Academic Editor: Brian Key, School of Biomedical Sciences, The University of Queensland, AUSTRALIA

Received: September 3, 2014

Accepted: January 22, 2015

Published: March 20, 2015

Copyright: © 2015 Pfirrmann et al. This is an open access article distributed under the terms of the [Creative Commons Attribution License](https://creativecommons.org/licenses/by/4.0/), which permits unrestricted use, distribution, and reproduction in any medium, provided the original author and source are credited.

Data Availability Statement: All relevant data are within the paper and its Supporting Information files.

Funding: The project was supported by funding from the Fonds der Chemischen Industrie, Frankfurt and the Wilhelm Roux program (FKZ 26/22), Halle (Saale). The funders had no role in study design, data collection and analysis, decision to publish, or preparation of the manuscript.

Competing Interests: The authors have declared that no competing interests exist. Funding by "Fonds

Abstract

In *Saccharomyces cerevisiae* the Gid-complex functions as an ubiquitin-ligase complex that regulates the metabolic switch between glycolysis and gluconeogenesis. In higher organisms six conserved Gid proteins form the CTLH protein-complex with unknown function. Here we show that Rmnd5, the Gid2 orthologue from *Xenopus laevis*, is an ubiquitin-ligase embedded in a high molecular weight complex. Expression of *rmnd5* is strongest in neuronal ectoderm, prospective brain, eyes and ciliated cells of the skin and its suppression results in malformations of the fore- and midbrain. We therefore suggest that *Xenopus laevis* Rmnd5, as a subunit of the CTLH complex, is a ubiquitin-ligase targeting an unknown factor for polyubiquitination and subsequent proteasomal degradation for proper fore- and midbrain development.

Introduction

Previously, we isolated nine GID (glucose-induced degradation deficient) genes necessary for the glucose-induced degradation of fructose-1,6-bisphosphatase (FBPase) from yeast [1]. Seven of these proteins are part of a high molecular mass protein complex. In *Saccharomyces cerevisiae* the so-called Gid-complex functions as an ubiquitin-ligase complex that targets key gluconeogenic enzymes for polyubiquitination and subsequent proteasomal degradation to initiate an irreversible shutdown of the gluconeogenic pathway [2–4].

The ubiquitin proteasome system (UPS) regulates the targeted temporal and spatial degradation of proteins. The covalent modification of a protein with ubiquitin requires a set of three classes of enzymes, the ubiquitin-activating enzyme (E1), the ubiquitin-conjugating enzyme (E2) and finally the ubiquitin-ligase (E3) [5]. In humans there exist an estimated number of 600 ubiquitin-ligases that all share the E3 typical RING or HECT domain. Classical RING domains bind two zinc atoms by a Cys3HCys4 motif [6]. The *Saccharomyces cerevisiae* Gid

der Chemischen Industrie" does not alter the authors' adherence to PLOS ONE policies on sharing data and materials.

complex contains two proteins with non-canonical RING domains Gid2 and Gid9, the orthologs of RMND5 and MAEA of the vertebrate CTLH complex [3, 4].

Most subunits of the Gid-complex are conserved with a remarkable sequence and domain-distribution conservation throughout the eukaryotic kingdom [7]. GID1, GID2, GID4, GID5, GID7, GID8 and GID9 have their closest human relatives in RanBP9, RMND5, C17ORF39, ARMC8, MKLN1, C20ORF1 (aka Twa1) and MAEA respectively. All subunits except C17ORF39 are part of the human CTLH-complex [8, 9] and a similar complex in *Arabidopsis thaliana* [10] and other eukaryotes [7] exists.

While function and topology of the yeast Gid-complex subunits are well described, the function of the vertebrate counterpart remains poorly understood. Most subunits carry a CTLH-domain (C-terminal to LisH motif domain) and a LisH-domain (lis homology domain) [11]. The latter is often associated with syndromes involving malformations of the central nervous system [12]. For example, the mammalian CTLH/LisH subunit MKLN1, the ortholog of yeast Gid7 [4, 8], is expressed in the hippocampus and the cerebellum [13] and was recently found to be involved in dynein dependent GABA_A-receptor transport along actin filaments and microtubuli [14]. A similar function is described for ARMC8 [15].

RMND5A the human ortholog of yeast Gid2 also contains a CTLH/LisH- and the E3 typical RING-domain. Interestingly, mammals encode for two *GID2* orthologous genes called *RMND5A* and *RMND5B*, but only *RMND5A* is part of the CTLH-complex. Nevertheless, *RMND5B* associates with several ubiquitin-conjugating enzymes [16]. Therefore it is likely that both proteins function as ubiquitin-ligases. A recent report describes human *RMND5A* expression to be regulated by the small non-coding RNA miRNA-138. In conjunction with RanBP10 and Exportin5, *RMND5A* is described to protect Exportin5 from proteasomal degradation [17]. Clinical data concerning *RMND5A* are restricted to a recent case report that describes a giant occipitoparietal meningoencephalocele in a newborn baby. This rare neurodevelopmental defect coincides with a 80.65-kb gain within chromosome band 2p11.2 resulting in a duplication of the *RMND5A* gene [18].

We show that *Xenopus laevis* *Rmnd5* functions as an ubiquitin ligase, most probably in the context of the CTLH-complex. *Rmnd5* transcript is mainly present in ectodermal derivatives in *Xenopus laevis*. The suppression of *rmnd5* function leads to defects of the prospective prosencephalon and mesencephalon, pointing towards a role of *Rmnd5* during neural development. We speculate that *Rmnd5* targets a yet unknown neurospecific factor for degradation.

Results and Discussion

Xenopus laevis *Rmnd5* protein is structurally and functionally related to human RMND5A

We set out to gain knowledge of the phylogenetic distribution of yeast Gid2 orthologous proteins by comparison of the protein sequences. The Gid2/*Rmnd5* protein sequences of the indicated organisms were obtained from NCBI and used for multiple sequence analysis with the T-Coffee algorithm [19]. Further reconstruction and analysis of phylogenetic relationships were done by the Phylogeny.fr software [20] and are displayed in Fig. 1A. It can be seen that Gid2/*Rmnd5* is conserved throughout the eukaryotic kingdom. In fungi (*Saccharomyces cerevisiae*, *Candida albicans*, *Aspergillus niger*), nematodes (*Caenorhabditis elegans*), plants (*Arabidopsis thaliana*), insects (*Drosophila melanogaster*), amphibians (*Xenopus laevis*) and birds (*Falco peregrinus*, *Gallus gallus*) only a single isoform is present (shown in black), while mammals (*Homo sapiens*, *Ornithorhynchus anatinus*, *Sarcophilus harrisi*, *Canis lupus*, *Mus musculus*, *Rattus norvegicus*) possess two isoforms (homolog A in blue, homolog B in red) that are highly similar. Interestingly, the single isoforms existing in *Xenopus laevis*, *Gallus gallus* and

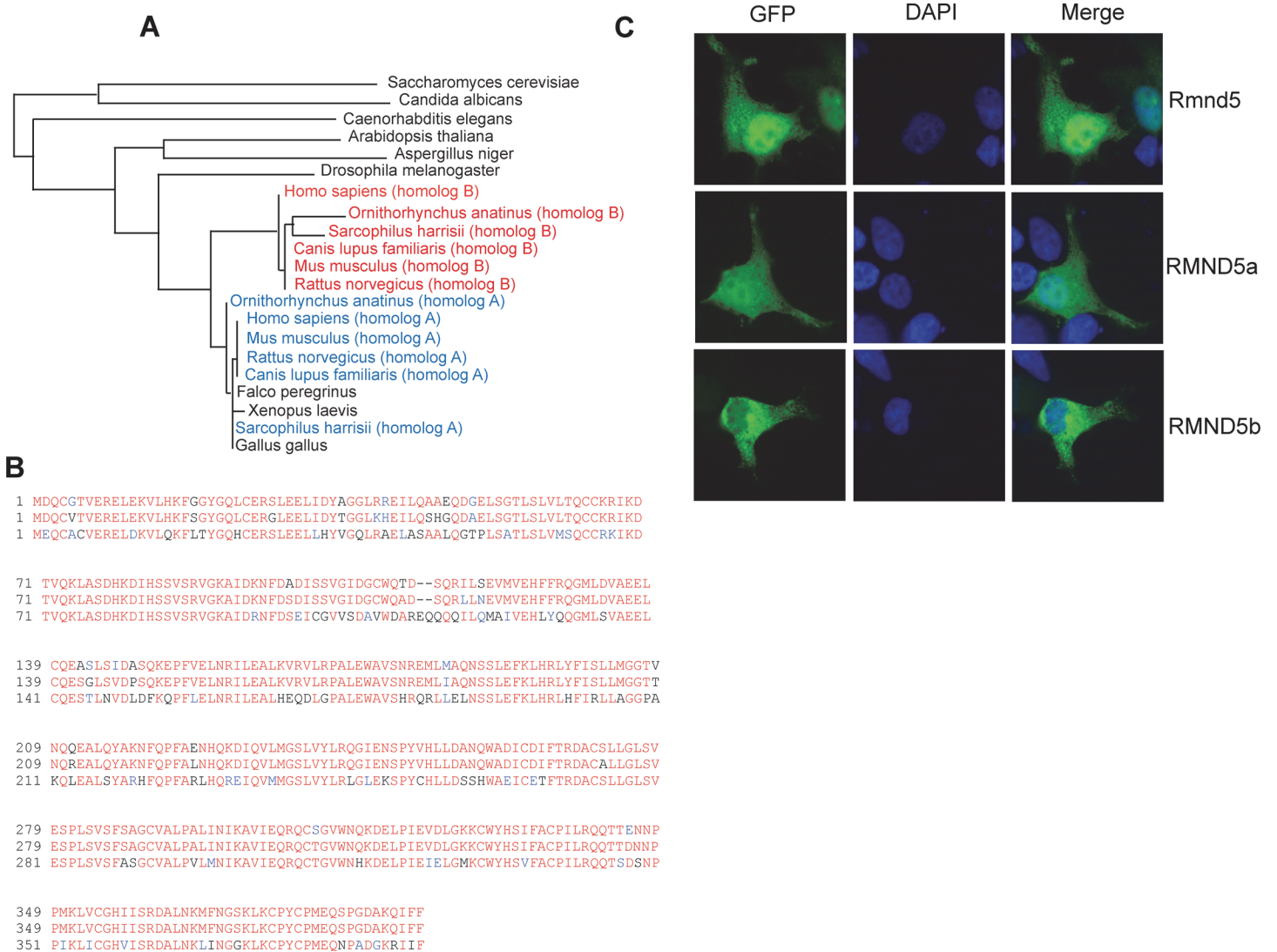


Fig 1. *Xenopus laevis* Rmnd5 protein is structurally and functionally related to human RMND5A. (A) Phylogenetic tree of Rmnd5 orthologs. The taxonomic tree of representative eukaryotic species rendered by Phylogeny.fr software [20]. Respective Gid2/Rmnd5 sequences obtained from NCBI with indicated accession numbers (*Saccharomyces cerevisiae* [NP_010541.3], *Candida albicans* [XP_712238.1], *Aspergillus niger* [XP_001388791.2], *Caenorhabditis elegans* [NP_508444.1], *Arabidopsis thaliana* [NP_196525.1], *Drosophila melanogaster* [NP_611536.3], *Xenopus laevis* [NP_001086276.1], *Falco peregrinus* [XP_005229906.1], *Gallus gallus* [XP_004936301.1], *Homo sapiens* [NP_073617.1; NP_073599.2], *Ornithorhynchus anatinus* [XP_007670084.1; XP_001515875.2], *Sarcophilus harrisii* [XP_003758697.1; XP_003756956.1], *Canis lupus familiaris* [XP_852129.1; XP_531873.2], *Mus musculus* [NP_077250.2; NP_079622.1], *Rattus norvegicus* [XP_232051.4; NP_001017473.1]); homolog A (blue), homolog B (red). (B) Sequence alignment of *Xenopus laevis* Rmnd5 (top), *Homo sapiens* RMND5A (middle) and RMND5B (bottom). Identical residues (red), similar residues (blue), others (black). Identities (%): *Xenopus laevis* Rmnd5 to human RMND5A (94%), to human RMND5B (70%). (C) Localization of *Homo sapiens* RMND5A (RMND5a, middle panel), RMND5B (RMND5b, bottom panel) and *Xenopus laevis* Rmnd5 (Rmnd5, top panel) in HEK293 cells. GFP signal (left column), DAPI signal (middle column), merged signals (right column).

doi:10.1371/journal.pone.0120342.g001

Falco peregrinus are phylogenetically closer to the mammalian isoform A (Fig. 1B). While the human RMND5A is 94% identical to *Xenopus laevis* Rmnd5, the human RMND5B isoform only shows 70% identity (calculated by T-Coffee). In previous studies, we have shown that human RMND5A localises to the cytosol and to the nucleus, while human RMND5B is entirely cytosolic [21]. In Fig. 1C representative cells transfected with either *Xenopus laevis* rmd5 (Rmnd5, upper panel), human RMND5A (RMND5A, middle panel) or RMND5B (RMND5B)

can be seen. Respective protein localisation is shown in the left column (GFP), the nuclei in the middle (DAPI) and an overlay in the right column (merge). As shown before, human RMND5A is distributed to the cytosol and the nucleus, while human RMND5B is cytosolic. *Xenopus laevis* Rmnd5 shows a localisation pattern similar to human RMND5A and therefore is not only structurally but also functionally closer to human RMND5A.

Interestingly, two isoforms of RMND5 only exist in mammals with the genomic location of the human *RMND5A* gene on chromosome 2 (2p11.2) and the *RMND5B* gene on chromosome 5 (5q35.3). The appearance of *RMND5B* is therefore a relatively late event in evolution and most probably a consequence of gene duplication. Despite the high degree of structural conservation, it is not clear if both proteins have redundant, overlapping or completely different functions in the cell. It is also unclear if both isoforms can be part of the CTLH-complex as exchangeable subunits. Therefore, to avoid redundancy effects between RMND5A and RMND5B, we consider *Xenopus laevis* as an ideal model organism to study Rmnd5 function during early development.

Rmnd5 is expressed during early embryonic development

To study a potential role of Rmnd5 during development of the neural system, we first analyzed its spatio-temporal expression pattern in embryos of *Xenopus laevis*. We started out looking at the temporal expression of *rmnd5* by semi-quantitative RT-PCR using total RNA from consecutive developmental stages of *Xenopus laevis* embryos. In [Fig. 2A](#) a specific signal at the expected size of 305 bp indicated the existence of *rmnd5* transcript (upper panel), while ODC1 primers were used to control the amount of input RNA (lower panel). The expression of *rmnd5* receives a strong maternal contribution, as RT-PCR products are detectable at NF (Nieuwkoop and Faber) stage 3 and declines steadily until gastrulation (NF stage 12). Zygotic transcripts of *rmnd5* are detectable through all further stages analyzed, though on a much lower level compared to NF stage 3. This finding is confirmed on the protein level, but a comparable decline in Rmnd5 levels is not visible ([Fig. 2B](#)). Whole mount *in situ* hybridisation (WMISH) reveals first expression of *rmnd5* at the four-cell stage ([Fig. 2C-A](#), NF stage 3) and the eight-cell stage ([Fig. 2C-C](#), NF stage 4). Here *rmnd5* transcript is mostly present in the animal pole (top), an area developing into derivatives of ectoderm and mesoderm. During gastrulation (NF-stage 12) increasing levels of *rmnd5* transcripts appear enhanced in the prospective head region ([Fig. 2C-D](#)) and during neurulation ([Fig. 2C-E](#), NF stage 18) in the neuronal ectoderm (red arrow) and subpopulations of skin cells, most likely the ciliated cells of the skin ([Fig. 2C-E](#), -H; yellow arrow). In a later stage of development (NF stage 34, [Fig. 2C-J](#), -K), the expression of *rmnd5* is mainly restricted to head structures and demarcates neural tissues and derivatives. Strong expression is observed in the eyes ([Fig. 2C-J](#), -K, -L; green arrow) and the prosencephalon ([Fig. 2C-J](#), -K, -L, -M; red arrow).

Our results show, that in *Xenopus laevis* *rmnd5* transcripts and Rmnd5 protein are present continuously within the investigated time frame. The localisation of transcripts in neuronal ectoderm, prospective prosencephalon, the eyes and subpopulations of the skin suggests a function during neural development.

Rmnd5 is important for proper early development of the embryonic forebrain

In order to analyze the function of Rmnd5, we inhibit the translation of *rmnd5* via injection of targeted antisense morpholino oligonucleotides. We injected 2.5 pmol *rmnd5*-morpholino together with 100 pg synthetic beta-*gal* RNA as a tracer into one cell of two-cell stage embryos and fixed them at NF stage 32–34. For further analysis, embryos were subjected to

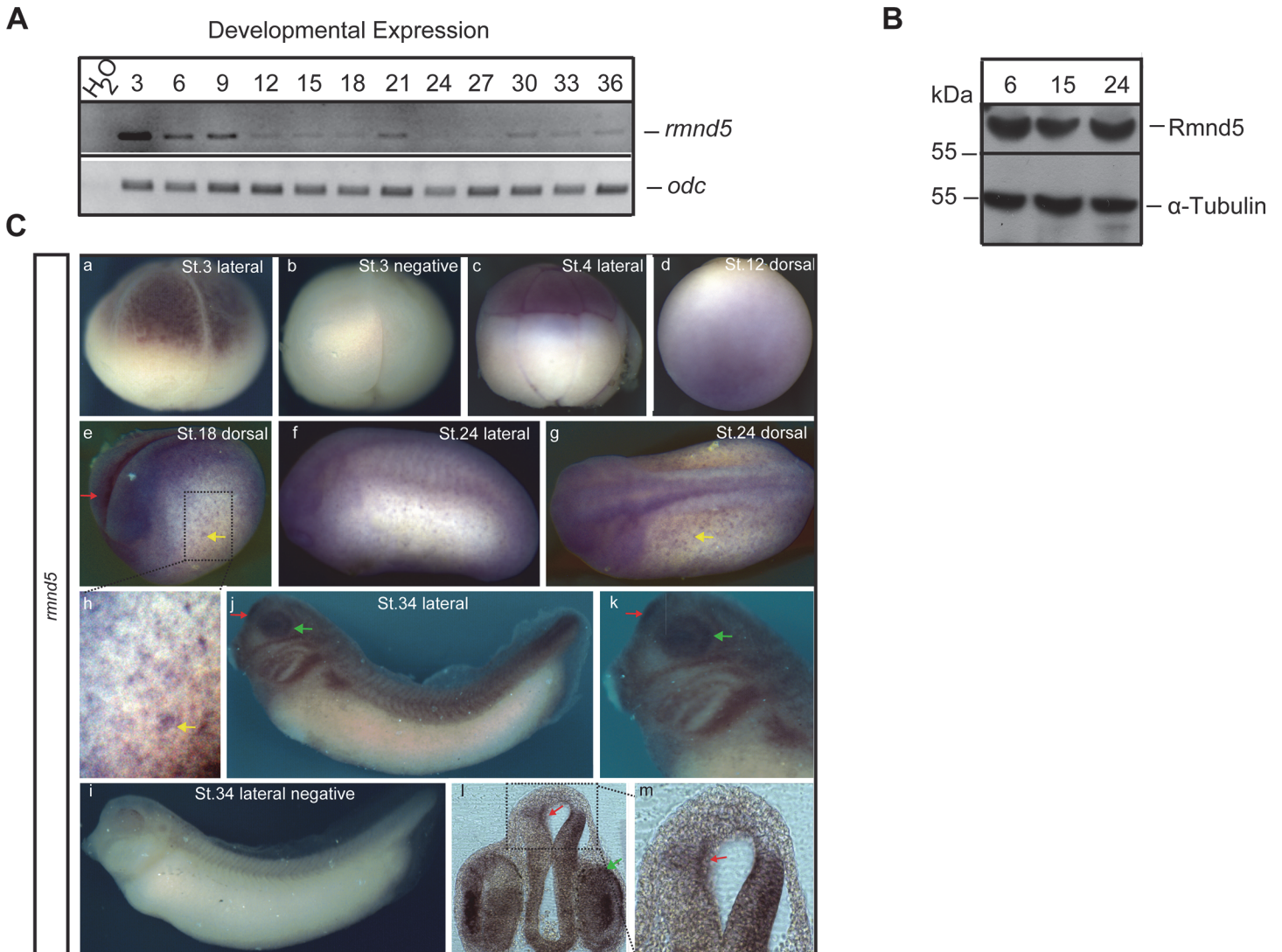


Fig 2. *rmnd5* is expressed during early embryonic development. (A) Temporal RT-PCR analysis of *rmnd5* expression (top panel); different developmental stages (NF-stages) indicated at the top. ODC1 functions as RNA input control (bottom). (B) Rmnd5 protein at different developmental stages. Western blot analysis of embryo lysate from indicated stages (top). α -RMND5A (Novus Biological; rabbit, 1:1000); α -Tubulin (AbD Serotec, rat, 1:2500). (C) Spatial analysis of *rmnd5* expression. Whole mount *in situ* hybridisation (Wmish) of wild type *Xenopus laevis* embryos at different developmental stages. NF stage 3 (panel a, left) and stage 4 (panel c) *rmnd5* transcript in the animal pole (top), NF-stage 12 (panel d) *rmnd5* transcripts around the prospective head, NF-stage 18; 24 (panel e, f, g, h) neuronal ectoderm (red arrow, panel e) and ciliated cells of the skin (yellow arrow, panel e, g, h), NF-stage 34 (panel j, k, l, m) proencephalon (red arrow) and eyes (green arrow). Negative controls with sense probes (panel b, i).

doi:10.1371/journal.pone.0120342.g002

whole-mount *in situ* hybridisation (WMISH) after fixation and beta-Gal staining. A set of probes was employed to cover different states of differentiation and morphogenesis during the development of the central nervous system. Noticeable, loss of Rmnd5 function suppresses mostly the proper development of the mesencephalon, the prosencephalon and the eye. For example *pax6* expression at stage 34 is specific to amacrine and bipolar cells of the retina, epithelium of the lens, prospective prosencephalon and interneurons [22]. As a prominent phenotype, expression of *pax6* in the *rmnd5*-morpholino injected side (IS) is completely absent from the prospective prosencephalon (Fig. 3A-B, yellow arrow) while expression in the mid-/hindbrain was shifted to posterior (Fig. 3A-B, compare green/ red arrow). In a frontal section

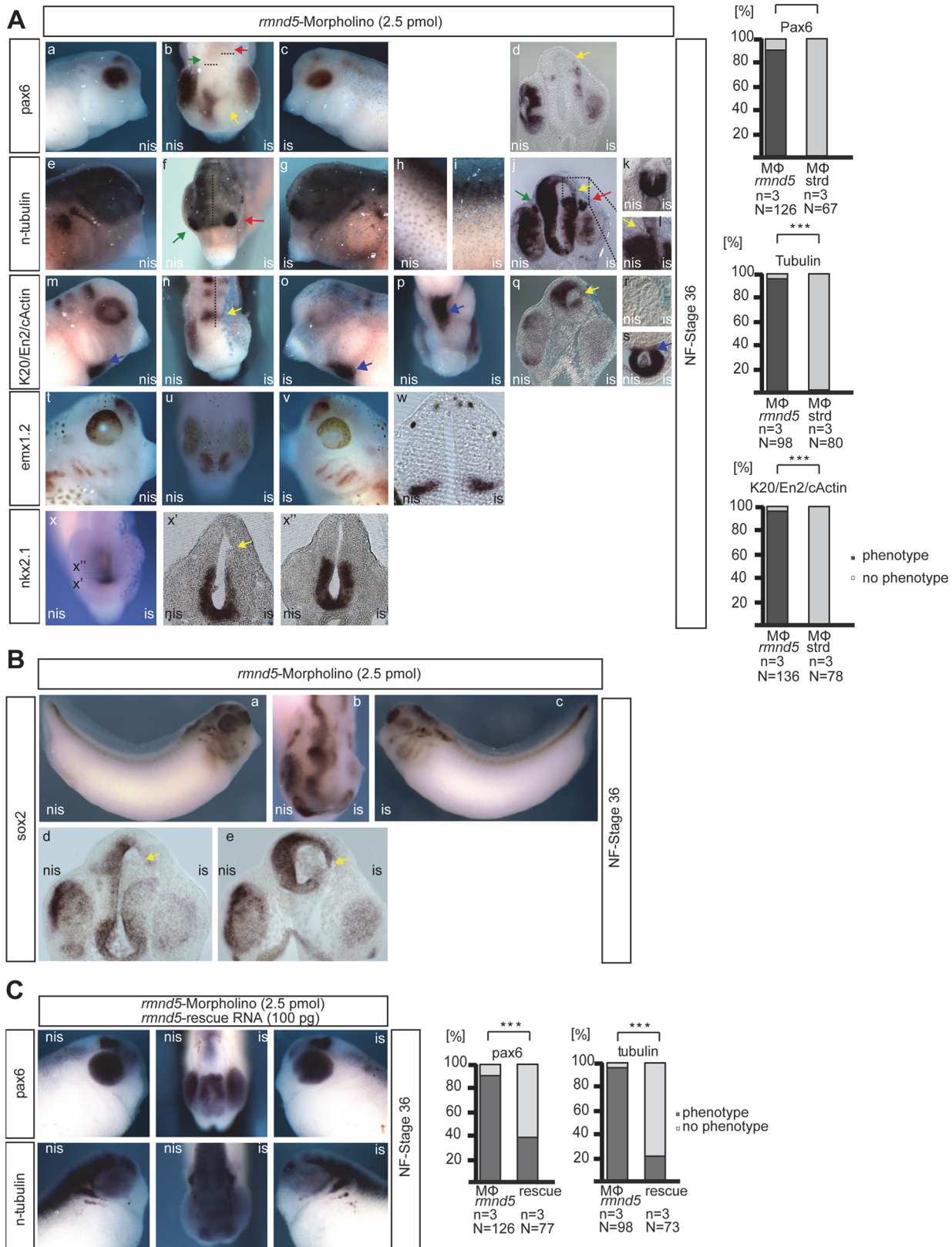


Fig 3. The CTLH complex functions during early embryonic neurogenesis. (A) *rmnd5*-mo injected embryos were used for *in situ* hybridisation with indicated marker probes; *pax6* (upper lane), *n-tubulin* (middle lane), *k20/en22/rx1/c-actin*, *emx1.2*, *nkx2.1* (bottom lanes). Abbreviations: IS, injected side; NIS, non-injected side. Quantitative representation of phenotypes are presented as a bar graph (percent embryos with phenotype to total amount (%); black, phenotype; grey, no phenotype); n = number of independent experiments, N = number of injected embryos analysed for respective marker, * $P \leq 0.05$, *** ≤ 0.001 (Chi Square test). (B) As (A) with *sox2* as probe. (C) *Xenopus* embryos co-injected with *rmnd5* morpholino (2.5 pmol/embryo) and synthetic capped RNA (100 pg/embryo) were used for *in situ* hybridisation and quantified as shown in A.

doi:10.1371/journal.pone.0120342.g003

the lack of *pax6* signal in the dorsal area of the prospective prosencephalon is obvious, since the respective tissue is almost absent (Fig. 3A-D, yellow arrow). Thus, the lack of expression can be observed with all other marker genes (Fig. 3A-J, -L, [*n-tubulin*], -n, -q [*en2*], -x' [*nkx2.1*] and Fig. 3B, -B, -D, -E, [*sox2*]; yellow arrow). Strikingly, the expression of *n-tubulin* in subpopulations of skin cells is also severely reduced (Fig. 3A-H, -I), while expression in the prospective spinal cord is not altered (Fig. 3A-K). In contrast, structures arising from placodes such as the olfactory placodes (Fig. 3A-F, green/red arrow) and the trigeminal nerve (3A-J, green/red arrow) or of mesodermal origin such as the heart tube (3A-M, -O, -P, -S, c-Actin, blue arrow) appear normal. The non-injected sides (NIS) of these embryos and standard morpholino injected embryos (S2 Fig.) do not expose such phenotypes. To control for off-target effects of the *rmnd5* morpholino, we performed rescue experiments, injecting a synthetic *rmnd5* RNA that cannot be targeted by the *rmnd5*-morpholino. In the presence of the rescuing RNA, the *rmnd5* knockdown phenotype can be partially restored (Fig. 3C). Together our data suggests a role of Rmnd5 during the early development of dorsal areas of the pro- and mesencephalon, the eyes and most likely the ciliated cells of the skin. Its specific expression in these territories strongly supports a direct function of *rmnd5* during these processes (Fig. 2C-E, -H, -J, -K, -L, -M).

Rmnd5 is part of an ubiquitin-ligase complex

In *Saccharomyces cerevisiae* we have shown that the Rmnd5 ortholog Gid2 is part of a specific ubiquitin-ligase complex targeting key gluconeogenic enzymes for polyubiquitination [3, 4]. In higher organisms the function of the CTLH-complex remains enigmatic. Several lines of evidence support the hypothesis that Rmnd5 functions as an ubiquitin-ligase as well. First, the non-canonical RING domains in Gid2/RMND5 and in Gid9/MAEA are evolutionary highly conserved. Second, human RMND5B interacts with several ubiquitin-conjugating enzymes (E2s) [16]. And finally, several protein interaction partners are putative CTLH complex substrates and are degraded by the 26S proteasome [23]. Therefore, we tested whether *Xenopus laevis* Rmnd5 is part of a high molecular mass protein complex and whether it exhibits ubiquitin-ligase activity. *Xenopus laevis* stage 36 embryo lysates were subjected to glycerol density centrifugation (Fig. 4A). Fractionation revealed that Rmnd5 is mostly present in fraction 6 and 7 at 200–300 kDa and fraction 1 at 50 kDa. The predicted molecular mass of Rmnd5 is 44 kDa; the protein appears to be partially associated with other proteins most probably in the context of the CTLH complex. Another subunit of the human CTLH-complex is ARMC8 [8]. The *Xenopus* ortholog has a predicted molecular mass of 40 kDa. However, it is detected in fraction 5 and 6 (150–250 kDa, lower panel) and thus partially cofractionates with Rmnd5 under these conditions. We conclude, that Rmnd5 cofractionates with known subunits of the CTLH complex and thus most likely is an integral part of it. In a next step, we wanted to test if Rmnd5 has E3 ubiquitin-ligase activity. Fig. 4B shows the result of an *in vitro* polyubiquitination assay [4]. Only in the presence of active *Xenopus laevis* Rmnd5 a strong polyubiquitination signal was detected. The Rmnd5 mutant protein containing a mutation in the conserved RING cysteine residue (C354S) and the respective negative controls do not show any autoubiquitination (Fig. 4B,

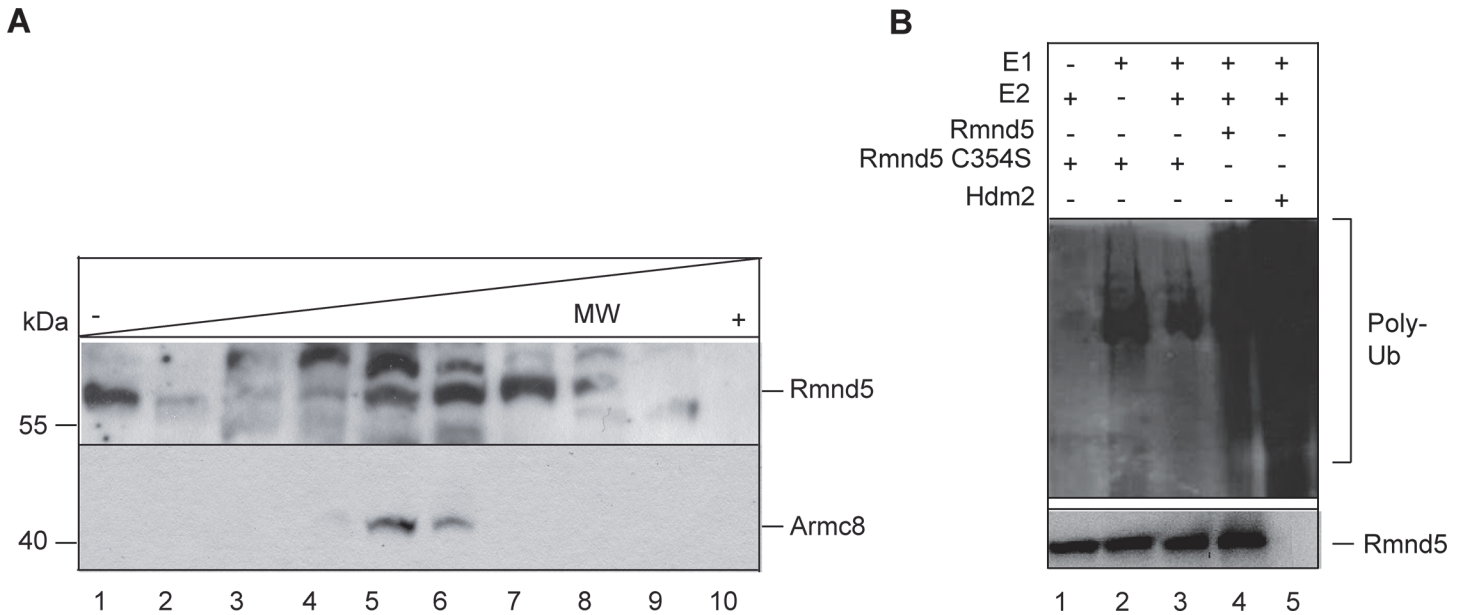


Fig 4. Rmnd5 is part of an ubiquitin ligase complex. (A) Glycerol step gradient of *Xenopus laevis* NF stage 36 embryo lysates. Molecular mass (MW) standard: albumin (67 kDa), fraction 1, 2; LDH (140 kDa), fraction 4; catalase (232 kDa), fraction 6,7. Western blot analysis with α -RMND5A (Rmnd5; upper panel) (1:1000) and α -ARMC8 (lower panel) (1:1000). (B) *In vitro* polyubiquitination assay with recombinant *Xenopus* Rmnd5 and Rmnd5-C354S (lane 3, 4). Reactions are performed in the presence (+) or absence (-) of E1 (lane 1), E2 (lane 2) and purified Rmnd5 protein. HDM2 is used as a positive control (lane 5). Polyubiquitination (Poly-Ub) is detected with α -HA and α -RMND5A as control.

doi:10.1371/journal.pone.0120342.g004

lane 1, 2, 3). As a positive control, the human ubiquitin ligase HDM2 was included in the test. We conclude that vertebrate Rmnd5 possesses E3 ligase activity and is part of a multimeric protein complex, most probably the CTLH complex. Given the close evolutionary relationship between the *Gid2/Rmnd5* proteins we asked whether *Xenopus laevis* Rmnd5 is able to complement a *gid2Δ* deletion phenotype in *Saccharomyces cerevisiae*. We expressed a yeast codon optimized *Xenopus laevis* *rmnd5* (sequence available upon request) in a *gid2Δ* deletion strain and measured the half-life of the gluconeogenic enzyme FBPase. Even elevated amounts of Rmnd5 are not able to rescue the Δ *gid2* phenotype (S1 Fig.). Additionally, no interaction between Rmnd5 and the yeast *Gid* complex can be measured. Despite the high degree of conservation, the structural differences of the protein binding domains appear to be too strong to allow incorporation of Rmnd5 into the yeast complex.

Taken together, we show for the first time that Rmnd5 of a higher organism is part of an ubiquitin-ligase complex. Unexpectedly, the suppression of *rmnd5* function during embryonic development leads to malformations specifically in dorsal parts of the pros- and mesencephalon, the eyes and of ciliated cells of the skin. Therefore, the accumulation of an unknown Rmnd5 substrate might disturb the proper regulation of e.g. neural progenitor proliferation, cell specification, neuronal differentiation, cell migration or ciliogenesis. Recently, the human transcription factor Sox2 was shown to interact with the entire CTLH-complex [24]. Sox2 is essential for the maintenance of neural stem cell pluripotency with a key role during the development of pituitary, forebrain and the eyes [25, 26] and shows a similar expression pattern as *rmnd5* (compare Fig. 2C and Fig. 3B). We therefore assume that the CTLH complex regulates Sox2 stability and thus may explain the manifestation of Rmnd5 dependent malformations of neural structures in our animal model and the patient [18].

Material and Methods

Capped mRNA and morpholino injections

Capped *rmnd5* m-RNA was generated using the mMESSAGE mMACHINE kit (Ambion, Austin, TX). NotI linearized pTP251 was used as a template for SP6 transcription and 5 nl of capped mRNA (~2.5 ng) was injected into one blastomere of a 2-cell stage embryo together with *rmnd5* morpholino. 25-mer morpholinos (MOs; Gene Tools, LLC Philomath, Oregon) were designed to target the ATG translation start site for *rmnd5* (NM_001092807.1) mRNA transcripts (sequence: GCTCCACCGTGCCGCACTGATCCAT). A mismatch standard MO was used as control (sequence: CCTCTTACCTCAGTTACAATTTATA). Both were injected (2.5 pmol) into one blastomere of 2-cell stage embryos.

Glycerol Density Gradient Fractionation

100 μ l aliquots of embryo extract were layered on top of a glycerol step gradient in lysis buffer (950 μ l each of 50%, 40%, 30%, 20 and 10% of glycerol) and centrifuged at 340000 g in a SW60TI rotor (Beckman Coulter) for 22h at 16°C. Thereafter, 330 μ l fractions were collected, total protein precipitated with trichloroacetic acid (10% final), solubilised in urea buffer and analyzed by Western blotting.

Purification of recombinant His-tagged protein

Expression and purification of recombinant Rmnd5 was performed as described before [27].

RNA preparation and reverse transcription

RNA was prepared from whole *Xenopus* embryos using a Qiagen RNeasy Kit following the instructions provided by the manufacturers. First strand cDNA was prepared from 500 ng total RNA using oligo-dT or random primer and reverse transcriptase (Gibco).

Whole mount *in situ* hybridization and RT-PCR

To analyze the spatio-temporal expression of *rmnd5* during *Xenopus laevis* embryogenesis, a DIG-labeled *antisense* RNA probe was generated by linearizing pTP221 with HindIII-HF (NEB) and *in vitro* transcription with T7 RNA Polymerase (Roche) as described before [28]. *Xenopus* embryos were fixed at consecutive developmental stages and whole-mount *in situ* hybridization was carried out as previously described [29]. Embryos probed with antisense RNAs of *n-tubulin*, *pax6*, and *rx1-en2-krox20*, *sox2*, *emx1.2*, *nkx2* and *rmnd5* respectively were vibratome sectioned (30 μ m) and photographed.

Oligonucleotides and plasmids

Plasmids and primers used in this work are listed in Table 1 and Table 2, respectively and are available upon request. Plasmid pTP250 contains the *Xenopus laevis rmnd5* ORF amplified from pTP221 with primers TP250fwd and TP250rev, inserted via XhoI and HindIII into pEGFP-C1 (Clontech). pTP221 contains the *Xenopus laevis rmnd5* ORF amplified from cDNA, which was inserted into EcoRI/XhoI linearized pTP213 by yeast homologous recombination and selection on CSD—URA medium. pTP230 is a pCA528 derivative containing *Xenopus laevis rmnd5* that was cut from pTP221 and inserted into pCA528 via XhoI and BamHI. pTP241 is a pTP230 derivative with a C354S mutation in the RMND5A gene SOMA-generated with primer TP226 [21]. Site-directed mutagenesis of plasmids was performed using SOMA [21].

Table 1. Primers used in this study.

Primer	Description	Reference
TP251	CCCATCGATTGCAATTCGAATGACCAATGTGGTACCGTAGAACGGGAGCTGGAGAAGGTGC	This work
TP250fwd	CATCATCTCGAGAAGATCAGTGCGGCACGGTG	This work
TP250rev	CATCATAAGCTTGAGTCAGAAAAAGATTTGTTTGGCGTCTC	This work
TP221fwd	TTGCAGGATCCCATCGATTGCAATTCGAATGATCAGTGCGGCACGGTG	This work
TP221rev	TACGACTCACTATAGTTCTAGAGGCTCGAGTCAGAAAAAGATTTGTTTGGCG	This work
TP226	CCTATGAAGCTTGTTCGGACACATTATATCC	This work
XL-Rmd5fwd	GAGCGGGAGCTGGAGAAGGT	This work
XL-Rmd5rev	CAGCCATCAATCCCCACGCT	This work
XL-ODC-F	GCCATTGTGAAGACTCTCTCCATTC	This work
XL-ODC-R	TTCGGGTGATTCTTGCCAC	This work

doi:10.1371/journal.pone.0120342.t001

Organisms and maintenance

Frogs were obtained from a commercial supplier (NASCO, USA). Production and rearing of embryos was performed as described previously [29] and embryos were maintained at 15°C and staged according to Nieuwkoop and Faber. All procedures were performed according to guidelines set by the German animal use and care laws (Tierschutzgesetz) and approved by the German state administration Saxony-Anhalt (Projekt/AZ: 42502-3-600 MLU). HEK293 cells were maintained in Dulbecco's modified Eagle's medium supplemented with 10% fetal calf serum (v/v). Transfections were performed using Lipofectamin 2000 (Invitrogen). For microscopy studies cells were grown on cover slips pretreated with poly-L-lysine solution, 0,1% (Sigma-Aldrich) for 5 min.

Western blotting

Western blotting was performed as described earlier [4]. Embryo extracts were prepared by homogenizing embryos with an injection needle (Braun, 0,7 × 30 mm) in one pellet volume of lysis buffer (20 mM Tris (pH8), 100 mM NaCl, 1mM EDTA, 0,5% Triton X-100, 10% glycerol, 0,1 mM PMSF, 10 µg/ml leupeptin, 1 µg/ml pepstatinA, 5 µg/ml aprotinin). Total protein was determined with the Bradford assay to load 20–30 µg total protein per lane. Antibodies were

Table 2. Plasmids used in this study.

Name	Description	Source
pTP230	pCA528 based vector with the <i>Xenopus laevis</i> open reading frame <i>rmnd5</i> (NM_001092807.1)	This work
pTP241	pTP230 with a C354-S mutation in <i>rmnd5</i>	This work
pTP221	pTP213 containing <i>Xenopus laevis</i> <i>rmnd5</i> (NM_001092807.1)	This work
pTP213	pCS2 ⁺ containing CEN/ARS and URA3 gene from <i>S. cerevisiae</i>	[21]
pCA528	E.coli expression vector for T7-promoted expression of His ₆ -SUMO fusion proteins	[30]
pTP250	pEGFP-C1 containing <i>rmnd5</i> (<i>Xenopus laevis</i>)	This work
pTP224	pEGFP-C1 containing RMND5b (homo sapiens)	[21]
pTP225	pEGFP-C1 containing RMND5a (homo sapiens)	[21]
pTP251	<i>Rmnd5</i> binding site silently mutated in pTP221	This work

doi:10.1371/journal.pone.0120342.t002

purchased from Abcam (Polyclonal ARMC8; WB 1:1000), Novus Biological (Polyclonal RMND5A; WB 1:1000).

Autoubiquitination assay

A 25 μ l ubiquitination reaction contained 0.25 μ g of E1 (yeast), 0.6 μ g of UbcH5b, 10 μ g of HA-ubiquitin, 1 μ l of energy regeneration solution (all BostonBiochem, Cambridge), 2 μ l ATP (100 mM, pH7.5), 2.5 μ l ubiquitin reaction buffer (500 mM Tris-HCl, pH7.5, 500 mM NaCl, 100 mM MgCl₂, 10 mM DTT, and 250 μ M ZnCl₂) and 2.25 μ g of purified Rmnd5 or HDM2 (Enzo Lifescience) as a positive control. The reactions were incubated at 30°C for 3 h. Ubiquitination of protein was monitored by Western blot analysis with polyclonal anti-HA antibody (Sigma).

Supporting Information

S1 Fig. Complementation assay of *Xenopus laevis* Rmnd5 in yeast *Agid2*. Catabolite degradation of fructose-1,6-bisphosphatase (FBPase) in yeast. *Agid2* (YWO0906) was transformed with plasmid pRM41 harbouring V5-tagged *rmnd5*. YWO0906 and YWO2023 (containing *GID2-V5*) were transformed with empty plasmid pRS426 as controls. Cells were grown for 12h in synthetic complete medium without uracil containing 2% glucose. After addition of 2% glucose 1.5 OD₆₀₀ of cells were taken at the indicated time points. Total protein was extracted and precipitated with trichloroacetic acid, resuspended in urea buffer and subjected to Western blot analysis with polyclonal FBPase antiserum, Pgk antibody (Molecular probes) and V5 antibody (Thermo Scientific), respectively. Digital data were quantified using TotalLab Quant and Excel; FBPase signals were normalised with 3-phosphoglycerate kinase (Pgk) (A) Representative Western blot of a complementation experiment. (B) Quantification of FBPase signal after glucose addition. Graphs include data from n = 10 (Rmnd5, blue), n = 7 (*gid2* = *Agid2*, red) and n = 5 (*GID2*, purple) experiments, respectively. (TIF)

S2 Fig. The CTLH complex functions during early embryonic neurogenesis. As Fig. 3 with standard morpholino injected embryos (TIF)

Acknowledgments

We thank the members of the Hollemann laboratory for constructive comments throughout the course of this work. Many thanks go to Astrid Fink for helping with statistical questions.

Author Contributions

Conceived and designed the experiments: TP TH DW PVL. Performed the experiments: TP RM AS. Analyzed the data: TP DW RM TH PVL. Contributed reagents/materials/analysis tools: TP DW TH. Wrote the paper: TP PVL.

References

1. Regelmann J, Schule T, Josupeit FS, Horak J, Rose M, Entian KD, et al. Catabolite degradation of fructose-1,6-bisphosphatase in the yeast *Saccharomyces cerevisiae*: a genome-wide screen identifies eight novel GID genes and indicates the existence of two degradation pathways. *Mol Biol Cell*. 2003; 14(4):1652–63. Epub 2003/04/11. doi: [10.1091/mbc.E02-08-0456](https://doi.org/10.1091/mbc.E02-08-0456) PubMed PMID: PMID: [12686616](https://pubmed.ncbi.nlm.nih.gov/12686616/).
2. Menssen R, Schweiggert J, Schreiner J, Kusevic D, Reuther J, Braun B, et al. Exploring the Topology of the Gid Complex, the E3 Ubiquitin Ligase Involved in Catabolite-induced Degradation of

- Gluconeogenic Enzymes. *J Biol Chem.* 2012; 287(30):25602–14. Epub 2012/05/31. doi: [10.1074/jbc.M112.363762](https://doi.org/10.1074/jbc.M112.363762) PubMed PMID: PMID: [22645139](https://pubmed.ncbi.nlm.nih.gov/22645139/); PubMed Central PMCID: PMC3408164.
3. Braun B, Pfirrmann T, Menssen R, Hofmann K, Scheel H, Wolf DH. Gid9, a second RING finger protein contributes to the ubiquitin ligase activity of the Gid complex required for catabolite degradation. *FEBS Lett.* 2011. Epub 2011/11/03. S0014-5793(11)00789-7 [pii]doi: [10.1016/j.febslet.2011.10.038](https://doi.org/10.1016/j.febslet.2011.10.038) PubMed PMID: PMID: [22044534](https://pubmed.ncbi.nlm.nih.gov/22044534/).
 4. Santt O, Pfirrmann T, Braun B, Juretschke J, Kimmig P, Scheel H, et al. The yeast GID complex, a novel ubiquitin ligase (E3) involved in the regulation of carbohydrate metabolism. *Mol Biol Cell.* 2008; 19(8):3323–33. Epub 2008/05/30. E08-03-0328 [pii]doi: [10.1091/mbc.E08-03-0328](https://doi.org/10.1091/mbc.E08-03-0328) PubMed PMID: PMID: [18508925](https://pubmed.ncbi.nlm.nih.gov/18508925/).
 5. Sommer T, Wolf DH. The ubiquitin-proteasome-system. *Biochim Biophys Acta.* 2014; 1843(1):1. Epub 2013/09/24. doi: [10.1016/j.bbamcr.2013.09.009](https://doi.org/10.1016/j.bbamcr.2013.09.009) PubMed PMID: PMID: [24055503](https://pubmed.ncbi.nlm.nih.gov/24055503/).
 6. Deshaies RJ, Joazeiro CA. RING domain E3 ubiquitin ligases. *Annu Rev Biochem.* 2009; 78:399–434. Epub 2009/06/06. doi: [10.1146/annurev.biochem.78.101807.093809](https://doi.org/10.1146/annurev.biochem.78.101807.093809) PubMed PMID: PMID: [19489725](https://pubmed.ncbi.nlm.nih.gov/19489725/).
 7. Francis O, Han F, Adams JC. Molecular Phylogeny of a RING E3 Ubiquitin Ligase, Conserved in Eukaryotic Cells and Dominated by Homologous Components, the Muskelin/RanBPM/CTLH Complex. *PloS one.* 2013; 8(10):e75217. Epub 2013/10/22. doi: [10.1371/journal.pone.0075217](https://doi.org/10.1371/journal.pone.0075217) PubMed PMID: PMID: [24143168](https://pubmed.ncbi.nlm.nih.gov/24143168/); PubMed Central PMCID: PMC3797097.
 8. Kobayashi N, Yang J, Ueda A, Suzuki T, Tomaru K, Takeno M, et al. RanBPM, Muskelin, p48EMLP, p44CTLH, and the armadillo-repeat proteins ARMC8alpha and ARMC8beta are components of the CTLH complex. *Gene.* 2007; 396(2):236–47. Epub 2007/05/01. S0378-1119(07)00120-5 [pii]doi: [10.1016/j.gene.2007.02.032](https://doi.org/10.1016/j.gene.2007.02.032) PubMed PMID: PMID: [17467196](https://pubmed.ncbi.nlm.nih.gov/17467196/).
 9. Umeda M, Nishitani H, Nishimoto T. A novel nuclear protein, Twa1, and Muskelin comprise a complex with RanBPM. *Gene.* 2003; 303:47–54. Epub 2003/02/01. S0378111902011538 [pii]. PubMed PMID: PMID: [12559565](https://pubmed.ncbi.nlm.nih.gov/12559565/).
 10. Tomastikova E, Ceniklova V, Kohoutova L, Petrovska B, Vachova L, Halada P, et al. Interactions of an Arabidopsis RanBPM homologue with LisH-CTLH domain proteins revealed high conservation of CTLH complexes in eukaryotes. *BMC plant biology.* 2012; 12:83. Epub 2012/06/09. doi: [10.1186/1471-2229-12-83](https://doi.org/10.1186/1471-2229-12-83) PubMed PMID: PMID: [22676313](https://pubmed.ncbi.nlm.nih.gov/22676313/).
 11. Gerlitz G, Darhin E, Giorgio G, Franco B, Reiner O. Novel functional features of the Lis-H domain: role in protein dimerization, half-life and cellular localization. *Cell Cycle.* 2005; 4(11):1632–40. Epub 2005/11/01. PubMed PMID: PMID: [16258276](https://pubmed.ncbi.nlm.nih.gov/16258276/).
 12. Emes RD, Ponting CP. A new sequence motif linking lissencephaly, Treacher Collins and oral-facial-digital type 1 syndromes, microtubule dynamics and cell migration. *Human molecular genetics.* 2001; 10(24):2813–20. Epub 2001/12/06. PubMed PMID: PMID: [11734546](https://pubmed.ncbi.nlm.nih.gov/11734546/).
 13. Tagnaouti N, Loebrich S, Heisler F, Pechmann Y, Fehr S, De Arcangelis A, et al. Neuronal expression of muskulin in the rodent central nervous system. *BMC neuroscience.* 2007; 8:28. Epub 2007/05/04. doi: [10.1186/1471-2202-8-28](https://doi.org/10.1186/1471-2202-8-28) PubMed PMID: PMID: [17474996](https://pubmed.ncbi.nlm.nih.gov/17474996/); PubMed Central PMCID: PMC1876237.
 14. Heisler FF, Loebrich S, Pechmann Y, Maier N, Zivkovic AR, Tokito M, et al. Muskelin regulates actin filament- and microtubule-based GABA(A) receptor transport in neurons. *Neuron.* 2011; 70(1):66–81. Epub 2011/04/13. doi: [10.1016/j.neuron.2011.03.008](https://doi.org/10.1016/j.neuron.2011.03.008) PubMed PMID: PMID: [21482357](https://pubmed.ncbi.nlm.nih.gov/21482357/); PubMed Central PMCID: PMC3101366.
 15. Tomaru K, Ueda A, Suzuki T, Kobayashi N, Yang J, Yamamoto M, et al. Armadillo Repeat Containing 8alpha Binds to HRS and Promotes HRS Interaction with Ubiquitinated Proteins. *Open Biochem J.* 2010; 4:1–8. Epub 2010/03/13. doi: [10.2174/1874091X01004010001](https://doi.org/10.2174/1874091X01004010001) PubMed PMID: PMID: [20224683](https://pubmed.ncbi.nlm.nih.gov/20224683/); PubMed Central PMCID: PMC2835868.
 16. van Wijk SJ, de Vries SJ, Kemmeren P, Huang A, Boelens R, Bonvin AM, et al. A comprehensive framework of E2-RING E3 interactions of the human ubiquitin-proteasome system. *Mol Syst Biol.* 2009; 5:295. Epub 2009/08/20. msb200955 [pii]doi: [10.1038/msb.2009.55](https://doi.org/10.1038/msb.2009.55) PubMed PMID: PMID: [19690564](https://pubmed.ncbi.nlm.nih.gov/19690564/).
 17. Li J, Chen Y, Qin X, Wen J, Ding H, Xia W, et al. MiR-138 downregulates miRNA processing in HeLa cells by targeting RMND5A and decreasing Exportin-5 stability. *Nucleic acids research.* 2014; 42(1):458–74. Epub 2013/09/24. doi: [10.1093/nar/gkt839](https://doi.org/10.1093/nar/gkt839) PubMed PMID: PMID: [24057215](https://pubmed.ncbi.nlm.nih.gov/24057215/); PubMed Central PMCID: PMC3874158.
 18. Vogel TW, Manjila S, Cohen AR. Novel neurodevelopmental disorder in the case of a giant occipitoparietal meningoencephalocele. *Journal of neurosurgery Pediatrics.* 2012; 10(1):25–9. Epub 2012/06/12. doi: [10.3171/2012.3.PEDS11559](https://doi.org/10.3171/2012.3.PEDS11559) PubMed PMID: PMID: [22681319](https://pubmed.ncbi.nlm.nih.gov/22681319/).

19. Notredame C, Higgins DG, Heringa J. T-Coffee: A novel method for fast and accurate multiple sequence alignment. *Journal of molecular biology*. 2000; 302(1):205–17. Epub 2000/08/31. doi: [10.1006/jmbi.2000.4042](https://doi.org/10.1006/jmbi.2000.4042) PubMed PMID: PMID: [10964570](https://pubmed.ncbi.nlm.nih.gov/10964570/).
20. Dereeper A, Guignon V, Blanc G, Audic S, Buffet S, Chevenet F, et al. Phylogeny.fr: robust phylogenetic analysis for the non-specialist. *Nucleic acids research*. 2008; 36(Web Server issue):W465–9. Epub 2008/04/22. doi: [10.1093/nar/gkn180](https://doi.org/10.1093/nar/gkn180) PubMed PMID: PMID: [18424797](https://pubmed.ncbi.nlm.nih.gov/18424797/); PubMed Central PMCID: PMC2447785.
21. Pfirrmann T, Lokapally A, Andreasson C, Ljungdahl P, Hollemann T. SOMA: a single oligonucleotide mutagenesis and cloning approach. *PloS one*. 2013; 8(6):e64870. Epub 2013/06/12. doi: [10.1371/journal.pone.0064870](https://doi.org/10.1371/journal.pone.0064870) PubMed PMID: PMID: [23750217](https://pubmed.ncbi.nlm.nih.gov/23750217/); PubMed Central PMCID: PMC3672168.
22. Hirsch N, Harris WA. *Xenopus Pax-6 and retinal development*. *Journal of neurobiology*. 1997; 32(1):45–61. Epub 1997/01/01. PubMed PMID: PMID: [8989662](https://pubmed.ncbi.nlm.nih.gov/8989662/).
23. Suzuki T, Ueda A, Kobayashi N, Yang J, Tomaru K, Yamamoto M, et al. Proteasome-dependent degradation of alpha-catenin is regulated by interaction with ARMc8alpha. *Biochem J*. 2008; 411(3):581–91. Epub 2008/01/25. doi: [10.1042/BJ20071312](https://doi.org/10.1042/BJ20071312) PubMed PMID: PMID: [18215130](https://pubmed.ncbi.nlm.nih.gov/18215130/).
24. Cox JL, Wilder PJ, Gilmore JM, Wuebben EL, Washburn MP, Rizzino A. The SOX2-interactome in brain cancer cells identifies the requirement of MSI2 and USP9X for the growth of brain tumor cells. *PloS one*. 2013; 8(5):e62857. Epub 2013/05/15. doi: [10.1371/journal.pone.0062857](https://doi.org/10.1371/journal.pone.0062857) PubMed PMID: PMID: [23667531](https://pubmed.ncbi.nlm.nih.gov/23667531/); PubMed Central PMCID: PMC3647065.
25. Kelberman D, de Castro SC, Huang S, Crolla JA, Palmer R, Gregory JW, et al. SOX2 plays a critical role in the pituitary, forebrain, and eye during human embryonic development. *The Journal of clinical endocrinology and metabolism*. 2008; 93(5):1865–73. Epub 2008/02/21. doi: [10.1210/jc.2007-2337](https://doi.org/10.1210/jc.2007-2337) PubMed PMID: PMID: [18285410](https://pubmed.ncbi.nlm.nih.gov/18285410/); PubMed Central PMCID: PMC3479085.
26. Rizzino A. Sox2 and Oct-3/4: a versatile pair of master regulators that orchestrate the self-renewal and pluripotency of embryonic stem cells. *Wiley interdisciplinary reviews Systems biology and medicine*. 2009; 1(2):228–36. Epub 2009/12/18. doi: [10.1002/wsbm.12](https://doi.org/10.1002/wsbm.12) PubMed PMID: PMID: [20016762](https://pubmed.ncbi.nlm.nih.gov/20016762/); PubMed Central PMCID: PMC2794141.
27. Panavas T, Sanders C, Butt TR. SUMO fusion technology for enhanced protein production in prokaryotic and eukaryotic expression systems. *Methods Mol Biol*. 2009; 497:303–17. Epub 2008/12/25. doi: [10.1007/978-1-59745-566-4_20](https://doi.org/10.1007/978-1-59745-566-4_20) PubMed PMID: PMID: [19107426](https://pubmed.ncbi.nlm.nih.gov/19107426/).
28. Cornesse Y, Pieler T, Hollemann T. Olfactory and lens placode formation is controlled by the hedgehog-interacting protein (Xhip) in *Xenopus*. *Developmental biology*. 2005; 277(2):296–315. Epub 2004/12/25. doi: [10.1016/j.ydbio.2004.09.016](https://doi.org/10.1016/j.ydbio.2004.09.016) PubMed PMID: PMID: [15617676](https://pubmed.ncbi.nlm.nih.gov/15617676/).
29. Hollemann T, Bellefroid E, Pieler T. The *Xenopus* homologue of the *Drosophila* gene *tailless* has a function in early eye development. *Development*. 1998; 125(13):2425–32. Epub 1998/06/04. PubMed PMID: PMID: [9609825](https://pubmed.ncbi.nlm.nih.gov/9609825/).
30. Andreasson C, Fiaux J, Rampelt H, Mayer MP, Bukau B. Hsp110 is a nucleotide-activated exchange factor for Hsp70. *J Biol Chem*. 2008; 283(14):8877–84. Epub 2008/01/26. doi: [10.1074/jbc.M710063200](https://doi.org/10.1074/jbc.M710063200) PubMed PMID: PMID: [18218635](https://pubmed.ncbi.nlm.nih.gov/18218635/).